Lappeenranta
University of Technology

Davood Gudarzi

CATALYTIC DIRECT SYNTHESIS OF HYDROGEN PEROXIDE IN A NOVEL MICROSTRUCTURED REACTOR.

Thesis for the degree of doctor of science (Technology) to be presented with due permission for public examination and criticism in the Auditorium 1381 at Lappeenranta University of Technology, Lappeenranta, Finland on the 2th of December, 2014, at noon.

Acta Universitatis
Lappeenrantaensis 601

Supervisor

Professor Ilkka Turunen
Department of Chemical Technology
Lappeenranta University of Technology
Finland

Reviewers

Professor Jiří Hanika
Institute of Chemical Process Fundamentals
Academy of Science of the Czech Republic
Czech Republic

Professor Juan García Serna
Department of Chemical Engineering and Environmental Technology
University of Valladolid
Spain

Opponent

Professor Juan García Serna
Department of Chemical Engineering and Environmental Technology
University of Valladolid
Spain

Custos

Professor Ilkka Turunen
Department of Chemical Technology
Lappeenranta University of Technology
Finland

ISBN 978-952-265-680-3
ISBN 978-952-265-681-0 (PDF)
ISSN-L 1456–4491
ISSN 1456-4491

Lappeenrannan Teknillinen Yliopisto
Yliopistopaino 2014

ABSTRACT

Davood Gudarzi

Catalytic direct synthesis of hydrogen peroxide in a novel microstructured reactor.

Lappeenranta 2014
115 P.

Acta Universitatis Lappeenrantaensis 601
Diss. Lappeenranta University of Technology

ISBN 978-952-265-680-3, ISBN 978-952-265-681-0 (PDF)
ISSN-L 1456-4491, ISSN 1456-4491

The direct synthesis from hydrogen and oxygen is a green alternative for production of hydrogen peroxide. However, this process suffers from two challenges. Firstly, mixtures of hydrogen and oxygen are explosive over a wide range of concentrations (4-94% H_2 in O_2). Secondly, the catalytic reaction of hydrogen and oxygen involves several reaction pathways, many of them resulting in water production and therfore decreasing selectivity.

The present work deals with these two challenges. The safety problem was dealed by employing a novel microstructured reactor. Selectivity of the reaction was highly improved by development a set of new catalysts. The final goal was to develop an effective and safe continuous process for direct synthesis of hydrogen peroxide from H_2 and O_2.

Activated carbon cloth and Sibunit were examined as the catalysts' supports. Palladium and gold monometallic and palladium-gold bimetallic catalysts were thoroughly investigated by numerous kinetic experiments performed in a tailored batch reactor and several catalyst charachterization methods. A complete set of data for direct synthesis of H_2O_2 and its catalytic decomposition and hydrogenation was obtained. These data were used to assess factors influencing selectivity and activity of the catalysts in direct synthesis of H_2O_2 as well as its decomposition and hydrogenation.

A novel microstructured reactor was developed based on hydrodynamics and mass transfer studies in prototype microstractural plates. The shape and the size of the structural elements in the microreactor plate were optimized in a way to get high gas-liquid interfacial area and

gas-liquid mass transfer. Finally, empirical correlations for the volumetric mass transfer coefficient were derived.

A bench-scale continuous process was developed by using the novel microstructral plate reactor. A series of kinetic experiments were performed to investigate the effects of the gas and the liquid feed rates and their ratio, the amount of the catalyst, the gas feed composition and pressure on the final rate of H_2O_2 production and selectivity.

Keywords: Hydrogen peroxide, Direct synthesis of H_2O_2, Palladium catalysts, Palladium-gold catalysts, Decomposition of H_2O_2, Hydrogenation of H_2O_2, Microreactors, Hydrodynamics, Mass transfer.

UDC 544.478:66.023:661.491:542.057:66.021.3

PREFACE

The present work was carried out in the Laboratory of Process and Product Development, Department of Chemical Technology, Faculty of Technology at Lappeenranta University of Technology. The Finnish Funding Agency for Technology and Innovation (TEKES), The Academy of Finland, and The Center of Separation Technology (CST) are gratefully acknowledged for funding.

I would like to express my deepest appreciation to Professor Ilkka Turunen for giving me the opportunity to work at the laboratory and freedom to conduct the research. It has been a great honour to be supervised by such highly valuable top professional.

I would like to thank my colleagues from the Laboratory of Industrial Chemistry and Reaction Engineering at Åbo Akademi University for interesting discussions and inputs related to my work. My special thanks go to Academy Professor Tapio Salmi for letting me to do some experiments and characterization tests in the laboratory. The Laboratory Manager Dr. Kari Eranen deserves extra recognition for his faithful cooperation and helps.

I am grateful to Markku Heinonen from University of Turku for assisting in the XPS measurements and meticulous treatment of the spectra.

I would like to thank Dr. Warin Ratchananusorn for his enthusiastic cooperation and friendship. I am also grateful to all of my friends and colleagues at the Department of Chemical Technology.

Finally, I would like to express an immense and warm appreciation to my family in Iran, especially my mother for her unconditional care and support throughout the years.

The last, but not the least; I express my wholehearted thanks to my beloved wife and son, Nahid and Arman, for their infinite patience, supports and love. This thesis is dedicated to them.

Lappeenranta, on a snowy day of autumn
November 7th, 2014
Davood Gudarzi

TABLE OF CONTENTS

LIST OF PUBLICATIONS

This thesis is based on the following publications, which are referred to in the text by Roman numbers I-VII:

I. **D. Gudarzi**, W. Ratchananusorn, I. Turunen, T. Salmi, M. Heinonen. Preparation and study of Pd catalysts supported on activated carbon cloth (ACC) for direct synthesis of H_2O_2 from H_2 and O_2. *Topics in Catalysis* 56 (2013) 527–539.

II. **D. Gudarzi**, W. Ratchananusorn, I. Turunen, M. Heinonen, T. Salmi. Factors affecting catalytic destruction of H_2O_2 by hydrogenation and decomposition over Pd catalysts supported on activated carbon cloth (ACC). *Catalysis Today* (2014), http://dx.doi.org/10.1016/j.cattod.2013.12.050.

III. **D. Gudarzi**, W. Ratchananusorn, I. Turunen, M. Heinonen, T. Salmi. Promotional effects of Au in Pd-Au bimetallic catalysts supported on activated carbon cloth (ACC) for direct synthesis of H_2O_2 from H_2 and O_2. *Catalysis Today* (2014), http://dx.doi.org/10.1016/j.cattod.2014.04.011.

IV. **D. Gudarzi**, I. Turunen, M. Heinonen. T. Salmi, Factors influencing hydrogenation and decomposition of H_2O_2 over Pd-Au catalysts supported on activated carbon cloth (ACC). *Submitted to Topics in Catalysis*.

V. **D. Gudarzi**, O. A. Simakova, J. R. Hernández Carucci, P. D. Biasi, K. Eränen, E. Kolehmainen, I. Turunen, D. Y. Murzin, T. Salmi. Direct synthesis of H_2O_2 from H_2 and O_2 over carbon supported Au, Pd and Au-Pd/C bimetallic catalysts. *Chemical Engineering Transaction* 21 (2010) 925-930.

VI. W. Ratchananusorn, **D. Gudarzi**, I. Turunen. Catalytic direct synthesis of hydrogen peroxide in a novel microstructured reactor. *Chemical Engineering and Processing: Process Intensification* (2014), http://dx.doi.org/10.1016/j.cep.2014.01.005.

VII. W. Ratchananusorn, D. Semyonov, **D. Gudarzi**, E. Kolehmainen, I. Turunen. Hydrodynamics and mass transfer studies on a plate microreactor. *Chemical Engineering and Processing: Process Intensification* 50 (2011) 1186-1192.

Author's contribution in the publications

Publications I-V: The author was the prime contributor and responsible for the design, development and characterization of the catalysts. He had a major role in conducting the experiments, analyzing the data, drawing the conclusions and writing the papers.

Publication VI: The author contributed in design and making the experimental set-up, carried out the experiments with co-authors and participated in writing the paper.

Publication VII: The author contributed in design of the microstructured plate reactor and making the experimental set-ups, carried out the experiments with co-authors and participated in writing the paper.

Related conference presentations

I. **D. Gudarzi**, Z. Wukui, I. Turunen. Computational modeling and experimental investigation of liquid-liquid separation in a coalescer. *18th International Congress of Chemical and Process Engineering*, Prague, Czech Republic, 24th-28th August 2008. Oral presentation.

II. W. Ratchananusorn, D. Semyonov. **D. Gudarzi**, E. Kolehmainen, I. Turunen. Hydrodynamic and mass transfer studies in a microreactor plate. *2th European Process Intensification Conference*, Venice, Italy, 14-17 June 2009. Oral presentation.

III. **D. Gudarzi**, O. A. Simakova, J. R. H. Carucci, E. Kolehmainen, D. YU. Murzin, T. Salmi, I. Turunen. Direct Synthesis of H_2O_2 from H_2 and O_2 over Carbon Supported Au, Pd and Au-Pd/C Bimetallic Catalysts. *19th International Congress of Chemical and Process Engineering and 7th European Congress of Chemical Engineering*, Prague, Czech Republic, 28 August-1 September 2010. Oral presentation.

IV. **D. Gudarzi**, W. Ratchananusorn, I. Turunen. Micro structured plate reactor for direct synthesis of hydrogen peroxide. *8th International Symposium on Catalysis in Multiphase Reactors and 7th International Symposium on Multifunctional Reactors*, Naantali, Finland, 22-25 May 2011. Poster presentation.

V. **D. Gudarzi**, W. Ratchananusorn, I. Turunen. Preparation and study of Pd-Au catalysts supported on activated carbon cloth (ACC) for direct synthesis of H_2O_2 from H_2 and O_2, *15th Nordic Symposium on Catalysis*, Åland, Finland, 10-12 June 2012. Poster presentation.

VI. **D. Gudarzi**, W. Ratchananusorn, I. Turunen. Factors influencing decomposition of H_2O_2 over Pd catalysts supported on activated carbon cloth. *ANQUE International Congress of Chemical Engineering*, Seville, Spain, 24-27 June 2012. Poster presentation.

VII. **D. Gudarzi**, W. Ratchananusorn, I. Turunen. Preparation and study of Pd catalysts supported on activated carbon cloth (ACC) for direct synthesis of H_2O_2 from H_2 and O_2. *15th International Congress on Catalysis*, Munich, Germany, 1-6 July 2012. Poster presentation.

VIII. **D. Gudarzi**, W. Ratchananusorn, I. Turunen. Factors influencing decomposition of H_2O_2 over Pd-Au catalysts supported on activated carbon cloth. 9th European Congress of Chemical Engineering, Hague, Netherlands, 21-25 April 2013. Poster presentation.

IX. W. Ratchananusorn, **D. Gudarzi**, I. Turunen. Hydrogen peroxide direct synthesis on Pd catalysts in a microreactor. 9th European Congress of Chemical Engineering, Hague, Netherlands, 21-25 April 2013. Oral presentation.

X. **D. Gudarzi**, I. Turunen. Hydrogenation and decomposition of H_2O_2 over Pd-Au bimetallic catalysts supported on activated carbon cloth (ACC). 16th Nordic Symposium on Catalysis, Oslo, Norway, 15-17 June 2014. Poster presentation.

LIST OF SYMBOLS

a	specific surface area	$m^2\ m^{-3}$
A	area	m^2
C	concentration	$mol\ m^{-3}$
C^*	saturation concentration	$mol\ m^{-3}$
D	diffusivity	$m^2\ s^{-1}$
h	hold up	–
H	Henry's constant	$dm^3\ bar\ mol^{-1}$
k	volumetric mass transfer coefficient	$m\ s^{-1}$
L	length	m
p	partial pressure	bar
P	total pressure	bar
$\dot{V}$	volumetric flow rate	$m^3\ s^{-1}$
S_{N_2}	specific surface area	$m^2\ g^{-1}$

Greek symbols

ε	volume fraction	–
υ	superficial velocity	$mm\ s^{-1}$

Subscript

cr	cross sectional
f	fluid
g	gas
l	liquid
norm	normalized
per	perimeter
r	reactor
s	structured plate reactor
sq	square structure plate reactor
tot	total
tri	triangular structure plate

Abbreviations

ACC	activated carbon cloth
DTA	differential thermal analysis
EDS	energy dispersive spectroscopy
OACC	oxidized activated carbon cloth
ODE	ordinary differential equations
SEM	scanning electron microscopy
STEM	scanning transmission electron microscopy
TGA	thermal gravimetric analysis
TPD	temperature programmed desorption
XPS	X-ray photoelectron spectroscopy
UHRFESEM	ultra-high resolution field emission scanning electron microscopy

1. INTRODUCTION

1.1. Hydrogen peroxide

Hydrogen peroxide (H_2O_2) is an important commodity chemical and one the most popular oxidants because of its reactivity and green nature. It has a wide range of applications in many large scale processes (Fig. 1). It is also known as an environmentally friendly alternative to chlorine and chlorine-containing bleaching agents and oxidants [1]. The global production of H_2O_2 in 2013 was around 3 million tons per annum and the growth of its market is estimated around 4% per annum [2].

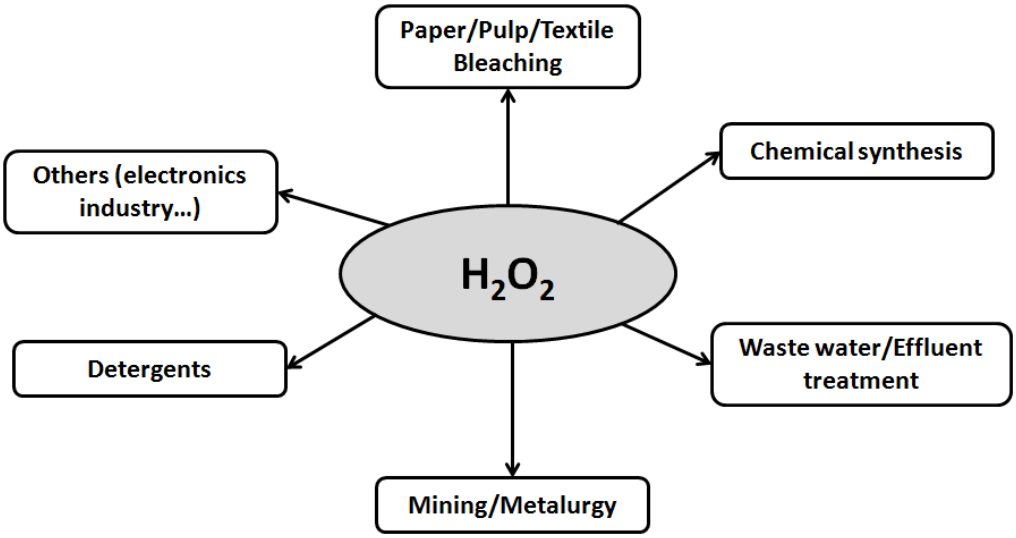

Figure 1. Global applications of hydrogen peroxide [3]

Hydrogen peroxide was discovered by well-known French chemist Louis-Jacques Thenard in 1818 [4]. Until the beginning of the 20th century, about 3% H_2O_2 solutions were produced by the hydrolysis of barium peroxide with sulfuric acid [1]. Later, it was also produced by the electrolysis of ammonium sulphate. Commercially, all H_2O_2 is now produced by the auto-oxidation (AO) of anthraquinone compounds [5] according to the reaction scheme shown in Fig. 2.

The AO process suffers from several drawbacks, such as the use of a complex solvent system which requires frequent analyzing and maintenance activities. In addition, the large amount of organic solution in the process represents environmental and safety risks. The deactivation of hydrogenation catalyst also requires periodic regeneration activities.

According to Piccinini et al [6], this process is economical only at large scale and at high product concentrations. However, H_2O_2 is often required at lower concentrations. Transportation of concentrated solution of H_2O_2 causes additional safety concerns since it can be explosive if it violently decomposes. These issues have encouraged scientists and engineers for many years to develop a more cost-effective and cleaner process for manufacturing this large-volume environmentally friendly chemical.

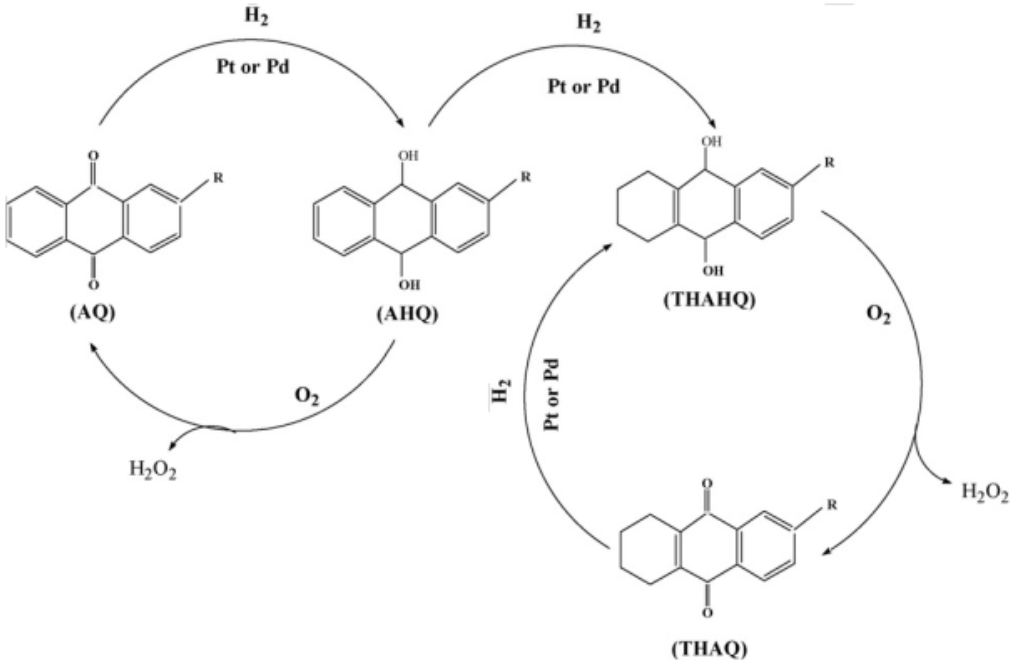

Figure 2. Production of H_2O_2 via anthraquinone auto-oxidation reactions.

1.2. Direct synthesis

The synthesis of hydrogen peroxide directly from gaseous H_2 and O_2 is an attractive alternative and the main challenger to the traditional anthraquinone process. Direct synthesis over a Pd-based catalyst was first reported by Henkel and Webel in 1914 [7] and since then it has been under research. Commercialization has not yet been taken place, probably because of challenges in safety and selectivity. Mixtures of hydrogen and oxygen are explosive over a wide range of concentrations (4-94% H_2 in O_2) [8].The selectivity problem can be understood by looking at the reaction scheme in Fig. 3. In addition to hydrogen peroxide, water is produced via several reaction routes. The highest cost in the process is the price of hydrogen and therefore we should maximize its conversion to hydrogen peroxide and minimize the

production of water. Therefore, selectivity is crucial to the economy of the process.

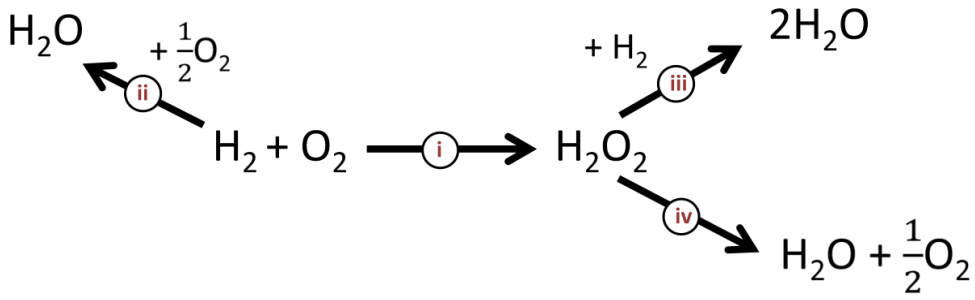

Figure 3. Reactions involved in the direct reaction of H_2 and O_2.

Pd-based catalysts are commonly used in the liquid-phase oxidation of H_2 by O_2 to H_2O_2, affecting all of the reactions in Fig. 3. The support material has an important role in their performance. Pd catalysts supported on acidic materials, e.g. Pd/SiO_2, were reported to be more active than Pd on basic supports (Pd/Al_2O_3) [9-10]. A majority of studies concerning the direct synthesis have focused on the factors maximizing the rate of H_2O_2 synthesis (reaction i, Fig. 3) while suppressing the water production (reactions ii–iv, Fig. 3). V.R. Choudhary et al [11-13] reported that the H_2O_2 destruction activity (reactions iii and iv, Fig. 3) of Pd catalysts were highly influenced by the oxidation state of Pd particles. They showed that palladium oxide (PdO) is substantially less destructive than palladium in zero valent state (Pd^0). Indeed, it was demonstrated that supported PdO catalysts are more selective but less active than the corresponding Pd^0 catalysts [14-19]. Several promoters have been examined to enhance the selectivity. Using of halide ions (especially Br^-) in reaction medium and/or directly in the catalyst along with protons (H^+) can raise the selectivity [11-13, 20-34]. The halide ions together with protons (H^+) promote the selectivity mainly by reducing the non-selective oxidation of H_2 to water through inhibiting the dissociative chemisorption of oxygen on catalyst surface and also by decreasing the consecutive decomposition/hydrogenation of H_2O_2 formed in the reaction [1]. Fu et al [35] demonstrated that surface chemistry of supports affects more the yield and selectivity than the metal particle size and specific surface area.

The addition of a second metal (e.g. Pt, Au, Ru, Rh) to Pd catalysts has been reported to affect catalytic activity and selectivity [10, 26-47]. Addition of Au or Pt (at favorable concentration) to a Pd catalyst was reported to enhance catalyst selectivity, while the presence of Rh or Ru exhibited an adverse effect [45].

Solvent affects, of course, also the direct synthesis rate by changing the overall rate of mass

transfer of gaseous reactants to the surface of catalyst via changing the solubility of the gases. Water, methanol or a mixture of them are commonly used as solvent. The solubility of H_2 in methanol is 4–5 times higher than in water while that of O_2 may increase up to eightfold [48]. Indeed, the rate of H_2O_2 production in alcohol medium was found much higher than that in an aqueous medium [48]. Rueter et al. [49] have disclosed that the addition of small amounts of a water soluble organic additive (e.g. methanol or ethanol) can significantly influence the direct synthesis of H_2O_2 from H_2 and O_2.

1.3. Microreactor technology

Microreactors, with their small volumes, short residence time and excellent heat and mass transfer properties open new possibilities to develop efficient, inherently safe, environmentally benign, and compact processes.. Today, microstructured devices are commercially available and are offered by different manufactures and engineering companies such as Velocys, BTS, Ehrfeld, CPC, IMM, Mikroglas, Microinnova, Little Things Factory etc. Modern fabrication techniques and machines enable production of novel microstructural process equipment which open new possibilities in chemical engineering.

Improved safety is one of the main advantages of microreactors [50]. This advantage can be achieved via several mechanisms. Firstly, the fluid hold-up in microreactors is small leading to smaller amount of explosive or burning substances. Secondly, the small dimensions of microchannels might suppress the initiated explosion prohibiting it to proceed. Both of these mechanisms might be useful in the connection of the direct synthesis. In the best case it might even be possible to run the synthesis in the explosive concentration ranges. This might lead to improved reaction rate and yield.

Direct synthesis in a microreactor is also suitable for on-site production of hydrogen peroxide. Therefore, there might be no need to concentrate the hydrogen peroxide solution, because dilute hydrogen peroxide can be used directly in various applications. As a result, it is possible to avoid energy consuming distillation and minimize the transportation of water.

1.4. Scope of this research and outlines

As it was discussed earlier, direct synthesis of hydrogen peroxide suffers from two technical challenges. Firstly, mixtures of hydrogen and oxygen are explosive over a wide range of concentrations (4-94% H_2 in O_2). Secondly, the catalytic reaction of hydrogen and oxygen involves several reaction pathways, most of them result in the production of water decreasing

the selectivity (Fig. 3)

In the present work, the safety risk was reduced by employing a novel microstructural reactor. Selectivity of the reaction was highly improved by development a set of new selective catalysts. The final goal was to develop an effective and safe continuous process for direct synthesis of hydrogen peroxide from H_2 and O_2.

Activated carbon materials have been reported as best supports for palladium based catalysts [47] in direct synthesis of hydrogen peroxide. Textural forms of activated carbon materials, such as activated carbon cloths and activated carbon felts, represent noticeable advantageous characteristics with respect to the usual granular activated carbons [39]. High surface area is normally in the range of 1500-3000 m^2 g^{-1} [40], and the porous network is mainly formed by deep pores in a narrow range of sizes, especially micropores [41]. Because of mechanical elasticity and geometric flexibility, fibrous cloths can be easily bent and rolled to fit in particular uses. Cloths woven from thin μm-sized fibers reduce the diffusion distance and produce a low-pressure drop in fixed beds and in multi-phase reactors where one or more dissolved species have to react with gaseous compounds of limited solubility [42]. Fast adsorption/desorption rates have been claimed as an additional advantage [43-44]. Moreover, in the novel microstructured reactor, ACC catalyst is an attractive alternative because it can be replaced quickly and easily when needed.

Activated carbon cloth and Sibunit were examined as supports for the catalysts. However, catalysts on activated carbon cloth were finally selected to be used in the novel microreactor. Palladium and palladium-gold bimetallic catalysts were thoroughly investigated (**Publications I, III and V**).

Since destruction of H_2O_2 can result in the loss of selectivity and yield, it is important to have a deep understanding of the factors affecting the H_2O_2 decomposition reactions (reactions iii and iv, Fig. 3). Therefore, as a part of the catalyst development, destruction of H_2O_2 over the catalysts supported on activated carbon cloth were also thoroughly investigated (**Publications II and IV)**.

A prototype of structured microreactor plates with 300 μm deep flow channels was developed for the three phase (gas-liquid-solid) reactions (**Publication VI**). Two plates with different static mixing elements, square and triangular, were used in the study. Hydrodynamic parameters and volumetric mass transfer coefficients were determined at various gas-liquid flow conditions.

Finally, direct synthesis of hydrogen peroxide was studied is in a bench-scale continuous process using the novel microstructured reactor (**Publication VII).** The effects of the process conditions, e.g. the gas composition, the gas and the liquid feed rates, pressure and the amount and composition of catalyst on the rate of H_2O_2 production were investigated.

2. EXPERIMENTATION

2.1. Materials and chemicals

A commercial activated carbon cloth ACC-5092-20 (Kynol Europa GmbH), after cleaning and a chemical treatment, was employed as a catalyst support. Sibunit was also used as a catalyst support in publication V. Sibunit is a synthetic carbon composite material combining advantages of graphite (chemical stability and electric conductivity) and active carbons (high specific surface area and adsorption capacity).

The specification of the main chemicals were used in the catalyst preparation, direct synthesis reactions, H_2O_2 hydrogenation and decomposition reactions, and the chemical analysis are reported in Table 1.

Table 1. Specification of the used chemicals

Chemical	Source	Purity
Carbon dioxide	AGA Oy	99.99 mol%
Oxygen	AGA Oy	99.99 mol%
Hydrogen	AGA Oy	99.999 mol%
CO_2/H_2 mixture	AGA Oy	(5% H_2)
Nitrogen	AGA Oy	99.99 mol%
Palladium (II) chloride	Sigma-Aldrich	99.999 wt%
Chloroauric acid	Aldrich	99.999 wt%
Methanol	Merck	99.9 wt%
Nitric acid	Merck	65 wt%
Acetic acid	Merck	100 wt%
Potassium Iodide	Merck	Analytical grade
Potassium dichromate	Aldrich	99.99 wt%
Sodium thiosulphate penta-hydrate	Merck	Analytical grade
Starch	Merck	Analytical grade
Hydranal (reagent)	Sigma-Aldrich	Titrant 2
Hydranal (solvent)	Sigma-Aldrich	-
Hydrogen peroxide	VWR	50 wt%
Sodium carbonate	Merck	Analytical grade
polyvinyl alcohol	Merck	Analytical grade
Sodium tetrahydridoborate	Aldrich	-

Palladium (II) chloride ($PdCl_2$) and gold (III) chloride hydrate ($HAuCl_4$) were used as metal precursors. Nitric acid, and sometimes acetic acid, was used for acid pretreatment of the

support. Methanol was used as a solvent (Merck) in all catalytic reactions, unless specified otherwise. Methanol was used as a solvent allowing higher solubility of gases. Potassium iodide (KI), acetic acid (CH_3COOH), potassium dichromate ($K_2Cr_2O_7$), Starch, and Sodium thiosulphate penta-hydrate ($Na_2S_2O_3 \cdot 5H_2O$) were used in iodometric titration of hydrogen peroxide. Hydranal reagent and Hydranal solvent were used in water content measurement.

2.2. Catalyst preparation

2.2.1. Catalysts supported on activated carbon cloth

The activated carbon cloth (ACC) was first treated in an oven at 100 °C for about 12 h. Then it was cleaned with 50 % solution of methanol at room temperature for 1 h, and finally washed with plenty of deionized water. For wet oxidation, the cleaned ACC was treated with 20 % solution of nitric acid at room temperature for 40 h. This is the main method for wet oxidation of ACC in this work, unless specified otherwise. Moreover, for compression few samples were also wet oxidized by acetic acid. After the oxidative treatment, the samples were washed with deionized water until neutral conditions were reached and then dried at 60 °C over night. These samples are referred as oxidized ACC (OACC). Acid pre-treatment step was used to create oxygen-containing functional groups on the surface of activated carbon and to modify the surface as suggested by several authors [44-47, 50-53].

The Pd catalysts on non-oxidized and oxidized activated carbon cloth were prepared by impregnation of the supports with an aqueous acidic solution of $PdCl_2$ at room temperature for 12 h. Appropriate concentrations of the metal precursor were used to finally obtain palladium loading in the range 1-5 wt.%. The impregnation was done in a 100 ml reactor with stirring rate about 700 rpm. The ratio of the solution volume to catalyst mass was 200 ml/g. After impregnation, the catalysts were washed with deionized water and left at room temperature for 3 h, and then dried at 60 °C over night.

The Pd-Au bimetallic catalysts on non-oxidized and oxidized activated carbon cloth were prepared by simultaneous co-impregnation of the supports with an aqueous acidic solution of $PdCl_2$ and $HAuCl_4$ at room temperature for 6-7 h. The impregnation was done in a glass reactor with stirring rate of 400-500 rpm. The rate of the stirring was adjusted to get uniform distribution of the metal particles in the catalysts. The ratio of the solution volume to catalyst mass was 500 ml/g. The amount of the precursor (Pd + Au) between 7.2 and 17.3 mg per 200 mg of the support in a 200 ml glass reactor gave metal loading (Pd + Au) in the range of 1–5

wt%. After impregnation, the catalysts were washed with deionized water and left at room temperature for 3 h, and then dried at 60 °C over night. This is the main method used to make the Pd-Au bimetallic catalysts in this work, unless specified otherwise. Moreover, in order to study the effects of catalyst preparation method, a series of bimetallic catalysts were also prepared by consequent impregnation of supports by Pd and Au precursors.

The reduction process was done by treating the fresh dried catalysts with H_2 at 185 °C under 3.5 bar for about 12 h. A series of calcined catalysts were prepared by oxidizing the fresh dried catalysts at temperature 185-275 °C in air for 12 h. The calcination temperatures were selected based on the TGA/DTA results in order to be in the safe thermal treatment region of the supports and their surface functional groups (in the case of oxidized ACC) (see Section 3.1.1.1.2).

2.2.2. Catalysts supported on Sibunit

Catalysts on both non-oxidized and pre-oxidized Sibunit were prepared almost with the same procedure. The pre-oxidized Sibunit was prepared by immersing it in 5 wt% nitric acid at room temperature overnight. Preparation of Au on carbon was started by dissolving $HAuCl_4$ (ABCR, Darmstad, 49% Au) in deionized water, then polyvinyl alcohol was added to form gold sol [54]. After a few minutes of mixing, gold sols were reduced by freshly prepared 0.1 M $NaBH_4$ solution. The ruby red Au^0 sols were immobilized immediately by adding the carbon support (Sibunit) under vigorous stirring. After 2 h the slurry was filtered and washed with deionized water. The catalyst was dried overnight at 60 °C.

Preparation of Pd on carbon was started by mixing with alkali solution of Na_2CO_3 at pH equal to 8 [55] then aqueous solution of H_2PdCl_4 was added. The slurry was mixed overnight at room temperature, then filtered and washed with deionized water. The catalyst was reduced in hydrogen flow at 150°C.

Au-Pd-catalyst on carbon was prepared by a two-steps procedure [56]. First Au was loaded on Sibunit as discussed above. The obtained slurry was mixed with a palladium sol, formed by mixing aqueous solution of H_2PdCl_4 with polyvinyl alcohol and hydrogen bubbled at room temperature (50 mL/min) for 2 h. Then the slurry was mixed in air atmosphere overnight, filtered and washed with water. The catalyst was dried at 60°C over night.

2.3. Catalyst characterization

The pore size distribution of the different supports and the catalysts were measured via nitrogen adsorption/desorption isotherms at liquid nitrogen temperature (-350 °C) using an automated gas sorption system (Sorptomatic 1900, Carlo Erba Instruments). The samples were degassed by heating at 100 °C in a vacuumed tube ($1.06* 10^{-3}$ Pa) for about 3 hours prior to the measurements. This treatment removed water, volatile impurities and other gases adsorbed or trapped in the porous. The specific surface area (S_{N2}) was calculated by using Dubinin-Radushkevich equation.

Atomic adsorption spectroscopy (AAS) was used for the quantitative determination of palladium and gold incorporated in the catalysts. Moreover, it was used to determine the amount of Pd and Au leached out into the reaction medium during the direct synthesis test. Latter figure was found out by determining the residual Pd and Au contents of the used catalyst and comparing it with that of the fresh catalyst. Atomic absorption spectroscopy was performed with a Thermo Scientific ICE 3000 series atomic absorption spectrometer using an air-acetylene flame. Samples for analysis were prepared by dissolving about 200 mg of the dried catalyst in an aqua regia solution followed by the addition of 500 ml of deionized water to dilute the solution.

Thermal behavior and properties of the supports and the catalysts were characterized by simultaneous differential thermal analysis (DTA) and thermal gravimetric analysis (TGA) using a NETZSCH STA 449 C Jupiter analyzer. Weight loss and heat flow during linear heating were measured. The analyses were done in oxidized conditions. Helium (He) was used as protective gas and oxygen as purge gas. The flow rates of He and O_2 were 40 ml/min and 20 ml/min, respectively. The furnace was heated up from 20 °C to 700 °C with heating rate 5 °C/min. The observed thermal effects in the TGA/DTA curves were interpreted according to the methodology presented by G. E. Shter et al. [57].

Temperature programmed desorption (TPD) approach was employed to study oxygen-containing surface functional groups in the supports and catalysts. The TPD tests were run in a set-up made of a U-shaped tubular reactor, placed inside an electrical furnace coupled to a Blazers Omnistar mass spectrometer for gas analyses. 200 mg of the sample was heated up to 1000 °C with a constant heating rate of 50 °C/min. During the tests, helium was passed through the reactor with the flow rate of 60 ml/min. The amounts of CO and CO_2 desorbed from the samples were recorded by the mass spectrometer for further analysis.

Scanning electron microscopy (SEM), Ultra-high resolution field emission scanning electron microscopy (UHRFESEM) and scanning transmission electron microscopy (STEM) were hired to assess particle size, shape and distribution, surface morphology, and to monitor the agglomeration tendency of metal particles. The UHRFESEM, STEM, and energy dispersive spectroscopy (EDS) analyses were done by a Hitachi S-4800 microscope with an X-ray detector for micro-analytical x-ray mapping and quantitative analysis. The active area of the x-ray detector for quantitative analysis was 10 mm^2. The SEM/EDS analysis was done by using a JEOL JSM-5800 microscope with X-ray detector for microanalysis (Noran Instrument Co.).

The oxidation states of the active components (Pd and Au) were determined by X-ray photoelectron spectroscopy (XPS). The spectra were obtained with a Perkin Elmer 5400 spectrometer, by using the Mg Ka (1,253.6 eV) radiation of twin anode in a constant analyzer energy mode with pass energy of 37.75 eV. The pressure of the analysis chamber was maintained at 2×10^{-7} Pa. The binding energy scale was calibrated by setting the Au 4f7/2 transition to 84.0 eV. The spectra were analyzed by using Unifit peak-fitting program.

2.4. Catalytic reactions

2.4.1. Direct synthesis in batch reactor

In order to evaluate catalytic performance during the catalyst development part, a batch reactor was employed. The experimental setup is shown in Fig. 4. The direct synthesis was conducted in a stainless steel autoclave (Parr Instruments Ltd) with a nominal volume of 450 ml and a maximum working pressure of 140 bar. The autoclave was equipped with an overhead stirrer (0–2000 rpm) and facilities to measure the temperature and pressure. Hydrogen (18 mmol) was fed into the reactor through a gas-holder with a volume of 33 ml and through a flow controller. The gas-holder was used to measure the precise amount of hydrogen. A circulation line equipped with a six-way valve was installed for sampling at different times (Fig. 4). The sampling line was designed to cause minimum pressure changes and gas losses during sampling. Typically, the reactor was charged with about 60 mg of catalyst and successively with carbon dioxide up to 15.2 bar at room temperature. The pressure was thereafter elevated to 20.2 bar with oxygen and further to 35.2 bar with carbon dioxide again at room temperature. For the sake of safety and increasing the solubility of H_2 and O_2 in the solvent, CO_2 was used [58]. Catalysts were fixed in the reactor by means of a

metal stand as shown in Fig. 5. Methanol was employed as a reaction medium. 175 g of methanol was pumped in and the reactor was cooled down to about -1 °C. Stirring (1250 rpm) was begun after 2/3 of the methanol had been fed. Hydrogen was fed when the desired temperature was reached. The reaction time now began. The gas-liquid and liquid-solid mass transfer effects were eliminated by adjusting the stirring speed. This was done beforehand by carrying out a series of tests varying the stirring rate. It was found out that 1250 rpm was a sufficient stirring rate to eliminate the mass transfer limitations.

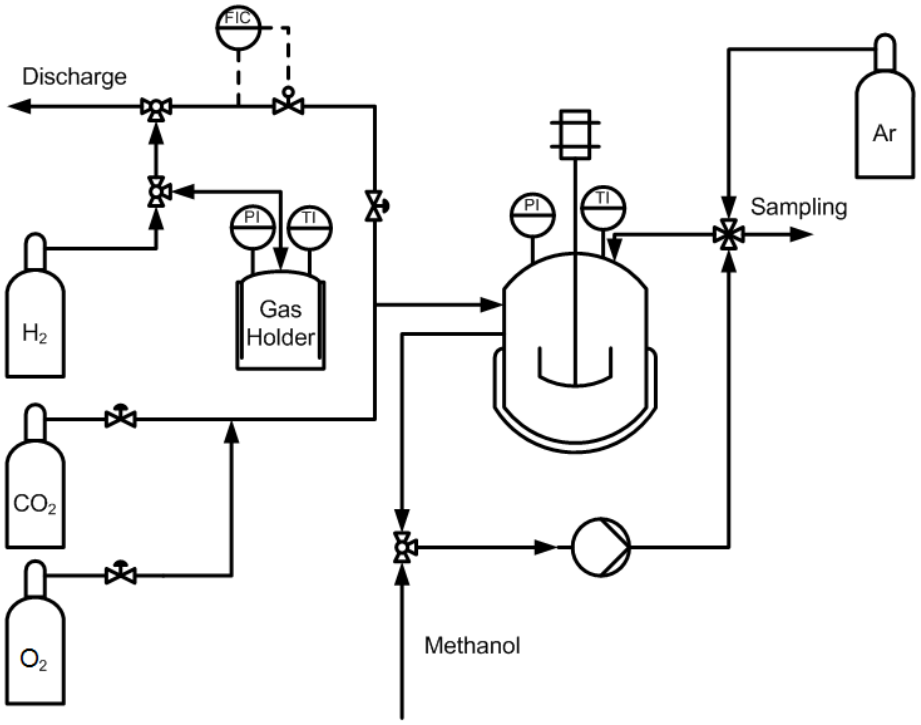

Figure 4. Experimental setup for the batch-wise H_2O_2 direct synthesis.

The concentration of H_2O_2 formed in the reaction was measured quantitatively by a volumetric iodometry titration. The produced water was determined by coulometric Karl–Fischer titration using a Mettler DL35 Karl-Fischer titrator. The water content in the solvent was measured prior to each experiment, before feeding hydrogen.

Catalytic performance was evaluated by the means of the following parameters: the final concentration of the produced hydrogen peroxide and water (wt %), selectivity (%), yield (%), and total H_2 conversion (%). The last three parameters are defined as follows:

$$\text{Selectivity}\,(\%) = \frac{\text{Moles of produced } H_2O_2}{\text{Moles of produced } H_2O_2 + \text{Moles of produced } H_2O} \times 100 \qquad (2\text{-}1)$$

$$\text{Yield}\,(\%) = \frac{\text{Moles of produced } H_2O_2}{\text{Moles of } H_2 \text{ fed}} \times 100 \qquad (2\text{-}2)$$

$$\text{Conversion}\,(\%) = \frac{\text{Moles of produced } H_2O_2 + \text{Moles of produced } H_2O}{\text{Moles of } H_2 \text{ fed}} \times 100 \qquad (2\text{-}3)$$

Another parameter which can be used in order to take in to account the metal content of the catalysts in their activities is Productivity:

$$\text{Productivity} = \frac{\text{Moles of produced } H_2O_2\ (\text{mol})}{\text{Reaction time (h)} \times \text{The metal content of the catalyst (kg)}} \qquad (2\text{-}4)$$

Figure 5. The metal stand for catalyst installation in the autoclave.

2.4.2. H_2O_2 hydrogenation and decomposition reactions

The H_2O_2 hydrogenation and decomposition reactions were also performed batch-wise in a Parr stainless steel autoclave. Experimental set up was also the same as the direct synthesis

reaction (Fig. 4). However, O_2 bottle was replaced with N_2. Typically, the reactor was charged with about 60 mg of catalyst and successively with 200 g of 1wt % hydrogen peroxide solution in methanol. In the case of decomposition tests, first the air in the reactor was displaced by N_2 and then the reactor was filled with N_2 up to 4 bar. For hydrogenation reaction, the air in the reactor was replaced with H_2 and then the reactor was filled with H_2 up to 4 bar. Stirring (1250 rpm) was begun immediately after H_2 feeding and the reaction time was started. Therefore, the possible decomposition of H_2O_2 during the H_2 feeding does not matter. The gas-liquid and liquid-gas mass transfer effects were eliminated by maintaining the sufficient stirring speed (1250 rpm). The amount of water and hydrogen peroxide in the solvent were measured prior to each experiment, just before starting the reaction. The destruction of H_2O_2 by hydrogenation ($H_2O_2 + H_2 \rightarrow 2\ H_2O$) or decomposition ($H_2O_2 \rightarrow H_2O + {}^1/_2O_2$) was measured as follow:

$$\left| H_2O_2 \text{ destructed} \right| (\%) = \frac{C_{H_2O_2,t=0} - C_{H_2O_2,t}}{C_{H_2O_2,t=0}} \times 100 \qquad (2\text{-}5)$$

2.4.3. Continuous direct synthesis in a novel microstructured reactor

2.4.3.1. Plate type microstructural reactor

In this section, the general specification of the final microstructural plate reactor used in the continuous H_2O_2 direct synthesis is presented.

The reactor is made of stainless steel and consists of several sections shown in Fig. 6. The gas is fed through the cover plate installed against the microreactor plate. The liquid is fed through a bifurcation configuration to improve liquid distribution and prevent channeling. The microreactor plate was installed vertically to locate the gas and liquid inlets on the top. Therefore, the microstructured section, catalyst bed or reaction section, gas-liquid separation section and outlet were placed under the inlets. The width of the microstructured section was 32 mm, height 300 mm and depth 300 μm. It consists of triangular elements arranged in staggered arrays (see Fig. 6). The size of each element is 1 mm × 2 mm × 300 μm (base × height × depth). The gas/liquid holdup was 3.84 cm^3 (the void fraction is 75%). The microstructural elements were designed to improve mixing of the two phases and to generate high interfacial area. The width of the reaction section was 32 mm, height 100 mm and depth 300 μm. A single layer of the catalysts supported on activated carbon cloth is slightly pressed in the reaction section by the cover plate.

2.4.3.2. The bench-scale process

The continuous bench scale process for the direct synthesis is shown in Fig. 7. The stainless steel equipment was firstly passivated with 20% citric acid at 60 ºC for 12 h to minimize the decomposition of hydrogen peroxide. Methanol was used as a solvent. Solvent was saturated with oxygen in the saturation vessel at 20 bar. Excess oxygen was used in order to also strip away dissolved CO_2 and H_2 left in the recycled solvent. The vessel was cooled to maintain solvent temperature at 0 ºC. From the saturation vessel, solvent saturated with oxygen was fed into the microreactor together with a mixture of CO_2 and H_2 (5% H_2). The fluids were flowing co-currently downwards in the reactor. At the bottom, gas and liquid phases were separated by gravity. Pressure was controlled by the gas outflow. Part of the out flowing liquid was taken as a product and the rest was recycled back to the saturation vessel. The volume of the solvent in the saturation vessel was kept constant by means of a liquid level controller. Another liquid level controller was installed to prevent flooding in the reactor. The instrumentation is shown in Fig. 7. Typical conditions in the reactor were 0 ºC and 20 bar. At the beginning, the saturation vessel was filled with methanol (0.35 l).Cooling of the liquid was started by feeding ethylene glycol through the jacket of the saturation vessel. Then oxygen flowed through the saturation vessel was initiated. Gas sparger was utilized to achieve sufficient gas–liquid interface. After that, circulation of solvent saturated with oxygen through the process was started. Next, the pressure of the reactor was raised to sufficient level by feeding inert gas. After reaching proper conditions in the whole process, the inert gas feed was changed to the mixture of CO_2 and H_2 and the reaction was started. The variables in the experiments were flow rates of gas and liquid fed into the reactor, pressure, wt % of Pd in the catalysts and the amount of catalyst. In addition, two alternative inert gases, CO_2 and N_2, were utilized with H_2 as gas feed. Temperature was 0 ºC in all tests. Concentration of hydrogen peroxide and water was determined in the product stream.

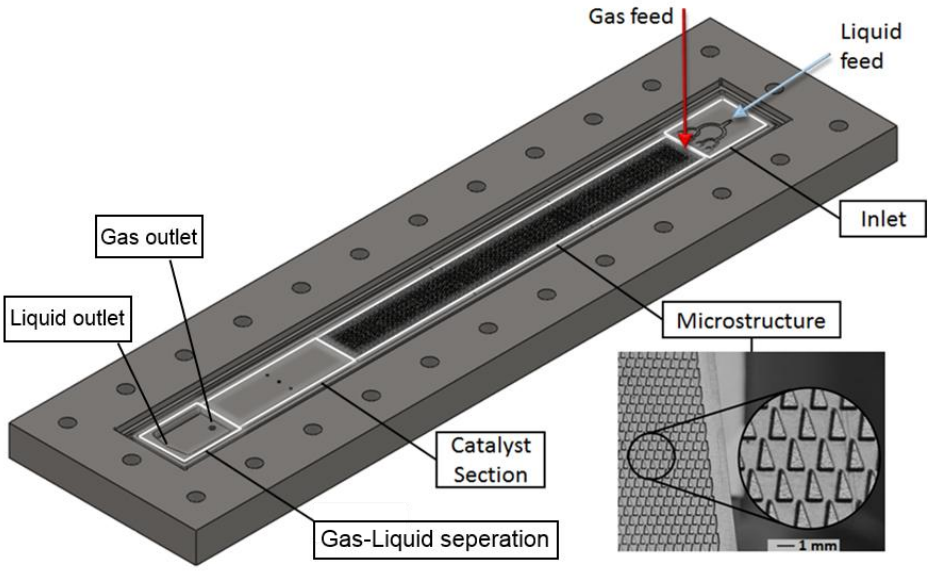

Figure 6. The microstructural plate reactor used in the continuous H_2O_2 direct synthesis.

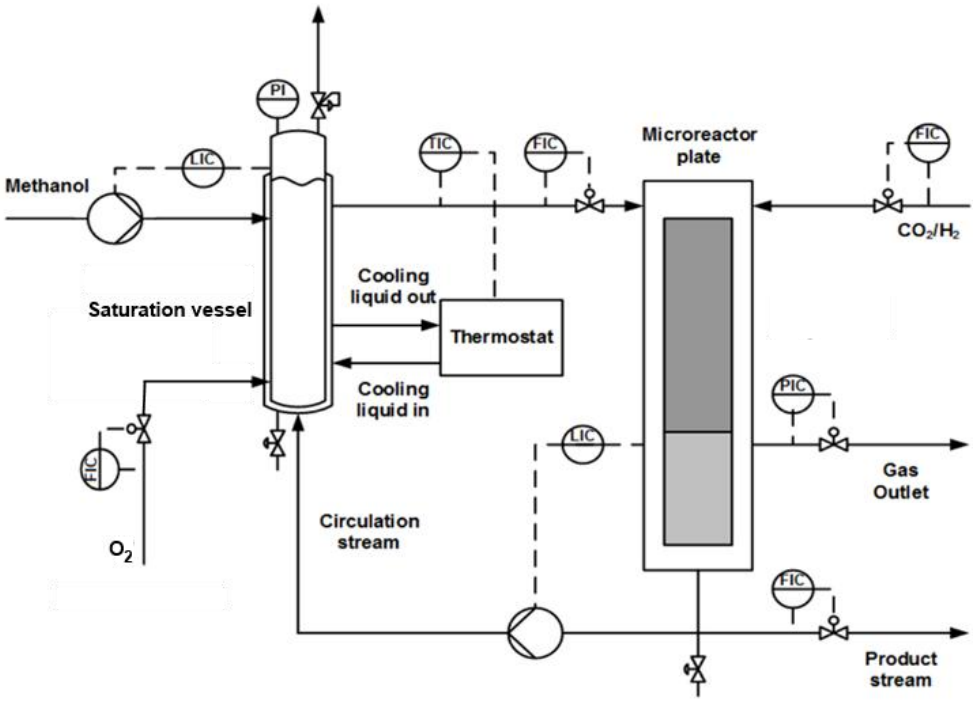

Figure 7. Experimental setup for continuous direct synthesis of H_2O_2 in the microstructural plate reactor

3. RESULTS AND DISCUSSION

3.1. Catalyst development

3.1.1. Pd catalysts supported on activated carbon cloth

3.1.1.1. Catalyst characterization results

3.1.1.1.1.Surface morphology and textural characteristics

Pore structure characteristics of the non-oxidized ACC (NACC) and ACC oxidized with nitric acid (OACC) are presented in Table 2. It can be observed that the pretreatment with HNO_3 decreased the specific surface area (SSA) and porosity of the activated carbon cloth. This occurs because activation of carbon makes the pore walls thinner and, thus, more easily destroyable by the oxidizing agent [59]. However, the pore size distribution almost remained constant. The effects of impregnation with Pd on the specific surface area (SSA) of oxidized and non-oxidized ACC are demonstrated in Fig. 8. These effects will be explained with the aid of SEM images in the following paragraphs.

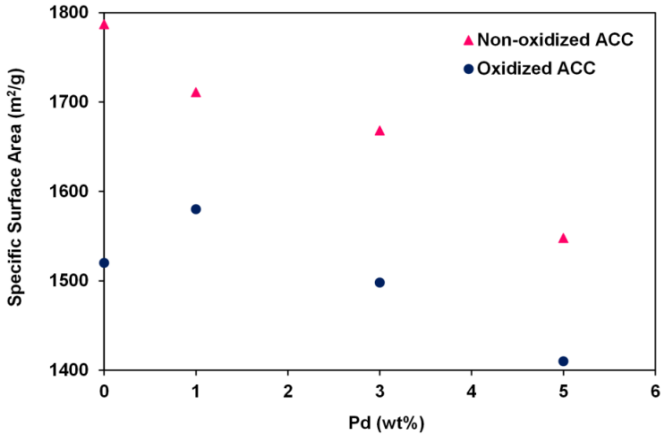

Figure 8. Specific surface area vs. Pd content of the Pd catalysts

Table 2. Textural properties of Non-oxidized and oxidized ACC with HNO_3

Sample	S_{N_2} (m^2g^{-1})	Pore volume (cm^3g^{-1})	Pore size distribution (nm)
Non-oxidized ACC	1788	0,63	9-25
Oxidized ACC	1520	0,54	8-25

The SEM images of the virgin oxidized ACC and oxidized ACC impregnated with different wt% of palladium are shown as Fig. 9. The virgin oxidized ACC (Fig. 9a) almost looks like a plain fiber without any visible pores, cavities or bulk solid on the surface. This also agrees well with the results of the specific surface area and pore size distribution measurements (Table 2). It demonstrates that the ACC fibers contain mainly micropores which are invisible in the SEM image. The SEM image of oxidized ACC impregnated with 1 wt% Pd (Fig. 9b) almost looks like the virgin oxidized ACC. This observation demonstrates that Pd mainly formed small particles (in the range of microposize) mostly located inside the micropores and, thus, they are invisible in the SEM image. Surface morphology in the catalysts with 3 and 5 wt% Pd are considerably changed due to the formation of the big Pd particles on the outer surface of ACC fibers (Fig. 9c-9d). Formation of the big Pd particles resulted in clogging of some of the ACC micropores and consequently resulted in reducing the specific surface area. This fact is in well agreement with specific surface area measurements (Fig. 8). In fact, increasing Pd content from 1 to 5 wt% decreased the specific surface area (from 1580 to 1409 m^2/g). Impregnation with 1 wt% Pd even slightly increases the specific surface area (from 1520 to 1580 m^2/g). Locating of small Pd particles in the pores can increase the roughness of their surface and consequently result in a small increase in specific surface area (Fig. 10).

Unlike oxidized ACC, impregnation of the non-oxidized ACC even with 1 wt% Pd leads to formation of a very thin layer of small Pd particles on the outer surface of the ACC fibers (Fig. 11). The metallization of the outer surface of carbon fibers can be even observed visually. The outer surface of the black ACC turned grey which is typical for palladium, while their interior, as seen upon cleavage of the fibers, remained black. Formation of the Pd particles and their crust-like distribution on the outer surface of the ACC fibers resulted in clogging of the ACC micropores. This fact is well confirmed with specific surface area measurements (Fig. 8). The specific surface area in the catalyst with 1 wt% Pd is decreased to 1711 from 1787 m^2/g. Increasing further the wt% of Pd results to formation bigger Pd particles and denser layer of them on the outer surface of the ACC fibers (Fig.11c-11d).

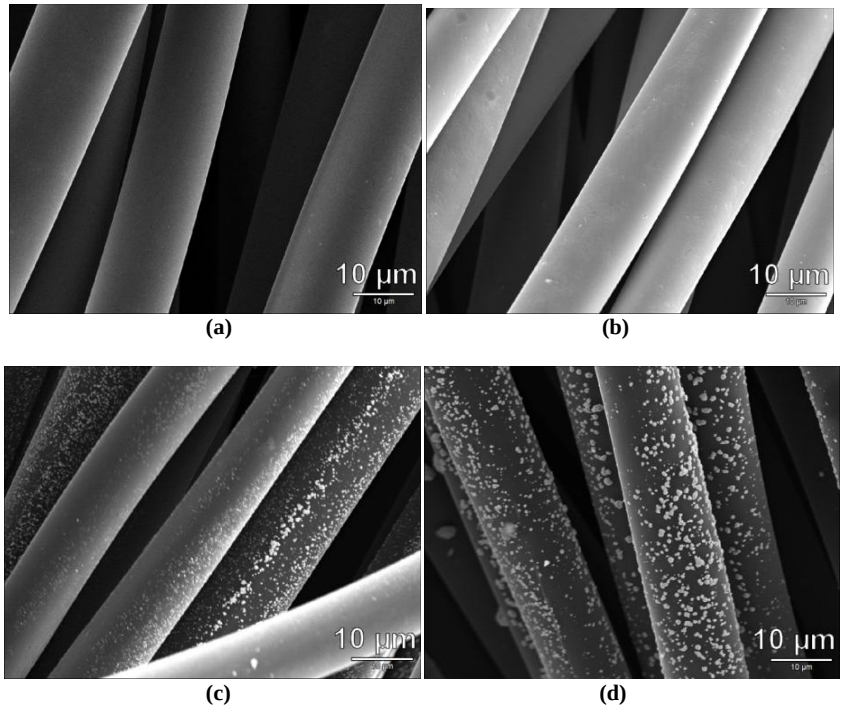

Figure 9. SEM images of (a) virgin oxidized ACC and the corresponding catalysts with: (b) 1 wt% Pd, (c) 3 wt% Pd and, (d) 5 wt% Pd.

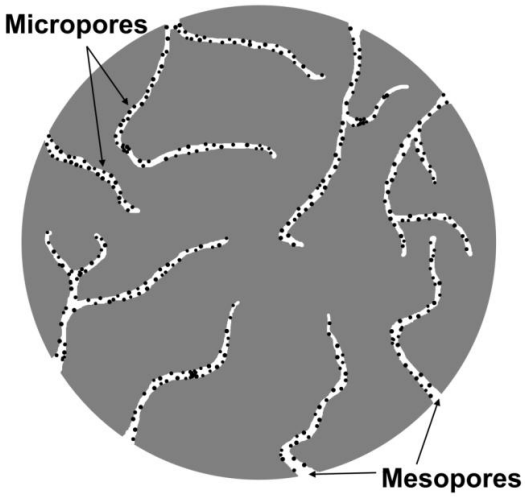

Figure 10. Schematic representation of the effect of small Pd particles

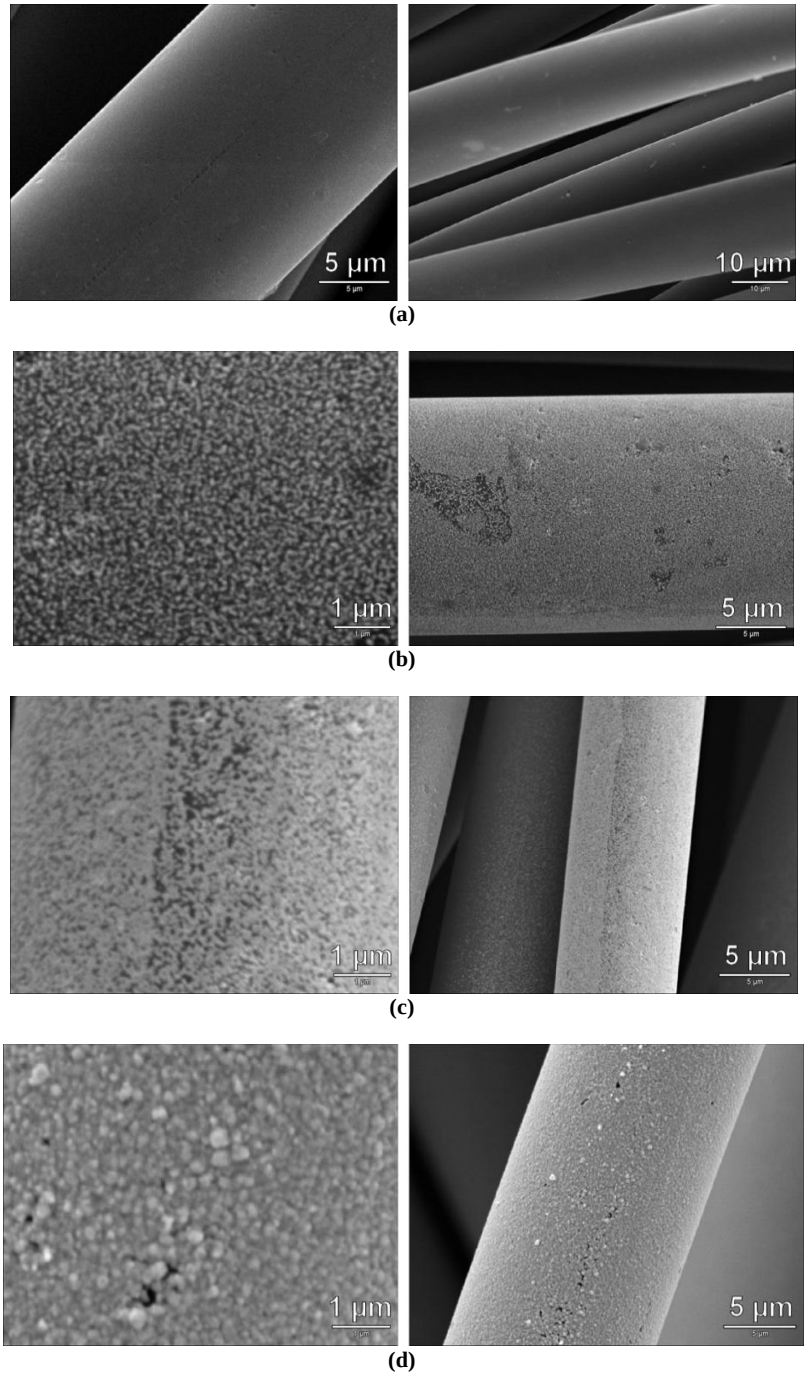

Figure 11. SEM images of (a) the virgin non-oxidized ACC and the corresponding catalysts with: (b) 1 wt% Pd, (c) 3 wt% Pd, and (d) 5 wt% Pd.

Surface morphology of the Pd catalysts is mainly governed by the interaction (attraction or repulsion) between the surface of the ACC fibers and Pd ions in the metal precursor. This interaction is typically determined by the differences between the pH of the palladium precursor and the isoelectric point (IEP or pH_{IEP}) of the ACC [60-61]. The pH_{IEP} of the ACC is depended on the surface chemistry of the ACC fibers which is characterized by the nature and the amount of surface functional groups. Actually, IEP or pH_{IEP} is the pH at which a surface carries no net electrical charge.

Wet oxidation of activated carbon cloth with nitric acid leaded to form acidic oxygen-containing functional groups on the surface of ACC fibers (see Section 3.1.1.1.3). These functional groups charge negatively the surface and affect the final interaction between the surface of ACC fibers and Pd ions in the metal precursor. Indeed, according to Fig. 12, they decrease the pH_{IEP} of ACC surface from around 5 to 3.5. When $pH>pH_{IEP,}$ the carbon surface, covered by deprotonated acidic groups, attracts cations from solution; while $pH<pH_{IEP}$ it attracts anions [62]. This is illustrated in Fig. 13.

Simonov et al. [61] showed that ionic palladium (Pd^{2+}) in acidic solution of palladium dichloride ($PdCl_2$) appears mainly as tetrachloropalladic ion complex ($PdCl_4^{2-}$). The pH of the Pd precursor during the impregnation of the ACC was in the range of 3.5-4. According to isoelectric point measurements (Fig. 12), the pH_{IEP} of the oxidized and non-oxidized ACC were 3.5 and 5 respectively. Based on the discussion above, the surface morphology changes of the non-oxidized and oxidized ACC impregnated with Pd could be explained as follow:

a) During the impregnation of non-oxidized ACC with Pd precursor, the pH of the precursor is considerably less than pH_{IEP} of the surface of the ACC. So, the electrostatic attraction between the positively charged surface ($pH<pH_{IEP}$) and the catalyst precursor anions ($PdCl_4^{2-}$) facilitate the adsorption of Pd anions ($PdCl_4^{2-}$) on the surface of the ACC fibers. Whereas the outer surface of the fibers is directly exposed to the Pd precursor, the rapid adsorption of ($PdCl_4^{2-}$) leads to formation of the crust-like distribution of the Pd particles on the outer surface. It can be observed visually that the pale yellow color of the precursor disappears after a short contact of non-oxidized ACC with precursor. Indeed, the adsorption equilibrium was found to be established in ca. 20 minutes on the non-oxidized ACC and in about atleast 3 hours on the oxidized one.
b) Since carbon is essentially not hydrophilic in nature, it has a very low affinity for

solvents of polar character such as water [63]. The metal precursor will be mostly exposed to the outer surface of the carbon particle when using water, but it will penetrate to the interior pores when the hydrophobicity of carbon decreases. Acidic functional groups introduced by the pretreatment with HNO_3 decreases the hydrophobicity of the carbon [60] thus making the interior of the micropores more accessible to the aqueous solution of the metal precursor during impregnation. Indeed, acid pretreatment of the ACC facilitates the access to the interior surfaces of the ACC fibers. This effect along with low attraction between the surface of the oxidized ACC with the Pd anions lead to form small and well distributed Pd particles, during the impregnation, also in the interior areas.

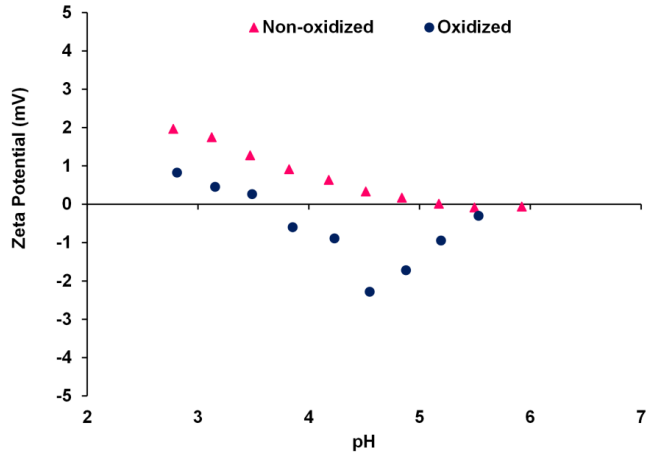

Figure 12. Isoelectric point measurements of oxidized and non-oxidized ACC

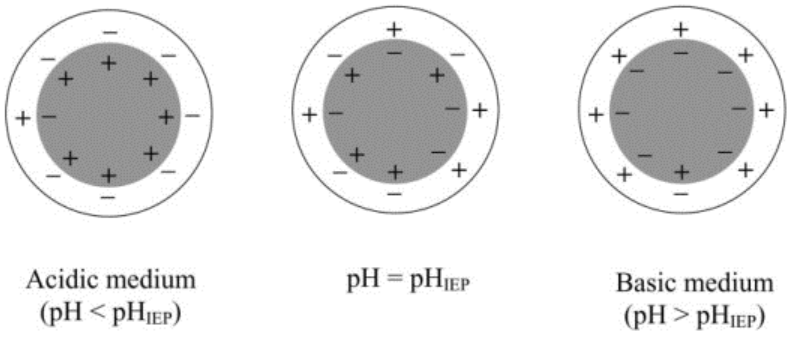

Figure 13. Schematic representation of the amphoteric character of carbon [62].

3.1.1.1.2.Thermal analysis

DTA and TGA profiles of the non-oxidized ACC, ACC oxidized with nitric acid, and their corresponding catalysts with 1-5 wt% Pd are shown in Figs. 14-16. No thermoeffect was detected by DTA for non-oxidized ACC below 455 °C. The only exothermic effect starts at 455 – 465 °C followed by a large and sharp weight loss in the TGA curve (Fig. 16). This effect corresponds to the burn-off of the ACC fibers and, T_g is the temperature at which the burn-off of the ACC fibers starts.

The DTA thermogram for oxidized ACC includes two exothermic effects. The first starts at around 310 – 320 °C and shows a peak at 350 °C with a small weight loss (about 4%) in the corresponding TGA profile (Fig. 15b, Table 4). The burn-off of the ACC fibers starts at 400 – 415 °C and is followed by a drastic and sharp weight loss in the TGA profile (Fig. 15a). The first slight observed peak corresponds to the decomposition of the oxygen-containing surface functional groups to CO and CO_2 [57]. T_c is the temperature at which the first thermoeffect starts.

For Pd catalysts on oxidized ACC, it can be observed:

a) T_c was shifted to lower values and it was dependent on the Pd content (Table 3, Fig. 15b). The reduction rate in T_c value for impregnated ACC, at the beginning was very sharp and T_c was reduced to 215 – 220 °C for 1% Pd/ACC (Table 4). After that, the rate of change of T_c as a function of Pd content was decreased. T_c is an important criterion in selection of calcination temperatures for Pd catalysts on oxidized ACC. In fact, treating of the catalysts above their T_c temperatures could damage and finally destroy the oxygen-containing surface functional groups introduced by acid pretreatment of ACC.
b) In the same way as T_c values, T_g in the Pd catalysts were considerably decreased (Table 3). The value of reduction in T_g also depended on the Pd content.
c) Impregnating the oxidized ACC with Pd leads to the sharper and more intensive exothermic peaks and weight loss corresponding to burn-off of the ACC fibers.

The DTA curve of impregnated non-oxidized ACC with 3%Pd, the same as the virgin non-oxidized ACC, shows only exothermic effect which is related to the burn-off of the ACC fibers (Fig. 16). However, burn of the ACC fibers are started earlier (T_g=300-320 °C) in 3%Pd/ACC compare to the virgin non-oxidized ACC (Table 3).

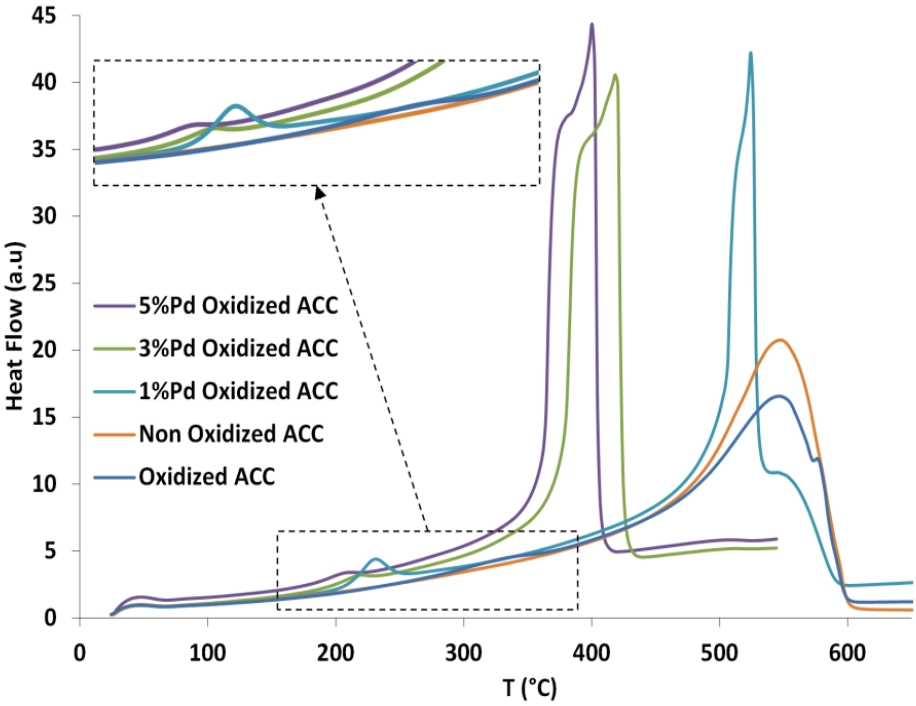

Figure 14. DTA curves for oxidized ACC and the corresponding Pd catalysts in an oxidative atmosphere.

Table 3. The characteristic temperatures in DTA/TGA curves. (T_c: The temperature at which oxygen starts to attack the ACC oxygen surface functional groups; T_g: The temperature at which oxygen starts to attack the carbon fiber skeleton; $T_{burn\text{-}off}$: The burn-off temperature of the ACC).

Sample	T_c (°C)	T_g (°C)	Burn-off (°C)
Non-oxidized ACC		455-465	495-595
3 wt% Pd/Non-oxidized ACC		300-320	460-580
Oxidized ACC	310-320	400-415	495-585
1 wt% Pd/Oxidized ACC	215-220	355-370	500-580
3 wt% Pd/Oxidized ACC	200-205	290-300	380-420
5 wt% Pd/Oxidized ACC	195-200	275-285	360-405

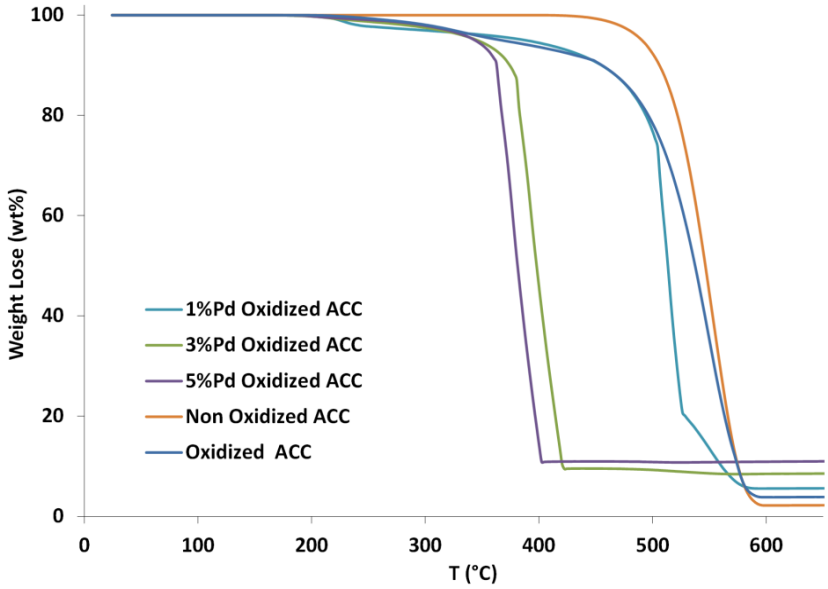

(a)

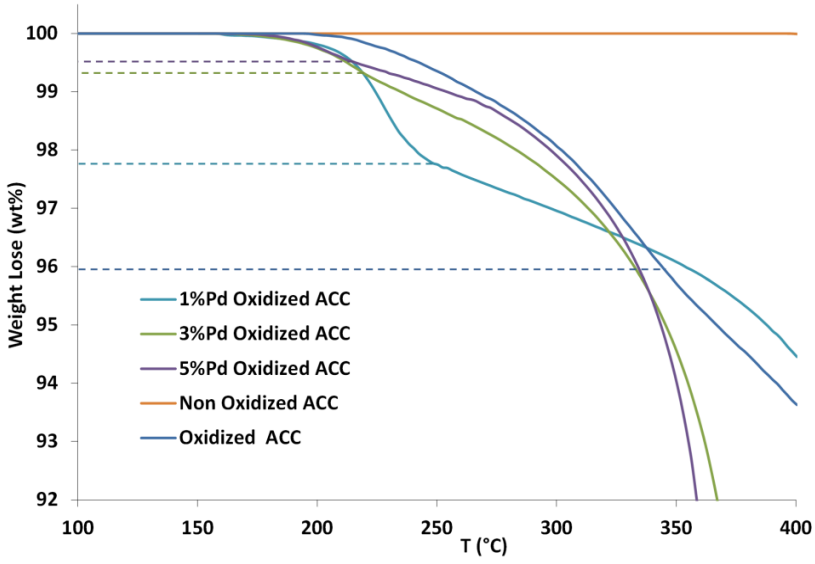

(b)

Figure 15. TGA curves (a) and corresponding close-up of the first exothermic effect (b) for oxidized ACC and the corresponding Pd catalysts in an oxidative atmosphere.

Table 4. Weight loss corresponding to the decomposition of the oxygen surface functional groups.

Sample	Weight loss (wt%)
Oxidized ACC	4.12
1 wt% Pd/Oxidized ACC	2.32
3 wt% Pd/Oxidized ACC	0.71
5 wt% Pd/Oxidized ACC	0.41

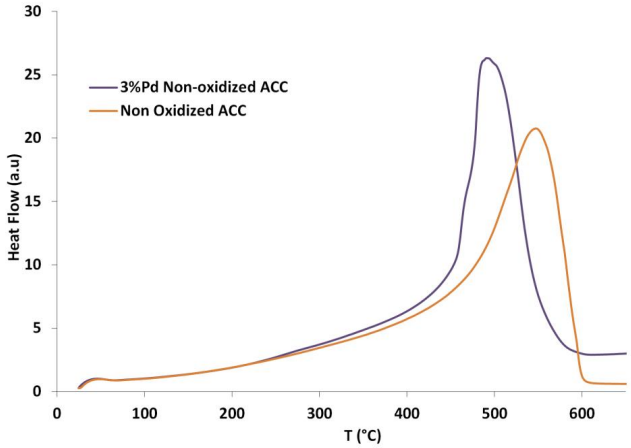

(a)

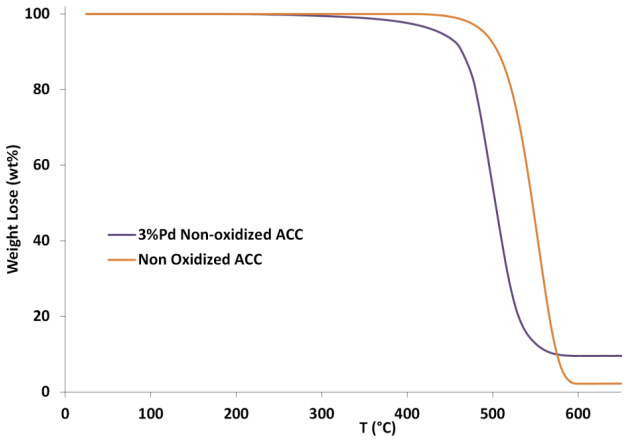

(b)

Figure 16. DTA (a) and TGA (b) curves for non-oxidized ACC and the corresponding catalyst with 3 wt% Pd in an oxidative atmosphere.

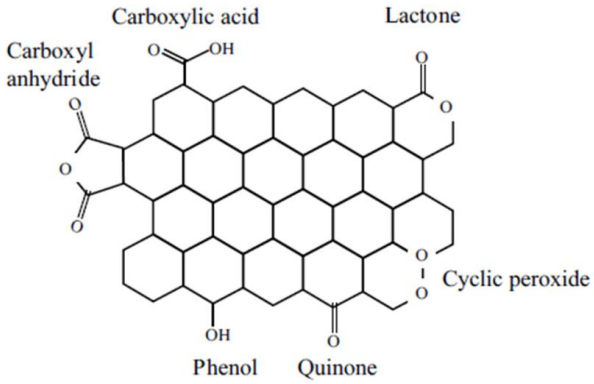

Figure 17. Different types of oxygen-containing surface groups on graphitic carbon [63].

3.1.1.1.3.Surface chemistry of the support

Wet oxidation treatments of carbon materials result in the formation of different oxygen-containing surface groups. These functional groups consist of strong acidic ones (like carboxylic and anhydride groups) and weak acidic ones (like lactones, phenols and carbonyl groups) [9, 52]. The oxygen-containing functional groups (Fig. 17) can be characterized by thermal programmed desorption (TPD) test. Strong and weak acidic oxygen-containing groups are responsible for CO_2 and CO desorption in TPD, respectively [9, 59, and 62].

The CO- and CO_2-TPD profiles of the non-oxidized ACC and ACC oxidized with nitric acid are compared in Fig. 18. The CO_2-TPD profile of the oxidized ACC shows a wide peak which starts at approximately 180 °C and reaches a maximum at approximately 620 °C. The corresponding CO-TPD profile begins to release CO at higher temperature (220 °C) and continuing this with increasing flow rate up to 900 °C. Indeed, These CO- and CO_2-TPD profiles demonstrate that the pretreatment of the ACC with HNO_3 introduces considerable amounts of oxygen-containing functional groups on the surface of ACC fibers.

The CO_2- and CO-TPD profiles of the oxidized ACC (virgin oxidized ACC and the one reduced with H_2 at 185 °C) and the corresponding catalysts with 3 wt% Pd are presented in Fig. 19. It can be seen:

a) The CO_2-TPD profiles of the different 3 wt% Pd catalysts started to release CO_2 at around 150 °C while in virgin oxidized ACC it started at around 200 °C.
b) Increasing the calcination temperature reduced the amount of the released CO_2 represented by the area under the CO_2 curve (Table 5). In other words, calcination of the Pd catalyst in air resulted in destruction of the stronger acidic surface functional

groups. This agrees well with the DTA/TGA results (see Section 3.1.1.1.2).

c) Minimum amount of CO_2 was released of the Pd catalyst reduced in H_2 at 185 °C. While the same treatment of the virgin oxidized ACC did not change the CO_2-TPD profile considerably (Table 5). This fact implies that the presence of Pd accelerates destruction of the oxygen-containing functional groups by the heat treatments.

d) CO-TPD profiles of the Pd catalysts show that the calcination in air slightly increases the amount of released CO (Table 5 and Fig. 19b). It could be related to the destruction of the stronger acidic group partly to the weaker ones.

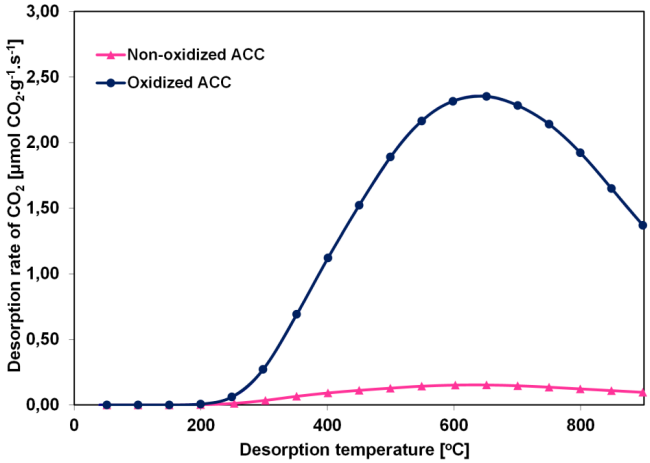

(a)

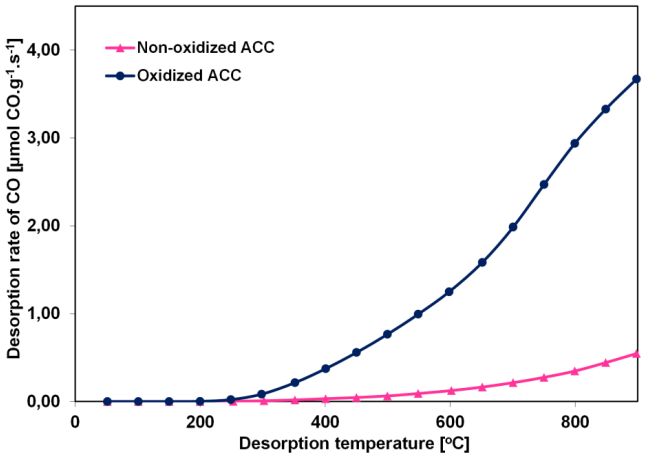

(b)

Figure 18. The CO_2 (a); and CO (b) temperature programmed desorption profiles of the non-oxidized and oxidized of ACC

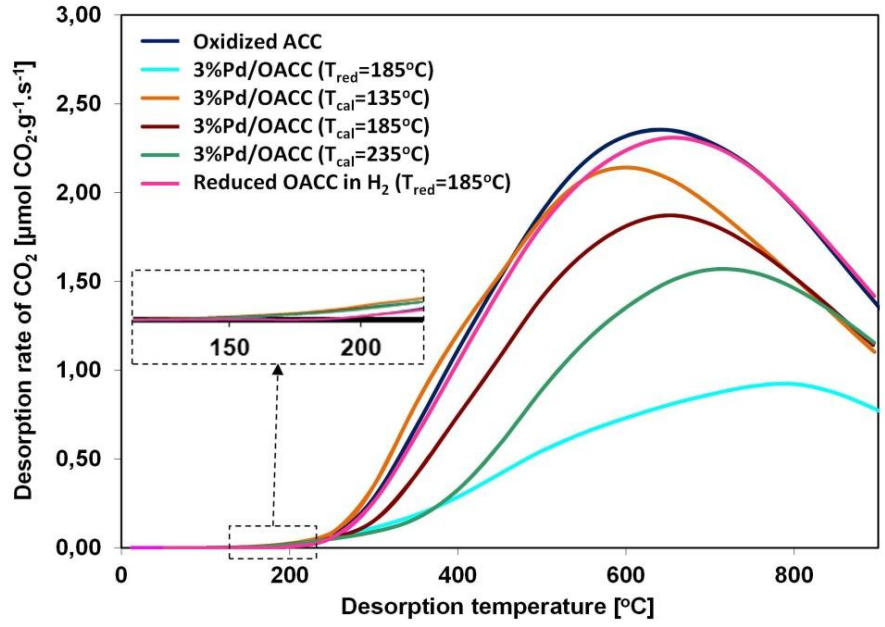

(a)

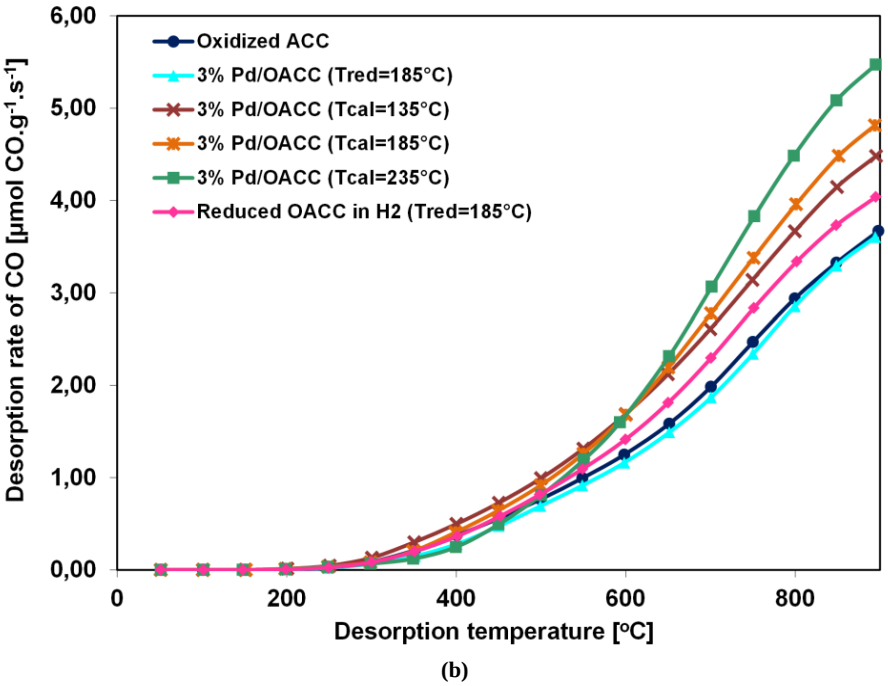

(b)

Figure 19. The CO_2 (a); and CO (b) temperature programmed desorption profiles of the oxidized ACC and the corresponding catalysts with 3 wt% Pd.

Table 5. Total amounts of CO and CO_2 desorbed according to temperature programmed desorption curves

Sample	CO (μmol/g)	CO_2 (μmol/g)
Non-oxidized ACC	130.13	91.73
Oxidized ACC (OACC)	1137.82	1296.30
Reduced OACC with H_2 (T_{red}=185 °C)	1206.19	1224.44
3%Pd/OACC (T_{red}=185 °C)	1050.86	470.43
3%Pd/OACC (T_{cal}=135 °C)	1369.89	1135.57
3%Pd/OACC (T_{cal}=185 °C)	1392.24	943.12
3%Pd/OACC (T_{cal}=235 °C)	1492.78	734.22

3.1.1.1.4. Oxidation state of the Pd particles

The Pd3d XPS spectra of the different 3 wt% Pd catalysts supported on oxidized ACC are presented in Fig. 20. It can be seen (from the segregation of the Pd3d XPS spectra of the catalysts) that:

a) Palladium in the fresh catalyst is almost in zero-valence or in metallic state (Pd^0, the two peaks with binding energy at around 335 and 340.2 eV) and only traces of the palladium are in the form of Pd^{+2} (the two peaks with binding energy at around 338 and 343.4 eV) originated from palladium dichloride $PdCl_2$. The appearance of Pd^0 species in the virgin catalyst can be due to a reducing effect of the activated carbon fibers during the impregnation step, because of the native charge of their surfaces (see Section 3.1.1.1.3)
b) The XPS spectrum of the catalyst reduced with H_2 at 185 °C (Fig. 20b) shows that Pd in the reduced catalyst appears only in the metallic state (Pd^0).
c) Palladium in the catalyst calcined in air at 135 °C is almost in zero-valence (Pd^0, the two peaks with binding energy at around 335 and 340.2 eV). However, a small amount of palladium (about 5.5 wt%) also appears in the form of palladium oxide (PdO, the two peaks with binding energy at around 337 and 342.2 eV).
d) Increasing further the calcination temperature increases the amount of palladium oxide (PdO). The catalyst calcined at 235 ^oC contains the maximum amount of palladium oxide (around 72 wt% of total metal phase).

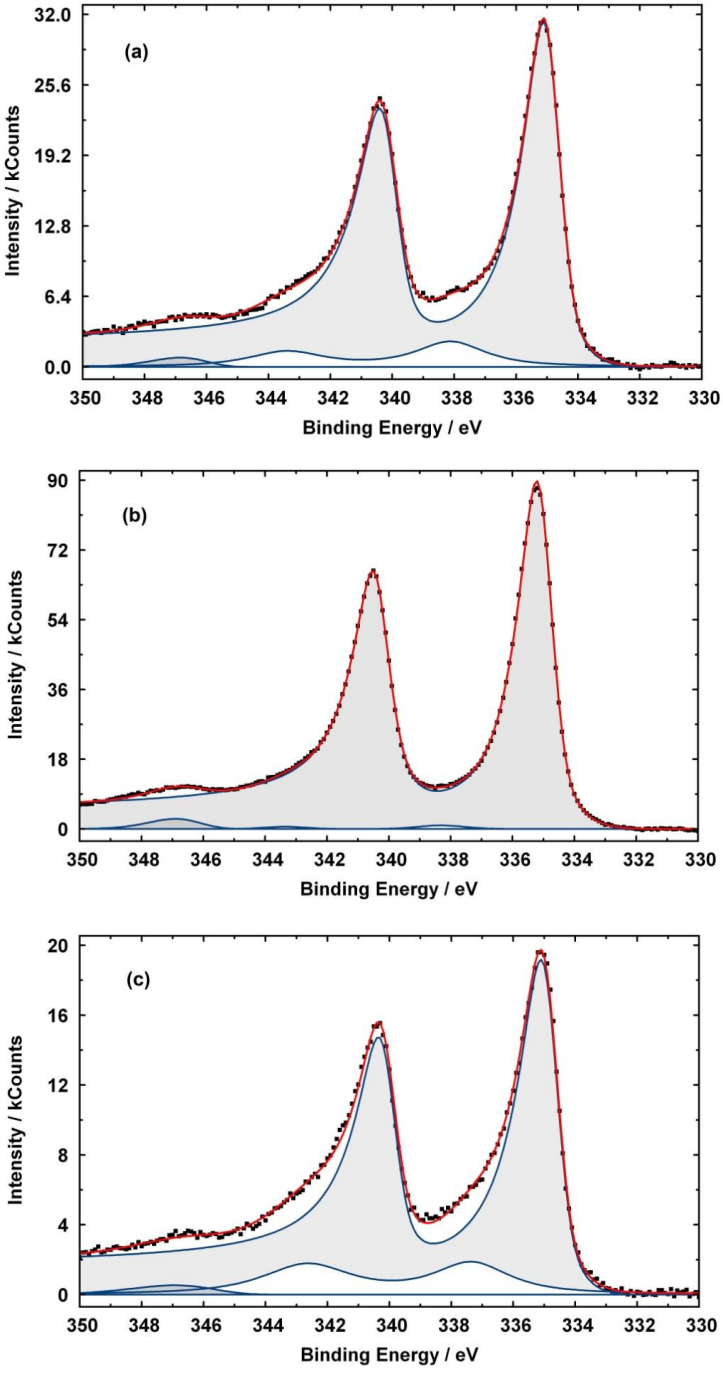
(a)
Intensity / kCounts
32.0
25.6
19.2
12.8
6.4
0.0
350 348 346 344 342 340 338 336 334 332 330
Binding Energy / eV
(b)
Intensity / kCounts
90
72
54
36
18
0
350 348 346 344 342 340 338 336 334 332 330
Binding Energy / eV
(c)
Intensity / kCounts
20
16
12
8
4
0
350 348 346 344 342 340 338 336 334 332 330
Binding Energy / eV

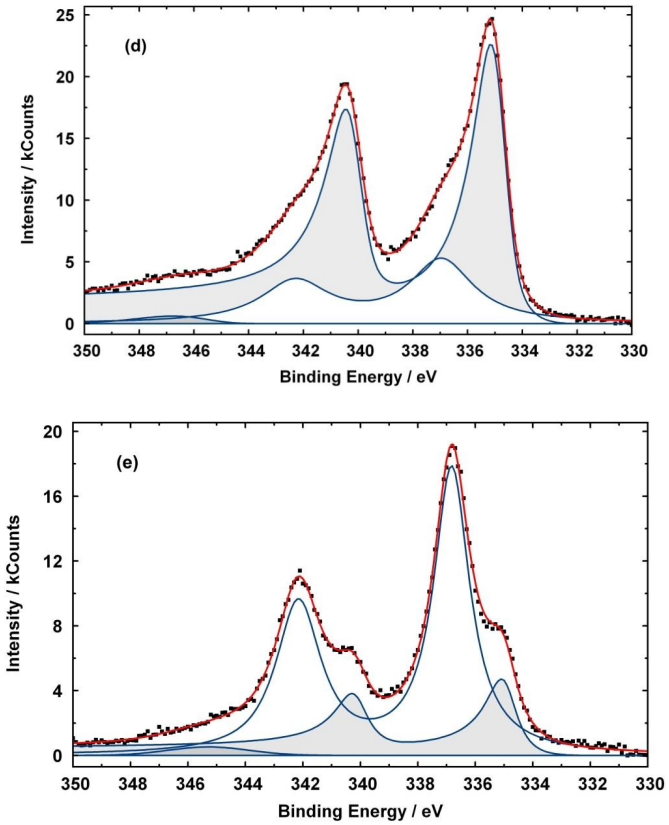

Figure 20. The Pd3d XPS spectra of 3 wt.% Pd/OACC (a) fresh dried one ; (b) reduced one with H_2 at 185 °C and the calcined ones in the air at (c) 135 °C; (d) 185 °C; (e)235°C.

3.1.1.2. Direct synthesis results

The results of the direct synthesis of hydrogen peroxide over 3 wt% Pd catalysts on oxidized and non-oxidized ACC are shown in Fig. 21 and Fig. 22, respectively. It can be observed:

a) The calcined catalysts are more active and selective than the corresponding reduced catalysts.

b) In the case of catalysts on non-oxidized ACC, increasing the calcination temperature improves the selectivity. These results (a, b) imply that the presence of oxidized state of Pd (PdO) in the catalyst makes the catalyst more active and selective than the corresponding Pd^0 catalyst.

c) In the case of catalysts on oxidized ACC, increasing the calcination temperature up to 185 °C improves both the activity and selectivity. Increasing further the calcination temperature to 235 °C leads to slightly more active but less selective catalyst.

d) Pd catalysts on oxidized ACC are significantly more selective than the corresponding Pd catalysts on non-oxidized ACC. This observation implies that the presence of the oxygen-containing surface functional groups make the Pd catalyst more selective.

Heat treatment of oxidized ACC in the presence of Pd at temperatures higher than 190 °C can seriously damage the oxygen-containing functional groups (see Section 3.1.1.1.3). Because of this, calcination at 235 °C resulted in slightly degrease in selectivity. This was the case even though the amount of palladium oxide (PdO) was higher in the catalyst calcined at 235 °C.

Heat treatment of oxidized ACC in H_2 causes the substantial damage to the oxygen-containing functional groups (see Section 3.1.1.1.3). Moreover, there is no palladium oxide in the reduced Pd catalysts. Lack of PdO and damaged oxygen-containing functional groups (in the case of the catalyst on oxidized ACC) result in poor performance of the reduced catalysts.

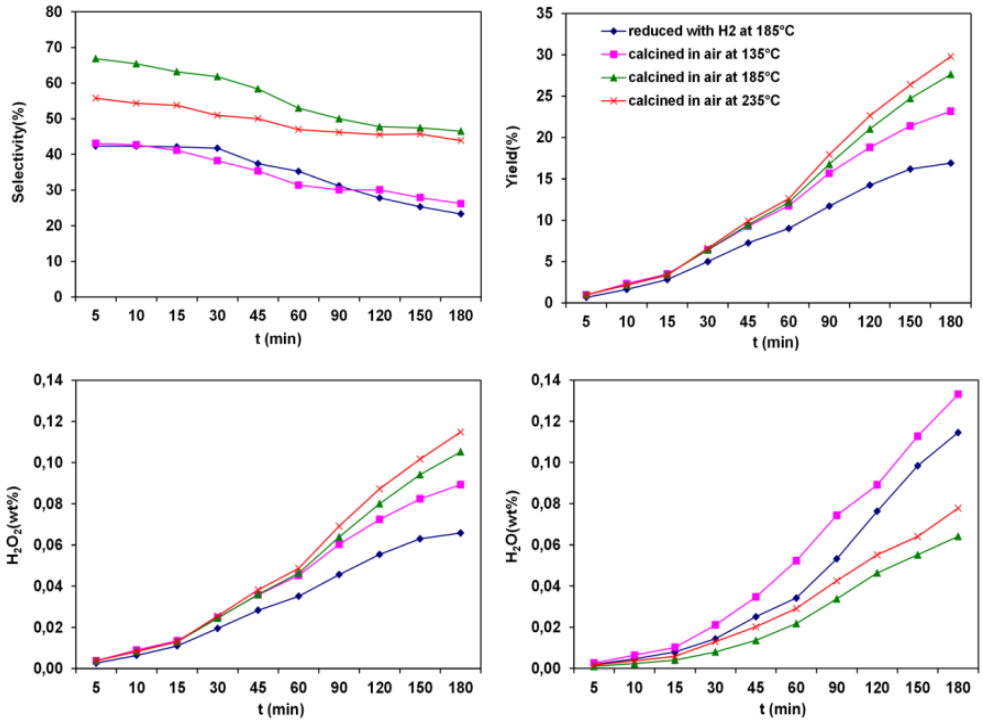

Figure 21. The activity the 3% Pd catalysts on oxidized ACC in Direct synthesis of H_2O_2 (mass of catalyst = 55 mg, temperature = 0 **°C).**

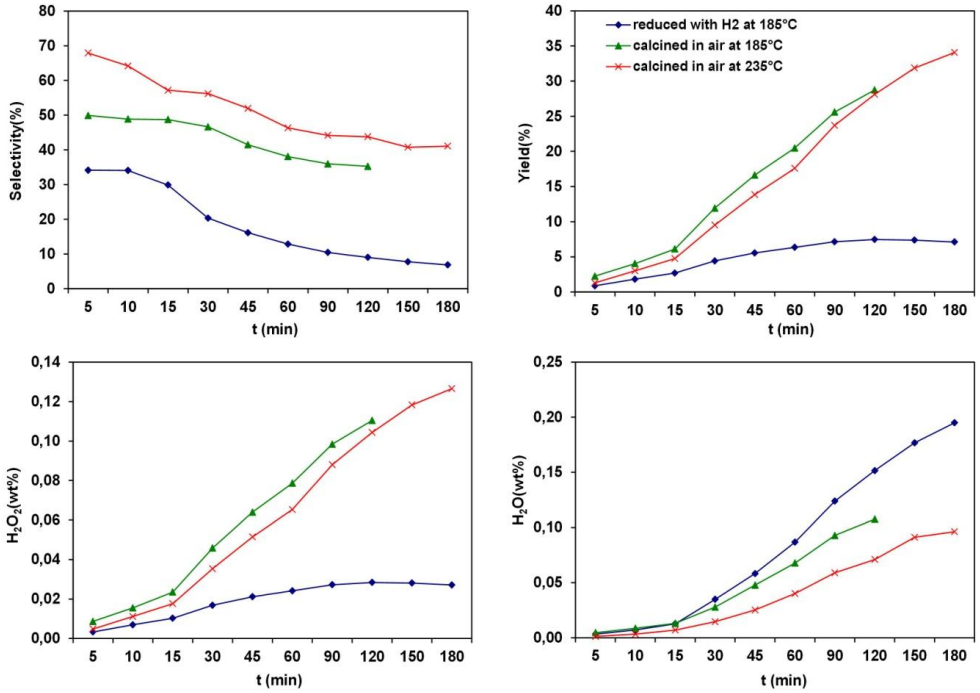

Figure 22. The activity of the 3 wt% Pd on non-oxidized ACC in direct synthesis of H_2O_2 (mass of catalyst = 55 mg, temperature = 0 °C).

3.1.1.3. Destruction of H_2O_2 by hydrogenation

3.1.1.3.1. The effects of pretreatment of ACC with different acids

Hydrogenation of H_2O_2 over 3 wt% Pd catalysts supported on non-oxidized ACC, ACC oxidized with nitric acid, and ACC oxidized with acetic acid versus time are presented in Fig. 23. This figure shows that the hydrogenation activity of the catalyst supported on ACC oxidized with nitric acid is substantially less than of the other ones. The catalysts supported on non-oxidized ACC and ACC oxidized with acetic acid show almost the same hydrogenation activity.

Based on the CO_2- and CO-TPD desorption profiles, pretreatment of ACC with acetic acid does not change the surface chemistry of the ACC fibers. The same surface chemistry resulted in almost the same surface morphology in the Pd catalysts supported on non-oxidized ACC and the ACC oxidized with acetic acid. Therefore, these two catalysts show almost the same activity in the hydrogenation of H_2O_2.

Different surface chemistry of the ACC oxidized with nitric acid (see Section 3.1.1.1.1)

and consequently different surface morphology of the its corresponding pd catalysts (see Section 3.1.1.1.3) compare to the catalysts supported on non-oxidized ACC and the ACC oxidized with acetic acid resulted in the different hydrogenation activities (Fig. 23).

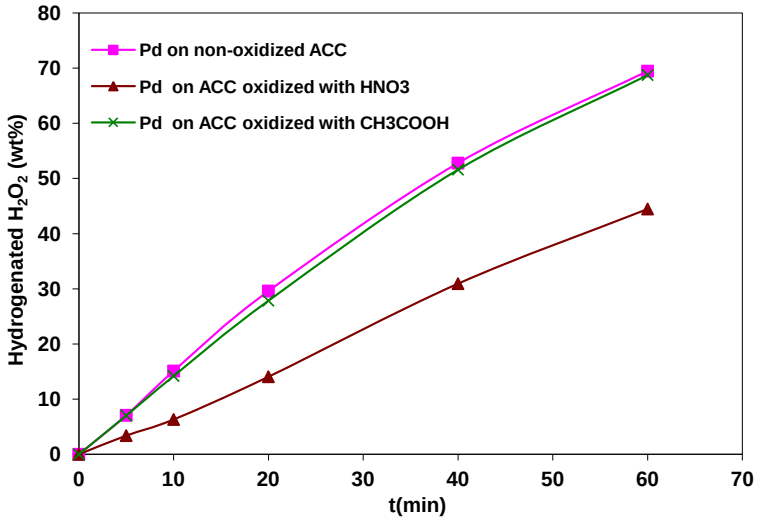

Figure 23. Hydrogenation of H_2O_2 over catalysts with 3 wt% Pd supported on different ACCs and calcined in air at 185 °C; $T_{reaction}$= 21°C, $m_{catalyst}$= 60mg, P_{H2}=4 bar.

3.1.1.3.2.The effects of the heat treatment in H_2 and air

Destruction of H_2O_2 by hydrogenation over the catalysts with 3 wt% Pd supported on non-oxidized ACC and ACC oxidized with nitric acid are shown in Fig. 24. It can be observed that:

a) For catalysts supported on non-oxidized ACC, the hydrogenation activity of all different catalysts is almost the same. Especially the reduced catalyst is almost as active as the calcined ones (Fig. 24a).

b) In the case of the catalysts supported on oxidized ACC, the calcined catalysts almost show the same H_2O_2 destructive activities. However, the catalyst which was calcined at 185 °C still demonstrates a lower activity. The catalyst reduced by H_2 at 185 °C is substantially more active than the other calcined catalysts.

c) The calcined catalysts supported on oxidized ACC are less H_2O_2 destructive than the corresponding ones on non-oxidized ACC.

It was demonstrated (see Section 3.1.1.1.4) that the calcination of Pd catalysts in air at 135-235 ºC was partly oxidized palladium to palladium oxide (PdO). With increasing the

calcination temperature the amount of palladium oxide (PdO) was also increased. However, the Pd3d XPS spectra of the Pd catalysts which were used in the hydrogenation reaction revealed that the oxidation state of palladium was dramatically influenced by H_2 during H_2O_2 hydrogenation reaction (Table 6). The XPS results (see also the corresponding XPS profiles in publication II) reveal that:

a) In the case of calcined catalyst at 235 °C, after 5 min of hydrogenation reaction, the amount of palladium oxide (PdO) in the catalyst was dropped to 19% (wt %) from about 70%. With continuing the reaction up to half an hour, the amount of the PdO was futher decreased to 5%. Almost all PdO were reduced to zero-valance (Pd^0) after the reaction time of nearly 1 h (Table 6).
b) In the case of the calcined catalyst at 185 °C, the amount of oxidized palladium was only about 11% of the total amount of Pd. Almost all of the palladium oxide (PdO) was reduced to zero valences (Pd^0) after 5 min of the H_2O_2 hydrogenation reaction (Table 6).
c) Therefore, palladium was in the reduced state (Pd^0) in the all catalysts were being used in hydrogenation reaction.

Based on the discussion above, it can be concluded that the oxidation state of palladium could not have an important role in causing the observed difference in Fig. 24b.

Moreover, the ultra-high resolution field emission scanning electron microscope (UHRFESEM) images confirmed that the heat treatment in H_2 at 185 °C and in air up to 235 °C had no noticeable effects on the surface morphology of the Pd particles in the catalysts.

However, it was shown (see Section 3.1.1.1.3) that the heat treatment of the oxidized ACC in air or H_2, especially in the presence of palladium, leads to damage of the oxygen-containing surface functional groups. Actually it was demonstrated:

a) Heat treatment of oxidized ACC in H_2 at 185 ºC causes the substantial damage to these surface functional groups.
b) Calcination of the Pd catalyst at temperature above 190 ºC could also damage these surface functional groups.

Based on the discussion above and the hydrogenation activity of the catalysts shown in Fig. 24b, it can be concluded that the oxygen-containing surface functional groups has an important role in the final hydrogenation activity. Indeed, damage in these functional groups increases the hydrogenation activity. Because of this fact, the reduced catalyst showed the

highest hydrogenation activity in Fig. 24b.

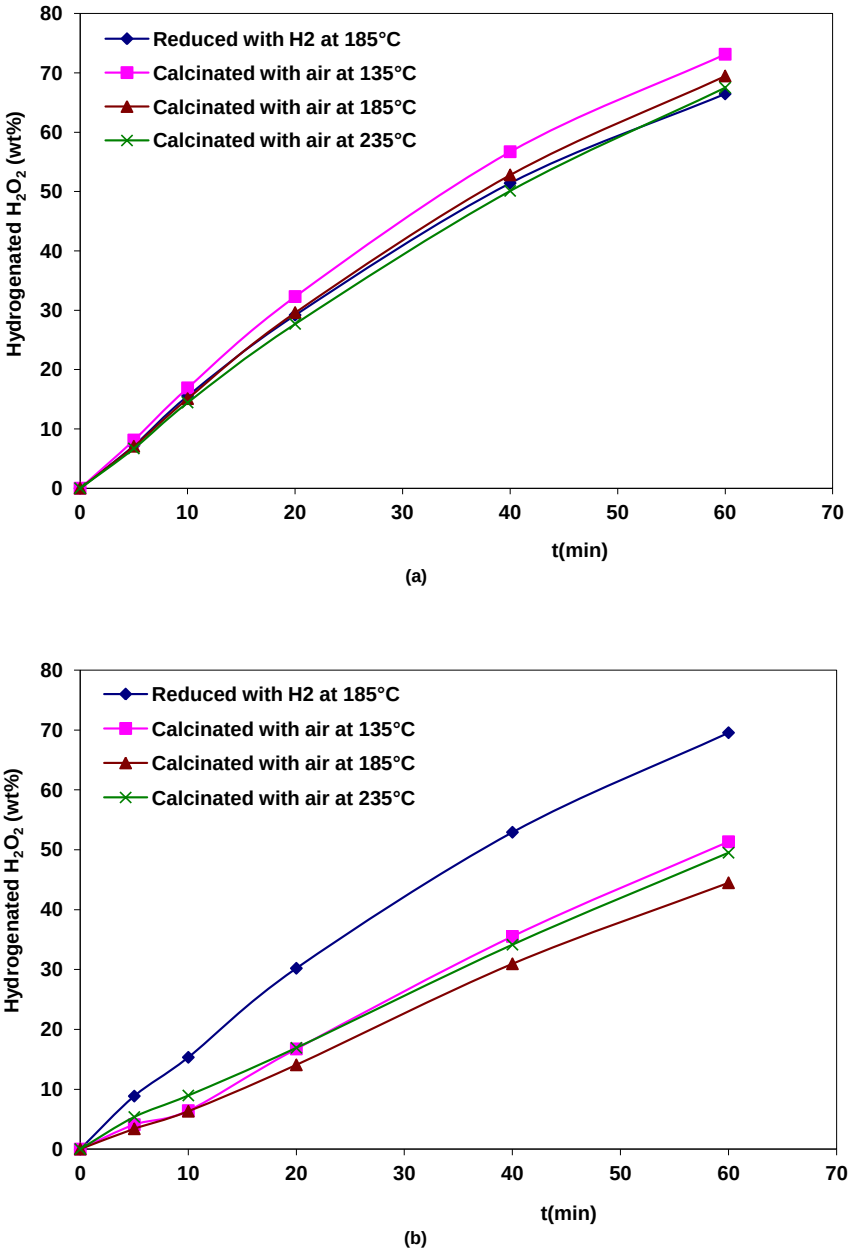

Figure 24. Hydrogenation of H_2O_2 over the catalysts with 3 wt% Pd supported on (a) non-oxidized ACC and (b) ACC oxidized with nitric acid; $T_{reaction}$= 21°C, $m_{catalyst}$= 60mg, P_{H2}=4 bar.

Table 6. Total amount (wt %) of palladium in the form of palladium oxide (PdO) in the samples were introduced in Fig. 24b, according to the results of x-ray photoelectron spectroscopy.

Sample	PdO (wt %)
3%Pd/OACC$_N$ ($T_{calcination}$=235 °C)	69.12
3%Pd/OACC$_N$ ($T_{calcination}$=235 °C); after hydrogenation reaction ($t_{reaction}$=5 min)	19
3%Pd/OACC$_N$ ($T_{calcination}$=235 °C); after hydrogenation reaction ($t_{reaction}$=15 min)	9
3%Pd/OACC$_N$ ($T_{calcination}$=235 °C); after hydrogenation reaction ($t_{reaction}$=30 min)	5
3%Pd/OACC$_N$ ($T_{calcination}$=235 °C); after hydrogenation reaction ($t_{reaction}$=60 min)	2
3%Pd/OACC$_N$ ($T_{calcination}$=185 °C)	10.21
3%Pd/OACC$_N$ ($T_{calcination}$=185 °C); after hydrogenation reaction ($t_{reaction}$=5 min)	1
3%Pd/OACC$_N$ ($T_{calcination}$=185 °C); after decomposition reaction ($t_{reaction}$=60 min)	10

3.1.1.3.3.The effects of the Pd content

The effects of Pd content on the hydrogenation activity of the catalysts on non- oxidized and oxidized ACC (with nitric acid) are shown in Fig. 25 and Table 7. It can be seen that:

a) In both cases, with increasing the wt% of Pd from 1 to 5%, the activity of the catalysts was increased. This could be expected, because increasing the amount of Pd in the catalyst will increase the number of the active sites.
b) In the case of non-oxidized ACC, increasing wt% of Pd from 1 to 3% resulted in a big jump in the H_2O_2 destruction activity. However, increasing further the amount of Pd did not considerably affect. Therefore, increasing wt% of Pd from 3 to 5% slightly increased the activity.
c) In the case of the catalysts supported on oxidized ACC, the effect of the Pd content is not completely the same as non-oxidized one. In fact, increasing Pd content from 1 to 5% enhanced the catalytic activity almost with a constant rate.

In the case of 3 wt% Pd catalyst supported on non-oxidized ACC, the whole outer surfaces of the ACC fibers were almost covered with the Pd particles (Fig. 11c in section 3.1.1.1.1). Therefore, additional increase of Pd content did not change considerably the number of the Pd active sites and consequently the activity of the catalyst.

The ultra-high resolution field emission scanning electron microscope (UHRFESEM) images of the catalysts with 1, 3, and 5 wt% Pd supported on ACC oxidized with nitric acid are shown in Fig. 26. These images reveal that with increasing Pd content from 1 to 3 and finally to 5 wt %, the number of small ($\leq$ 10 nm) and bigger ($\geq$20 nm) Pd particles were

grown on the outer surface of ACC fibers. Therefore, the number of the active sites and consequently the activity of the catalysts were also enhanced. In fact, bigger particles were formed at high Pd contents (≥ 3 wt %).

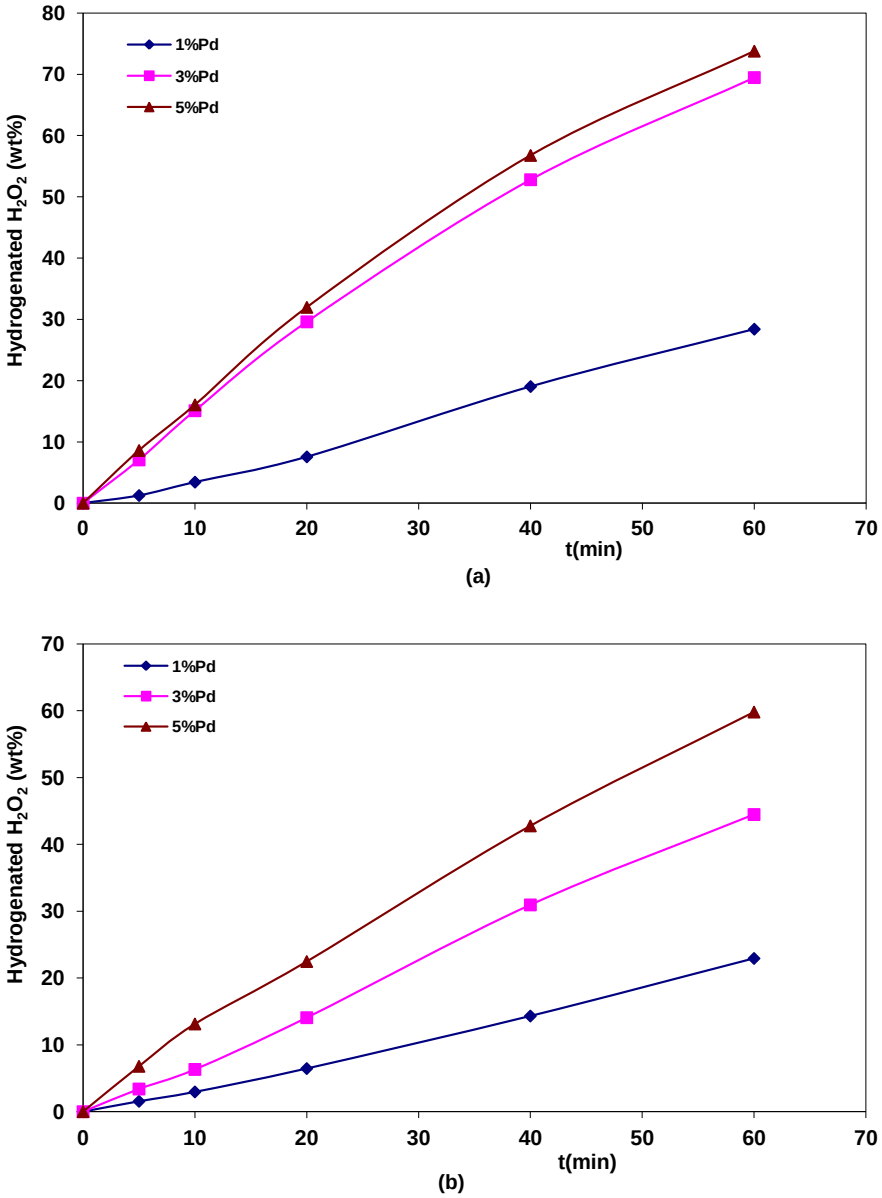

Figure 25. Hydrogenation of H_2O_2 over the catalysts with 1, 3, and 5 wt% Pd supported on (a) non-oxidized ACC and (b) oxidized ACC with nitric acid

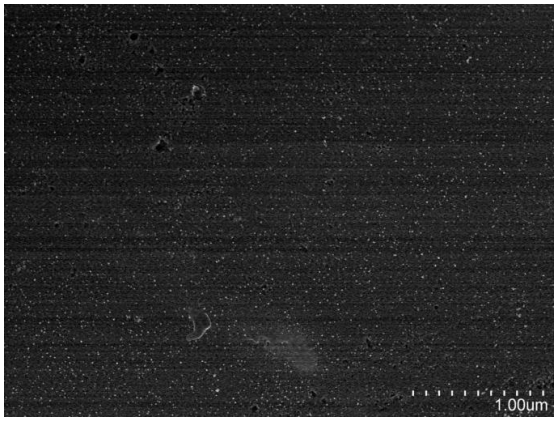

(a)

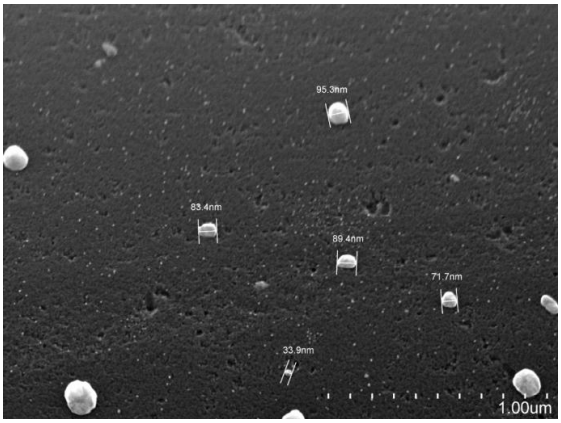

(b)

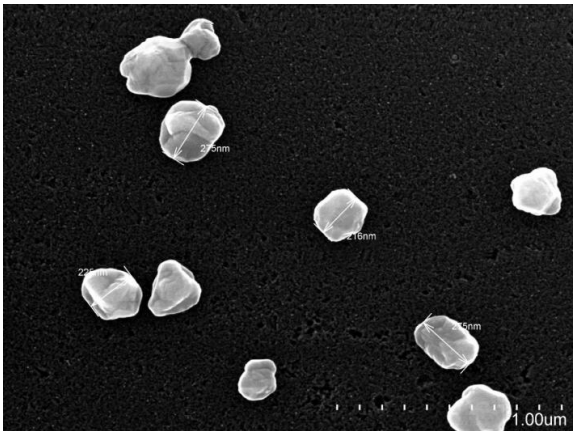

(c)

Figure 26. High resolution SEM images of the catalysts with (a) 1 wt%, (b) 3 wt% and, (c) 5 wt% Pd supported on ACC oxidized with nitric acid

Table 7. Average destruction rate (wt %/min), the destruction rate at the first 5 minute of the reaction time (wt %/min), and maximum destruction of H_2O_2 (wt%) via hydrogenation over the different Pd catalysts supported on non-oxidized ACC (NACC) and ACC oxidized with nitric acid (OACC).

catalyst	Initial decomposition rate (wt %/min)	Average decomposition rate (wt %/min)	Maximum decomposition (wt %)
1 wt % Pd/OACC	0.31	0.38	22.93
3 wt % Pd/OACC	0.50	0.73	43.96
5 wt % Pd/OACC	1.36	1.00	59.81
1 wt % Pd/NACC	0.25	0.47	28.40
3 wt % Pd/NACC	1.41	1.16	69.47
5 wt % Pd/NACC	1.72	1.23	73.78

3.1.1.4. Destruction of H_2O_2 by decomposition

The results of the destruction of H_2O_2 by its decomposition over the catalysts with 3 wt% Pd supported on ACC oxidized with nitric acid are presented in Fig. 27. It can be observed that:

a) The decomposition activity of the catalyst calcined at 185 °C was almost zero.
b) The catalyst reduced by H_2 at 185 °C had maximum H_2O_2 decomposition activity.
c) The calcined catalyst at 235 °C is less active than the corresponding one which was calcined at 135 °C.
d) The destruction of H_2O_2 by decomposition is really low and negligible as compared to the H_2O_2 destruction by hydrogenation (Fig. 24b).

It seems that the decomposition activity is influenced by the same factors as the H_2O_2 hydrogenation reaction (see Section 3.1.1.3). The main difference in decomposition test is the lack of H_2 in the reaction medium and atmosphere. Therefore, oxidation state of Pd can also affect the final activity of the catalysts. In fact, unlike the hydrogenation tests, the XPS results indicate that the oxidation state of palladium in the catalyst did not change during the decomposition test (Table 6). Therefore, surface chemistry of the supports along with the oxidation state of palladium are the two main factors leading to the observed different decomposition activities. In the case of the calcined catalysts, the one calcined at 235 °C has maximum amount of oxidized palladium, around 70 wt% of the total Pd (Table 6). However, calcination of catalyst at 235 ^{o}C damaged the oxygen-containing surface functional groups more than the same procedure at lower temperatures. Smaller decomposition activity of the

calcined catalyst at 235 °C than at 135 °C implies that the existence of oxidized state of Pd (PdO) makes the catalyst less active in H_2O_2 decomposition than the corresponding zero valances Pd (Pd^0).

Highly damage in oxygen-containing surface functional groups (see Section 3.1.1.1.3) and lack of palladium oxide (PdO) in the catalyst reduced by H_2, maximized its decomposition activity.

Based on the discussion above, it can be concluded that a combination of these two factors (the amount of oxygen-containing functional groups and the presence of palladium oxide in the catalyst) determined the final differences in the decomposition activity of the catalysts with 3 wt% Pd.

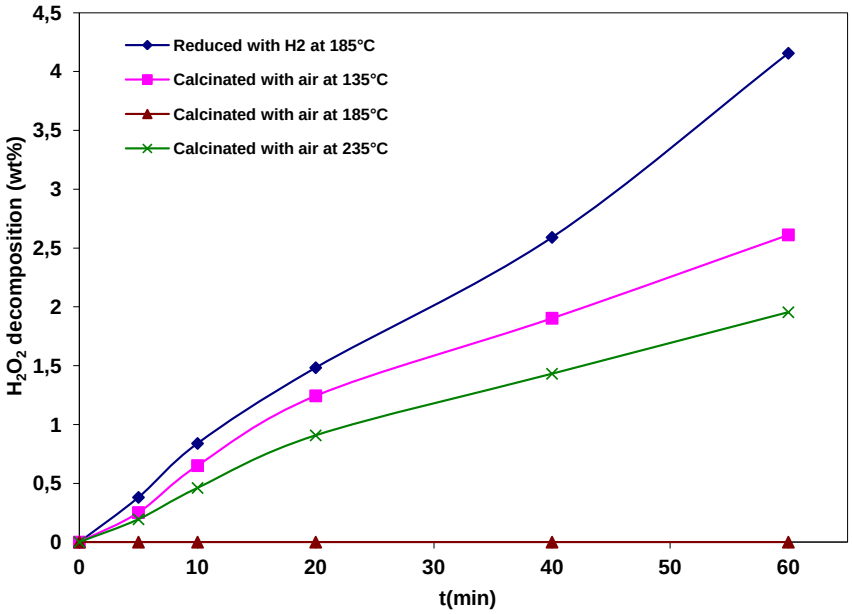

Figure 27. Destruction of H_2O_2 by its decomposition over the catalysts with 3 wt% Pd supported on ACC oxidized with nitric acid.

3.1.2. Pd-Au bimetallic catalysts supported on activated carbon cloth

3.1.2.1. Direct synthesis results

3.1.2.1.1. The effects of Au/Pd ratio and metal content

3.1.2.1.1.1. Increasing the amount of gold with a constant amount of palladium

The Results of the direct synthesis of H_2O_2 over the Pd-Au bimetallic catalysts with 1 wt % Pd and 1-5 wt % Au supported on the ACC oxidized with nitric acid are presented in Fig. 28. For comparison, the results with 1 wt % Pd monometallic catalyst are also shown. It can be observed that:

a) All Pd-Au bimetallic catalysts are more selective than the Pd monometallic catalyst. Especially in the first 60 min of the reaction time, almost all of the Pd-Au bimetallic catalysts are considerably more selective than the Pd monometallic catalyst (Fig. 28).
b) In the case of Pd-Au bimetallic catalysts, with increasing the amount of gold, the selectivity drops, especially during the first 60 min. However, at reaction times above 1.5 h, the differences between the selectivity of the different Pd-Au catalysts became smaller (see the exact values in Table 8).
c) In the case of Pd-Au bimetallic catalysts, the activity (yield, productivity and H_2 conversion rates) was increased when increasing the amount of gold (Fig. 28, Table 8).
d) The Pd-Au catalysts with less than 3 wt% Au are less active in water production than the 1 wt % Pd catalyst. Especially the catalysts with 1 and 2 wt % gold produced substantially lower amount of water (more than 50% less) when compared to the Pd monometallic catalyst (see the exact values in Table 8). However, increasing the Au content from 3 wt % to 4 wt % seems to cause a sudden increase in water production (see the exact values in Table 8).
e) Indeed the catalyst with 1 wt% Pd and 4 wt% Au was substantially more active than the other catalysts in both H_2O_2 and water production.
f) Fig. 28 demonstrates that the selectivity of the catalysts (at least in the case of Pd-Au bimetallic catalysts) could be changed with the reaction time. This is because of the direct synthesis of H_2O_2 has a complex mechanism and could be influenced by different parameters. Therefore, in comparison of the performance of different catalysts, it is needed to consider the results versus time.

In general and according to the results presented in Table 8, the Pd-Au catalysts are more

selective but less active (have lower yield and productivity) than the Pd monometallic catalyst even with lower total metal content. The only exception is the catalyst with 4 wt % Au. This catalyst is substantially more active in H_2O_2 and water production than the other bimetallic and monometallic Pd catalysts. Its selectivity is almost constant and does not change with the reaction time. However, the selectivity of the other Pd-Au catalysts is strongly dependent on reaction time, especially up to 1 h.

3.1.2.1.1.2. Increasing the amount of palladium with a constant amount of gold

In order to study the effect of increasing the amount of palladium, a series of Pd-Au catalysts with constant amount of gold (1 wt %) and maximum 4 wt % palladium were prepared. The results of the catalytic performance are presented in Fig. 29. It can be observed that:

a) When increasing the amount of palladium from 1 wt % to 2, 3, and 4 wt %, the selectivity of the Pd-Au bimetallic catalysts were decreased a lot, especially in the first hour of the reaction time. It was dropped more than 37% during the first 15 min. At the reaction times above 1.5 h, the differences between the selectivity of the different Pd-Au catalysts became smaller (less than 15% in the worst cases; see Table 8).
b) The Pd-Au bimetallic catalysts with 1 wt% gold and more than 1 wt % Pd almost demonstrated constant selectivity versus time (Fig. 29), otherwise than the corresponding catalysts presented in Fig. 28.
c) When increasing the amount of palladium, the rate of H_2O_2 production, yield, and H_2 conversion were increased almost with similar trends (Fig. 29, Table 8). When increasing palladium from 1 to 2 wt % and from 2 to 3 wt %, the rate of H_2O_2 production, yield, productivity, and H_2 conversion were increased a lot (see exact values in Table 8). However, when increasing palladium from 3 to 4 wt %, these quantities did not change considerably. Indeed, the catalyst with 3 and 4 wt %Pd produced almost the same yields (see exact values in Table 8).
d) When increasing the amount of palladium, the production rate of H_2O was also increased. However, when increasing palladium from 2 to 3 wt %, the rate did not change so much.
e) Based on the results presented in Figs. 28-29 and Table 8, it can be said that the bimetallic catalysts with 1 wt% Au and equal or more than 2 wt% Pd are more active (have higher yield and productivity) than the corresponding bimetallic catalysts with 1 wt% Pd and equal or more than 2 wt% Au, and Pd monometallic catalysts with the same

metal content (Pd+Au).

In general, it can be concluded that increasing the amount of palladium in the Pd-Au bimetallic catalysts resulted in better activity but worse selectivity. Moreover, it should be mentioned that gold monometallic catalysts did not show any noticeable activity in direct synthesis of H_2O_2.

3.1.2.1.1.3. Changing the Au/Pd ratio with a constant total metal content

The effects of the Au/Pd ratio on the final performance of the Pd-Au bimetallic catalysts with constant total metal content (Pd + Au = 5 wt %) are presented in Fig. 30. It can be observed that:

a) All the Pd-Au catalysts with $\frac{Au}{Pd} \geq 1$ are more selective when compared to the monometallic catalyst with 5 wt % Pd, and the bimetallic catalysts with $\frac{Au}{Pd} < 1$.
b) All the Pd-Au bimetallic catalysts are more selective than the monometallic catalyst with 5 wt % Pd when the reaction time is above 1.5 h.
c) The bimetallic catalysts with $\frac{Au}{Pd} < 1$ are less selective when compared to the monometallic catalyst with 5 wt % Pd when the reaction time is less than 1.5 h.
d) The most selective one is the catalyst with 2 wt% of Pd and 3 wt% of Au. However, it is also the least active catalyst. The rate of water production and H_2 conversion with this catalyst is considerably low when compared to the others (see exact values in Table 8).
e) The catalyst with 4 wt% of Pd and 1 wt% of Au is substantially more active than the others (see exact values in Table 8). The rate of H_2O_2 and water production and consequently yield and H_2 conversion rate with this catalyst are considerably higher than with the others. However, it is the least selective one, especially when the reaction time is below 1.5 h.
f) The second active catalyst is the one with 1 wt% of Pd and 4 wt% of Au. It is also one of the most selective ones. However, its activity is considerably less than the most active catalyst (4 wt% Pd_1 wt% Au).
g) The third active catalyst is the one with 2.5 wt% of Pd and 2.5 wt% of Au. It is also one the most selective ones. Indeed, its selectivity was a little smaller than with the most selective catalyst (2 wt% Pd_3 wt% Au).
h) The rate of water production and H_2 conversion of all of the catalysts are almost the

same, except with catalysts 4 wt% Pd_1 wt% Au and 2 wt% Pd_3 wt% Au.

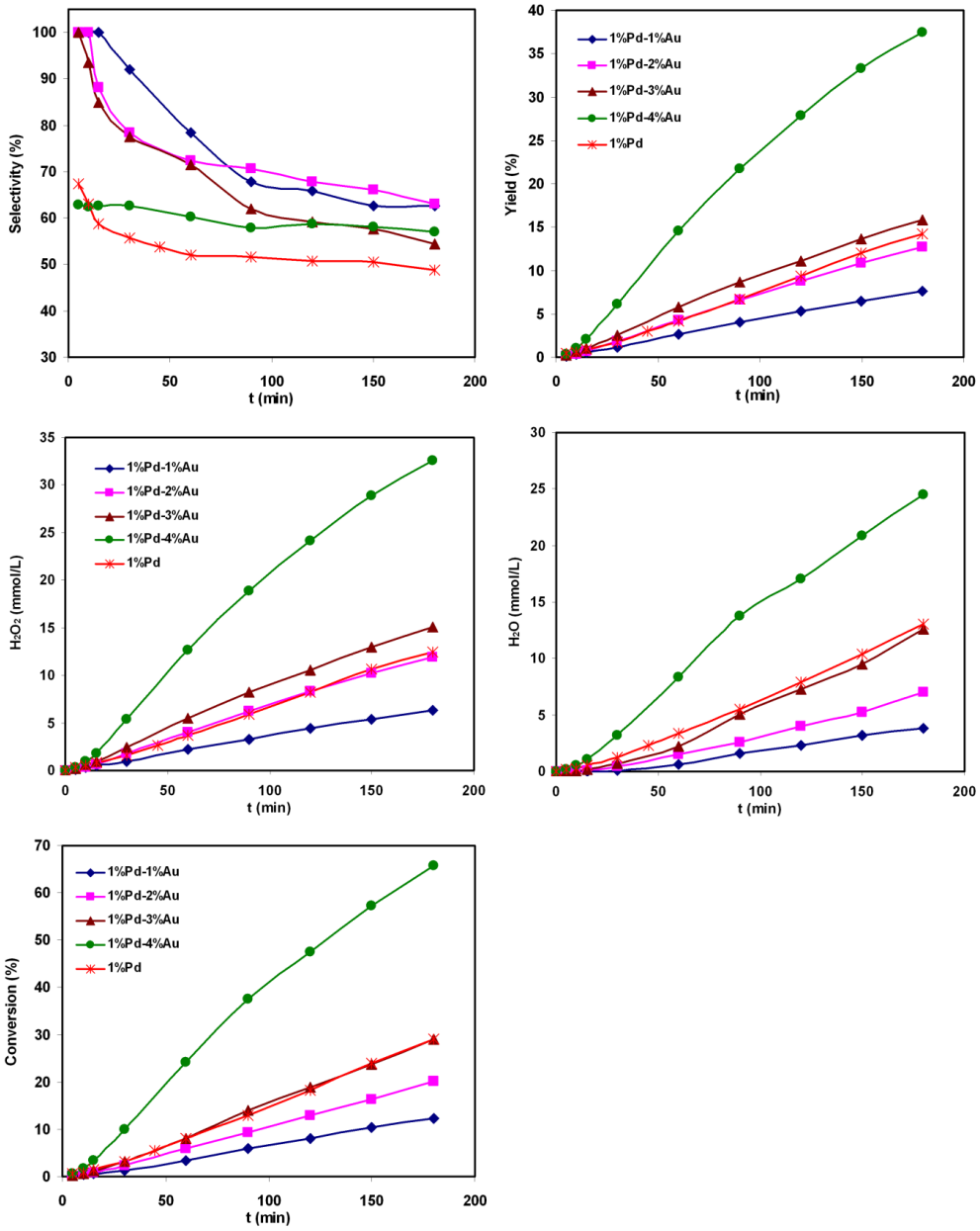

Figure 28. The effect of increasing the amount of gold on the catalytic activity of Pd-Au bimetallic catalysts supported on ACC oxidized with nitric acid; mass of catalyst = 56 mg, $T_{reaction}$= 0 °C , and all catalysts were calcined in air at 185 °C.

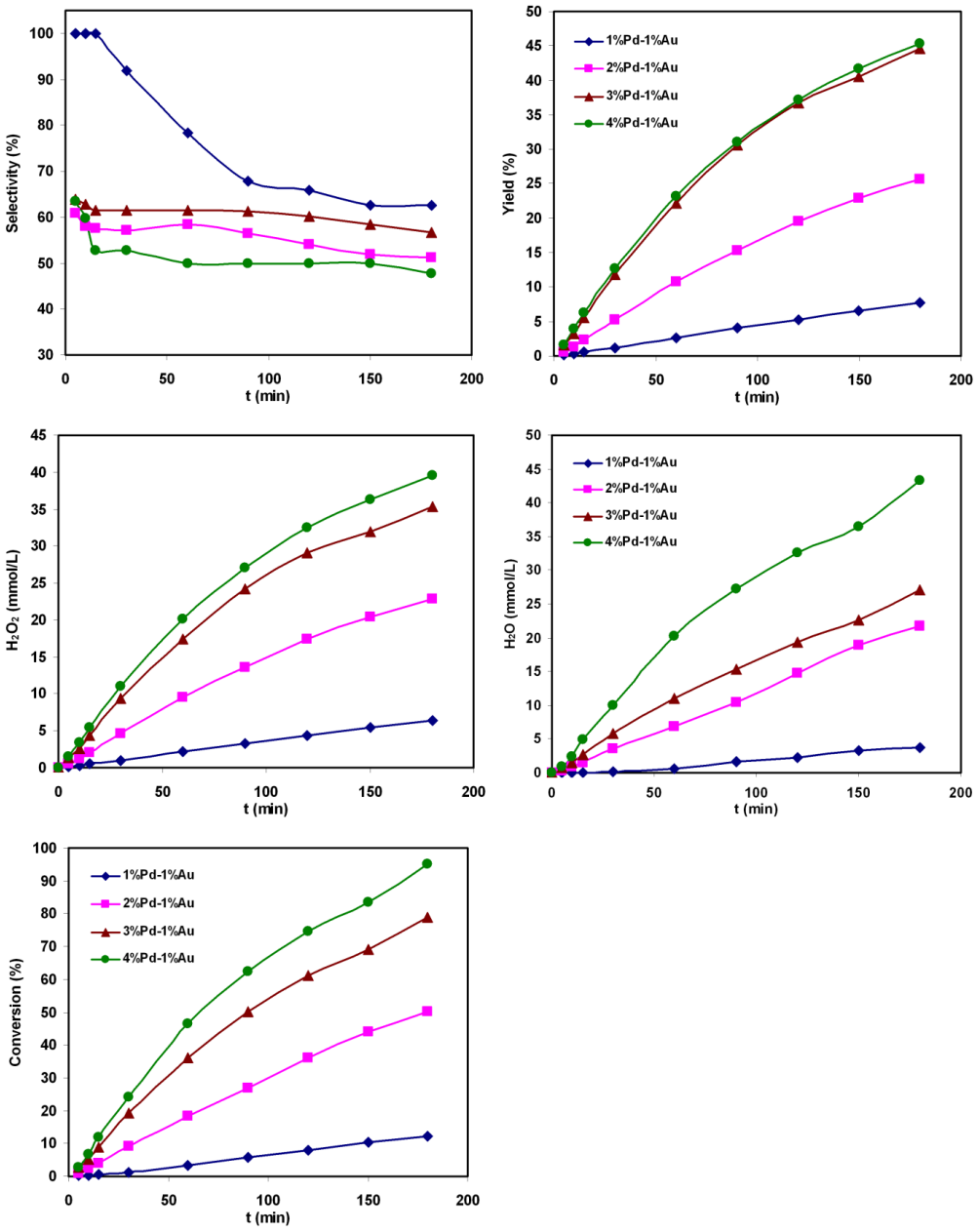

Figure 29. The effect of increasing the amount of palladium on the catalytic activity of Pd-Au bimetallic catalysts supported on ACC oxidized with nitric acid; mass of catalyst = 56 mg, $T_{reaction}$= 0 °C , and all catalysts were calcined in air at 185 °C.

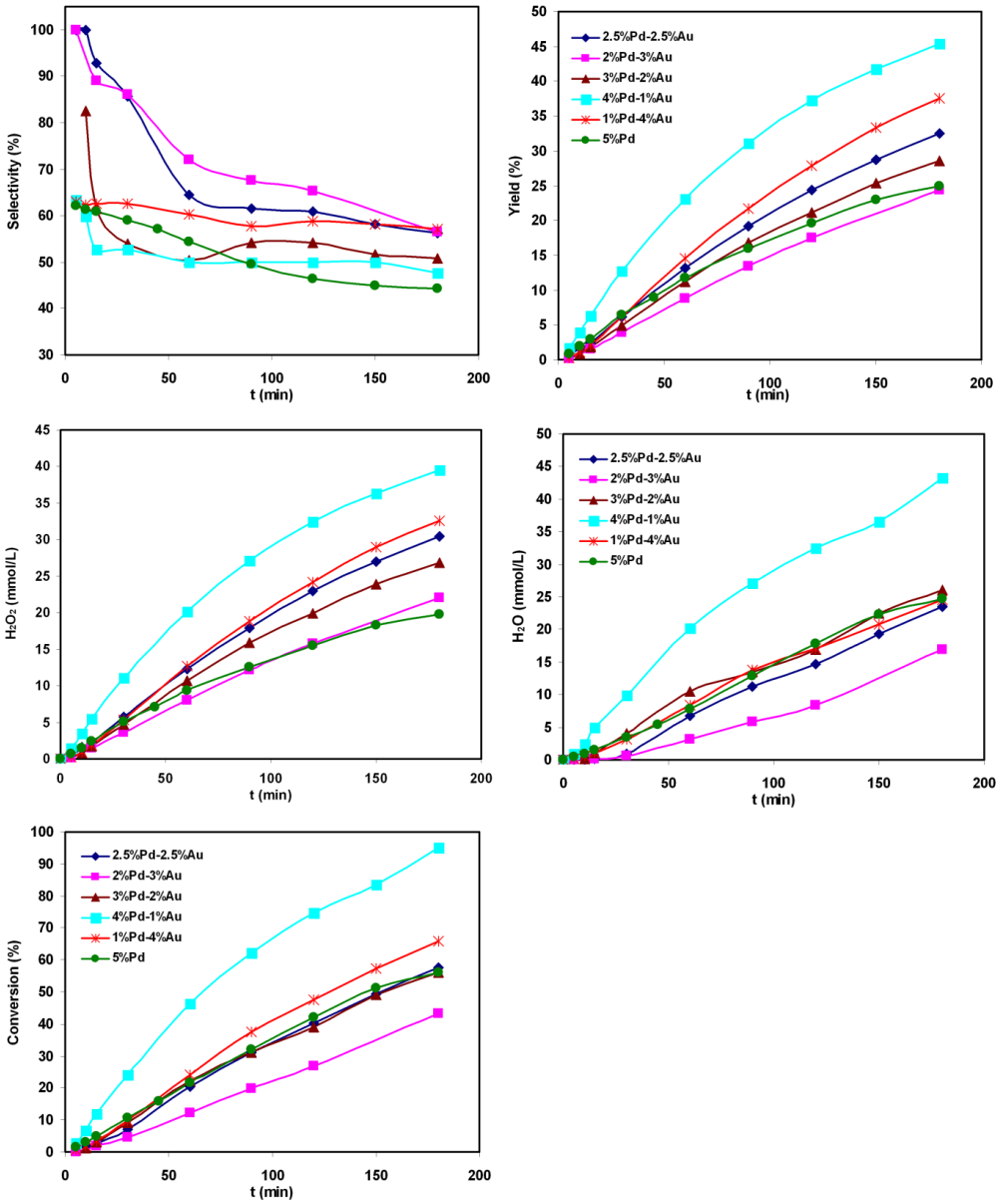

Figure 30. The effect of the Pd/Au ratio on the catalytic activity of Pd-Au bimetallic catalysts supported on ACC oxidized with nitric acid with constant amount of metal content (Pd+Au=5 wt%); mass of catalyst = 56 mg, $T_{reaction}$= 0 °C and all catalysts were calcined in air at 185 °C.

Table 8. The catalytic activity of the Pd mono metallic, and Pd-Au bimetallic catalysts supported on ACC oxidized with nitric acid after 3h of the reaction time (in H_2O_2 direct synthesis). All catalysts were calcined in air at 185 °C.

Catalyst	H_2O_2 (mmol/L)	H_2O (mmol/L)	Selectivity (%)	Yield (%)	Productivity ($\frac{mol_{H_2O_2}}{h_{reaction}.kg_{cat}}$)	H_2 Conversion (%)
1% Pd	12.47	13.04	48.88	14.20	1467	29.05
3% Pd	24.45	28.13	46.49	27.63	985	59.42
5% Pd	19.72	24.75	44.34	24.87	520	56.09
1% Pd_1% Au	6.33	3.77	62.63	7.67	408	12.24
1% Pd_2% Au	11.96	7.02	63.00	12.66	514	20.10
1% Pd_3% Au	15.03	12.60	54.40	15.81	522	29.05
1% Pd_4% Au	32.56	24.49	57.08	37.51	846	65.71
2% Pd_1% Au	22.85	21.77	51.22	25.68	984	50.15
3% Pd_1% Au	35.28	27.08	56.58	44.62	1141	78.88
4% Pd_1% Au	39.51	43.32	47.70	45.34	1025	95.07
3% Pd_2% Au	26.88	26.03	50.81	28.52	693	56.13
2% Pd_3% Au	21.98	16.99	56.41	24.36	570	43.18
2.5% Pd_2.5% Au	30.41	23.57	56.34	32.45	791	57.59

Table 9. The effect of impregnation of oxidized ACC (with nitric acid) with different amount of gold and palladium, on the specific surface area of the final bimetallic catalysts.

Sample	S_{N_2} (m^2g^{-1})
Oxidized ACC (OACC)	1550
(1% Pd_1% Au)/ OACC	1521
(1% Pd_2% Au)/ OACC	1480
(1% Pd_3% Au)/ OACC	1468
(3% Pd_1% Au)/ OACC	1424
(2.5% Pd_2.5% Au)/ OACC	1397

3.1.2.1.1.4. Discussion

All of the catalysts presented in Figs. 28-30 were supported on the same carrier (ACC oxidized with nitric acid). Therefore, surface chemistry of the support was the same for all of them. However, different amount of the loaded metal could slightly affect the free available surface area of the support in the final catalyst (Table 9). Therefore, it can be concluded that

the surface chemistry of the support cannot cause the observed differences in the performance of different catalysts in Figs. 28-30.

Oxidation state of palladium and gold in the catalysts were determined by x-ray photo electron microscopy (XPS). XPS spectra of the presented bimetallic catalysts revealed that almost all of the palladium and gold were in zero-valent state or in metallic form (Pd^0). However, traces of palladium were in the ionic form (Pd^{+2}).

Ultra-High Resolution Field Emission Scanning Electron Microscope (UHRFESEM) images of the bimetallic catalysts with different amount of palladium and gold are presented in Fig. 31-33. It seems that the bimetallic catalysts consist of mainly small metal particles with the size mostly 5-15 nm and also relatively big ones (with different sizes in the order of 100 nm). All of them (small and big particles) are well dispersed through the support. Concerning the small metal particles, it can be said that:

a) In the case of catalyst with 1 wt% Pd and 1 wt%, the size of the small particles is mainly around 5 nm (Figs. 31b-31c).
b) When the amount of Pd is increased to 3 wt%, the size of the small particles is also increased to 10-15 nm (Figs. 32b-32c). However, some particles with size 20-50 nm can be found.
c) The catalyst with 1 wt% Pd and 3 wt% Au consist of considerable number of gold particles with different shape and size, mainly 20-50 nm (Fig. 33c). However, similar to the catalyst with 3 wt% Pd and 1 wt% Au, the small Pd particles are mostly 10-15 nm (Fig. 33d).
d) Based on EDS analysis of UHRFESEM images, small particles mainly consist of monometallic palladium and gold.
e) In the case of catalyst with 3 wt% Pd and 1 wt% Au, small particles mostly consist of monometallic Pd particles. However, in the case of catalyst with 1 wt% Pd and 3 wt% Au, the number of Au monometallic particles was considerable.

Ionic gold (Au^{3+}) in chloroauric acid ($HAuCl_4$) solution is mainly in the form of ($AuCl_4^-$) [64]. Ionic palladium (Pd^{2+}) in acidic solution of palladium dichloride ($PdCl_2$) appears mainly as ion complex ($PdCl_4^{2-}$) (see Section 3.1.1.1.1). It was discussed that (see Section 3.1.1.1.3) wet oxidation of activated carbon cloth (ACC) with nitric acid leads to formation of oxygen-containing functional groups on the surface of ACC fibers. These acidic groups charged negatively the surface of ACC fibers. The electrostatic interaction (repulsion) between the

metal precursors ($AuCl_4^-$, $PdCl_4^{2-}$) and the negatively charged surface of the oxidized ACC could result in good dispersion of metal precursors on the support surface. However, largely aggregated metallic particles (specially Au) were obtained principally due to the redox properties of activated carbon [65-66] In fact, the higher variety of activated carbon functionalities than those present on oxides (like silica and alumina) can promote other electrostatic interactions [65]. Concerning the big metal particles, it can be observed that:

a) In the case of the catalyst with 1 wt% Pd and 1 wt% Au, the images with higher magnification of a big metal particle (Figs. 31d-31e) and the Energy Dispersive X-ray Spectroscopy (EDS) analysis of STEM image of a Pd-Au particle (Fig. 34) reveal that these relatively round and big particles consist of a gold-rich core which was surrounded by a lot of small palladium particles. As a result, the outer surface of activated carbon cloth in 1 wt% Pd_1 wt% Au catalyst was changed to dark grey which is slightly lighter than the black color of the ACC. This pale grey color could possibly be assigned to the natural color of palladium.
b) When increasing the amount of palladium, like in the catalyst with 3 wt% Pd and 1 wt% Au, the small Pd particles seem to form a thicker and denser layer around the golden core (Fig. 32d). Therefore, they look bigger than in the catalysts with 1 wt% Pd and 1 wt% Au.
c) When the amount of gold was increased, like in the catalyst with 1 wt% Pd and 3 wt% Au, the round core-shell morphological Pd-Au particles were formed over bigger thin spots of gold (Figs. 33d-33e). The round Pd-Au particles have almost the same morphology as the particles in 1% Pd_1% Au catalyst. The new morphology of Pd-Au particles is supported by EDS analysis of STEM images (Fig. 35). However, the changes of the color of the surface of the activated carbon cloth to pale yellow in the bimetallic catalysts with higher amount of gold can be seen.
d) The morphology of the metal particles in the catalyst with 2.5 wt% Pd and 2.5 wt% Au looked almost the same as the one with 1 wt% Pd and 3 wt% Au.
e) The big Pd-Au particles mainly consist of gold-rich core covered by small Pd particles with the size mostly less than 10 nm which, they cannot be inactive. Indeed, it is assumed that Au acts as an electronic promoter for the Pd-rich shell [10, 40-41].

Based on the discussion above, it can be concluded that the morphology and size of the metal particles in the bimetallic catalysts were determined by the amount of palladium, gold, and

their ratio. Consequently, the different selectivity and activity of the Pd-Au catalysts presented in Figs. 28-30 could mostly be related to their different morphology and size of the metal particles.

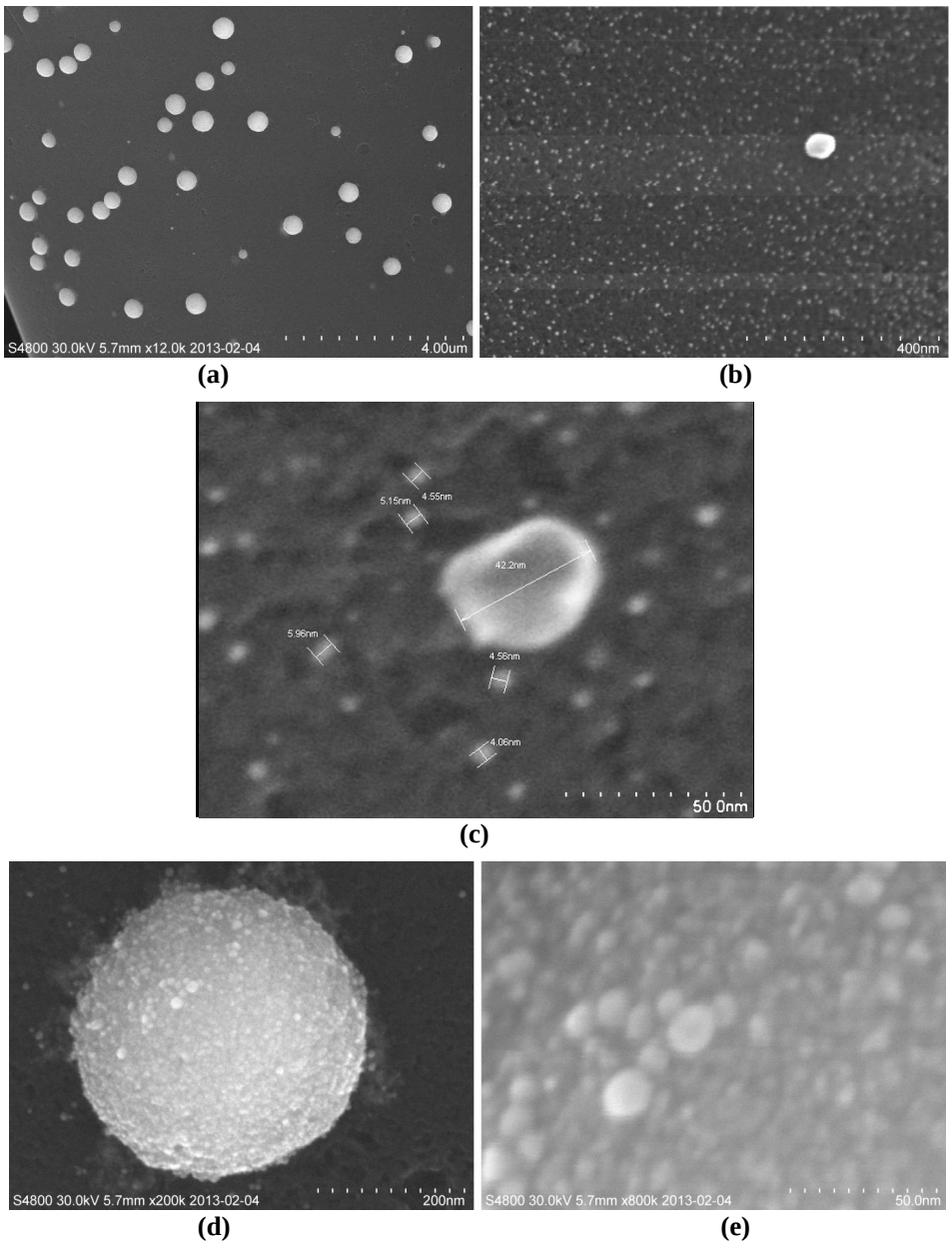

(a) **(b)**

(c)

(d) **(e)**

Figure 31. The ultra-high resolution field emission scanning electron microscopy (UHRFESEM) images (with different magnifications) of the catalyst with 1 wt % Pd and 1 wt % Au supported on the ACC oxidized with nitric acid.

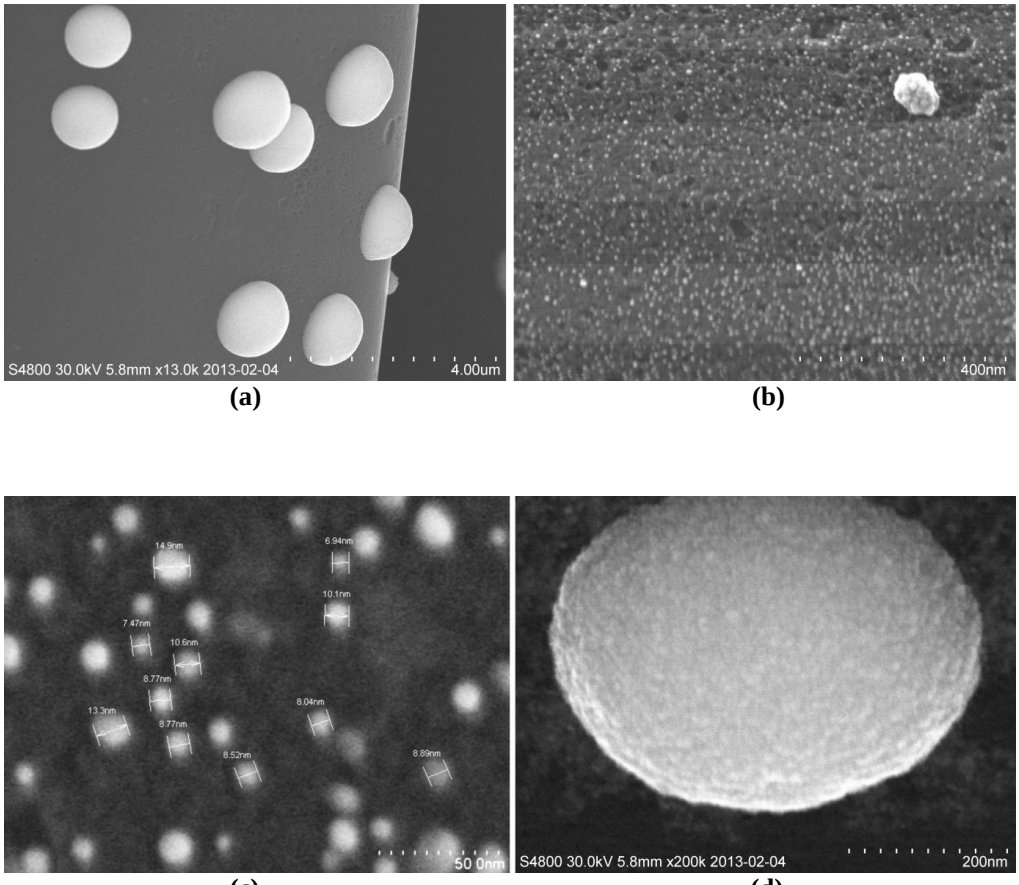

(a) **(b)**

(c) **(d)**

Figure 32. The ultra-high resolution field emission scanning electron microscopy (UHRFESEM) images (with different magnifications) of the catalyst with 3 wt % Pd and 1 wt % Au supported on the ACC oxidized with nitric acid.

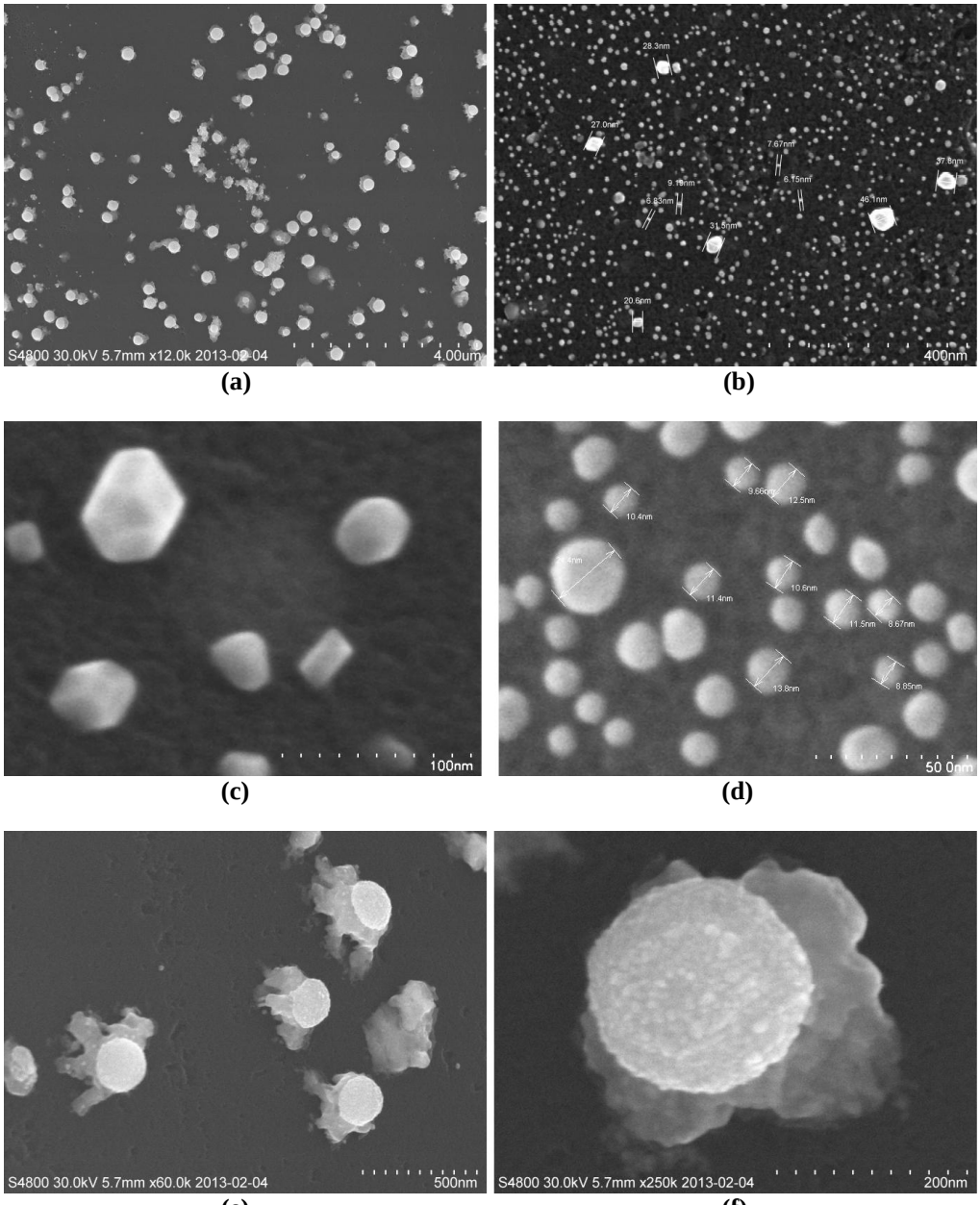

(a) **(b)**

(c) **(d)**

(e) **(f)**

Figure 33. The ultra-high resolution field emission scanning electron microscopy (UHRFESEM) images (with different magnifications) of the catalyst with 1 wt % Pd and 3 wt % Au supported on the ACC oxidized with nitric acid.

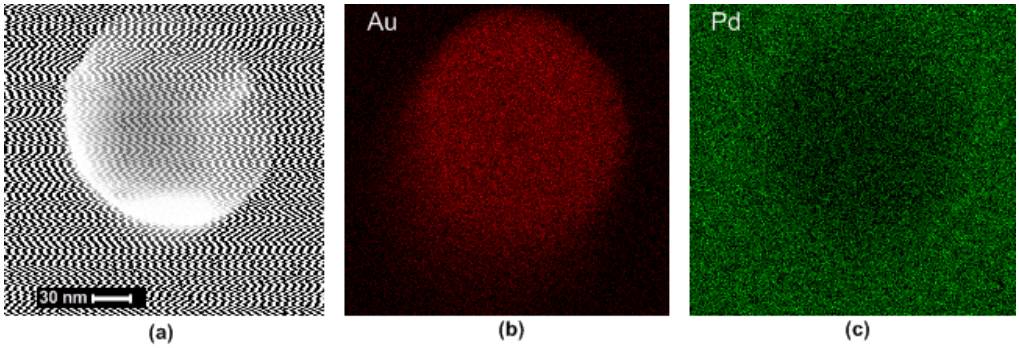

Figure 34. STEM-EDS mapping and analysis of a big particle in the 1 wt %_ 1 wt % Au bimetallic catalyst; (a) STEM image, (b) Au map, and (c) Pd map.

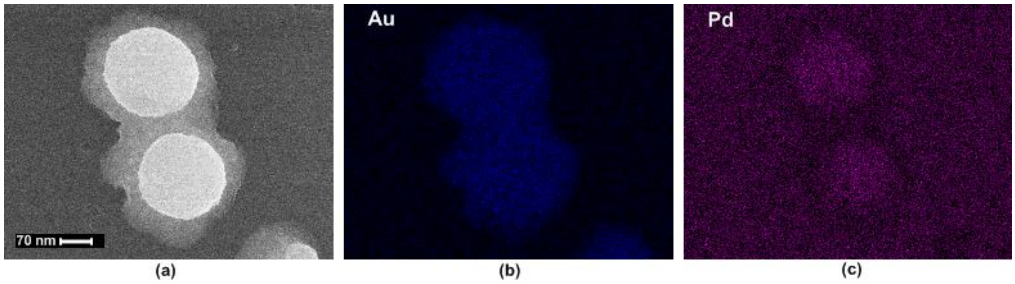

Figure 35. STEM-EDS mapping and analysis of two big particles in the 1 wt %_ 3 wt % Au bimetallic catalyst; (a) UHRFESEM image, (b) Au map, and (c) Pd map.

3.1.2.1.2.The effects of the oxidation state of the loaded metal

As it was discussed earlier (see Sections 3.1.1.1.1, 3.1.1.2, 3.1.1.3.1, 3.1.1.3.2), the presence of the oxygen-containing surface functional groups highly affect the final catalytic properties and activity. In the case of the non-oxidized ACC, lack of the oxygen-containing surface functional groups makes it possible to investigate merely the effects of the oxidation state of the metallic part of the catalysts.

The results of the catalytic activities of the different bimetallic catalysts with 3 wt% Pd and 1 wt% Au supported on non-oxidized ACC are presented in Fig. 36. One of the catalysts was calcined in air at 185 °C and, the other one at 275 °C. It can be observed that:

a) The yield and H_2O_2 production rates demonstrate that the catalyst calcined at 275 °C is more active in H_2O_2 production than the other.
b) However, the H_2 conversion and water production rates reveal that the catalyst calcined at 185 °C is more active in water production than the other.

c) Therefore, the catalyst calcined at 275 °C is more selective (more than 50%) than the other.

The X-ray photo electron microscopy spectra of the catalysts mentioned above reveal that (see Fig. 38):

a) Palladium in the catalyst calcined at 185 °C was almost in zero-valence or in metallic state (Pd^0, the two peaks with binding energy at around 335 and 340.2 eV) and only traces of the palladium are in the form of Pd^{+2} (the two peaks with binding energy at around 338 and 343.4 eV) originated from palladium dichloride $PdCl_2$.
b) When increasing the calcination temperature to 235 °C almost 8 wt % of the total amount of the palladium was oxidized to palladium oxide (PdO, the two peaks with binding energy at around 336.6 and 342 eV).
c) In the catalyst calcined at 275 °C, almost 63 wt % of the total amount of palladium was in the form of palladium oxide. Therefore, increasing the calcination temperature increases the amount of palladium oxide.
d) In the catalyst with 1 wt% Pd and 4 wt% Au calcined at 275 °C, only 8 % of the total amount of palladium was in the form of palladium oxide. This is much lower than what was observed for the catalyst with 3 wt% Pd and 1 wt% Au calcined at 275 °C.
e) In general, in the bimetallic catalysts with $\frac{Au}{Pd} > 1$, calcination at 235-275 °C resulted in smaller amount of palladium oxide than with $\frac{Au}{Pd} \leq 1$.
f) Gold in all calcined catalysts were in metallic or zero-valent state.

Based on the results presented in Fig. 36 and discussions above, it could be concluded that the presence of palladium oxide (PdO) made the Pd-Au bimetallic catalysts more selective and more active than the corresponding catalysts with Pd^0.

Low amount of PdO in the catalyst with 1 wt% Pd and 4 wt% Au calcined at 275 °C resulted in smaller differences in catalytic performance of the two catalysts calcined at 185 °C and 275 °C (Fig. 37) when compared to the corresponding differences observed for the catalysts with 3 wt% Pd and 1 wt% Au (Fig. 36).

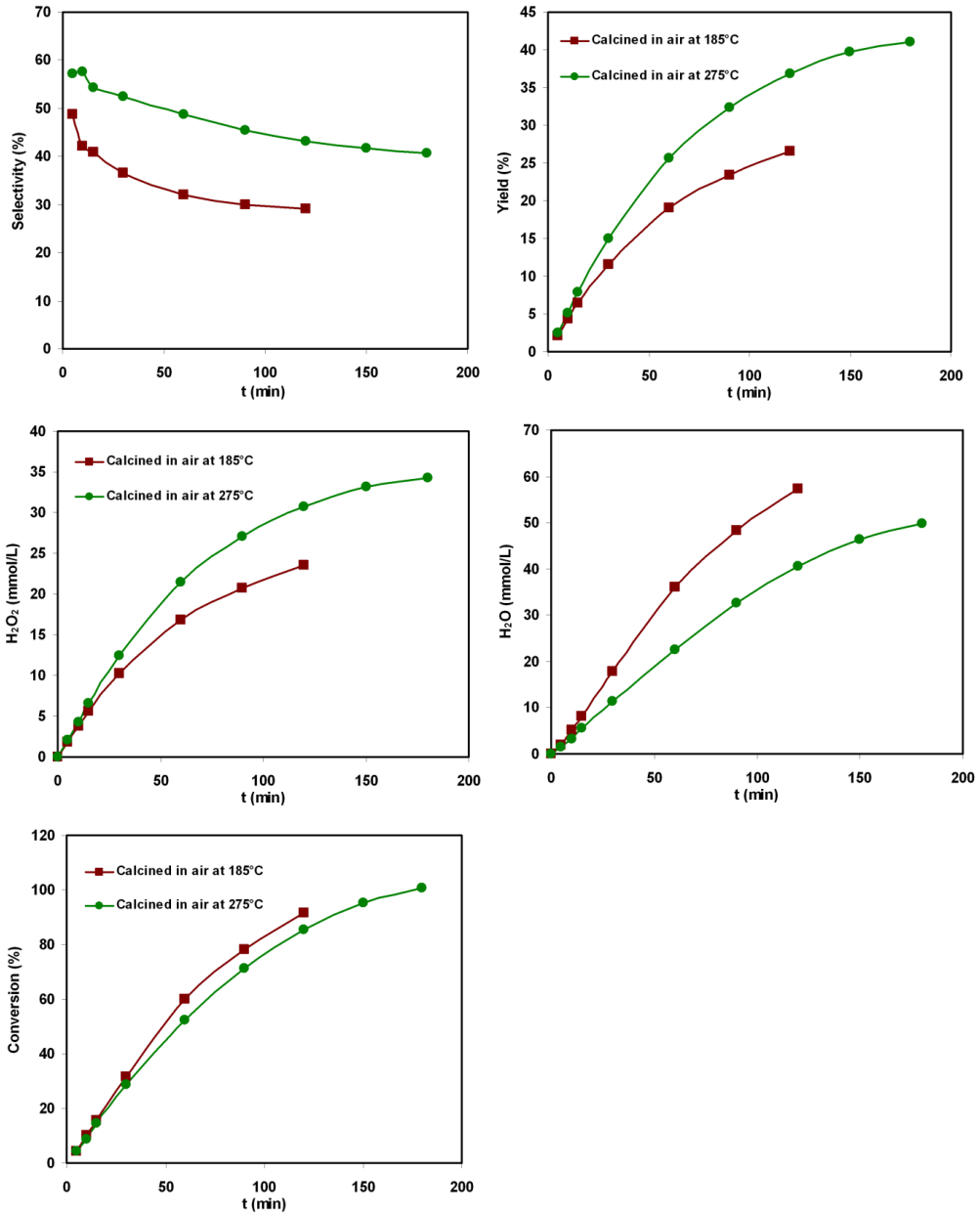

Figure 36. The results of the direct synthesis of H_2O_2 over the catalysts with 3 wt% Pd and 1 wt% Au supported on non-oxidized ACC and calcined in air at 185 °C and 275 °C.

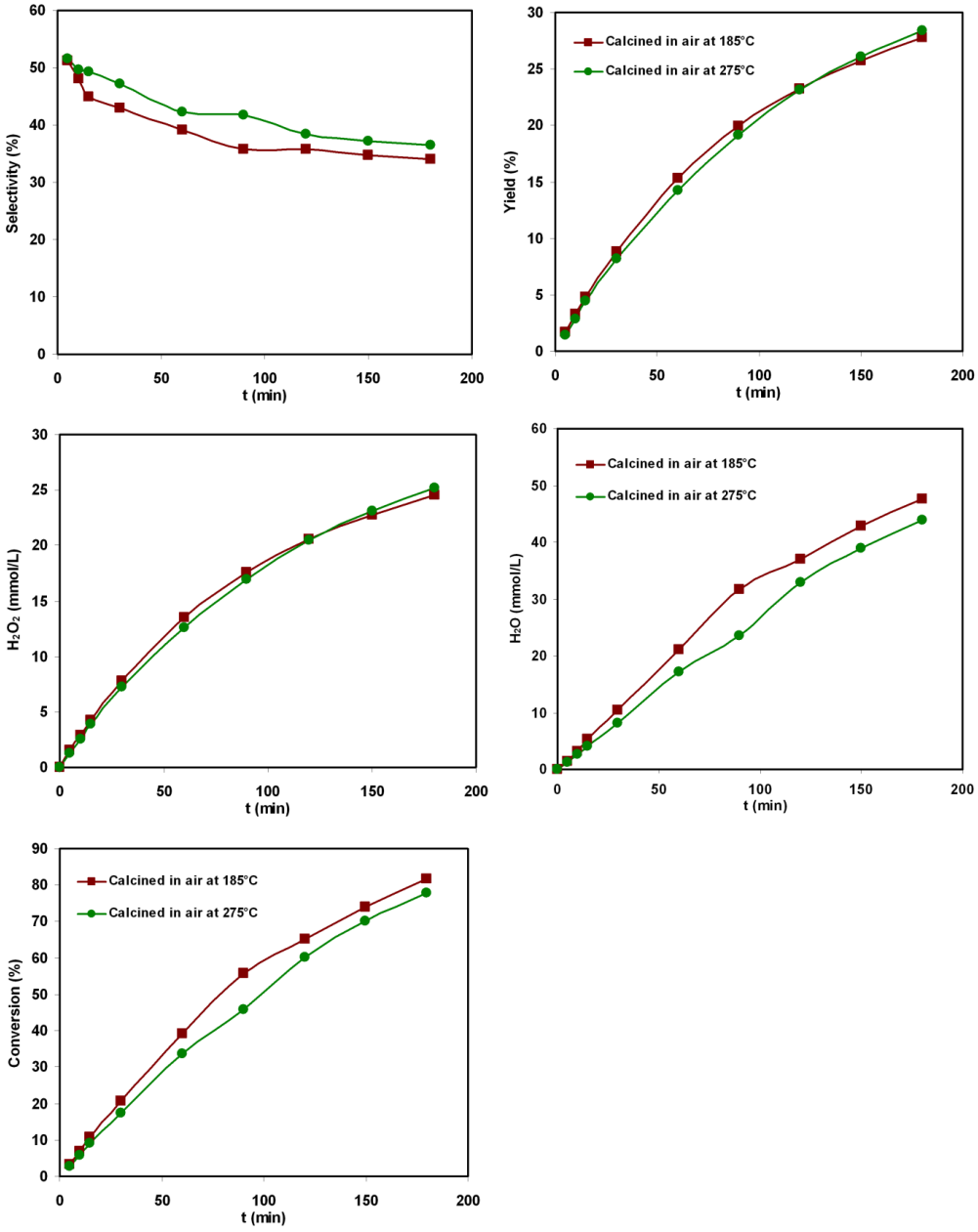

Figure 37. The results of the direct synthesis of H_2O_2 over the catalysts with 1 wt% Pd and 4 wt% Au supported on non-oxidized ACC and calcined in air at 185 °C and 275 °C.

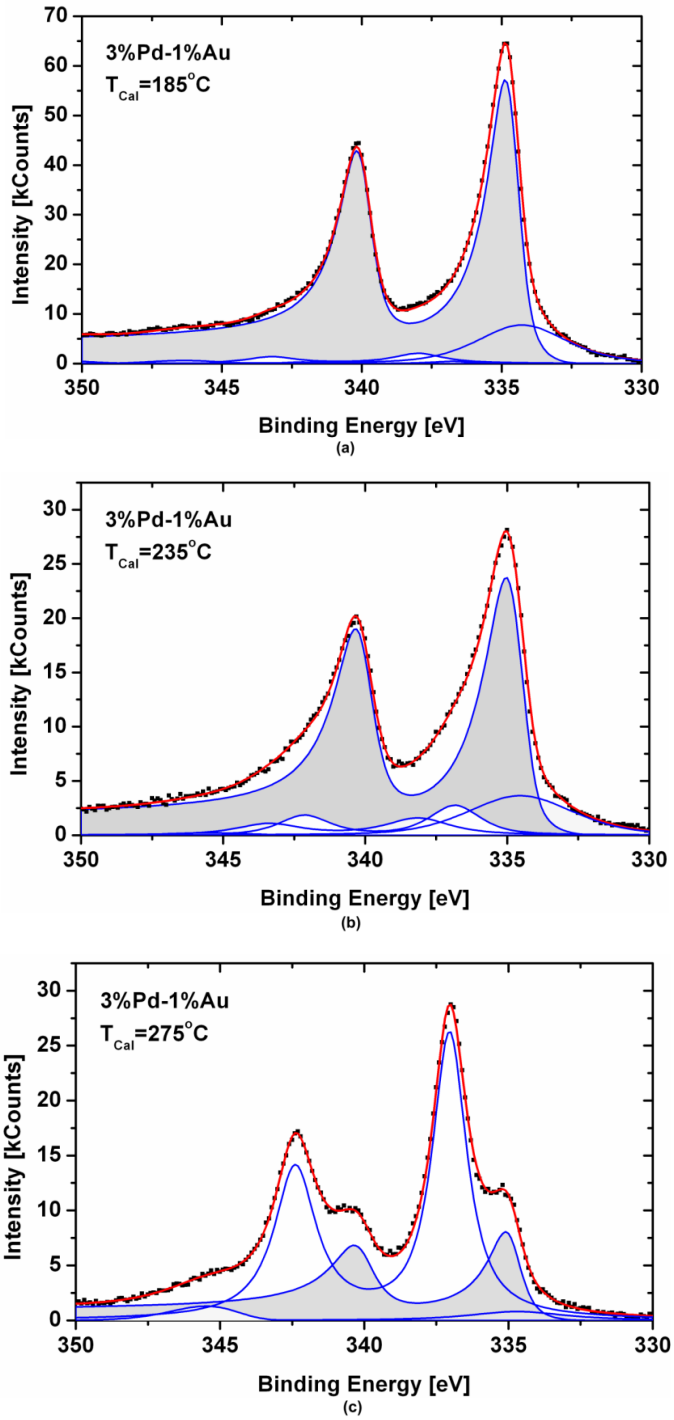

Figure 38. The Pd 3d XPS spectra of the catalyst with 3 wt % Pd and 1 wt % Au calcined in air at (a) 185 °C, (b) 235 °C, and (c) 275 °C.

3.1.2.1.3.The effects of the surface chemistry of the ACC fibers on the final catalytic performance and surface morphology of the Pd-Au bimetallic catalysts

The results of the direct synthesis of H_2O_2 over the catalysts with 3 wt% Pd and 1 wt% Au supported on the non-oxidized ACC (NACC) and the ACC oxidized with nitric acid (OACC) are presented in Fig. 39. It can be observed that:

a) The catalyst supported on oxidized ACC was almost 2 times more selective than the corresponding one on non-oxidized ACC.
b) According to the results of yield and rate of H_2O_2 production, the catalyst supported on oxidized ACC was also more active than the one on non-oxidized ACC.
c) H_2 conversion results and the rate of water production demonstrate that the catalyst supported on non-oxidized ACC was substantially more active in water production than the one on oxidized ACC.
d) Almost similar results were observed for the other bimetallic catalysts presented in this paper. The only difference was that in the case of bimetallic catalysts with $\frac{Au}{Pd} \geq 1$, the differences between performances of the catalysts supported on oxidized ACC and non-oxidized ACC were smaller than the catalysts with $\frac{Au}{Pd}$ <1. This can be explained as, in general, with increasing the amount of Au, bimetallic catalysts become more selective and less active. As an example, the results of the catalysts with 1 wt% Pd and 4 wt% Au supported on non-oxidized and oxidized ACC are shown in Fig. 40.

Different surface chemistry of the supports (lack of the oxygen-containing surface functional groups in the case of non-oxidized ACC) leads to different surface morphology. The surface morphology of the Pd-Au catalysts on oxidized ACC has been discussed in the section 3.1.2.1.1.4. In the case of non-oxidized ACC, similar to the Pd monometallic catalysts (see Section 3.1.1.1.1), palladium and gold form really big and joined particles at the outer surface of ACC fibers (Fig. 41). In most areas, the metal particles almost cover the outer surface of the ACC fibers. These completely different surface morphologies resulted in different catalytic performances. Formation of the big and almost jointed metal particles on the outer surface of the non-oxidized ACC can be a result of the electrostatic attraction between the surface of the ACC fibers and the anions of palladium and gold ($PdCl_4^{2-}$ and $AuCl_4^-$)in the precursor solution (see Section 3.1.1.1.1 and 3.1.2.1.1.4 for detailed explanation).

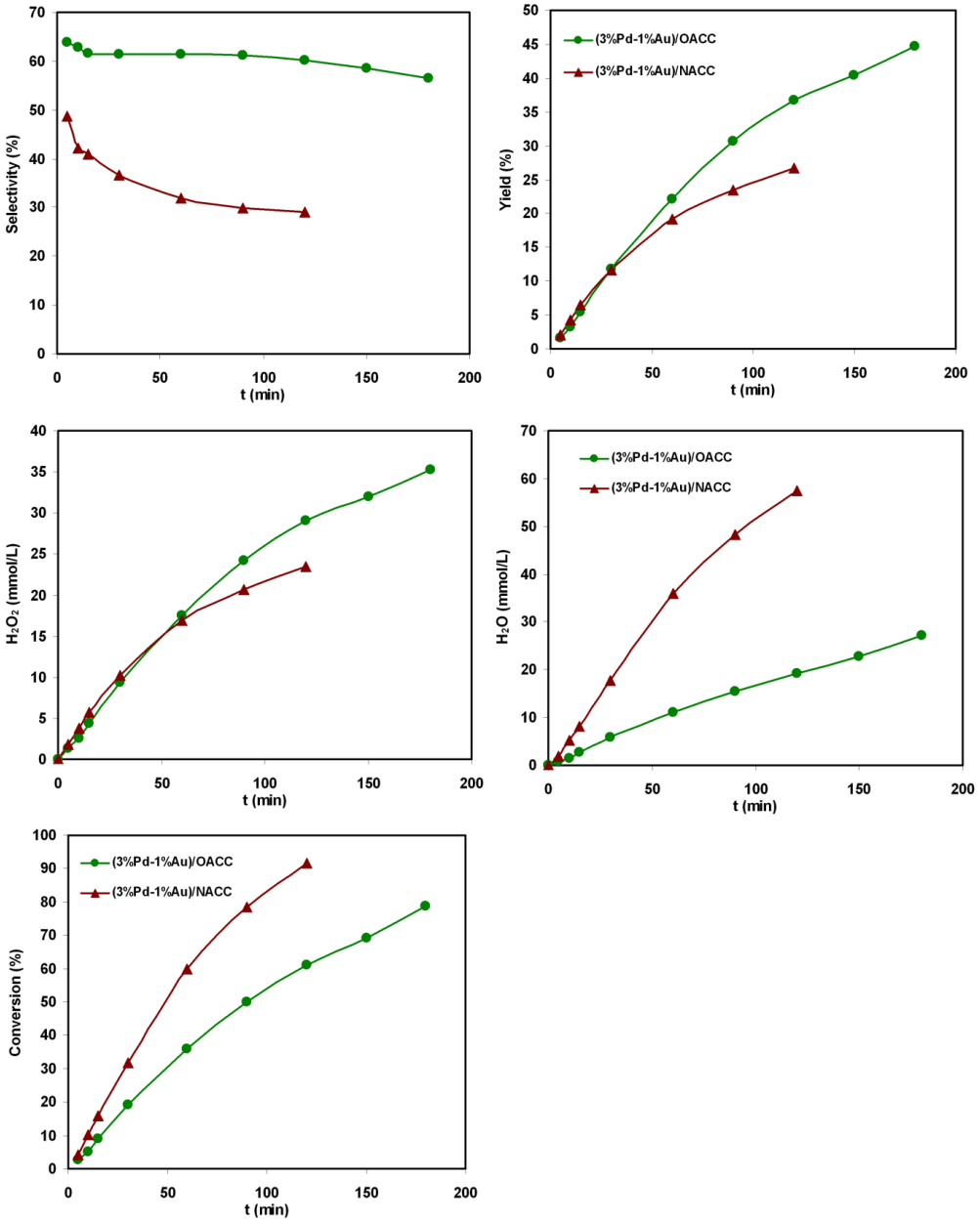

Figure 39. The results of the direct synthesis of H_2O_2 over the catalysts with 3 wt% Pd and 1 wt% Au supported on non-oxidized ACC and calcined in air at 185 °C and 275 °C.

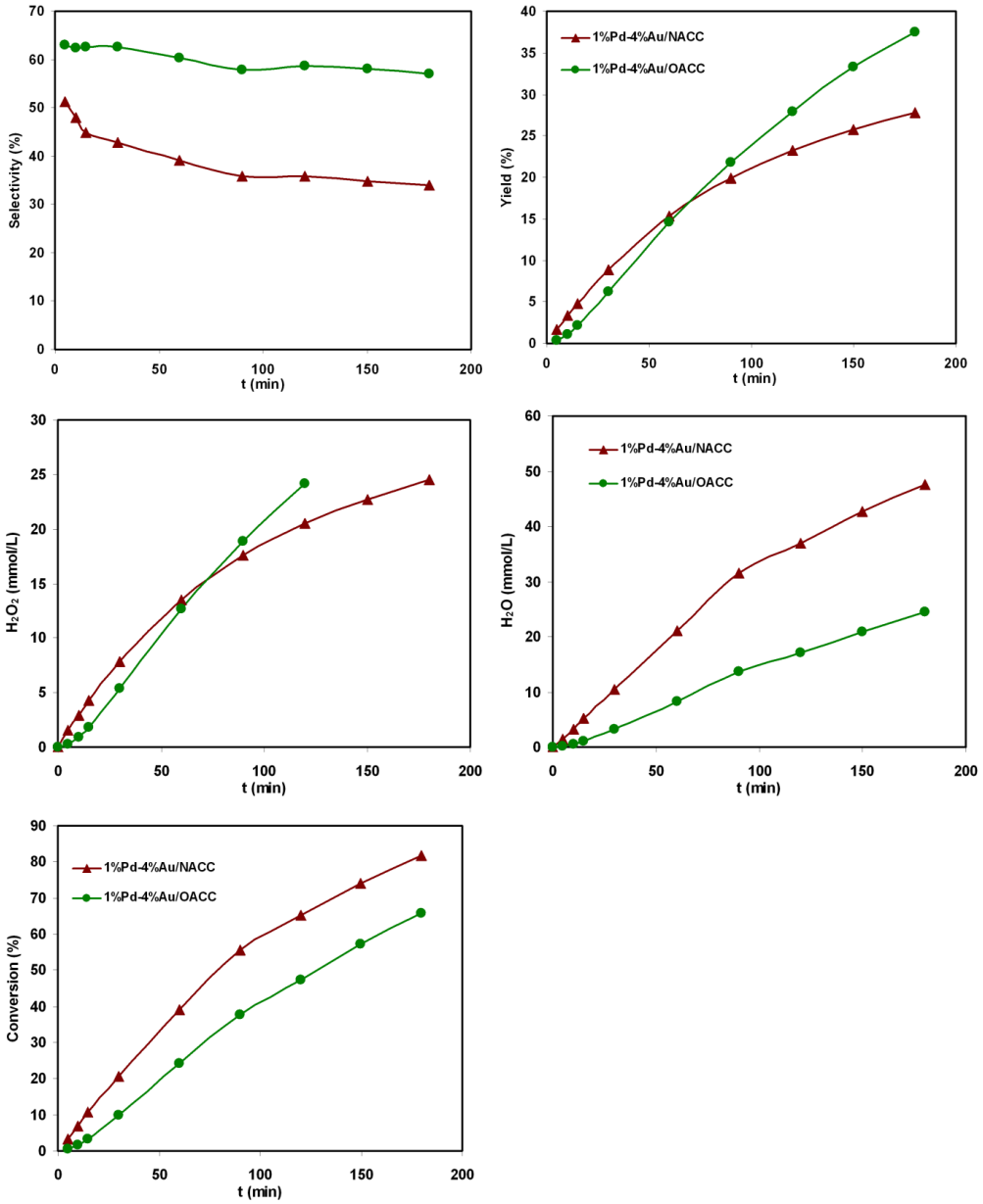

Figure 40. The results of the direct synthesis of H_2O_2 over the catalysts with 1 wt% Pd and 4 wt% Au supported on non-oxidized ACC and calcined in air at 185 °C and 275 °C.

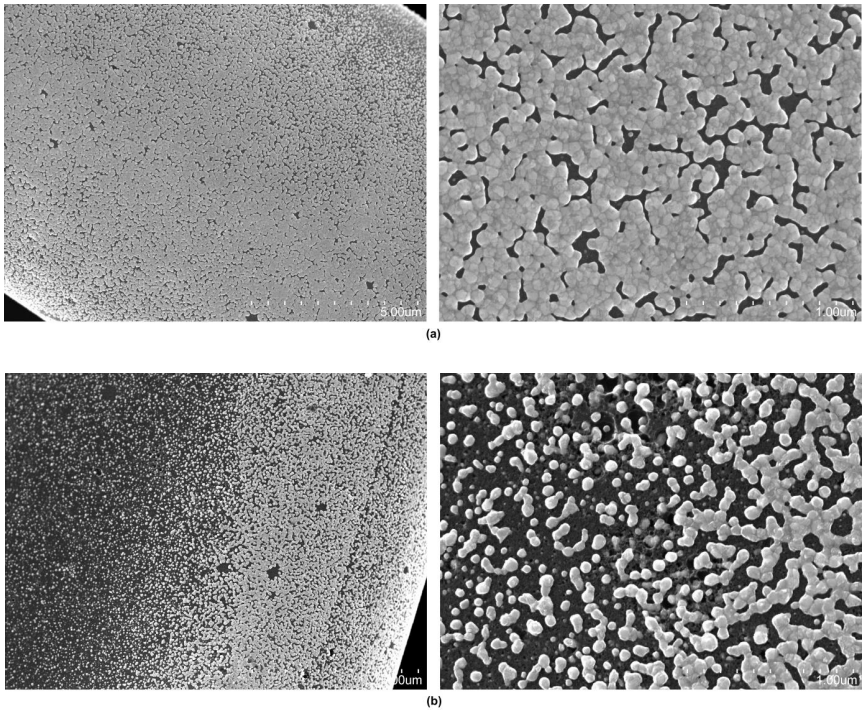

Figure 41. The ultra-high resolution field emission scanning electron microscopy (UHRFESEM) images (with different magnifications) of the catalyst with: (a) 1 wt% Pd and 4 wt% Au supported on non-oxidized ACC and (b) 3 wt% Pd and 1 wt% Au supported on non-oxidized ACC.

3.1.2.1.4.The effects of the heat treatment of the catalysts in H_2 and air

The results of the direct synthesis of H_2O_2 over the catalysts with 3 wt% Pd and 1 wt% Au supported on the ACC oxidized with nitric acid are presented in Fig. 42. It can be observed that:

a) The catalysts calcined in the air at 185-275 °C are almost 3 times more selective than the catalyst reduced by H_2 at 185 °C.
b) According to the results of yield and H_2O_2 production rate, the calcined catalysts are substantially more active in H_2O_2 production than the corresponding reduced one.
c) The catalyst reduced by H_2 is dramatically more active in water production than the calcined catalysts.
d) The catalyst calcined at 235 °C is considerably more active in H_2O_2 and also in water production than the other calcined catalysts.
e) In the case of calcined catalysts, the catalyst calcined at 185 °C has the highest

selectivity and, the one calcined at 235 °C has the lowest selectivity. However, the selectivity of the different calcined catalysts are quite close to each other.

f) In the case of calcined catalysts, the catalyst calcined at 275 °C shows lower activity in H_2O_2 and water production than the other ones.

g) Almost similar results were observed for the other bimetallic catalysts supported on oxidized ACC.

The ultra-high resolution field emission scanning electron microscope (UHRFESEM) images and EDS analysis confirmed that the heat treatment in H_2 at 185 °C and the calcination in air up to 275 °C had no noticeable effects on the morphology of the Pd-Au particles in the catalysts. However, the heat treatment of the oxidized ACC damages the oxygen-containing surface functional groups (Table 10). In the case of calcined catalysts, increasing the calcination temperature increased the damage, especially to the stronger acidic surface functional groups. As it was discussed (see Section 3.1.1.1.3), these groups are responsible for CO_2 releasing in temperature programmed desorption (TPD) test (Table 10). Heat treatment of the Pd-Au catalysts supported on oxidized ACC by H_2 at 185 °C causes maximum damage to the stronger acidic oxygen functional groups (Table 10).

From the other side, increasing the calcination temperature increases the amount of PdO in the final catalyst (see Section 3.1.1.1.4). Based on the results and discussions in section 3.1.1.2 and section 3.1.1.3, the presence of palladium oxide and the oxygen-containing surface functional groups (in the case of ACC oxidized with nitric acid) are favored for direct catalytic synthesis of H_2O_2. Therefore, increasing the calcination temperature has two opposite effects, namely the damage to the oxygen-containing surface functional groups (Table 10) and increasing the amount of palladium oxide, and the resultant of these two effects mainly determine the different activities observed in Fig. 42.

In the case of the catalyst reduced by H_2 at 185 °C, it seems that the lack of palladium oxide and high damages to the oxygen-containing surface functional groups (Table 10) caused the catalyst to be considerably less selective and less active in H_2O_2 production and substantially more active in water production than the calcined catalysts.

Table 10. Total amount of CO and CO_2 desorbed according to temperature programmed desorption test.

Sample	CO (μmol/g)	CO_2 (μmol/g)
Non-oxidized ACC	115.13	82.73
Oxidized ACC (OACC)	1147.52	1290.44
3%Pd_1% Au/OACC (T_{red}=185 °C)	1015.26	445.81
3%Pd_1% Au/OACC (T_{cal}=185 °C)	1390.23	935.57
3%Pd_1% Au/OACC (T_{cal}=235 °C)	1483.51	742.43
3%Pd_1% Au/OACC (T_{cal}=270 °C)	1569.35	529.53

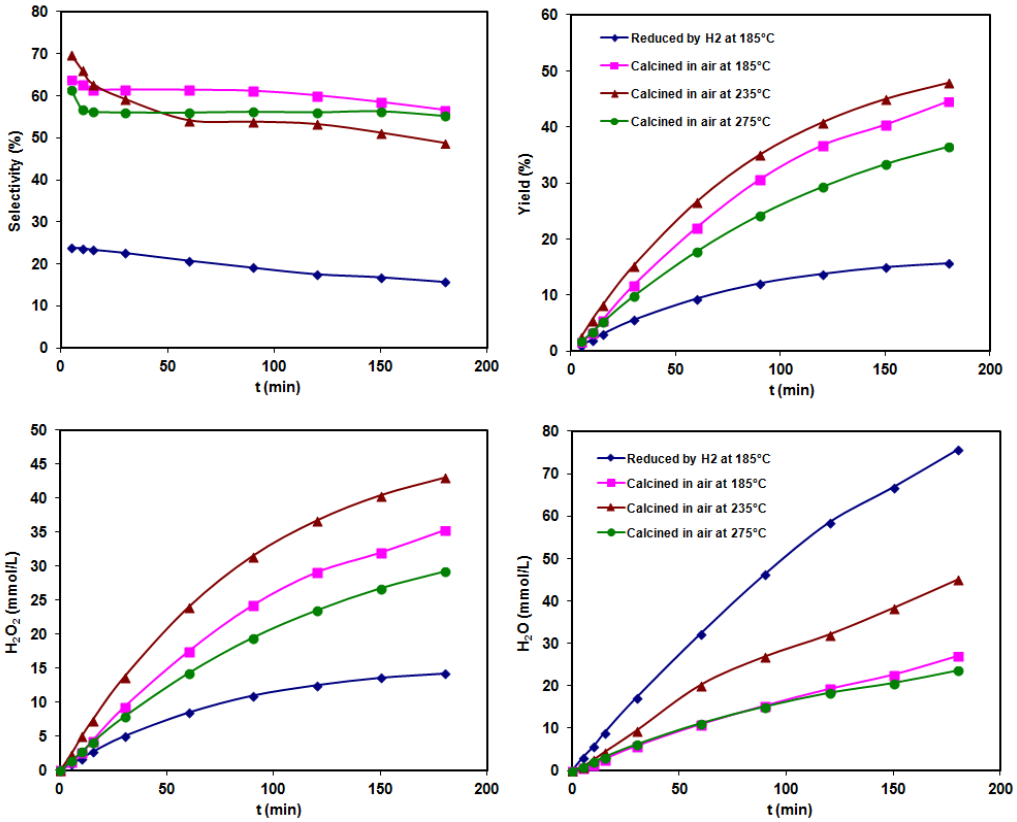

Figure 42. The catalytic activity of the catalysts with 3 wt % Pd and 1 wt % Au supported on oxidized ACC; mass of catalyst = 56 mg, $T_{reaction}$= 0 °C.

3.1.2.2. Destruction of H_2O_2 by hydrogenation

3.1.2.2.1. The effects of Au/Pd ratio and metal content

3.1.2.2.1.1. Increasing the amount of gold with a constant amount of palladium

The results of hydrogenation of H_2O_2 over a series of Pd-Au bimetallic catalysts supported on the ACC oxidized with nitric acid having 1 wt % Pd and 1-4 wt % Au are presented in Fig. 43. For comparison, the result with 1 wt % Pd monometallic catalyst is also shown. It can be observed that:

a) The bimetallic catalysts are substantially less destructive than the Pd monometallic catalyst. In other words, adding Au to Pd monometallic catalyst dramatically diminished its activity in hydrogenation of H_2O_2. Especially the catalyst with 1 wt% Pd and 1 wt% Au is almost 5 times less destructive than the monometallic catalyst with 1 wt% Pd (see the exact values in Table 11).
b) In the case of the bimetallic catalysts, when increasing the amount of gold from 1 wt% to 2 wt% the activity of the catalyst in hydrogenation of H_2O_2 increased about 1.8 times (see the exact values in Table 11). Further increase of Au from 2 to 3 and then to 4 wt% did not change so much the activity of the catalyst. In other words, the bimetallic catalysts with 2, 3 and 4 wt% of Au almost have the same hydrogenation activities, especially during the first half an hour of the reaction time.

3.1.2.2.1.2. Increasing the amount of palladium with a constant amount of gold

In order to study the effect of increasing the amount of palladium, a series of Pd-Au catalysts with constant amount of gold (1 wt %) and 1-4 wt % palladium were prepared. The results of the hydrogenation tests are presented in Fig. 44. For comparison, the results with 1, 3, and 5 wt % Pd monometallic catalysts are also shown. It can be observed that:

a) In the case of the bimetallic catalysts (Fig. 44a), when increasing the amount of palladium from 1 wt% to 2 wt%, the H_2O_2 hydrogenation activity of the catalyst was substantially increased. Indeed, the catalyst with 2 wt% Pd is about 6.5 times more active than the corresponding one with 1 wt% Pd (see the exact values in Table 11).
b) In the case of the bimetallic catalysts (Fig. 44a), increasing the amount of palladium from 2 to 3 wt%, slightly decreased the hydrogenation activity. Increasing further to 4 wt% again resulted in more active catalyst (see the exact values in Table 11).
c) In general and based on the results in Figs 44b-44d, it can be concluded that the

bimetallic catalysts with the same total metal content (wt% of Pd + wt% of Au), catalysts with higher amount of gold are less H_2O_2 destructive than the corresponding ones with higher amount of palladium.

d) The bimetallic catalysts are less H_2O_2 destructive than the corresponding monometallic Pd catalysts (Figs 44b-44d).

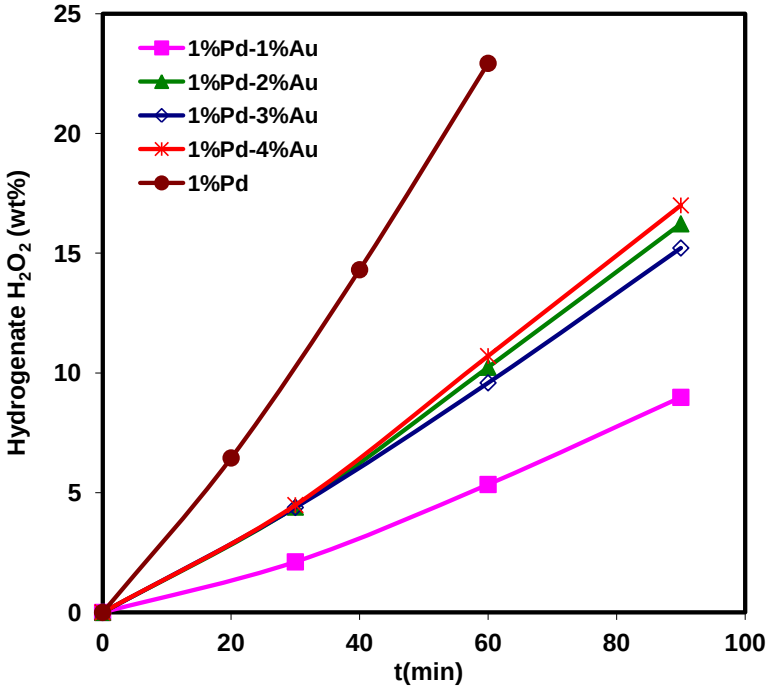

Figure 43. The effect of increasing the amount of gold on the hydrogenation activity of the Pd-Au bimetallic catalysts supported on ACC oxidized with nitric acid. Mass of catalyst = 56 mg, $T_{reaction}$= 21 °C, P_{H2}= 4 bar; all catalysts calcined in air at 185 °C.

3.1.2.2.1.3. Changing the Au/Pd ratio with a constant total metal content

The influence of varying the Au/Pd ratio on the hydrogenation activity of the Pd-Au bimetallic catalysts with constant total metal content (wt% of Pd + wt% of Au = 5 wt %) are presented in Fig. 45. It can be observed that:

a) The bimetallic catalysts were less H_2O_2 destructive than the Pd monometallic catalyst.

b) The bimetallic catalysts with $\frac{Au}{Pd} \geq 1$ were less active in hydrogenation of H_2O_2 when compared to the other bimetallic catalysts with $\frac{Au}{Pd} < 1$ (see exact values in Table 11).

c) The catalyst with 1 wt% Pd and 4 wt% Au is substantially less active than the others (see exact values in Table 11).

The observed differences in the hydrogenation activity of the catalysts presented in Figs. 45-47, can be explained in a way as discussed in section 3.1.2.1.1.4.

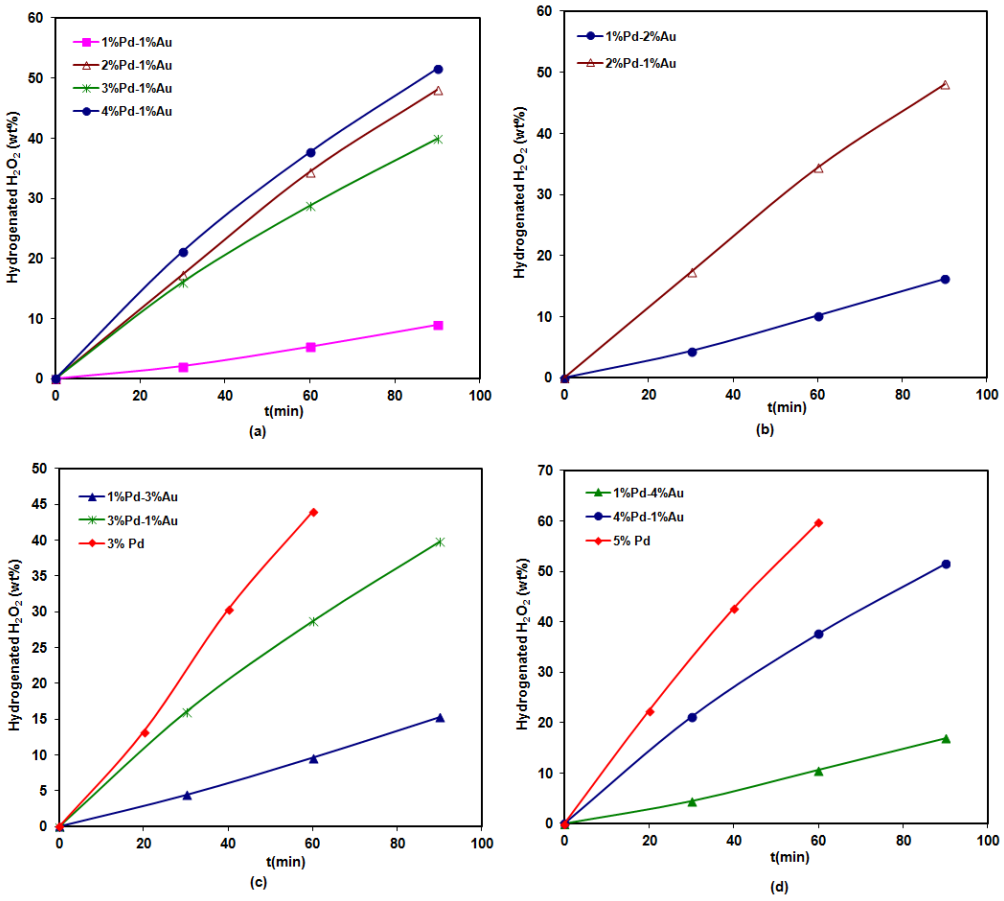

Figure 44. The effect of increasing palladium on the H_2O_2 hydrogenation activity of the Pd-Au bimetalic catalysts supported on ACC oxidized with nitric acid. Mass of catalyst = 56 mg, $T_{reaction}$= 21 °C, P_{H2}= 4 bar; all catalysts calcined in air at 185 °C.

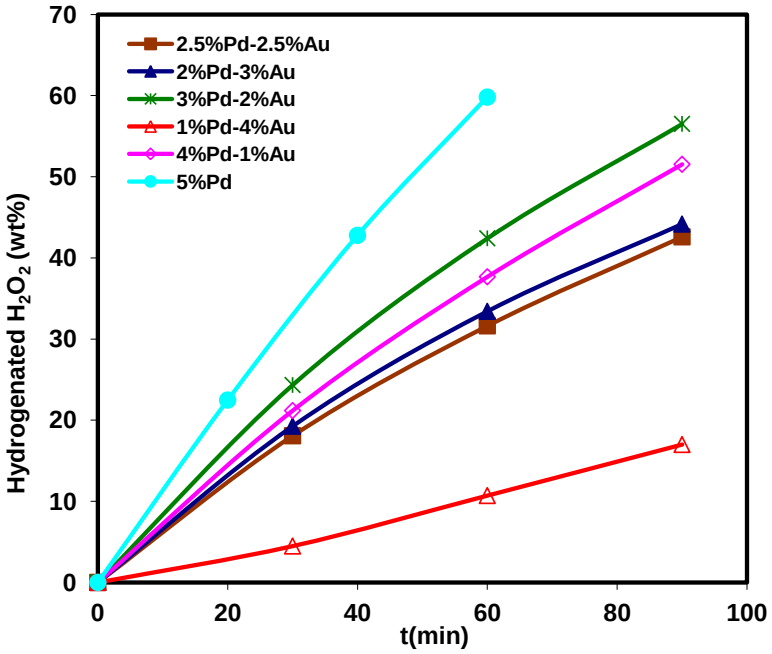

Figure 45. The effect of the Pd/Au ratio on the H_2O_2 hydrogenation activity of the Pd-Au bimetallic catalysts supported on ACC oxidized with nitric acid; Pd+Au= constant= 5 wt%, Mass of catalyst = 56 mg, $T_{reaction}$= 21 °C, P_{H2}= 4 bar; all catalysts calcined in air at 185 °C.

Table 11. Destruction of H_2O_2 by hydrogenation over Pd and Pd-Au bimetallic catalysts after 1 h. All catalysts supported on ACC oxidized with nitric acid and calcined in air at 185 °C.

Sample	Destruction of H_2O_2 by hydrogenation (wt%)
1 wt% Pd	22.93
3 wt% Pd	43.96
5 wt% Pd	59.81
1 wt% Pd_1 wt% Au	5.34
1 wt% Pd_2 wt% Au	10.24
1 wt% Pd_3 wt% Au	9.59
1 wt% Pd_4 wt% Au	10.71
2 wt% Pd_1 wt% Au	34.47
3 wt% Pd_1 wt% Au	28.75
4 wt% Pd_1 wt% Au	37.67
2.5 wt% Pd_2.5 wt% Au	31.62
2 wt% Pd_3 wt% Au	33.41
3 wt% Pd_2 wt% Au	42.41

3.1.2.2.2.The effects of the catalyst preparation method

The results of the hydrogenation of H_2O_2 over three different Pd-Au bimetallic catalysts supported on ACC oxidized with nitric acid (OACC) and prepared with different methods (see Section 2.2.1) are presented in Fig. 46. It can be seen that:

a) The catalysts prepared by co-impregnation method are less active than the corresponding ones prepared by the consequent impregnation with Pd and Au.

b) In the case of the catalysts with $\frac{Au}{Pd} \geq 1$, the catalysts prepared by first impregnating with Au and then with Pd are less active than the corresponding ones which were prepared by impregnating with Pd and then with Au.

c) However, in the case of the catalysts with $\frac{Au}{Pd} < 1$, the catalysts prepared by impregnating with Pd and then with Au are slightly less active than the corresponding ones prepared vice versa (first with gold and then with palladium).

d) The differences between hydrogenation activity of the catalysts prepared with the different methods are larger in the catalysts with $\frac{Au}{Pd} > 1$ (e.g. catalyst with 1 wt% Pd and 3 wt% Au) when compared to the catalysts with $\frac{Au}{Pd} \leq 1$. This means that the hydrogenation activity of the bimetallic catalysts is more affected by the catalyst preparation method if $\frac{Au}{Pd} > 1$

Surface morphology of the bimetallic catalysts prepared by co-impregnation approach was discussed in section 3.1.2.1.1.4. The UHRFESEM images of two bimetallic catalysts prepared by consequent impregnation methods are presented in Figs. 47-48. It can be seen that:

a) In the case of with 1 wt% Pd and 3 wt% Au, impregnation with Pd and then with Au resulted in the formation of big particles jointed together and almost formed a metal layer on the other surface of the ACC fibers (Fig. 47a)

b) In the case of catalyst with 1 wt% Pd and 3 wt% Au, impregnation with Pd and then with Au resulted in formation of big but separated metal particles (Fig. 47b). Based on the EDS analysis, these big particles are mainly gold monometallic particles. However, palladium formed mainly small particles (Fig. 47c).

c) In the case of catalyst with 3 wt% Pd and 1 wt% Au, consequent impregnation resulted in the formation of big and almost separate metal particles (Fig. 48). However,

impregnation with Pd and then with Au resulted in the formation smaller metal particles than the other approach (first with Au and then Pd, Fig. 48c). Almost similar morphology of the metal particles with these two preparation methods resulted in almost similar hydrogenation activities (Fig. 46c).

Based on the discussion above, the surface morphology of the Pd-Au bimetallic catalysts was affected strongly by the preparation method (see Section 3.1.2.1.1.4 for co-impregnation). These different surface morphologies led to different hydrogenation activities.

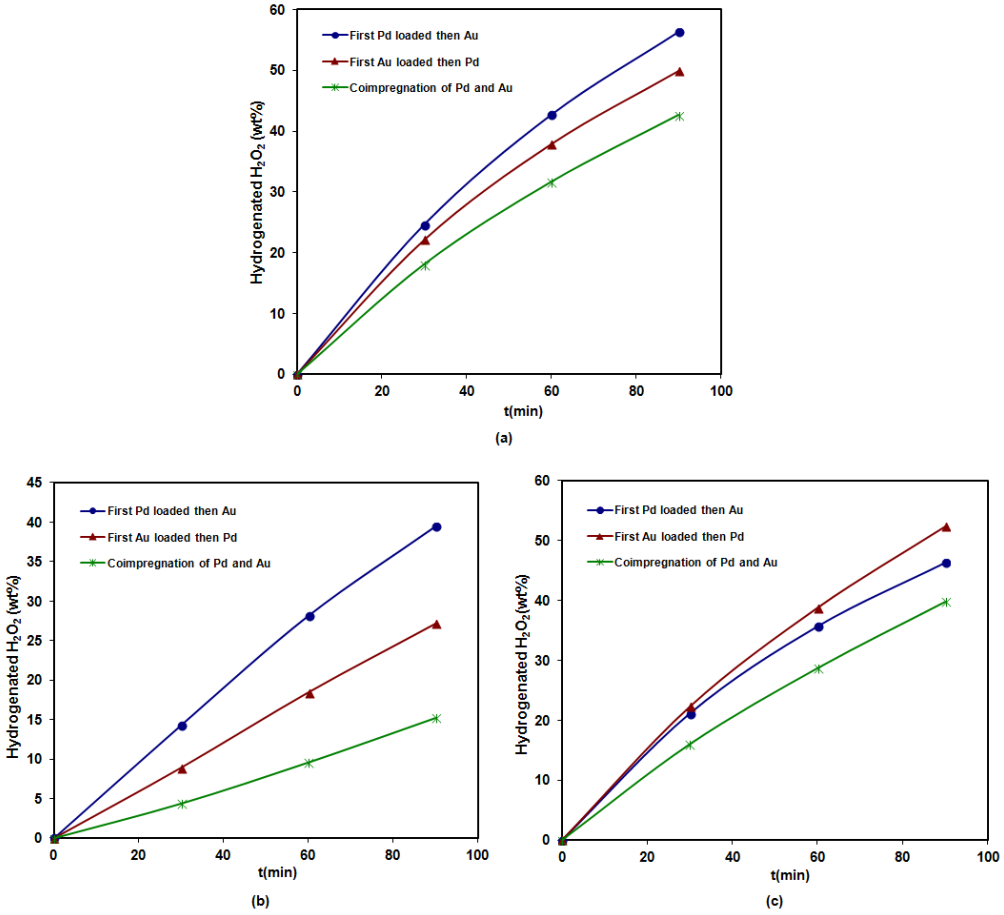

Figure 46. The effect of the catalyst preparation method on the final H_2O_2 hydrogenation activity of the bimetallic catalysts with (a) 2.5 wt% Pd and 2.5 wt% Au, (b) 1 wt% Pd and 3 wt% Au, and (c) 3 wt% Pd and 1 wt% Au. Mass of catalyst = 56 mg, $T_{reaction}$= 21 °C, P_{H2}= 4 bar; all catalysts supported on oxidized ACC (OACC) and calcined in air at 185 °C.

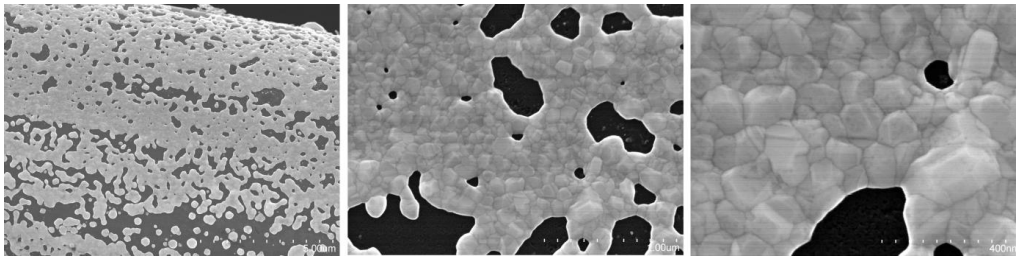

(a)

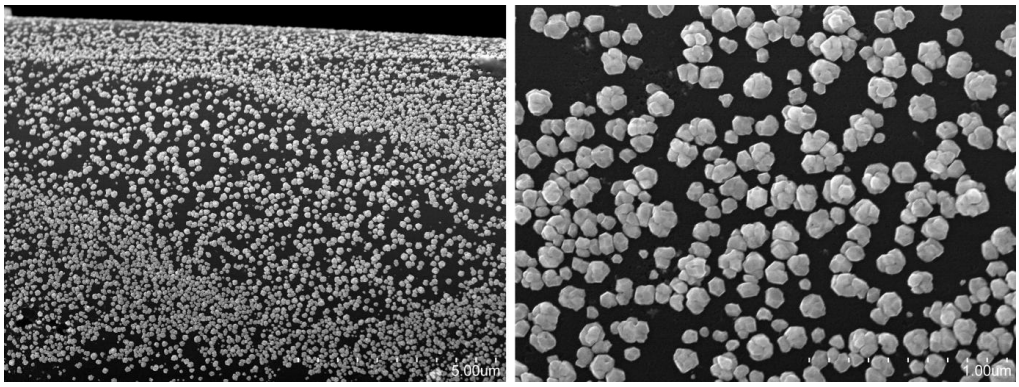

(b)

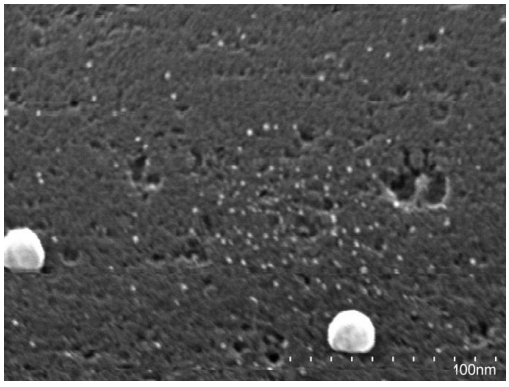

(c)

Figure 47. The ultra-high resolution field emission scanning electron microscopy (UHRFESEM) images with different magnifications of the catalyst with 1 wt % Pd and 3 wt % Au supported on oxidized ACC (OACC) and prepared by consequent impregnation of the support: (a) first with gold and then with palladium, (b) first with palladium and then with gold, and (c) also after impregnation with palladium and before consequent impregnation with gold.

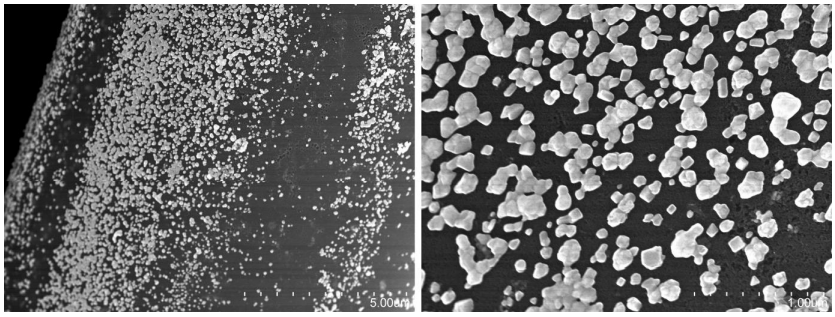

(a)

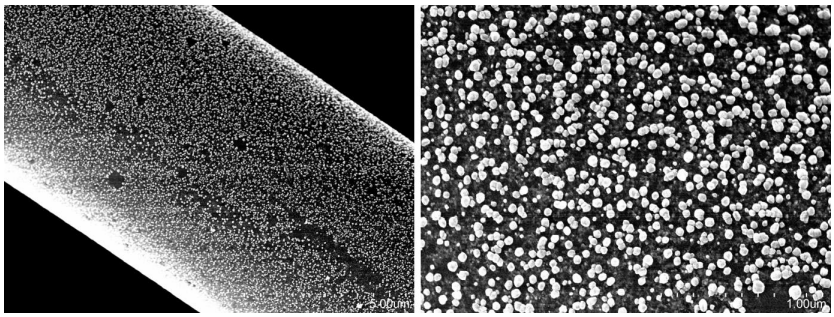

(b)

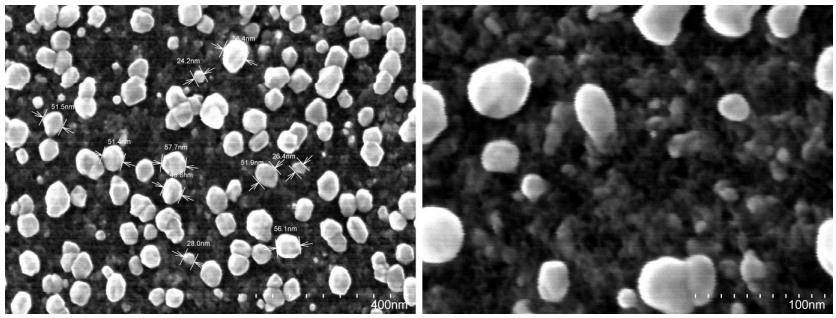

(c)

Figure 48. The ultra-high resolution field emission scanning electron microscopy (UHRFESEM) images with different magnifications of the catalyst with 3 wt % Pd and 1 wt % Au supported on oxidized ACC (OACC) and prepared by consequent impregnation of the support: (a) first with gold and then with palladium, (b-c) first with palladium and then with gold.

3.1.2.2.3.The effects of the surface chemistry of the ACC fibers

The results of the hydrogenation of H_2O_2 over three different bimetallic catalysts supported on the non-oxidized ACC and on the ACC oxidized with nitric acid are presented in Fig. 49. It can be observed that the catalysts supported on oxidized ACC are substantially less H_2O_2

destructive than the corresponding ones on non-oxidized ACC. Especially the catalyst with 1 wt% Pd and 1 wt% Au supported on non-oxidized ACC is about 10 times more destructive than the corresponding one supported on oxidized ACC.

Different surface chemistry of the ACC fibers in the non-oxidized ACC and the ACC oxidized with nitric acid (see Section 3.1.1.1.3) led to a huge differences in the surface morphology of their Pd-Au catalysts. The UHRFESEM images and the corresponding explanations about the surface morphology of the Pd-Au bimetallic catalysts supported on non-oxidized ACC and ACC oxidized with were already discussed in details in section 3.1.2.1.3 and section 3.1.2.1.1.4. These completely different surface morphologies can be the main reason for the behavior observed in Fig. 49.

Furthermore, in the case of oxidized ACC, the oxygen-containing surface functional groups might also affect directly the final hydrogenation activity of the catalysts. As it was discussed in section 3.1.1.1.1, these acidic groups negatively charge the surface of the carbon fibers and decrease their hydrophobicity. The affinity of the surface of oxidized ACC holding water molecules might also affect the final rate of water production by hydrogenation ($H_2O_2 + H_2 \rightarrow 2\ H_2O$) according to the Le Chatelier's principle**.**

3.1.2.2.4.The effects of heat treatment of the catalysts in H_2 and air

The results of the hydrogenation of H_2O_2 over three different sets of bimetallic catalysts supported on the ACC oxidized with nitric acid are presented in Fig. 50. Each set consists of the same catalysts which three of them were calcined in air at 185, 235, and 275 °C and one of them was reduced by H_2 at 185 °C. It can be observed that:

a) The catalysts calcined in air at 185-275 °C are less active than the corresponding catalysts reduced by H_2 at 185 °C. Especially in the case of catalyst with 1 wt% Pd and 1 wt% Au, the one reduced by H_2 is about 10 times more destructive than the corresponding calcined catalysts.
b) In the case of catalysts calcined in air, the ones calcined at 185 °C are less H_2O_2 destructive than the others. This is clearly visible for the catalyst with 1 wt% Pd and 3 wt% Au and the catalyst with 3 wt% Pd and 1 wt% Au.
c) It looks that in the case of catalysts with $\frac{Au}{Pd} > 1$, calcination at different temperatures affected more hydrogenation activity when compared to the catalysts with $\frac{Au}{Pd} \leq 1$.

d) In the case of catalysts calcined in air, increasing the calcination temperature from 185 °C to 275 °C resulted in more H_2O_2 destructive catalysts. Especially this can be clearly seen for the catalyst with 1 wt% Pd and 3 wt% Au and the catalyst with 3 wt% Pd and 1 wt% Au.

The heat treatment of the oxidized ACC damages the oxygen-containing surface functional groups. These groups are responsible for CO_2 releasing in the temperature programmed desorption (TPD) test (Table 12). In the case of calcined catalysts, increasing the calcination temperature increases damages, especially to the stronger acidic surface functional groups. Heat treatment in H_2 at 185 °C causes substantial damage to the stronger acidic oxygen-containing functional groups (Table 12).

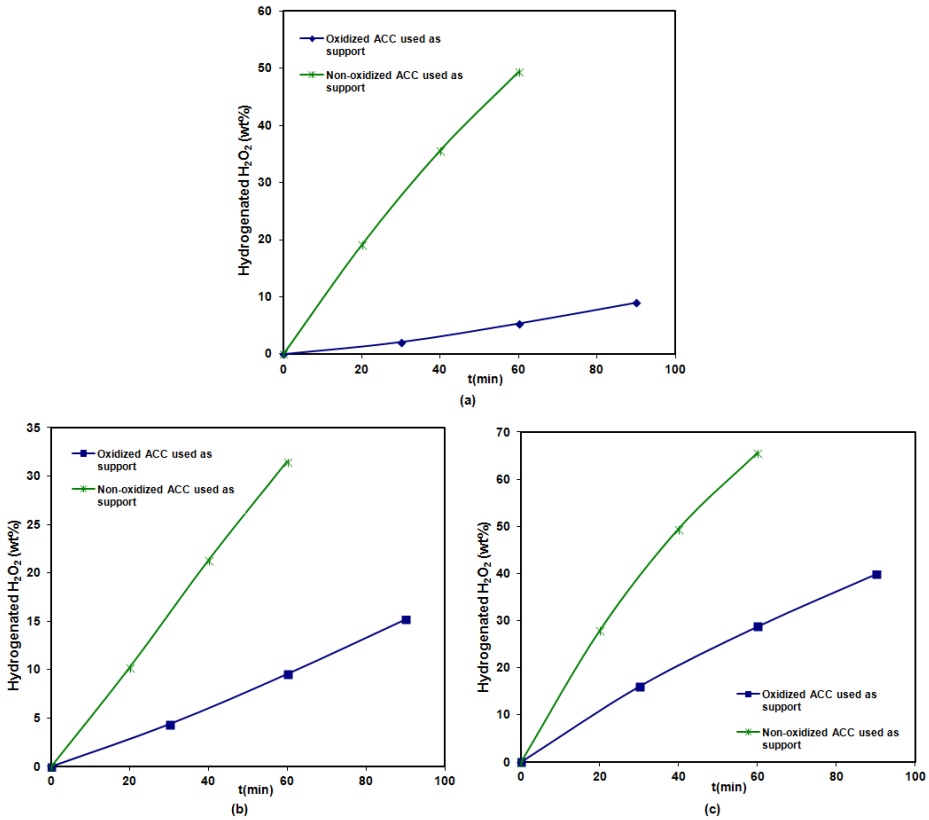

Figure 49. The hydrogenation of H_2O_2 over the bimetallic catalysts with: (a) 1 wt% Pd and 1 wt% Au, (b) 1 wt% Pd and 3 wt% Au, (c) 3 wt% Pd and 1 wt% Au. All catalysts were calcined in the air at 185 °C. Mass of catalyst = 56 mg, $T_{reaction}$= 21°C, P_{H2}= 4 bar.

Furthermore, and based on the X-ray photo electron microscopy (XPS) results, oxidation (calcination) of the fresh catalysts could result in production of palladium oxide in the catalysts. Higher calcination temperature could oxidize larger amount of active (metallic) part of the catalysts. The main results of the XPS test of the bimetallic catalysts with different amount of Pd and Au are presented in Table 13. It can be mentioned that:

a) Despite of the calcination temperature, gold was in the metallic or zero-valent state (Au^0) in all samples.
b) Palladium in the catalyst calcined at 185 °C was almost in zero valance or in the metallic state (Pd^0) and only traces of the palladium was in the form of Pd^{+2} originated from palladium dichloride $PdCl_2$.
c) In the case of the catalyst with 3 wt% Pd and 1 wt% Au, almost 8.5 wt % of the total amount of palladium was oxidized to palladium oxide (PdO) when increasing the calcination temperature to 235 °C. Almost 63 wt % of the total amount of palladium was in the form of palladium oxide in the catalyst calcined at 275 °C. Therefore, increasing the calcination temperature dramatically increases the amount of palladium oxide.
d) Calcination resulted in production of smaller amount of PdO in the catalyst with 1 wt% Pd and 3 wt% Au when compared to the catalyst with 3 wt% Pd and 1 wt% Au (Table 13). Indeed, when it was calcined at 275 °C, only 11.2 wt% of the total amount of palladium was oxidized to palladium oxide.
e) In the case of bimetallic catalysts with $\frac{Au}{Pd}>1$, calcination at 235-275 °C resulted in lower amount of palladium oxide when compared to the catalysts with $\frac{Au}{Pd}\leq 1$.

However, the Pd3d XPS spectra revealed that the oxidation state of palladium was considerably influenced by H_2 during hydrogenation reaction (Table 14). In fact, most of palladium oxide (PdO) was reduced to the zero-valent state (Pd^0) during the hydrogenation reaction ($H_2O_2 + H_2 \rightarrow 2\ H_2O$). Therefore, it can be concluded that the oxidation state of palladium could not have the main role in causing the observed differences in hydrogenation activity.

Summarizing the discussion above, the damages in the oxygen-containing surface functional groups caused by heat treatment are the main reason for different hydrogenation activities of the catalysts with equal amounts of Pd and Au. .

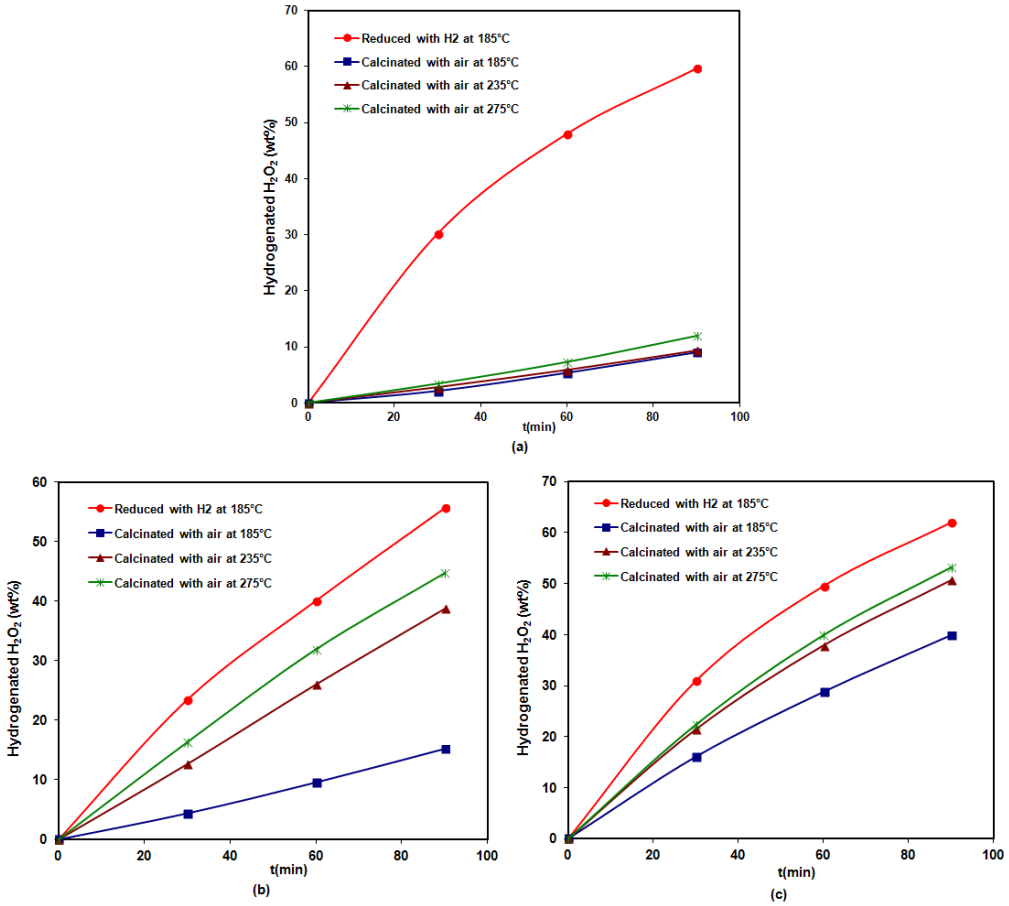

Figure 50. The hydrogenation of H_2O_2 over the bimetallic catalysts supported on oxidized ACC and reduced by H_2 at 185 °C or calcined in air at different temperatures; (a) the catalysts with 1 wt% Pd and 1 wt% Au, (b) the catalysts with 1 wt% Pd and 3 wt% Au, and (c) the catalysts with 3 wt% Pd and 1 wt% Au. Mass of catalyst = 56 mg, $T_{reaction}$= 21°C, P_{H2}= 4 bar.

Table 12. Total amount of CO and CO_2 desorbed according to the temperature programmed desorption (TPD) tests.

Sample	CO (μmol/g)	CO_2 (μmol/g)
Non-oxidized ACC	115.13	82.73
Oxidized ACC (OACC)	1147.52	1290.44
3%Pd_1% Au/OACC (T_{red}=185 °C)	1015.26	445.81
3%Pd_1% Au/OACC (T_{cal}=185 °C)	1390.23	935.57
3%Pd_1% Au/OACC (T_{cal}=235 °C)	1483.51	742.43
3%Pd_1% Au/OACC (T_{cal}=270 °C)	1569.35	529.53
1%Pd_3% Au/OACC (T_{red}=185 °C)	1091.29	480.72
1%Pd_3% Au/OACC (T_{cal}=185 °C)	1378.45	910.45
1%Pd_3% Au/OACC (T_{cal}=235 °C)	1432.52	795.14
1%Pd_3% Au/OACC (T_{cal}=275 °C)	1508.26	581.38

Table 13. Total amount (wt %) of palladium in the form of metallic state (Pd^0), palladium chloride (Pd^{+2}), and palladium oxide (PdO) in the bimetallic catalysts with the different amount of palladium and gold, Based on the results of x-ray photoelectron spectroscopy. The catalysts were supported on the ACC oxidized with nitric acid and calcined in air at different temperatures.

Catalyst	Pd^0 (wt%)	Pd^{+2} (wt%)	PdO (wt%)
1 wt% Pd_3 wt% Au, Tcal=185 °C	94.20	5.80	0.00
1 wt% Pd-3 wt% Au, Tcal=235 °C	90.94	5.65	3.42
1 wt% Pd-3 wt% Au, Tcal=275 °C	83.86	4.90	11.24
3 wt% Pd-1 wt% Au, Tcal=185 °C	93.54	5.79	0.67
3 wt% Pd-1 wt% Au, Tcal=235 °C	86.04	5.48	8.48
3 wt% Pd-1 wt% Au, Tcal=275 °C	36.86	0.00	63.14
2.5 wt% Pd-2.5 wt% Au, Tcal=185 °C	96.39	3.61	0.00
2.5 wt% Pd-2.5 wt% Au, Tcal=235 °C	97.06	2.80	3.26
2.5 wt% Pd-2.5 wt% Au, Tcal=275 °C	83.06	2.18	14.76
1 wt% Pd-1 wt% Au, Tcal=275 °C	60.11	0.56	39.33
2 wt% Pd-3 wt% Au, Tcal=275 °C	71.26	0.48	28.26
3 wt% Pd-2 wt% Au, Tcal=275 °C	67.16	0.68	32.16

Table 14. Total amount (wt %) of palladium in the form of palladium oxide (PdO) in the different samples of the catalysts with 3 wt% Pd and 1 wt% Au, and with 1 wt% Pd and 1 wt% Au supported on the ACC oxidized with nitric acid and calcined in air at 275 ºC, based on the results of x-ray photoelectron spectroscopy.

Sample	PdO (wt %)
3% Pd – 1% Au ($T_{calcination}$=275 °C)	63
3% Pd – 1% Au ($T_{calcination}$=275 °C); after H_2O_2 hydrogenation reaction (P_{H2}=4.1 bar, $T_{reaction}$= 298.15 K, $t_{reaction}$=5 min)	21
3% Pd – 1% Au ($T_{calcination}$=275 °C); after H_2O_2 hydrogenation reaction (P_{H2}=4.1 bar, $T_{reaction}$= 298.15 K, $t_{reaction}$=15 min)	20
3% Pd – 1% Au ($T_{calcination}$=275 °C); after H_2O_2 hydrogenation reaction (P_{H2}=4.1 bar, $T_{reaction}$= 298.15 K, $t_{reaction}$=30 min)	17
3% Pd – 1% Au ($T_{calcination}$=275 °C); after H_2O_2 hydrogenation reaction (P_{H2}=4.1 bar, $T_{reaction}$= 298.15 K, $t_{reaction}$=60 min)	14
1% Pd – 1% Au ($T_{calcination}$=275 °C)	39
1% Pd – 1% Au ($T_{calcination}$=275 °C); after H_2O_2 hydrogenation reaction (P_{H2}=4.1 bar, $T_{reaction}$= 298.15 K, $t_{reaction}$=5 min)	16
1% Pd – 1% Au ($T_{calcination}$=275 °C); after H_2O_2 hydrogenation reaction (P_{H2}=4.1 bar, $T_{reaction}$= 298.15 K, $t_{reaction}$=15 min)	15
1% Pd – 1% Au ($T_{calcination}$=275 °C); after H_2O_2 hydrogenation reaction (P_{H2}=4.1 bar, $T_{reaction}$= 298.15 K, $t_{reaction}$=30 min)	14
1% Pd – 1% Au ($T_{calcination}$=275 °C); after H_2O_2 hydrogenation reaction (P_{H2}=4.1 bar, $T_{reaction}$= 298.15 K, $t_{reaction}$=60 min)	12

3.1.2.2.5.The effect of the reaction temperature

The results in Fig. 51 demonstrate that the hydrogenation of H_2O_2 is strongly affected by the reaction temperature. The results show that:

a) Increasing the reaction temperature resulted in more H_2O_2 destruction. Maximum destruction was observed at 21 °C
b) The outstanding result is that in the case of the catalyst with 1 wt% Pd and 1 wt% Au and at reaction temperature equal to 0 °C, the hydrogenation of H_2O_2 was negligible. The hydrogenation of H_2O_2 at 0 °C and after 1h reaction time was about 0.78 wt% which it is really low.

c) In the case of catalyst with 1 wt% Pd and 3 wt% Au, hydrogenation activity of the catalyst at 21 °C is at least 3 times more than at 0 °C (see exact values in Table 11).

Temperature affects, of course, also the hydrogenation rate by changing the activation energy of the reaction and the solubility of hydrogen in methanol.

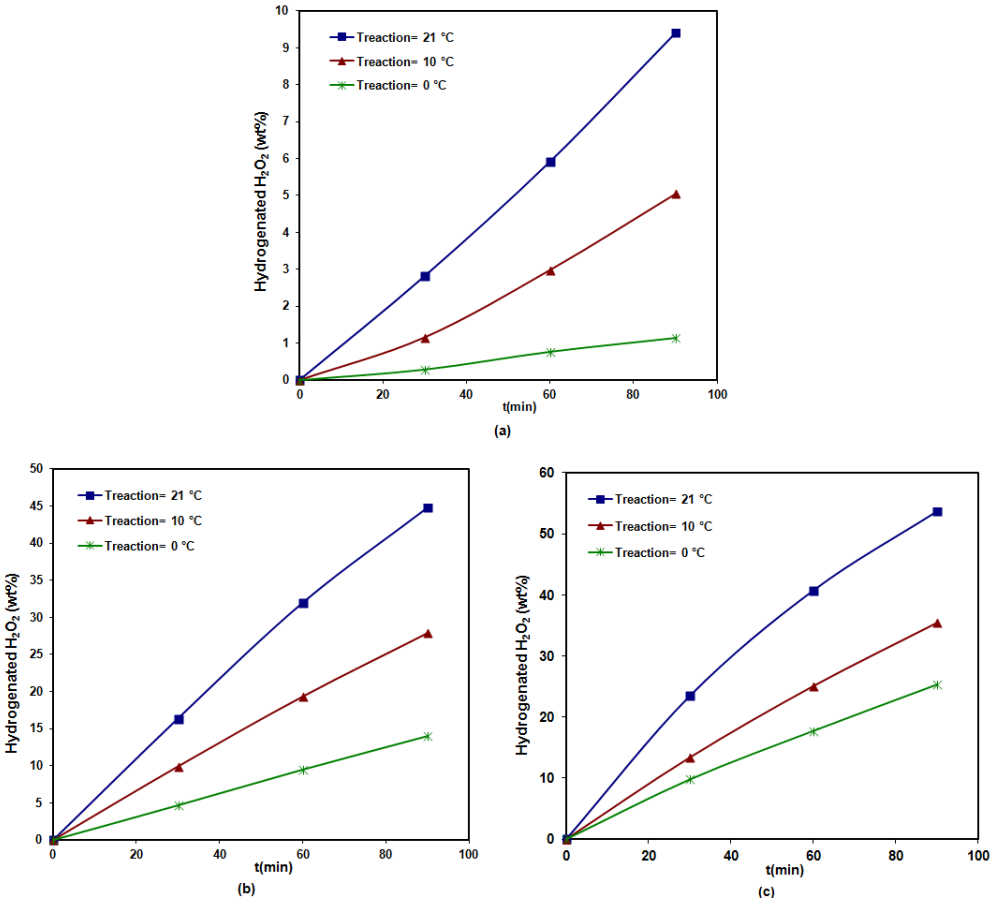

Figure 51. The effect of the reaction temperature on the final hydrogenation activity of the bimetallic catalysts with: (a) 1 wt% Pd and 1 wt% Au, (b) 1 wt% Pd and 3 wt% Au, (c) 4 wt% Pd and 1 wt% Au. All catalysts supported on oxidized ACC. Mass of catalyst = 56 mg and P_{H2}= 4 bar.

3.1.2.2.6.The effect of the solvent (reaction medium)

Hydrogenation rates of H_2O_2 in water and methanol are shown in Fig. 52. The results demonstrate that hydrogenation of H_2O_2 is highly affected by the reaction medium. It indicates that methanol significantly stabilized H_2O_2. Despite of higher solubility of H_2 in

methanol, hydrogenation of H_2O_2 in water was much faster than in methanol. According to S. Melada *et al.* [24], the most reactive sites of the catalyst could be blocked by formate compounds prohibiting HO-OH bond cleavage.

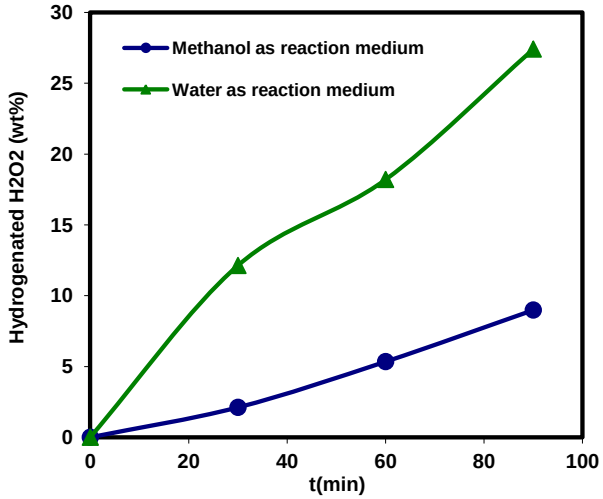

Figure 52. The effect of the reaction medium on the final hydrogenation activity of the catalyst with 1 wt% Pd and 1 wt% Au supported on oxidized ACC and calcined in air at 185 °C. Mass of catalyst = 56 mg, $T_{reaction}$= 21°C, and P_{H2}= 4 bar.

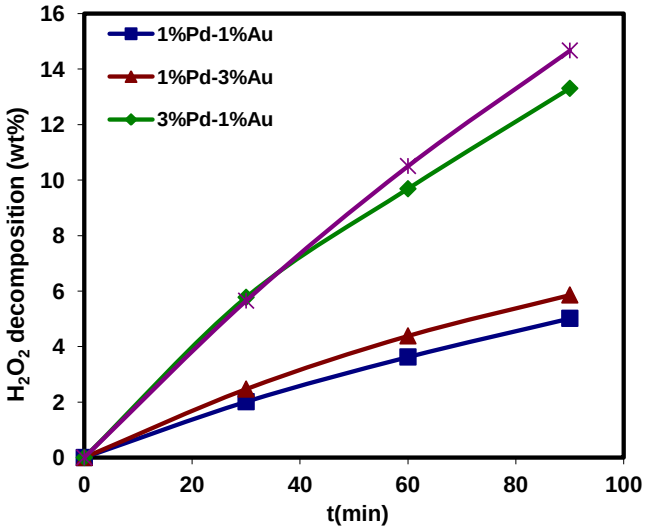

Figure 53. Destruction of H_2O_2 by its decomposition over the bimetallic catalysts supported on oxidized ACC and reduced by H_2 at 185 °C. Mass of catalyst = 56 mg, $T_{reaction}$= 21°C, and P_{N2}= 4 bar.

3.1.2.3. Destruction of H_2O_2 by its decomposition

3.1.2.3.1. Catalysts supported on the ACC oxidized with nitric acid

Based on the results of the decomposition of H_2O_2 over bimetallic catalysts supported on the ACC oxidized with nitric acid, it can be mentioned that:

a) In the case of the catalysts with 1 wt% palladium and calcined in air at 185 °C, decomposition of H_2O_2 was almost zero.
b) In the case of catalysts with 2 wt% palladium or more and calcined in air at 185 °C, decomposition of H_2O_2 was still negligible (less than 0.60 wt% after 1.5h).
c) Increasing the calcination temperature to 235 °C and 275 °C increased H_2O_2 decomposition. For the catalysts with 1 wt% palladium, the decomposition rate was still negligible (less than 0.55 wt% after 1.5h of the reaction time). For the catalysts with 2 wt% palladium or more, the decomposition rate was slightly higher (less than 1.5 wt % after 1.5 h of the reaction time) when compared to the catalysts with 1 wt% Pd. However, it is still much lower than the hydrogenation rates presented in Table 11.
d) Maximum H_2O_2 decomposition rate was obtained with the catalysts reduced by H_2 at 185 °C (Fig. 53). In these catalysts, the H_2O_2 decomposition activity was considerably increased with increasing the amount of palladium (see exact values in Table 15).

As it was already discussed in section 3.1.2.2.4, heat treatment of the catalysts supported on oxidized ACC caused damages on the oxygen-containing sufrace functional groups. These damages increase the rate of H_2O_2 decomposition.

3.1.2.3.2. Catalysts supported on the non-oxidized ACC

In the case of the catalysts supported on the non-oxidized ACC, decomposition rate was dependent on the amount and ratio of palladium and gold. However, independent of the heat treatment, it was changed between 1 to 5 wt% after 1.5 h of the reaction time (see exact value in Table 15). These decomposition rates are still quite low when compared to the hydrogenation rate of H_2O_2 (see the hydrogenation results in Table 11).

Table 15. Destruction of H_2O_2 by its decomposition over the bimetallic catalysts after 1.5 h.

Sample	H_2O_2 decomposition (wt%)
Catalysts supported on oxidized ACC	
(1% Pd_1% Au)/ OACC, Reduced by H_2 at 185 °C	5.02
(1% Pd_3% Au)/ OACC, Reduced by H_2 at 185 °C	5.86
(3% Pd_3% Au)/ OACC, Reduced by H_2 at 185 °C	13.30
(2.5% Pd_2.5% Au)/ OACC, Reduced by H_2 at 185 °C	14,67
Catalysts supported on non-oxidized ACC	
(1% Pd_1% Au)/ NACC, calcined in air at 185 °C	1.28
(1% Pd_1% Au)/ NACC, calcined in air at 275 °C	1.21
(1% Pd_1% Au)/ NACC, Reduced by H_2 at 185 °C	1.18
(1% Pd_3% Au)/ NACC, calcined in air at 185 °C	2.94
(1% Pd_3% Au)/ NACC, calcined in air at 275 °C	3.11
(1% Pd_3% Au)/ NACC, Reduced by H_2 at 185 °C	3.01
(3% Pd_1% Au)/ NACC, calcined in air at 185 °C	4.92
(3% Pd_1% Au)/ NACC, calcined in air at 275 °C	4.85
(3% Pd_1% Au)/ NACC, Reduced by H_2 at 185 °C	5.01

3.1.3. Catalysts supported on Sibunit

Direct synthesis of H_2O_2 over Pd and Pd-Au catalysts supported on Sibunit were almost followed the same behavior observed with activated carbon cloth as support. In other words:

a) Pd-Au bimetallic catalysts were more selective and active in H_2O_2 direct synthesis when compared to the Pd monometallic catalysts.
b) Pd and Pd-Au catalysts supported on Sibunit oxidized with nitric acid were almost more active and selective than the corresponding ones on non-oxidized Sibunit.

However, the catalysts on Sibunit were not studied and developed as much as the catalysts on the activated carbon cloth. This happened because of the following reasons:

a) The early results showed that the catalysts on the activated carbon cloth were substantially more active and selective than the corresponding ones on Sibunit.
b) Because of mechanical elasticity and geometric flexibility, activated carbon cloth can be easily fit and changed in the microstructural plate reactor.
c) The only way to fix Sibunit particles in the microstructural plate reactor was by means of glue. Using glue raised two new challenges. Firstly, changing and regeneration of the catalyst in the microstructral reactor were really challenging. Secondly, deactivation of the catalyst by glue.

Because of these reasons, further development of the catalysts on Sibunit, and in general on carbon materials in the granular form, was stopped.

3.2. Continuous direct synthesis in the novel microstructured reactor

3.2.1. Long-term experiments

The steady state continuous direct synthesis of H_2O_2 was obtained by running long-term experiments. The effects of the inert gas, CO_2 and N_2, and the total gas pressure on the final rate of H_2O_2 production were studied (see the experimental procedure in Section 2.4.3.2). The direct synthesis was over 3 wt% Pd catalyst supported on the ACC oxidized with nitric acid. The results are shown in Figs. 54-56. It can be seen that the presence of CO_2 as well as the total gas pressure, considerably increases the H_2O_2 production rate and selectivity. Carbon dioxide affects, of course, direct synthesis by increasing the solubility of H_2 and O_2 in methanol [58] and stabilizing the produced H_2O_2 [1].

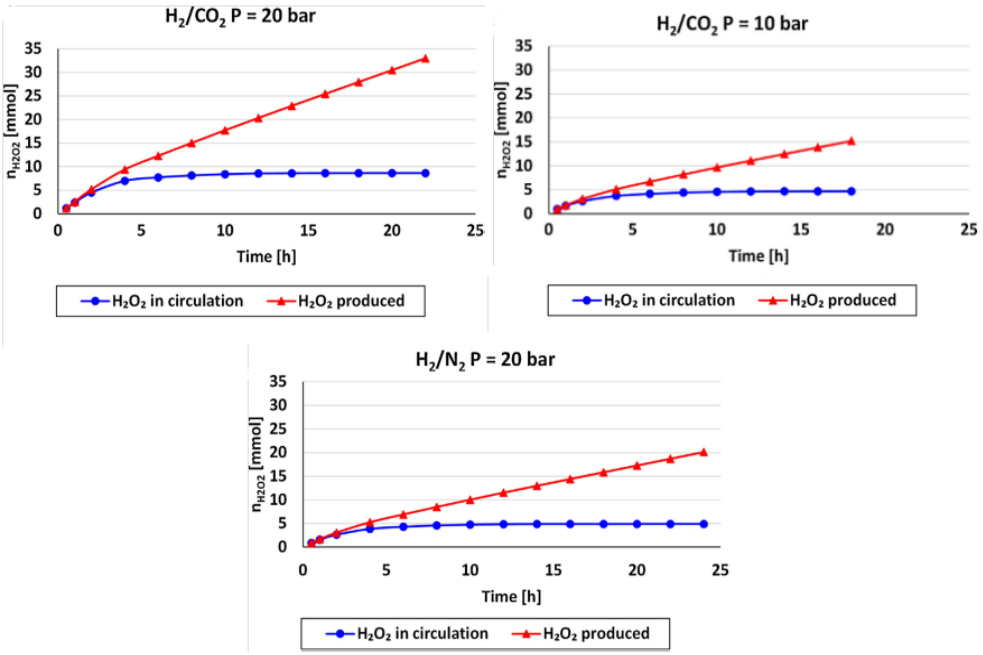

Figure 54. The cumulative amount of produced H_2O_2.

Table 16. Conditions in long-term experiments.

Liquid feed [ml/min]	Gas mixture	Gas feed [ml/min]	Product flow [ml/min]	Pressure [bar]	Catalyst	$m_{catalyst}$ [g]
68	CO_2/H_2	102	0.85	20	3 wt.% Pd	0.21
68	N_2/H_2	102	0.85	20	3 wt.% Pd	0.21
68	CO_2/H_2	102	0.85	10	3 wt.% Pd	0.21

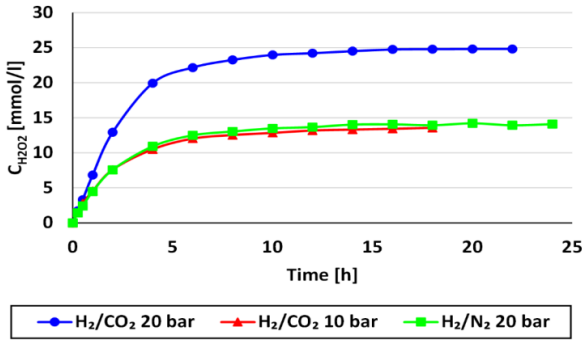

Figure 55. The H_2O_2 concentration in the product stream

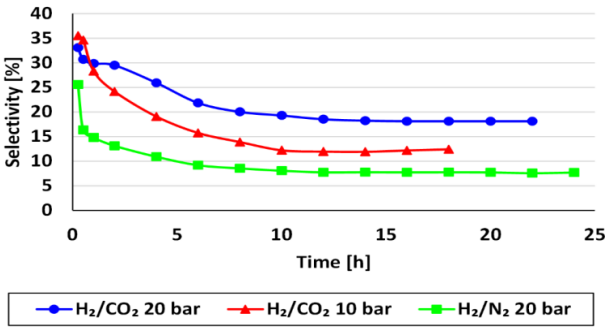

Figure 56. Selectivity

3.2.2. The effect of the liquid and gas feed rates

The effects of the liquid and gas feed rates were investigated by short-term experiments. The reaction time was 6 h. A set of experiments were run at different liquid and gas feed rates, while their ratio was kept constant (Table 17). The results are shown in Fig. 57. Another set of experiments were conducted with constant liquid feed rate, while the gas flow rate was changed in the reactor (Table 18). The results are shown in Fig. 58. All of the experiments were run at 20 bar and 0 ºC. The mass of catalyst was 0.21 g. The product stream taken out after the reactor was 0.85 ml/min.

Table 17. Experimental conditions for study the effect of liquid feed rate.

Liquid feed rate [ml/min]	Gas feed rate [ml/min]	Liquid/gas feed ratio
34	51	1.5
51	76.5	1.5
68	102	1.5

Table 18. Experimental conditions for study the effect of gas/liquid feed ratio.

Liquid feed [ml/min]	Gas feed [ml/min]	Gas/liquid feed ratio
68	51	0.75
68	102	1.00
68	150	2.21

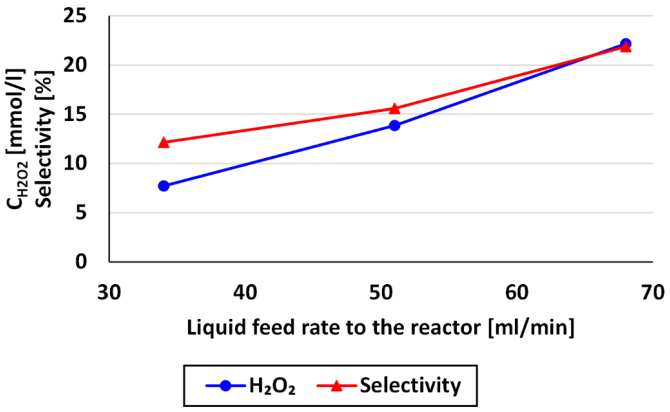

Figure 57. The effect of liquid feed rate

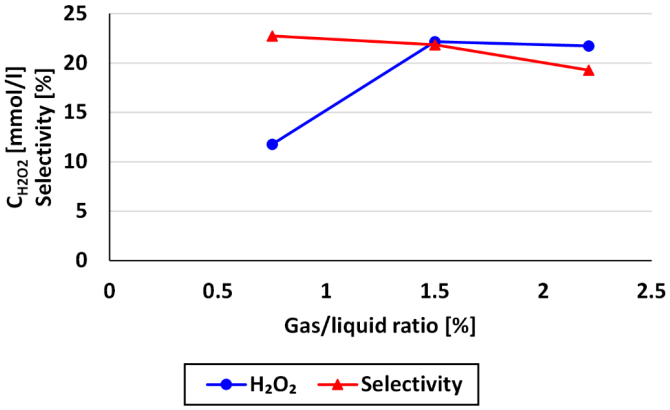

Figure 58. The effect of gas/liquid feed rates ratio.

3.3. Microstructured plate reactor development

The specification of the novel microstructured plate reactor was shown and discussed in section 2.4.3.1. This structure was selected in order to gain several advantages over more

conventional multichannel structures. Firstly, plugging problems were expected to be less severe and more uniform fluid distribution was anticipated. Secondly, changing and regeneration of the catalyst were assumed to be less complex, because the plates can be easily separated from each other. Two types of the structural elements, square and triangle, were used (Fig. 59). The final element's shape was selected based on the hydrodynamic properties and gas-liquid mass transfer measurements. High gas-liquid interfacial area and mixing enhance mass transfer between phases.

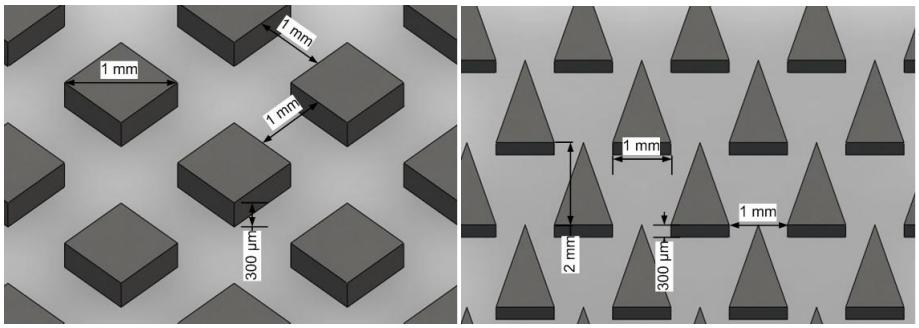

(a) **(b)**

Figure 59. Square structure layout (a) and triangular structure (b) layout and dimensions

3.3.1. Hydrodynamic study

In hydrodynamic studies, a transparent acrylic cover plate was used for visual observation. A high speed camera was used to capture still images from the flowing gas-liquid mixture in the plate reactor (Fig. 60). Water, as liquid phase, was fed with a flow rate of 20 to 100 ml/min. After water had filled the reactor, air was fed with a flow rate of 36 to 180 ml_n/min. The captured images were processed with ImagJ (a image process software) to determine gas hold up and gas-liquid interfacial area. For the sake of accuracy, several sample images from each flow combination were taken at different time spans. The results showed better hydrodynamic properties with the triangle elements (Fig. 61).

Gas holdup was in the range of 20–45%. The values of the total gas–liquid interfacial area were high up to 4800 and 5600 m^2m^{-3} for the square and triangular structure microreactor, respectively, which is much higher than in typical commercial gas–liquid reactors, where 1000 m^2m^{-3} is seldom exceeded.

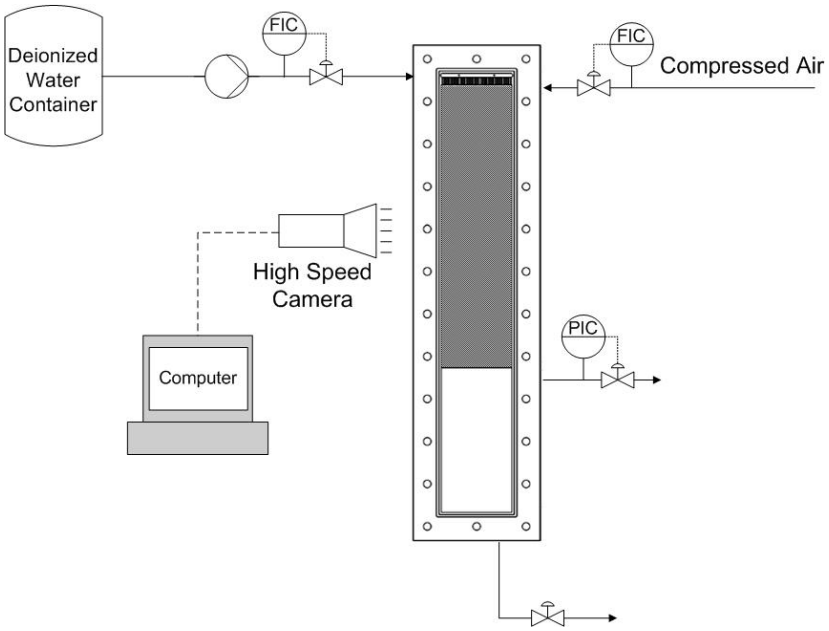

Figure 60. Experimental setup for the hydrodynamic studies.

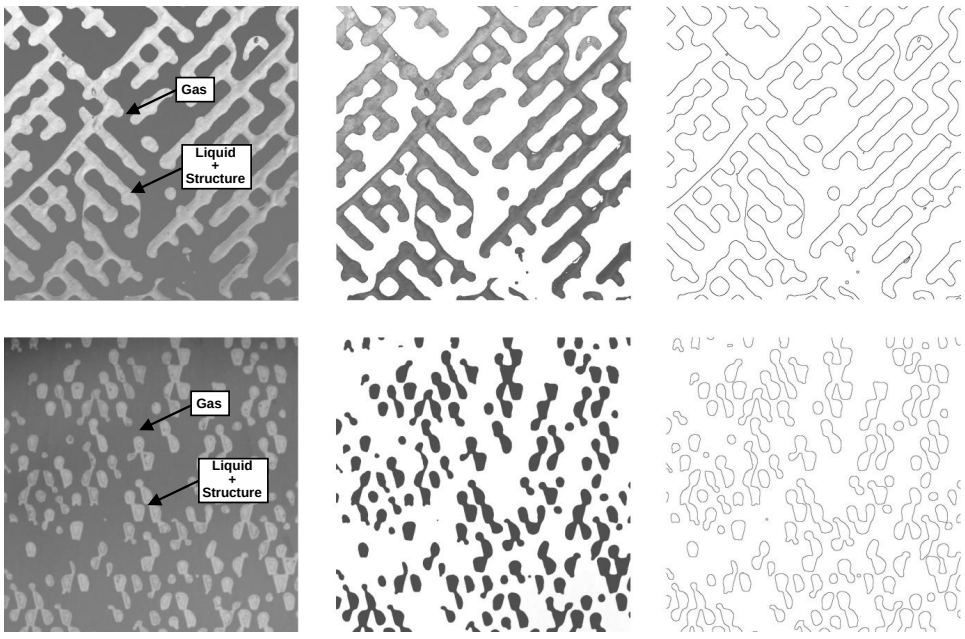

(a) (b) (c)

Figure 61. Image processing steps for gas holdup and gas-liquid interfacial area measurements: a) original image; b) processed image showing area of gas slugs; c) processed image showing perimeter of gas slugs.

3.3.2. Gas-liquid mass transfer measurements

A water–nitrogen–oxygen system was used for the mass transfer studies. Deionized water was saturated with oxygen, and nitrogen was used to strip oxygen out from the liquid phase in the plate reactor. The concentration of oxygen at the inlet and outlet of the reactor was measured by means of an in-line oxygen concentration analyzer (Fig. 62). The ranges of the gas and liquid flow rates were the same as in hydrodynamic study. Indeed, oxygen was transferred from the liquid phase to the gas phase and nitrogen vice versa. Changes in the oxygen and nitrogen molar flow in the gas phase along the microreactor can be described as:

$$\frac{d\dot{n}_{O_2}}{dL} = -k_l a\left(C^*_{O_2} - C_{O_2}\right)(1-\varepsilon_s)A_{cr} \tag{3-1}$$

$$\frac{d\dot{n}_{N_2}}{dL} = -\frac{D_{N_2}}{D_{O_2}} k_l a\left(C^{*}_{N_2} - C_{N_2}\right)(1-\varepsilon_s)A_{cr} \tag{3-2}$$

Concentrations of oxygen and nitrogen in liquid phase are changing according to the following equation:

$$\frac{dC_{O_2}}{dL} = k_l a\left(C^*_{O_2} - C_{O_2}\right)\frac{A_{cr}(1-\varepsilon_s)(1-\varepsilon_g)}{\dot{V}_l} \tag{3-3}$$

$$\frac{dC_{N_2}}{dL} = \frac{D_{N_2}}{D_{O_2}} k_l a\left(C^*_{N_2} - C_{N_2}\right)\frac{A_{cr}(1-\varepsilon_s)(1-\varepsilon_g)}{\dot{V}_l} \tag{3-.4}$$

The saturation concentrations of the nitrogen and oxygen are defined in Henry's law as:

$C^*_{N_2} = \frac{p_{N_2}}{H_{N_2}}$, and $C^*_{O_2} = \frac{p_{O_2}}{H_{O_2}}$,

$H_{N2} = 1639.34\frac{dm^3 \cdot bar}{mol}$, $H_{O2} = 769.23\frac{dm^3 \cdot bar}{mol}$

$p_{N_2} = \frac{\dot{n}_{N_2}}{\dot{n}_{O_2} + \dot{n}_{N_2}} \cdot P$, $p_{O_2} = \frac{\dot{n}_{O_2}}{\dot{n}_{O_2} + \dot{n}_{N_2}} \cdot P$

Given closed system of four ordinary differential equations (ODE) describes the two-phase mass transfer in the microreactor.

For the sake of simplicity and better numerical performance, the following normalized equation can be used:

$$k_l a = \alpha_1 \left(\frac{\upsilon_g}{\upsilon_{g,mean}} \right)^{\alpha_2} \left(\frac{\upsilon_l}{\upsilon_{l,mean}} \right)^{\alpha_3} \tag{3-5}$$

$k_l a$ values were estimated by minimizing the sum of the squared differences between the estimated and the measured values at the outlet of the reactor. Corresponding estimated optimal parameter values are shown in Table 19.

Table 19. Parameter values and correlation for mass transfer coefficient

Element type	α_1	α_2	α_3	**Correlation**
Square (◆)	0.177	0.874	0.179	$k_l a = 0.177 \left(\frac{\upsilon_g}{0.02} \right)^{0.874} \left(\frac{\upsilon_l}{0.02} \right)^{0.179}$
Triangular (▲)	0.175	0.899	0.432	$k_l a = 0.175 \left(\frac{\upsilon_g}{0.02} \right)^{0.899} \left(\frac{\upsilon_l}{0.02} \right)^{0.432}$

The mass transfer coefficient results are shown in Fig. 63. As it can be seen, higher mass transfer can be achieved with the triangle elements compare to the corresponding square elements. The maximum $k_l a$ value with the triangular elements was as high as 1.10 s−1, which was approximately 25% higher than in the square elements, where the highest value was 0.85 s−1. These values are one or two orders of magnitude higher than in conventional scale gas-liquid contactors (see publication VII).

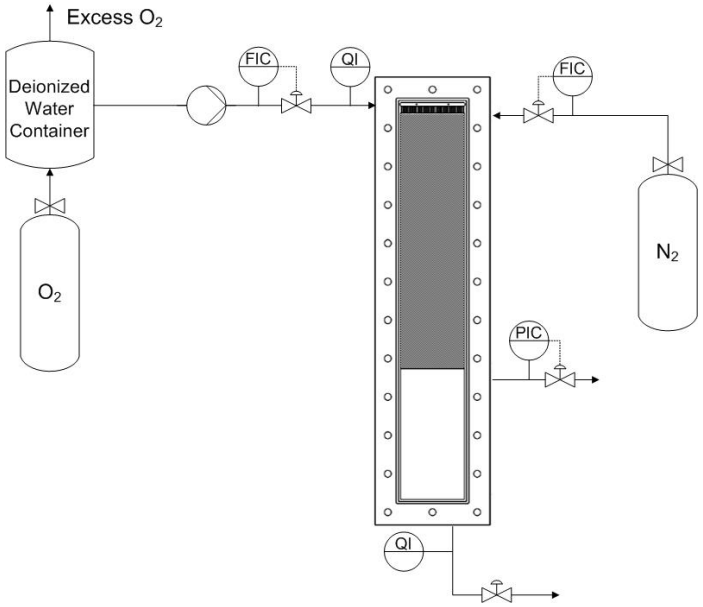

Figure 62. Experimental setup for mass transfer study.

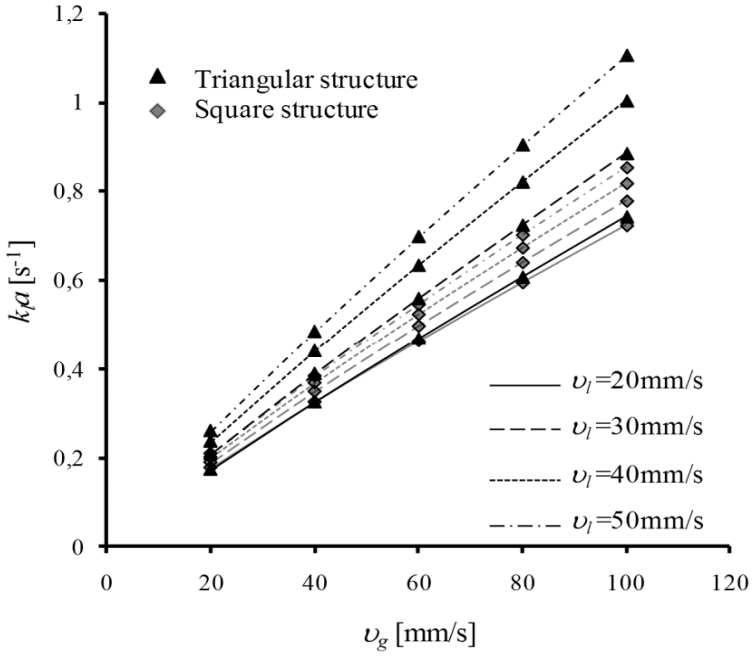

Figure 63. Estimated $k_l a$ dependency on υ_g and υ_l.

4. CONCLUSIONS

Direct synthesis from hydrogen and oxygen is a green alternative for production of hydrogen peroxide. However, it suffers from two challenges: safety of the process concerning the direct contact between hydrogen and oxygen and selectivity of the reaction in the presence of the other reaction pathways resulting in water production. A comprehensive study involving catalyst and microreactor development were carried out in order to offer a solution to these challenges.

A novel microstructured plate reactor was designed and developed. This plate structure avoids plugging problems and makes the changing and regeneration of catalyst easier. The microstructure was optimized based on the hydrodynamics and gas-liquid mass transfer. Substantial improvement in mass transfer and hydrodynamics was demonstrated when compared to conventional multiphase reactor. Also it was possible to optimize the microstruture in respect of mixing and mass transfer.

Palladium monometallic and palladium-gold bimetallic catalysts supported on Sibunit and activated carbon cloth were thoroughly studied. A set of new selective and active catalysts were developed. The early results showed that the catalysts supported on activated carbon cloth were substantially more active and selective than the corresponding ones on Sibunit. Furthermore, because of mechanical elasticity and geometric flexibility, activated carbon cloth can be easily fit and changed in the microstructured plate reactor. Therefore, it was selected as the main choice for the support of the final catalysts. It was observed that:

a) Wet oxidation of activated carbon cloth (ACC) with nitric acid resulted in formation of oxygen-containing functional groups on the surfaces of ACC fibers. These functional groups mainly control surface morphology, and consequently the selectivity and activity of the Pd and Pd-Au bimetallic catalyst. The catalysts supported on the ACC oxidized with nitric acid were substantially more selective and also more active in H_2O_2 production than the corresponding ones supported on non-oxidized ACC.
b) The presence of palladium oxide made the catalysts more selective and active in H_2O_2 production than the corresponding ones consisting of zero-valent palladium (Pd^0).
c) Heat treatment of the catalysts supported on the ACC oxidized with nitric acid in H_2 seriously damaged the oxygen-containing surface functional groups and resulted in substantial drop in the selectivity.

d) Almost all of the Pd-Au bimetallic catalysts were more selective than the Pd monometallic catalysts.
e) In the case of the bimetallic catalysts on the ACC oxidized with nitric acid, the size and morphology of the metal particles was also affected by the amounts of palladium, gold and their ratio.

Based on the H_2O_2 hydrogenation and decomposition results, it can be said:

a) The catalysts supported on the ACC oxidized with nitric acid were considerably less H_2O_2 destructive than the corresponding ones on non-oxidized ACC or ACC oxidized with acetic acid.
b) Almost all of the Pd-Au bimetallic catalysts were less destructive than the corresponding Pd monometallic ones.
c) In the case of the ACC oxidized with nitric acid as support, the catalysts calcined in air at 185 °C were the least destructive and the catalysts reduced by H_2 at 185 °C were the most destructive.
d) In the case of bimetallic catalysts, increasing the amount of gold and decreasing the amount of Pd resulted in low H_2O_2 destruction activity. Moreover, the bimetallic catalysts prepared by co-impregnation of Pd and Au, were less H_2O_2 destructive than the corresponding catalysts prepared by consequent impregnation approaches.
e) Using water instead of methanol as reaction medium substantially speeded up H_2O_2 destruction.
f) Furthermore, increasing the reaction temperature accelerated destruction of H_2O_2.
g) Finally, catalytic destruction of H_2O_2 via its decomposition was considerably low when compared to H_2O_2 hydrogenation.

A bench-scale continuous process was developed by employing the novel microstructured plate reactor. It was used to exploit the potential of the new selective catalysts. The effects of the process conditions were studied and promising results were obtained. The study demonstrated that the bench-scale process can be safely and effectively used in the laboratory for direct synthesis investigations. However, reactor and feed system modifications along with a separation unit would be needed to obtain higher concentrations of H_2O_2. Working in the explosive regime demands further safety studies. Finally, for commercial applications, a full-scale unit would have different design criteria and may be slightly different operation conditions.

It is also good to mention that the kinetic studies are going on by the same research group. The final goal is to apply gas-liquid mass transfer model along with the kinetics models to develop a full CFD model for the whole process of the continuous direct synthesis of H_2O_2 in the microstructured plate reactor.

REFERENCES

[1] C. Samanta, Appl. Catal. A: Gen. 350 (2008) 133–149

[2] http://www.arkema.com/sites/group/en/products/spotlight/h2o2.page.

[3] J. M. Campos-Martin, G. Blanco-Brieva, J. L. G. Fierro, Angew. Chem. Int. Ed. 45 (2006) 6962 – 6984.

[4] L. J. Thenard, Ann. Chim. Phys. 8 (1818) 306.

[5] H. J. Reidl, G. Pfleiderer (I.G. Farbenindustrie AG), US Patent 2,158,525 (1939).

[6] M. Piccinini, J. K. Edwards, J. A. Moulijn, G. J. Hutchings, Catal. Sci. Tech. 2 (2012) 1908–1913

[7] Henkel and W. Weber, US Patent110875, 1914

[8] C. E. Baukal, Oxygen-Enhanced Combustion, Second Ed., CRC, Boca Raton, 1998

[9] J.K. Edwards, G.J. Hutchings, Angew. Chem. Int. Ed. 47 (2008) 9192

[10] B. E. Solsona, J.K. Edwards, P. Landon, A.F. Carley, A. Herzing, C.J. Kiely, G.J. Hutchings, Chem. Mater. 18 (2006) 2689.

[11] A.G. Gaikwad, S.D. Sansare, V.R. Choudhary, J. Mol. Catal. A: Chem. 181 (2002) 143–149.

[12] V.R. Choudhary, A.G. Gaikwad, S.D. Sansare, Catal. Lett. 83 (2002) 235–239.

[13] V.R. Choudhary, S.D. Sansare, A.G. Gaikwad, Catal. Lett. 84 (2002) 81–87.

[14] C. Samanta, V.R. Choudhary, Catal. Commun. 8 (2007) 73–79.

[15] V.R. Choudhary, C. Samanta, T.V. Choudhary, Catal. Commun. 8 (2007) 1310–1316.

[16] C. Samanta, V.R. Choudhary, Appl. Catal. A: Gen. 326 (2007) 28–36.

[17] C. Samanta, V.R. Choudhary, Catal. Commun. 8 (2007) 2222–2228.

[18] C. Samanta, V.R. Choudhary, Chem. Eng. J. 136 (2008) 126-132.

[19] C. Samanta, V.R. Choudhary, Appl. Catal. A: Gen. 330 (2007) 23–32.

[20] V.V. Krishnan, A.G. Dokoutchaev, M.E. Thompson, J. Catal. 196 (2000) 366–374.

[21] D.P. Dissanayake, J.H. Lunsford, J. Catal. 214 (2003) 113–120.

[22] S. Abate, G. Centi, S. Melada, S. Perathoner, F. Pinna, G. Strukul, Catal. Today 104 (2005) 323–328.

[23] S. Melada, F. Pinna, G. Strukul, S. Perathoner, G. Centi, J. Catal. 235 (2005) 241-248.

[24] S. Melada, F. Pinna, G. Strukul, S. Perathoner, G. Centi, J. Catal. 237 (2006) 213-219.

[25] T.A. Pospelova, N.I. Kobozev, E.N. Eremin, J. Phys. Chem. 35 (1961) 143-147.

[26] T.A. Pospelova, N.I. Kobozev, J. Phys. Chem. 35 (1961) 262-265.

[27] K.P. Reis, V.K. Joshi, M.E. Thompson, J. Catal. 161 (1996) 62–67.

[28] D.P. Dissanayake, J.H. Lunsford, J. Catal. 206 (2002) 173–176.

[29] S. Chinta, J.H. Lunsford, J. Catal. 225 (2004) 249–255.

[30] Y-F. Han, J.H. Lunsford, J. Catal. 230 (2005) 313–316.

[31] Y-F. Han, J.H. Lunsford, Catal. Lett. 99 (2005) 13–19.

[32] Q. Liu, J.H. Lunsford, J. Catal. 239 (2006) 237–243.

[33] Q. Liu, J.H. Lunsford, Appl. Catal. A: Gen. 314 (2006) 94–100.

[34] V.Z. Radkevich, T.L. Senko, K. Wilson, L.M. Grishenko, A.N. Zaderko, V.Y. Diyuk, Appl. Catal. A: Gen. 335 (2008) 241–251.

[35] L. Fu, K. T. Chuang, R. Fiedorow, Stud. Surf. Sci. Catal. 72 *(*1992) 33–41.

[36] T. Danciu, E.J. Beckmann, T. Hancu, R.N. Cochran, R. Grey, D.M. Hajnik, J. Jewson, Angew. Chem. Int. Ed. 2 (2003) 1140–1142.

[37] E. N. Ntainjua, M. Piccinini, J. C. Pritchard, J K. Edwards, A. F. Carley, Ch. J. Kiely, G. J. Hutchings, Catal. Today 178 (2011) 47–50

[38] P. Landon, P.J. Papworth, C.J. Kiely, G.J. Hutchings, Chem. Commun. (2002) 2058–2059.

[39] P. Landon, P.J. Collier, A.F. Carley, D. Chadwick, A.J. Papworth, A. Burrows, C.J. Kiely, G.J. Hutchings, Phys. Chem. Chem. Phys. 5 (2003) 1917-1923.

[40] J.K. Edwards, B.E. Solsona, P. Landon, A.F. Carley, A. Herzing, C.J. Kiely, G.J. Hutchings, J. Catal. 236 (2005) 69–79.

[41] J.K. Edwards, B. Solsona, P. Landon, A.F. Carley, A. Herzing, M. Watanabe, C.J. Kiely, G.J. Hutchings, J. Mater. Chem. 15 (2005) 4595–4600.

[42] G. Li, J. Edwards, A.F. Carley, G.J. Hutchings, Catal. Today 122 (2007) 361–364.

[43] J.K. Edwards, A. Thomas, B.E. Solsona, P. Landon, A.F. Carley, G.J. Hutchings, Catal. Today 122 (2007) 397–402.

[44] G. Li, J. Edwards, A.F. Carley, G.J. Hutchings, Catal. Today 114 (2006) 369–371.

[45] V.R. Choudhary, C. Samanta, T.V. Choudhary, Appl. Catal. A: Gen. 308 (2006) 128–133.

[46] J. K. Edwards, A. F. Carley, A. A. Herzing, C. J. Kiely, G. J. Hutchings, Faraday Discuss. 138 (2008) 225–239.

[47] J. K. Edwards, E. Ntainjua, A. F. Carley, A. A. Herzing, C. J. Kiely, G. J. Hutchings, Angew. Chem., Int. Ed. 48 (2009) 8512–8515.

[48] V.V. Krishnan, A.G. Dokoutchaev, M.E. Thompson, J. Catal. 196 (2000) 366–374.

[49] M. Rueter, B. Zhou, S. Parasher (Headwaters Nanokinetix Inc.) US Patent 7,144,565 (2006).

[50] Y. Voloshin, A. Lawal, *Chem. Eng. Sci*. 65 (2010) 1028-1036.

[51] J. K. Edwards, B. Solsona, E. Ntainjua N., A. F. Carley, A. A. Herzing, C. J. Kiely, G. J. Hutchings, Science 20 Vol. 323 Nr. 5917 (2009) 1037-1041.

[52] K. Y. Lee, J. E. Na, J. Y. Lee, J. N. Kim, Bull. Korean chem.soc. 125 (2004) 1280–1282.

[53] Y. Lin, H. Teng , Carbon 41 (2003) 2865-2871.

[54] L. Prati, F. Porta, Appl. Catal. A: Gen. 291 (2005) 199-206.

[55] O. A. Simakova, P. A. Simonov, A. V. Romanenko, I. L. Simakova, React. Kinet. Catal. Lett. 95 (1) (2008) 3-12.

[56] A. Villa, C. Campione, L. Prati, Catal. Lett. 115 (2007) 133–136

[57] G.E Shter, Yu Shindler, Yu Matatov-Meytal, G.S Grader, M Sheintuch, carbon 40 (2002) 2547-2557

[58] N. Gemo, P. Biasi, T. Salmi, P. Canu, J. Chem. Thermo. 54 (2012) 1-9

[59] C. Moreno-Castilla, M.V. Lo´pez-Ramo´n, F. Carrasco-Mar´ın, Carbon 38 (2000) 1995-2001.

[60] S.R. de Miguel, J.I. Vilella, E.L. Jablonski, O.A. Scelza, C. Salinas-Martinez de Lecea, A. Linares-Solano, Appl. Catal. A: Gen. 232 (2002) 237-246.

[61] P. A. Simonov, A. V. Romanenko, I. P. Prosvirin, E. M. Moroz, A. I. Boronin, A. L. Chuvilin and V. A. Likholobov, Carbon 35 (1997) 73-82.

[62] M.L. Toebes, J.A. van Dillen, K.P. de Jong, J. Mol. Catal. A: Chem. 173 (2001) 75-98.

[63] F. Rodriguez-Reinoso, Carbon 36 (1998) 159-175.

[64] M. Haruta, Catalysis Today 36 (1997) 153–166.

[65] L. Prati, A. Villa, Catalysts 2 (2012) 24-37.

[66] L. Prati, Gold Bull. 32(1999) 96–101.

Publication I

D. Gudarzi, W. Ratchananusorn, I. Turunen, T. Salmi, M. Heinonen
Preparation and study of Pd catalysts supported on activated carbon cloth (ACC) for direct synthesis of H_2O_2 from H_2 and O_2
Topics in Catalysis 56 (2013) 527–539

Top Catal (2013) 56:527–539
DOI 10.1007/s11244-013-0014-5

Preparation and Study of Pd Catalysts Supported on Activated Carbon Cloth (ACC) for Direct Synthesis of H_2O_2 from H_2 and O_2

Davood Gudarzi · Warin Ratchananusorn · Ilkka Turunen · Tapio Salmi · Markku Heinonen

Published online: 16 April 2013

Abstract Activated carbon cloths (ACCs) were used as supports for Pd catalysts. The catalyst preparation was carried out by the impregnation method using acidic solution of palladium dichloride ($PdCl_2$) as metal precursor. The effects of the oxidation state of the loaded metal, heat treatment of the catalysts in different atmosphere (H_2, air) at different temperatures and surface chemistry of the support on the catalyst characterizations and the catalytic activities were investigated. Wet oxidation of ACC was done by nitric acid in order to induce oxygen-containing surface functional groups. Surface chemistry of the support and oxidation state of the metallic phase was investigated by means of XPS, TPD, SEM, DTA and TGA tests. Direct synthesis of hydrogen peroxide from H_2 and O_2 was performed batch wise in a stainless steel autoclave. The reactions were conducted under high pressure (38 bar) at 0 °C and methanol was used as reaction medium. The direct synthesis results showed that the oxygen-containing surface functional groups increase the selectivity of the catalysts by reducing the rate of water production. Existence of the oxidized state of Pd (PdO) also makes the catalyst more selective than the corresponding zerovalent state (Pd0). PdO affected on selectivity by increasing the rate of H_2O_2 production and reducing the amount of production of water, simultaneously.

Keywords Hydrogen peroxide · Direct synthesis · Palladium catalyst · Activated Carbon Cloth · Catalyst characterization

D. Gudarzi (✉) · W. Ratchananusorn · I. Turunen
Department of Chemical Technology, Lappeenranta University of Technology, Lappeenranta 53851, Finland
e-mail: davood.gudarzi@lut.fi

T. Salmi
Laboratory of Industrial Chemistry and Reaction Engineering, Åbo Akademi University, Turku 20500, Finland

M. Heinonen
Department of Physics and Astronomy, University of Turku, Turku 20014, Finland

1 Introduction

Hydrogen peroxide (H_2O_2) is one of the most powerful and environmentally friendly known oxidizers with a wide range of applications in pulp bleaching, waste water treatment, cosmetic and pharmaceutical industries. Commercially, hydrogen peroxide is mainly produced by the sequential hydrogenation and oxidation of an alkyl anthraquinone (auto-oxidation method). This method is more economical for large-scale production. The simplest method to produce hydrogen peroxide and the main challenger of anthraquinone auto-oxidation method is the direct catalytic synthesis of hydrogen peroxide from elemental hydrogen and oxygen. The direct method suffers from two serious technical challenges. Firstly, mixtures of hydrogen and oxygen are explosive over a wide range of concentrations (4–94 % H_2 in O_2) [1]. Secondly, the catalytic reaction of hydrogen and oxygen involves several reaction pathways and most of them result in the production of water (Scheme 1). Mainly because of these two challenges, the direct method has not been commercialized yet even though it has been widely studied.

Supported Pd catalysts are the most common ones for the direct synthesis of hydrogen peroxide [2]. The most common supports have been carbon, silica (high surface area materials), alumina and silica-alumina (relatively low surface area materials). From these, activated carbon

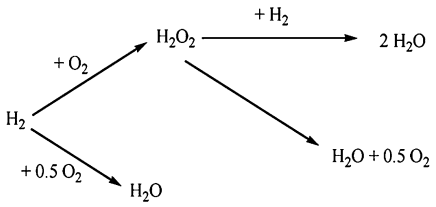

Scheme 1 Reactions involved in the direct synthesis of H_2O_2

materials as support have resulted in best activity and selectivity [3]. In addition, Pd on activated carbon has many advantages, e.g. chemical stability, availability, and easy recovery of Pd metal by just burning off carbon components [3]. Structured forms of activated carbons, such as activated carbon felts and activated carbon cloths (ACCs) represent promising alternatives due to their excellent characteristics and properties [4]. Literature concerning activated carbon cloths and felts as catalyst supports is relatively limited so far, while granular carbonaceous supports are well covered.

The direct catalytic synthesis of H_2O_2 from H_2 and O_2 has remained a challenging research target for over 90 years [5]. Choudhary et al. [6] have shown that catalyst properties such as particle size and surface area are less important than the oxidation state of Pd in determining selectivity of Pd catalysts for this reaction. They have claimed that existence of the oxidized state of Pd (PdO) makes the catalyst more selective than the corresponding zerovalent state (Pd^0) catalyst [7–9]. In contrast, some studies have declared that higher H_2O_2 activity and selectivity can be achieved with Pd^0 catalysts [10–12]. Fu et al. [13] demonstrated that metal particle size and specific surface area affect less on H_2O_2 yield and selectivity than the surface chemistry of the support. The acidity of the support is also an important characteristic of the Pd catalysts [5]. Pd catalysts on acidic support e.g. Pd/SiO_2 were found to be more active than basic catalysts (Pd/Al_2O_3) [5]. Using of halide ions (especially Cl^- and Br^-) and protons (H^+) as promoters, in order to improve the selective oxidation of H_2 to H_2O_2 over Pd-based catalysts, have been investigated in several papers [7–12, 14–26]. The catalytic performance of the Pd catalysts is also strongly dependent on the H_2:O_2 composition, total pressure, and the reaction temperature. Low temperature, high pressure, and the presence of a stabilizer in the reactant all lead to improved yields of H_2O_2 [5].

The goal of this paper is to study and test Pd catalysts on activated carbon cloth in the direct synthesis of H_2O_2. This kind of catalyst will be used in a novel microreactor [27].

2 Catalyst Preparations

A commercial activated carbon cloth ACC-5092-20 (Kynol Europa GmbH), after a thermal and a chemical treatment, was employed as support. Palladium (II) chloride ($PdCl_2$, purity 99.999 %, Sigma-Aldrich) was used as a precursor for the metallic palladium catalyst. Nitric Acid (Merck) was used for acid pretreatment of the support.

The activated carbon cloth was first treated in the oven at 100 °C for about 12 h. Then acid pretreatment was accomplished by a 20 % solution of nitric acid at room temperature for 40 h. After this oxidative treatment the samples were washed with distilled water until neutral conditions were reached, and then dried at 100 °C for 24 h. This sample is referred as oxidized ACC. Acid treatment is a common method to create oxygen-containing functional groups on the surface of activated carbon, to remove the mineral elements and to modify the surface of activated carbon materials [28–31].

A series of Pd catalysts on non-oxidized and oxidized activated carbon cloth were prepared by impregnation of the supports with an aqueous acidic solution of $PdCl_2$ at room temperature for 12 h. The impregnation was done in a 100 ml reactor with stirring rate of 1,000 rpm. The ratio of the solution volume to catalyst mass was 200 ml/g. The concentration of the metal precursor between 174.9 and 874.68 mg/l for 1 g of the support gave palladium loading in the range 1–5 wt%. After impregnation, the catalysts were left at room temperature for 3 h, and then dried at 60 °C during 24 h. To investigate the effects of the oxidation state of the metallic phase on the catalytic performances, the dried fresh catalysts were finally treated with different processes. The reduced samples were prepared by treating the fresh dried catalysts with H_2 at 185 °C under 3.5 bar overnight. A series of different calcined samples were prepared by oxidizing the fresh dried catalysts at temperatures 135, 185 and 235 °C in static air overnight. The calcination temperatures were selected according to the TGA/DTA results in order to be in the safe thermal treatment region of ACCs.

3 Characterization of the Catalysts

3.1 Textural Characterization

The distribution of pore volume with respect to pore size (pore-size distribution), the specific surface area and the pore volumes were deduced for each sample from N_2 adsorption and desorption isotherms at −196 °C in an automatic system Sorptomatic 1900 from Carlo Erba Instruments. Before N_2 adsorption tests, the samples were treated by degasification process. For degassing, about

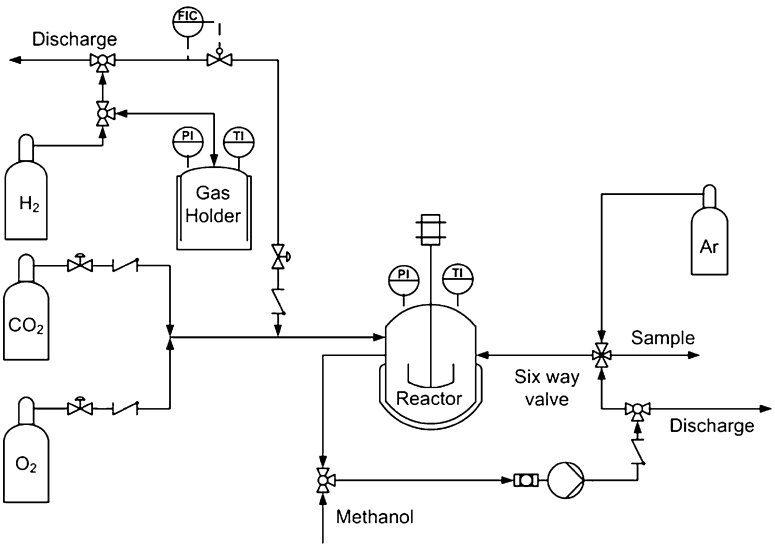

Fig. 1 Experimental set up for direct synthesis of H_2O_2

200 mg of the sample was put in the sample tube and left for constant heating at 100 °C until the pressure was stable at 1.06×10^{-3} Pa. This treatment removed water, volatile impurities and other gases adsorbed or trapped in the porous texture. The surface area obtained from N_2 adsorption (S_{N_2}) was calculated by using the Dubinin-Radushkevich equation.

3.2 Surface Morphology of the ACC and Pd/ACC Catalysts

Surface morphology of the ACC (oxidized and non-oxidized) and Pd/ACC catalysts were investigated by scanning electron microscopy (SEM). The SEM/EDS analysis was done by using a JEOL JSM-5800 microscope with X-ray detector for microanalysis (Noran Instrument Co.).

3.3 Thermal Analysis

Thermal characterization of the supports and the catalysts were done by differential thermal analysis (DTA) and thermogravimetry (TGA) using a NETZSCH STA 449 C Jupiter analyzer. Weight loss and heat flow during linear heating were measured. The analyses were done in oxidized conditions. He was used as protective gas and O_2 as purge gas. The flow rates of He and O_2 were 40 ml/min and 20 ml/min, respectively. The furnace was heated up from 20 to 700 °C with heating rate 5 °C/min.

The observed thermal effects in the TGA/DTA curves were interpreted according to the methodology presented by G. E. Shter et al. [32].

3.4 Characterization of the Surface Chemistry

The surface chemistry of the carbon materials is defined by the nature of the functional groups present on the surface. The surface chemistry of the oxidized and the non-oxidized activated carbon cloth was investigated by temperature programmed desorption (TPD) experiments. The TPD runs were carried out in a set-up made up of a U-shaped tubular reactor, placed inside an electrical furnace coupled to a Balzers OmniStar mass spectrometer for gas analysis. Around 200 mg of

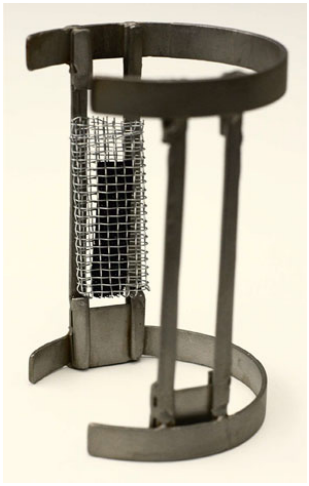

Fig. 2 Metal stand for catalyst installation in the autoclave

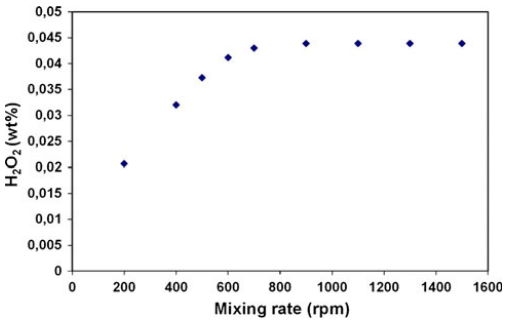

Fig. 3 The effect of the mixing rate on the reaction rate (3 % Pd/OACC, mass of catalyst = 55 mg, temperature = 0 °C)

the samples were heated with the rate of 50 °C/min up to 900 °C. During the tests, He was passed through the reactor with the flow rate equal to 60 ml/min [4]. The amounts of CO and CO_2 desorbed from the different samples were monitored and recorded with the mass spectrometer.

3.5 Metal Phase Characterization

3.5.1 The Amount of the Loaded Metal

Atomic absorption spectroscopy (AAS) was used to determine the amount of Pd in the support after impregnation, as well as the concentration (ppm) of Pd leached out into the solution during reaction. Latter figure was found out by determining the residual Pd content of the used catalyst and comparing it with that of the fresh catalyst. Atomic absorption spectroscopy was performed with a Thermo Scientific ICE 3000 series atomic absorption spectrometer using an air-acetylene flame.

3.5.2 Oxidation State of the Metal Phase

The chemical state of the metal phase in the different catalysts was investigated by X-ray photoelectron spectroscopy (XPS). The spectra were obtained with a Perkin Elmer 5400 spectrometer, by using the Mg Kα (1,253.6 eV) radiation of twin anode in the constant analyzer energy mode with pass energy of 37.75 eV. The pressure of the analysis chamber was maintained at 2×10^{-7} Pa. The binding energy scale was calibrated by setting the Au 4f7/2 transition to 84.0 eV. The spectra were analyzed by using Unifit peak-fitting program.

Table 1 Textural properties of Non-oxidized and oxidized ACC with HNO_3

Sample	S_{N_2} (m^2g^{-1})	Pore volume (cm^3g^{-1})	Pore size distribution (nm)
Non-oxidized ACC	1,788	0.63	9–25
Oxidized ACC	1,520	0.54	8–25

4 Catalytic Activity

The direct synthesis of hydrogen peroxide was carried out in a stainless steel autoclave (Parr Instruments Ltd) with a nominal volume of 450 ml and a maximum working pressure of 140 bar. The autoclave was equipped with an overhead stirrer (0–2,000 rpm) and facilities to measure the temperature and pressure. Hydrogen was fed into the reactor through a gas-holder with a volume of 33 ml and by means of a mass flow controller. The gas-holder was used to measure the precise amount of hydrogen fed to the system. A recirculation line equipped with a six-way valve was installed for sampling at different times (Fig. 1). The sampling line was designed in a way minimizing pressure changes (and consequently, loss of gases) in the reactor during sampling. ACC catalysts were fixed in the reactor by means of a metal stand (Fig. 2). The position of the catalyst and the stirrer in the autoclave were selected to generate similar flow condition as in the microreactor. Typically, the reactor was charged with about 55 mg of catalyst and successively with carbon dioxide up to 15.2 bar. The pressure was thereafter elevated to 20.2 bar with oxygen and further to 35.2 bar with carbon dioxide again. Methanol was employed as reaction medium. 175 g of methanol was pumped in and the reactor was cooled down to around −1 °C. Stirring (1,250 rpm) was begun after 2/3 of the methanol had been fed. Sufficient stirring speed for activity measurements was determined beforehand by carrying out a series of activity tests varying the stirring speed. As shown in Fig. 3, 1,250 rpm is sufficient speed to eliminate the effect of mass transfer phenomena. When the desired temperature was reached, the partial pressure of hydrogen was raised up to 3.2 bar by feeding

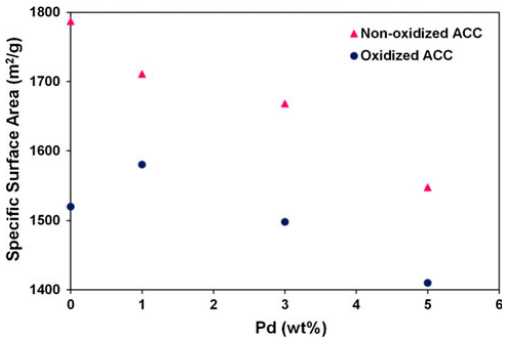

Fig. 4 Specific surface area vs. Pd content of the Pd catalysts

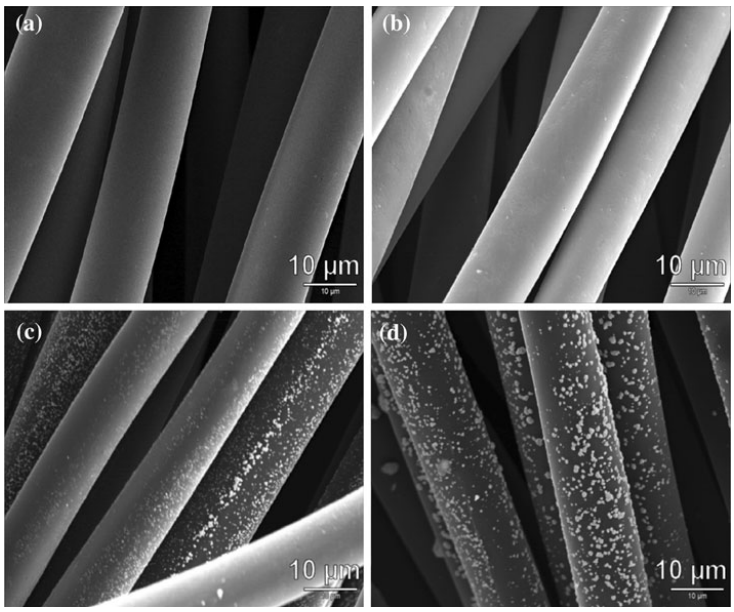

Fig. 5 SEM images of oxidized ACC with different Pd contents: **a** virgin oxidized ACC, **b** impregnated with 1 wt% Pd, **c** impregnated with 3 wt% Pd, **d** impregnated with 5 wt% Pd

from gas holder. The reaction time was now started. The tests were run for 3 h during which 11 samples were taken. During the experiments pressure went slightly down because hydrogen and oxygen were consumed.

The concentration of H_2O_2 which was formed in the reaction was measured quantitatively by a volumetric iodometry titration method, whereas the produced water was determined by coulometric Karl–Fischer titration using a Mettler DL35 Karl-Fischer titrator. The water content in the reaction medium before catalyst addition was determined prior to each experiment. Research grade oxygen, hydrogen and carbon dioxide were purchased from AGA Gases. Methanol with a purity of 99.9 % was used as solvent (Merck). KI (Merck), CH_3COOH (Purity 100 %, Merck), $K_2Cr_2O_7$ (purity 99.99 %, Aldrich) and $Na_2S_2O_3 \cdot 5H_2O$ (Merck) were used for iodometric titration of hydrogen peroxide. Water formation was determined by Karl-Fischer titration using hydranal reagents (Fluka).

5 Results and Discussions

5.1 Catalyst Properties

5.1.1 Surface Morphology and Textural Characterization of the ACC and Pd/ACC Catalysts

Textural characteristics of the non-oxidized and oxidized activated carbon cloth are shown in Table 1. It can be observed that the acid pretreatment with HNO_3 decreased the specific surface area (SSA) and porosity of the activated carbon cloth. This occurs because activation of carbon makes the pore walls thinner and, thus, more easily destroyable by the oxidizing agent [33]. However, the pore size distribution did not significantly change after the wet oxidation of ACC (Table 1). The effects of impregnation with Pd on the textural characteristic (SSA) of oxidized and non-oxidized ACC are shown in Fig. 4. These effects will be explained with the aid of SEM images in the following paragraphs.

The SEM images of the oxidized ACC without and with different Pd contents are presented in Fig. 5. The virgin oxidized ACC (Fig. 5a) almost looks like a flat fiber without any visible pores, cavities or bulk solid on the surface. This also agrees well with the results of the specific surface area and pore size distribution measurements (Table 1). It demonstrates that the ACC fibers contain mainly micropores with narrow size distribution between 8 to 10 nm which are invisible in the SEM image in Fig. 5a. The SEM image of oxidized ACC impregnated with 1 % Pd is almost the same as the virgin oxidized ACC. This observation demonstrates that almost all of the loaded Pd is located inside the micropores and, consequently, it is dispersed into very small sizes (less than the micropores size). Pd contents above 1 wt% lead to drastic morphology changes: large Pd particles on the outer surface of the ACC are clearly visible and presented in Fig. 5c-d for Pd loading of 3 and 5 %, respectively.

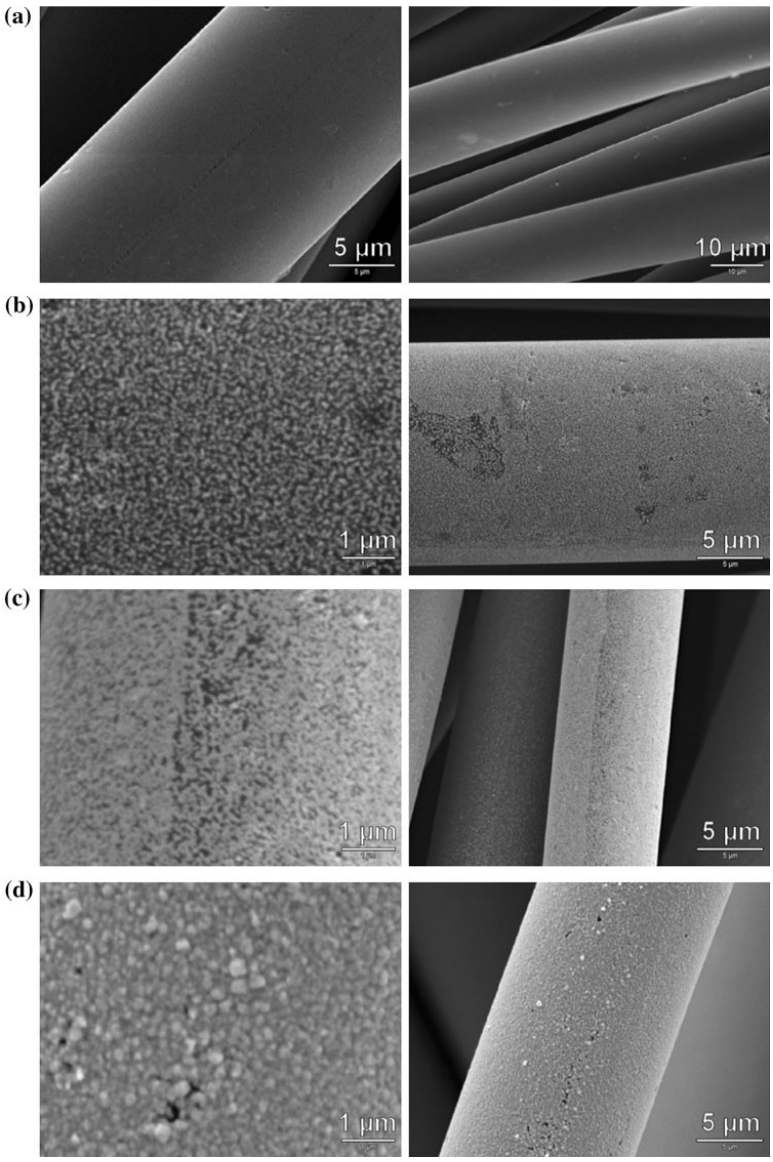

Fig. 6 SEM images of non-oxidized ACC with different Pd contents: **a** virgin non-oxidized ACC, **b** impregnated with 1 wt% Pd, **c** impregnated with 3 wt% Pd, **d** impregnated with 5 wt% Pd

The deposition of the big Pd particles on the outer surface of the ACC fibers resulted in clogging of ACC micropores and this fact is in well agreement with specific surface area measurements (Fig. 4). In fact, increasing Pd content from 1 to 5 wt% decrease the specific surface area (from 1,580 to 1,409 m^2/g). While impregnation with 1 wt% Pd even leads to an small increase in specific surface area (from 1,520 to 1,580 m^2/g). Locating of small Pd particles in the micropores can increase the roughness of the micropores' surface and consequently result in a small increase in micropores surface area.

Unlike oxidized ACC, impregnation of the non-oxidized ACC with Pd, even with low content of Pd, leads to form a very thin layer of small Pd particles on the outer surface of the ACC fibers (Fig. 6). The metallization of the outer surface of carbon fibers immersed in the acidic solution of

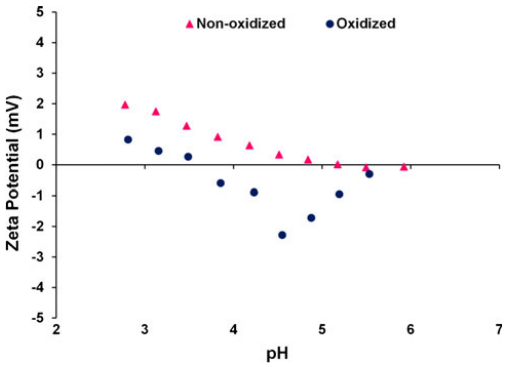

Fig. 7 Isoelectric point measurements of oxidized and non-oxidized ACC

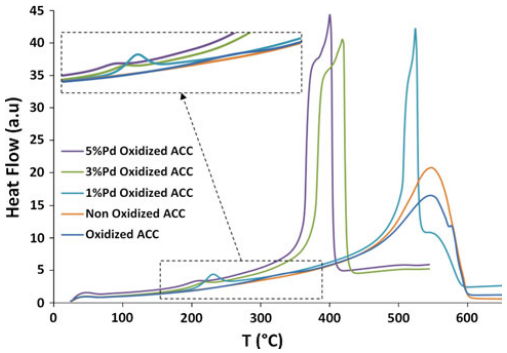

Fig. 8 DTA curves for oxidized ACC and Pd/ACC systems in oxidative atmosphere

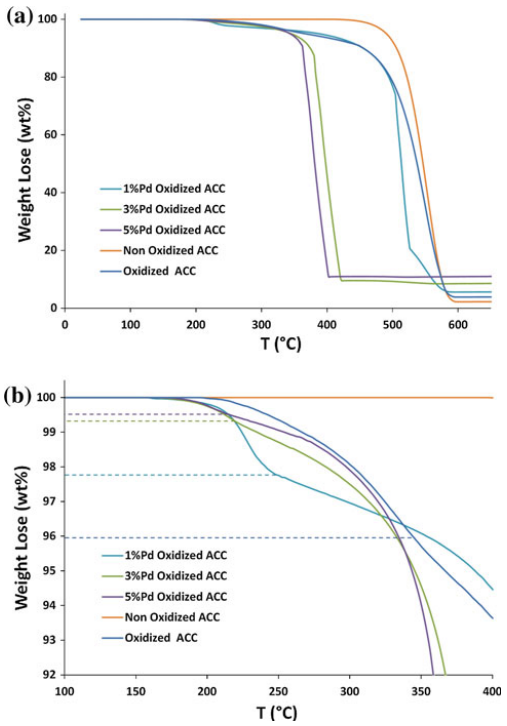

Fig. 9 TGA **a** curves and corresponding close-up of the first exothermic effect **b** for oxidized ACC and Pd/ACC systems in oxidative atmosphere

$PdCl_2$ can be even observed visually. The outer surface of the black ACC turned grey which is typical for palladium; while their interior, as seen upon cleavage of the fibers, remained black. Formation of the Pd particles and their crust-like distribution on the outer surface of the ACC fibers resulted in clogging of ACC micropores and this fact is well confirmed with specific surface area measurements (Fig. 4). In fact, impregnation with 1 % Pd results in a decrease in specific surface area (from 1,787 to 1,711 m^2/g). Increasing the amount of Pd content leads to bigger Pd particles and denser layer of Pd particles on the outer surface of the ACC fibers (Fig. 6c–d).

Simonov et al. [34] showed that ionic palladium (Pd^{2+}) in acidic solution of palladium dichloride ($PdCl_2$) appears mainly as tetrachloropalladic ion complex ($PdCl_4^{2-}$). The pH of the Pd precursor during the impregnation of the ACC was in the range of 3.5-4. According to isoelectric point measurements (Fig. 7), the pH_{IEP} of the oxidized and non-oxidized ACC were 3.5 and 5 respectively. The surface morphology changes of the non-oxidized and oxidized ACC impregnated with Pd could be explained as follow:

a) During the impregnation of non-oxidized ACC with Pd precursor, the pH of the precursor is considerably less than pH_{IEP} of the surface of the ACC. So, the electrostatic attraction between the positively charged surface ($pH < pH_{IEP}$) and the catalyst precursor anions ($PdCl_4^{2-}$) facilitate the adsorption of Pd anions ($PdCl_4^{2-}$) on the surface of the ACC fibers. Because the outer surface of the fibers is directly exposed to the Pd precursor, the adsorption of ($PdCl_4^{2-}$) occurs rapidly and leads to formation of the crust-like distribution of the Pd particles on the outer surface. It can be observed visually that the pale yellow color of the precursor disappears after a short contact of non-oxidized ACC with precursor. Indeed, the adsorption equilibrium was found to be established in ca. 20 min on the non-oxidized ACC and in about 3 h on the oxidized one.

b) Since carbon is essentially not hydrophilic in nature, it has a very low affinity for solvents of polar character

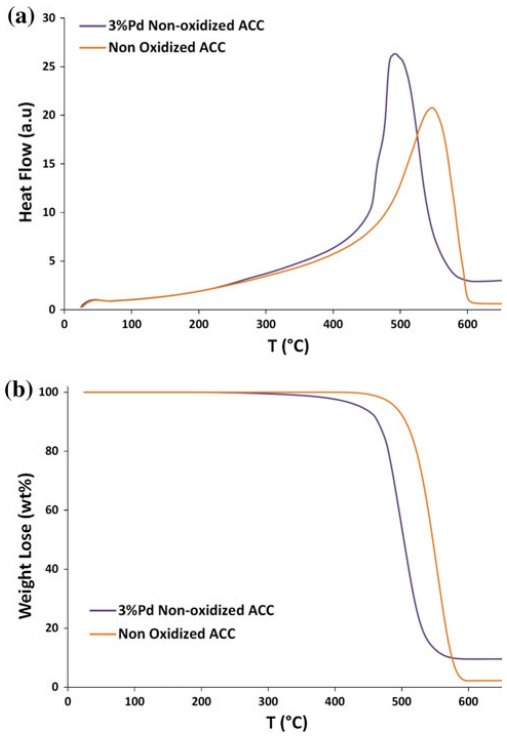

Fig. 10 DTA (**a**) and TGA (**b**) curves for non-oxidized ACC and 3 wt% Pd/ACC in oxidative atmosphere

Table 2 The characteristic temperatures in DTA/TGA curves

Sample	T_c (°C)	T_g (°C)	Burn-off (°C)
Non-oxidized ACC		455–465	495–595
3 % Pd/Non-oxidized ACC		300–320	460–580
Oxidized ACC	310–320	400–415	495–585
1 % Pd/Oxidized ACC	215–220	355–370	500–580
3 % Pd/Oxidized ACC	200–205	290–300	380–420
5 % Pd/Oxidized ACC	195–200	275–285	360–405

T_c the temperature at which oxygen starts to attack the ACC oxygen surface functional groups, T_g the temperature at which oxygen starts to attack the carbon fiber skeleton, $T_{burn\text{-}off}$ the burn-off temperature of the ACC

such as water [35]. The metal precursor will be mostly exposed to the outer surface of the carbon particle when using water, but it will penetrate to the interior pores when the hydrophobicity of carbon decreases. Acidic functional groups introduced by the treatment with HNO_3 decreases the hydrophobicity of the carbon [4] thus making the interior of the micropores more accessible to the aqueous solution of the metal precursor during impregnation. Indeed, acid pretreatment of the ACC facilitates the access to the interior surfaces of the ACC fibers. Therefore, it could lead to deposition of Pd particles during the impregnation in the interior surface area.

Table 3 Weight loss corresponding to the decomposition of the oxygen surface functional groups

Sample	Weight loss (wt%)
Oxidized ACC	4.12
1 % Pd/oxidized ACC	2.32
3 % Pd/oxidized ACC	0.71
5 % Pd/oxidized ACC	0.41

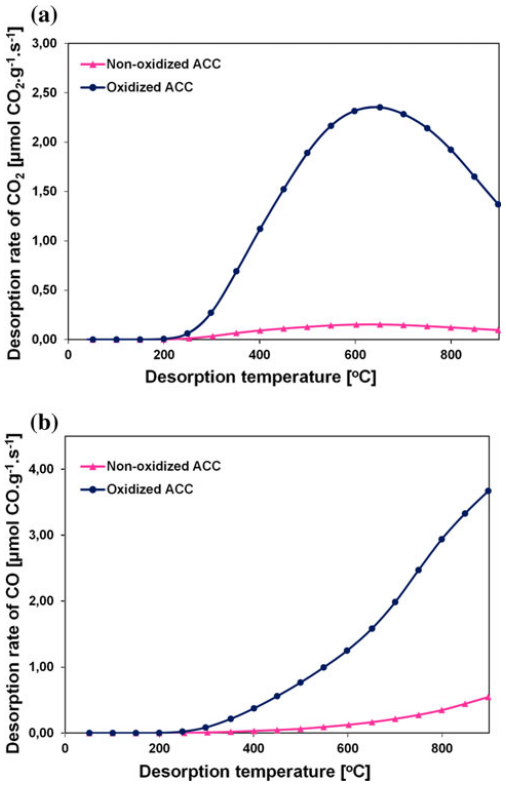

Fig. 11 The CO_2 (**a**), and CO (**b**) temperature programmed desorption profiles of the non-oxidized and oxidized of ACC

5.1.2 *Thermal analysis*

DTA and TGA profiles of virgin ACC (non-oxidized and oxidized) and impregnated ones with different Pd contents

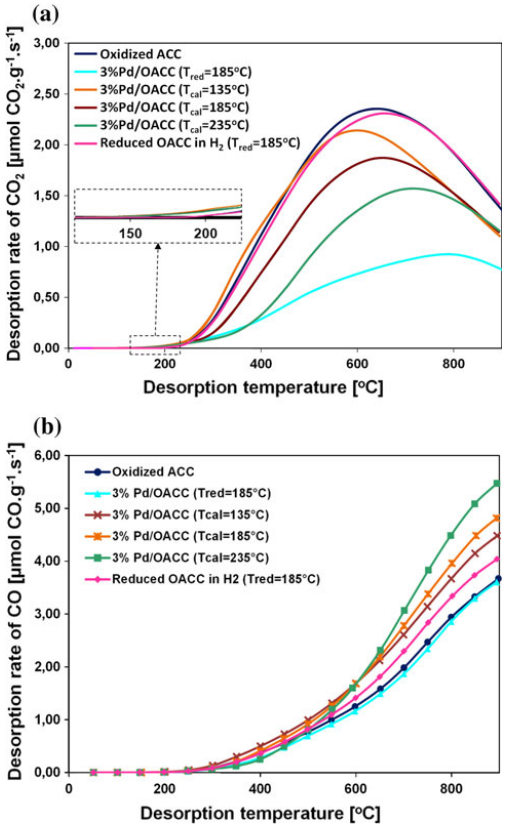

Fig. 12 The CO_2 (**a**), and CO (**b**) temperature programmed desorption profiles of the oxidized ACC and Pd catalysts on oxidized of ACC

are presented in Figs. 8, 9 and 10. No thermoeffect was detected by DTA for non-oxidized ACC below 455 °C. The only exothermic effect starts at 455–465 °C followed by a large and sharp weight loss in the TGA curve (Fig. 10). This effect corresponds to the burn-off of the ACC fibers and, T_g is the temperature at which the burn-off of the ACC fibers starts.

The DTA thermogram for oxidized ACC includes two exothermic effects. The first starts at around 310–320 °C and shows a peak at 350 °C with a small weight loss (about 4 %) in the corresponding TGA profile (Fig. 9b; Table 3). The burn-off of the ACC fibers starts at 400–415 °C and is followed by a drastic and sharp weight loss in the TGA profile (Fig. 9a). The first slight observed peak corresponds to the decomposition of the oxygen-containing surface functional groups to CO and CO_2 [32]. T_c is the temperature at which the first thermoeffect starts.

Table 4 Total amount of CO and CO_2 desorbed according to temperature programmed desorption curves

Sample	CO (µmol/g)	CO_2 (µmol/g)
Non-oxidized ACC	130.13	91.73
Oxidized ACC (OACC)	1,137.82	1,296.30
Reduced OACC with H_2 (T_{red} = 185 °C)	1,206.19	1,224.44
3 % Pd/OACC (T_{red} = 185 °C)	1,050.86	470.43
3 % Pd/OACC (T_{cal} = 135 °C)	1,369.89	1,135.57
3 % Pd/OACC (T_{cal} = 185 °C)	1,392.24	943.12
3 % Pd/OACC (T_{cal} = 235 °C)	1,492.78	734.22

For Pd catalysts on oxidized ACC the following observations can be made:

a) T_c was shifted to lower values and it was dependent on the Pd content (Table 2; Fig. 9b). The reduction rate in T_c value for impregnated ACC, at the beginning was very sharp and T_c was reduced to 215–220 °C for 1 % Pd/ACC (Table 2). After that, the rate of change of T_c as a function of Pd content was decreased. T_c is an important criterion in selection of calcination temperatures for Pd catalysts on oxidized ACC. In fact, treating of the catalysts above their T_c temperatures could damage and finally destroy the oxygen-containing surface functional groups which were introduced by acid pretreatment of ACC.

b) The maximum weight loss by the decomposition of the oxygen-containing surface functional groups (4.12 wt%) belongs to virgin oxidized ACC (Table 3). Impregnating oxidized ACC with Pd, reduced the bare surface of the ACC fibers for the first exothermic effect. This diminished the weight loss values because of the decomposition of the oxygen surface functional groups (Table 3).

c) In the same way as T_c values, T_g for the impregnated ACC with Pd were considerably decreased (Table 2). The value of reduction in T_g also depended on the Pd content.

d) Impregnating the oxidized ACC with Pd leads to the sharper and more intensive exothermic peaks and weight loss corresponding to burn-off of the ACC fibers.

The DTA curve of impregnated non-oxidized ACC with 3 % Pd, the same as the virgin non-oxidized ACC, showed no peak corresponding to the decomposition of oxygen surface functional groups (Fig. 10). But, burn of the ACC fibers were started earlier (T_g = 300–320 °C) in 3 % Pd/ACC compare to the virgin non-oxidized ACC (Table 2).

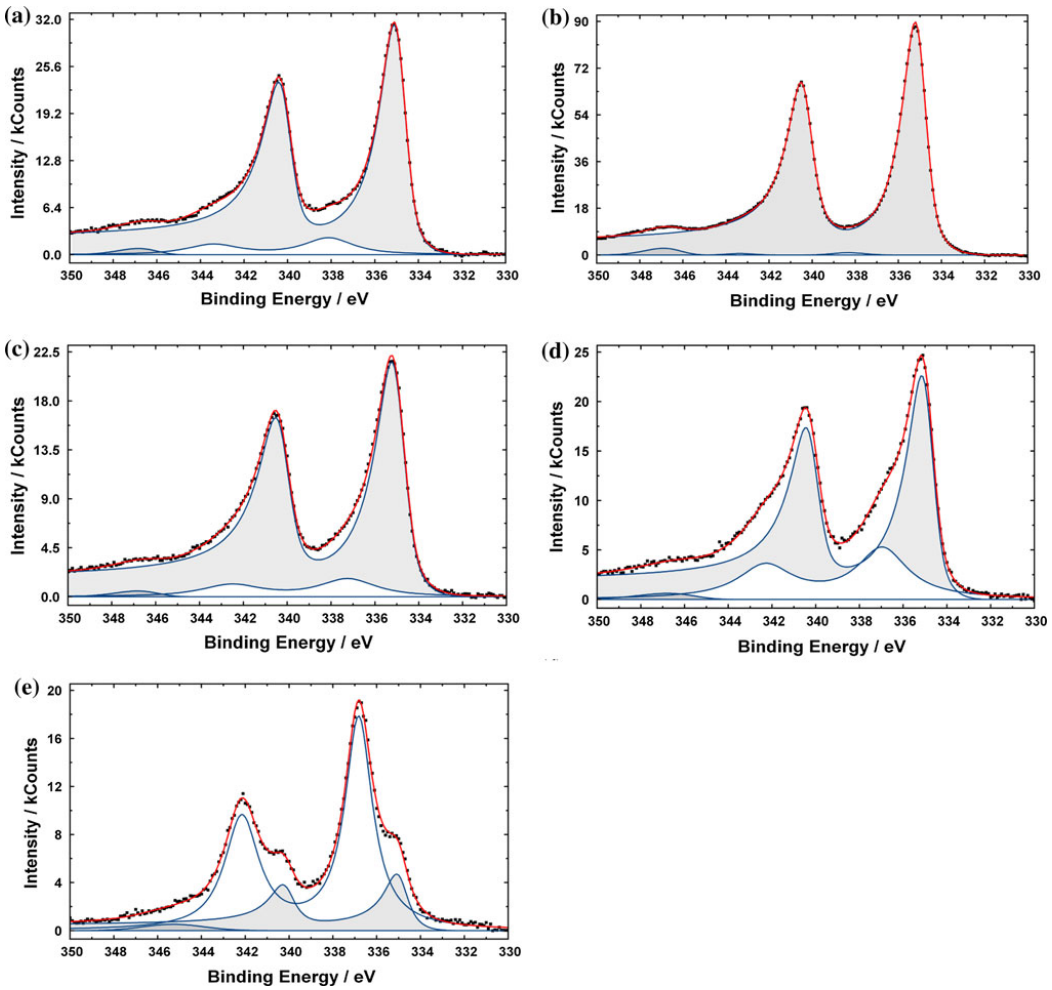

Fig. 13 The Pd3d XPS spectra of 3 wt% Pd/OACC **a** fresh virgin dried one, **b** reduced one with H_2 at 185 °C and the calcined ones in the air at **c** 135 °C, **d** 185 °C, **e** 235 °C

5.1.3 Surface chemistry of the support materials

Wet oxidation treatments of carbon materials result in the formation of different oxygen-containing surface groups. These functional groups consist of strong acidic ones (like carboxylic and anhydride groups) and weak acidic ones (like lactones, phenols and carbonyl groups) [5, 36]. These surface functional groups can be characterized by TPD desorption tests [33]. The stronger acidic groups lead to desorption of CO_2 at lower temperatures, while the weaker acidic ones show desorption zone of CO at higher temperatures [5, 29, 33]. The CO- and CO_2-TPD profiles of the non-oxidized and oxidized activated carbon cloths are shown in Fig. 11. The CO_2-TPD profile of the oxidized ACC shows a wide peak which starts at approximately 180 °C and reaches a maximum at approximately 620 °C. The corresponding CO-TPD profile begins to release CO at higher temperature (220 °C) and continuing this with increasing flow rate up to 900 °C. Indeed, it implies that the pretreatment of the ACC with HNO_3 introduces considerable amounts of oxygen containing functional groups on the surface of ACC fibers.

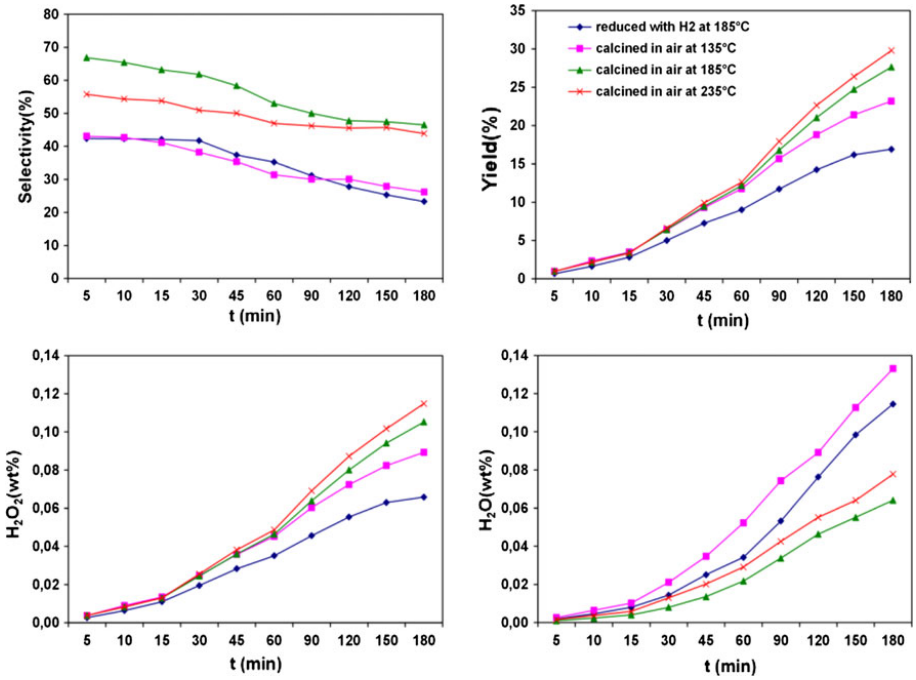

Fig. 14 Performance of 3 % Pd catalysts on oxidized ACC (mass of catalyst = 55 mg, temperature = 0 °C)

The CO_2- and CO-TPD profiles of the oxidized ACC (virgin oxidized ACC and the one reduced with H_2 at 185 °C) and the corresponding 3 wt% Pd catalysts are presented in Fig. 12. On the basis of them the following observations can be made:

a) The CO_2-TPD profiles of the different 3 wt% Pd catalysts started to release CO_2 at around 150 °C while in virgin oxidized ACC it started at around 200 °C.
b) Increasing the calcination temperature reduced the amount of the released CO_2 represented by the area under the CO_2 curve (Table 4). In other words, calcination of the Pd catalyst in the air resulted in decomposition of the stronger acidic surface functional groups. This agrees well with the DTA/TGA results (Sect. 5.1.3).
c) Minimum amount of the released CO_2 belongs to the reduced Pd supported catalyst in H_2 at 185 °C. While the same treatment of the virgin oxidized ACC did not change the CO_2-TPD profile considerably (Table 4).
d) Considering the CO_2- and CO-TPD profiles of Pd supported catalyst implies that the calcination of Pd catalysts in the air led to decomposition of the stronger acidic surface groups in the way which increased the thermal CO release (Table 4).

5.1.4 Metal Phase

The metal phase of Pd catalysts on oxidized ACC (the fresh dried catalyst, the one reduced with H_2 and the calcined ones) were characterized by the X-ray photoelectron spectroscopy (XPS). The Pd3d XPS spectra of the different 3 wt% Pd catalysts are displayed Fig. 13. The XPS spectrum of the catalyst reduced with H_2 at 185 °C (Fig. 13b) shows two peaks with binding energy at around 340.5 and 335.3 eV, corresponding to zerovalence of Pd (Pd^0) in the 3d3/2 and 3d5/2 level [37]. It indicates that the Pd species in the reduced catalyst appear in metallic state. From the segregation of the Pd3d XPS spectra of the catalysts which were calcined at 135, 185, and 235 °C (Fig. 13c, d, e), two doubles were obtained: one at a lower binding energy, which can be assigned to metallic palladium (Pd^0), and a second one at a higher binding energy, corresponding to Palladium oxide (PdO). The calcined Pd/OACC catalysts showed the presence of a PdO phase as well as a metallic phase (Pd^0), which indicated a partial oxidation of the Pd particles with calcination in static air. As it can be observed, with increasing the calcination temperature the amount of palladium oxide (PdO) is also increased. The catalyst which was calcined at

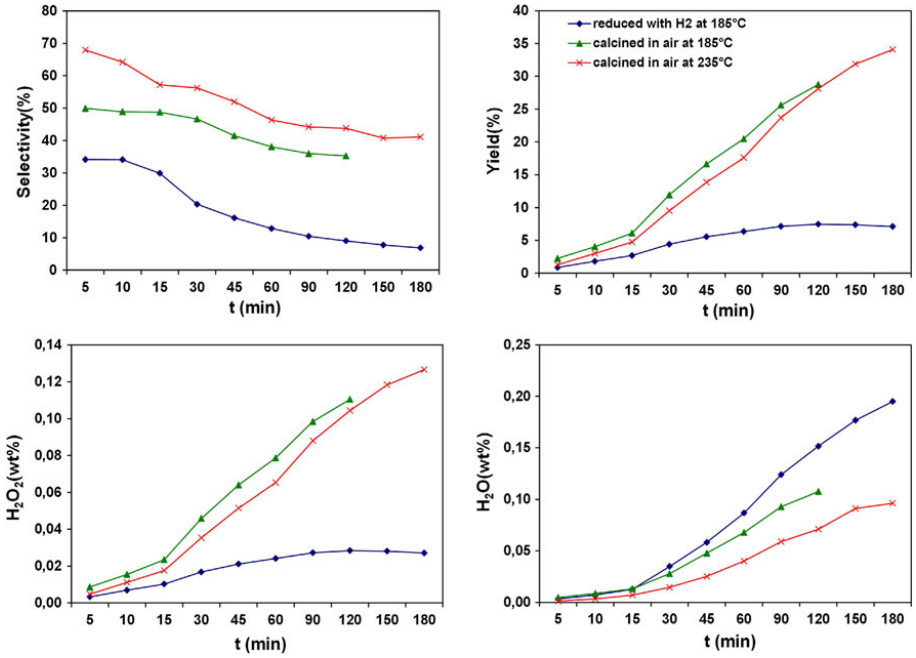

Fig. 15 Performance of 3 wt% Pd on non-oxidized ACC (mass of catalyst = 55 mg, temperature = 0 °C)

235 °C contained the maximum amount of palladium oxide (around 72.1 wt% of total metal phase).

The Pd3d XPS spectrum of the fresh virgin catalyst shows palladium mostly in the metallic form (Pd^0) instead of Pd^{2+}. The appearance of Pd^0 species in the virgin and oxidized catalysts could be due to a reducing effect of the activated carbon fibers during the impregnation step, because of the native charge of their surfaces (Fig. 7).

5.2 Catalytic activity

Activity of the catalysts was evaluated by yield and selectivity. These two parameters are defined as:

$$\text{Yield}\,(\%) = \frac{\text{Moles of produced } H_2O_2}{\text{Moles of } H_2 \text{ fed}} \times 100$$

$$\text{Selectivity}\,(\%) = \frac{\text{Moles of produced } H_2O_2}{\text{Moles of consumed } H_2} \times 100$$

The results of the direct synthesis of hydrogen peroxide over 3 wt% Pd catalysts on oxidized and non-oxidized ACC are shown in Figs. 14 and 15, respectively. From them, the following observations can be made:

a) The calcined catalysts are more active and selective than the corresponding reduced catalysts.

b) In the case of catalysts on non-oxidized ACC, increasing the calcination temperature improves the selectivity. These (a,b) imply that the oxidized state of Pd (PdO) in the catalyst makes the catalyst more active and selective than the corresponding Pd^0 catalyst.

c) In the case of catalysts on oxidized ACC, increasing the calcination temperature up to 185 °C improves both the activity and selectivity. Increasing the calcination temperature from 185 to 235 °C leads to slightly more active but less selective catalyst.

d) Pd catalysts on oxidized ACC are significantly more selective than the corresponding Pd catalysts on non-oxidized ACC, except the calcined catalysts at 235 °C. This observation implies that oxygen containing surface functional groups make the Pd catalyst more selective in the direct synthesis of H_2O_2.

Heat treatment of oxidized ACC in the presence of Pd at temperatures higher than 190 °C can seriously damage the oxygen-containing functional groups. Because of this, calcination at 185 °C led to better selectivity than at 235 °C. This was the case even though the amount of palladium oxide (PdO) was higher in the catalyst calcined at 235 °C.

Heat treatment of oxidized ACC in H_2 causes the substantial damage to the oxygen-containing functional groups (Figs. 11, 12). On the other hand, there is no palladium in the form of palladium oxide in the reduced Pd catalysts. Lack of PdO and damaged oxygen-containing functional groups result in poor performance of the reduced catalysts.

6 Conclusions

According to the observations and discussion, it can be concluded that activity and selectivity of the Pd catalysts on ACC in direct synthesis of H_2O_2 are greatly affected by two important characteristics of the catalyst: 1) oxidation state of Pd in metallic phase; 2) surface chemistry of the support which is determined by the nature and the amount of surface functional groups.

The existence of the oxidized state of Pd (PdO) makes the catalyst more active and selective than the corresponding zerovalent Pd^0 catalysts. PdO affected on selectivity by increasing the rate of H_2O_2 production and reducing the rate of water production, simultaneously.

Pd catalysts on oxidized ACC were significantly more selective than the corresponding ones on non-oxidized ACC. This implies that oxygen containing surface functional groups make the Pd catalyst more selective. Reduction of Pd catalysts supported on the oxidized ACC with H_2 at 185 °C substantially damaged the oxygen-containing functional groups. Moreover, calcination with the air at temperatures higher than 190 °C could also damage oxygen-containing functional groups.

Acknowledgments The authors thank Dr. Kari Eranen for helping with the TPD and SSA measurements and Toni Väkiparta for SEM images.

References

1. Baukal CE (1998) Oxygen-enhanced combustion. CRC, New York
2. Solsona BE, Edwards JK, Landon P, Carley AF, Herzing A, Kiely CJ, Hutchings GJ (2006) Chem Mater 18:2689
3. Harada T, Ikeda S, Miyazaki M, Sakata T, Mori H, Matsumura M (2007) J Mol Catal A 268:59
4. de Miguel SR, Vilella JI, Jablonski EL, Scelza OA, Salinas-Martinez de Lecea C, Linares-Solano A (2002) Appl Catal A 232:237
5. Edwards JK, Hutchings GJ (2008) Angew Chem Int Ed 47:9192
6. Choudhary VR, Jana P, Bhargava SK (2008) Catal Lett 125:296
7. Gaikwad AG, Sansare SD, Choudhary VR (2002) J Mol Catal A 181:143
8. Choudhary VR, Gaikwad AG, Sansare SD (2002) Catal Lett 83:235
9. Choudhary VR, Sansare SD, Gaikwad AG (2002) Catal Lett 84:81
10. Krishnan VV, Dokoutchaev AG, Thompson ME (2000) J Catal 196:366
11. Dissanayake DP, Lunsford JH (2003) J Catal 214:113
12. Burch R, Ellis PR (2003) Appl Catal B 42:203
13. Fu L, Chuang KT, Fiedorow R (1992) Stud Surf Sci Catal 72:33
14. Abate S, Centi G, Melada S, Perathoner S, Pinna F, Strukul G (2005) Catal Today 104:323
15. Melada S, Pinna F, Strukul G, Perathoner S, Centi G (2005) J Catal 235:241
16. Melada S, Pinna F, Strukul G, Perathoner S, Centi G (2006) J Catal 237:213
17. Pospelova TA, Kobozev NI, Eremin EN (1961) J Phys Chem 35:143
18. Pospelova TA, Kobozev NI (1961) J Phys Chem 35:262
19. Fu F, Chuang KT, Fiedorow R (1992) Stud Surf Sci Catal 72:33
20. Reis KP, Joshi VK, Thompson ME (1996) J Catal 161:62
21. Dissanayake DP, Lunsford JH (2002) J Catal 206:173
22. Chinta S, Lunsford JH (2004) J Catal 225:249
23. Han Y-F, Lunsford JH (2005) J Catal 230:313
24. Han Y-F, Lunsford JH (2005) Catal Lett 99:13
25. Liu Q, Lunsford JH (2006) J Catal 239:237
26. Liu Q, Lunsford JH (2006) Appl Catal A 314:94
27. Ratchananusorn W, Simonov D, Gudarzi D, kolehmainen E, Turunen I (2011) Chem Eng Process 50:1186
28. Radkevich VZ, Senko TL, Wilson K, Grishenko LM, Zaderko AN, Diyuk VY (2008) Appl Catal A 335:241
29. Toebes ML, van Dillen JA, de Jong KP (2001) J Mol Catal A 173:75
30. Gudarzi D, Simakova OA, Hernández Carucci JR, Biasi PD, Eränen K, Kolehmainenl E, Turunen I, Murzin DY, Salmi T (2010) Chem Eng Tran 21:925
31. Shen W, Li Z, Liu Y (2008) Recent Patent Chem Eng 1:27
32. Melada S, Pinna F, Strukul G, Perathoner S, Centi G (2006) J Catal 237:213
33. Moreno-Castilla C, López-Ramón MV, Carrasco-Marin F (2000) Carbon 38:1995
34. Simonov PA, Romanenko AV, Prosvirin IP, Moroz EM, Boronin AI, Chuvilin AL, Likholobov VA (1997) Carbon 35(1):73
35. Rodriguez-Reinoso F (1998) Carbon 36(3):159
36. Lee KY, Na JE, Lee JY, Kim JN (2004) Bull Korean Chem Soc 125, Nr.8:1280
37. Wang H, Wan Y (2009) J Mater Sci 44:6553

Publication II

D. Gudarzi, W. Ratchananusorn, I. Turunen, M. Heinonen, T. Salmi
Factors affecting catalytic destruction of H_2O_2 by hydrogenation and decomposition over Pd catalysts supported on activated carbon cloth (ACC)
Catalysis Today (2014)
Available online at http://dx.doi.org/10.1016/j.cattod.2013.12.050

G Model
CATTOD-8841; No. of Pages 11
ARTICLE IN PRESS

Catalysis Today xxx (2014) xxx–xxx

Contents lists available at ScienceDirect

Catalysis Today

journal homepage: www.elsevier.com/locate/cattod

Factors affecting catalytic destruction of H_2O_2 by hydrogenation and decomposition over Pd catalysts supported on activated carbon cloth (ACC)

Davood Gudarzi[a,*], Warin Ratchananusorn[a], Ilkka Turunen[a], Markku Heinonen[b], Tapio salmi[c]

[a] Department of Chemical Technology, Lappeenranta University of Technology, Lappeenranta FI-53851, Finland
[b] Department of Physics and Astronomy, University of Turku, Turku FI-20014, Finland
[c] Laboratory of Industrial Chemistry and Reaction Engineering, Åbo Akademi University, Turku/Åbo FI-20500, Finland

ARTICLE INFO

Article history:
Received 15 October 2013
Received in revised form 6 December 2013
Accepted 13 December 2013
Available online xxx

Keywords:
Hydrogen peroxide
Decomposition of H_2O_2
Hydrogenation of H_2O_2
Palladium catalysts
Activated carbon cloth

ABSTRACT

Destruction of hydrogen peroxide by its decomposition and hydrogenation over Pd catalysts supported on activated carbon cloth has been investigated. The catalysts were prepared by the impregnation method using acidic solution of palladium dichloride ($PdCl_2$) as a metal precursor. The reactions were performed batchwise in a Parr stainless steel autoclave. Tests were run at room temperature using either methanol or water as a reaction medium. The effects of oxidation pre-treatment of the support with different acids (nitric and acetic acid), the heat treatment of the catalysts in different atmospheres (H_2 and air), and Pd content on the final properties and H_2O_2 destruction activity of the catalysts were investigated. The results indicated that oxygen-containing surface functional groups have an important role in determining the physicochemical properties and H_2O_2 destruction activity of the catalysts. In fact, the presence of these groups stabilizes H_2O_2 in the solution and reduces its decomposition and hydrogenation. Furthermore, the presence of the oxidized state of Pd (PdO) in the catalyst makes it less active in H_2O_2 decomposition when compared to the corresponding zero valences (Pd^0) catalyst. Using water instead of methanol dramatically increased the H_2O_2 decomposition.

1. Introduction

Hydrogen peroxide (H_2O_2) is an important commodity chemical and environmentally friendly oxidant since the only by-product from the oxidation is water. One of the main applications of hydrogen peroxide is in pulp and paper industry, where it has been partially replaced chlorine-based bleaching agents because of the environmental concerns. It also has several applications in waste water treatment and as a raw material in chemical industry. Commercially, H_2O_2 is produced by an indirect process involving sequential hydrogenation and oxidation of anthraquinone compounds. This process suffers from a number of drawbacks, which have been described by several authors [1–8]. Moreover, this process is economically viable only at a large scale and at high product concentrations [9]. The high capital investment and operating costs disallow the utilization of anthraquinone process on-site at the end users, where H_2O_2 is often required in much smaller quantities and at lower concentrations.

The direct synthesis would allow small scale on-site production of dilute H_2O_2 solutions in a green and inexpensive manner. Moreover, the on-site direct process eliminates the safety concerns associated with the transportation of concentrated H_2O_2 solutions from the production plants to end users. Direct synthesis of hydrogen peroxide from hydrogen and oxygen has not yet been commercialized and has remained as a topic for research because of two main challenges. Firstly, mixtures of hydrogen and oxygen are explosive over a wide range of concentrations (4–94% H_2 in O_2) [10]. Secondly, in the direct catalytic oxidation of H_2 to H_2O_2, the selective generation of H_2O_2 ($H_2 + O_2 \rightarrow H_2O_2$) and non-selective generation of water ($H_2 + (1/2)O_2 \rightarrow H_2O$) occur simultaneously. Furthermore, H_2O_2 molecules are unstable in the presence of catalysts, which further facilitate its conversion to water (Fig. 1, reactions iii and iv). Therefore, it is difficult to achieve a high selectivity for H_2O_2 production.

Pd-based catalysts used to be the main choice for the direct synthesis of hydrogen peroxide. The major drawback of them is low selectivity, as they catalyze hydrogenation and decomposition of hydrogen peroxide (Fig. 1, reactions iii and iv) and also direct synthesis of water (Fig. 1, reaction ii). However, activity and selectivity of Pd catalysts are highly affected by the support materials. Pd catalysts on acidic support, e.g. Pd/SiO_2, were found to be more

* Corresponding author. Tel.: +358 445177734.
E-mail addresses: davood.gudarzi@lut.fi, d.goudarzi@gmail.com (D. Gudarzi).

0920-5861/$ – see front matter © 2014 Elsevier B.V. All rights reserved.
http://dx.doi.org/10.1016/j.cattod.2013.12.050

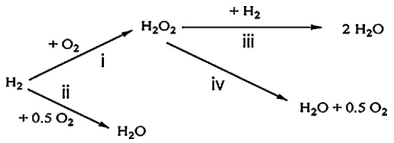

Fig. 1. Reaction pathways involved in the direct reaction of H_2 and O_2.

active and selective than basic catalysts (Pd/Al_2O_3) [10–12]. H_2O_2 decomposes more quickly in alkaline solution than in neutral or acidic medium [13]. The H_2O_2 decomposition activity of the supported Pd catalysts is strongly influenced by the oxidation state of Pd in the catalysts. The supported palladium oxide (PdO) catalysts have shown much lower H_2O_2 decomposition activity than the corresponding Pd^0 catalysts [5–7]. It was found that the H_2O_2 destruction (Fig. 1, reactions iii and iv) activity of Pd-based catalysts decreases drastically due to the addition of different halide anions (Cl^-, Br^- or I^-) in the catalyst [4] or in the acidic reaction medium [14–28]. However, the presence of halide ions together with H^+ ions in a reaction medium may cause the reaction medium to become strongly corrosive toward metallic reactor materials, particularly stainless steel. In addition, the halide ions together with H^+ ions form a complex reaction mixture from which the isolation of H_2O_2 and catalyst recovery is a difficult task [1]. Fu et al. [29] reported that Pd supported on hydrophilic supports are very active for decomposition of H_2O_2.

Activated carbons have been well established as support for palladium and platinum in liquid phase, due to their various industrial applications [30–32]. Textural forms of activated carbon materials, such as activated carbon cloths and activated carbon felts, represent noticeable advantageous characteristics with respect to the usual granular activated carbons [33]. High surface area is normally in the range of 1500–3000 $m^2\,g^{-1}$ [34], and the porous network is mainly formed by deep pores in a narrow range of sizes, especially micropores [35]. Because of mechanical elasticity and geometric flexibility, fibrous cloths can be easily bent and rolled to fit in particular uses. Cloths woven from thin μm-sized fibers reduce the diffusion distance and produce a low-pressure drop in fixed beds and in multi-phase reactors where one or more dissolved species have to react with gaseous compounds of limited solubility [36]. Fast adsorption/desorption rates have been claimed as an additional advantage [37,38]. Moreover, in our microstructured reactor [39], ACC catalyst is an attractive alternative because it can be replaced quickly and easily when needed. So far, the use of textural form of activated carbons (ACC and ACF) as catalyst supports is not well covered in scientific literature.

The preparation of Pd catalysts on activated carbon cloth for the direct synthesis was thoroughly studied in our previous work [8]. Since H_2O_2 decomposition can result in the loss of selectivity and yield, it is important to have a deep understanding of the factors affecting the H_2O_2 decomposition reactions (Fig. 1, reactions iii and iv). Destruction of H_2O_2 is a complex process and could be affected by different factors. In the present work, the effects of the reaction medium and the properties of the catalysts were studied.

The goal of this paper and our pervious work [8] is to develop a selective Pd catalyst supported on activated carbon cloth for the direct synthesis. This catalyst will be used in a novel microstructured reactor [39].

2. Experimentation

2.1. Catalysts preparation

A commercial activated carbon cloth ACC-5092-20 (Kynol Europa GmbH), after a cleaning and a chemical treatment, was employed as support. Palladium (II) chloride was used as metal precursors.

The activated carbon cloth was first treated in an oven at 100 °C for about 12 h. Then chemical cleaning was accomplished by a 50% solution of methanol at room temperature for 1 h, and then washed with plenty of deionized water. In order to oxidize activated carbon cloth, the cleaned ACC was treated with a 20% solution of nitric or acetic acid at room temperature for 40 h. After this oxidation treatment the samples were washed with deionized water until neutral conditions were reached, and then dried at 60 °C for 24 h. These samples are referred as oxidized ACC. Acid pre-treatment step was used to create oxygen-containing functional groups on the surface of activated carbon and to modify the surface as suggested by several authors [40–45].

Pd catalysts on non-oxidized and oxidized activated carbon cloth were prepared by impregnation of the supports with an aqueous acidic solution of $PdCl_2$ at room temperature for 6–7 h. The impregnation was done in a glass reactor with stirring rate of 600–700 rpm. The ratio of the solution volume to catalyst mass was 500 ml/g. The concentration of the metal precursor between 16.67 and 83.3 mg/L for 1 g of the support gave palladium loading in the range 1–5 wt%.

After impregnation, the catalysts were left at room temperature for 3 h, and then dried at 60 °C over night. To investigate the effects of the oxidation state of the metallic phase on the decomposition/hydrogenation activity, the dried fresh catalysts were finally treated with different processes. The reduced samples were prepared by treating the fresh dried catalysts with H_2 at 185 °C under 3.5 bar for around 12 h. A series of different calcined samples were prepared by oxidizing the fresh dried catalysts at temperatures 135, 185, and 235 °C in static air for 12 h. The calcination temperatures were selected on the basis of our earlier study [8] in order to be in the safe thermal treatment region of the supports and their surface functional groups.

2.2. Catalysts characterization

Pore size and surface area of different samples were measured via nitrogen adsorption/desorption isotherms at liquid nitrogen temperature (−196 °C) using an Automated Gas Sorption System (Sorptomatic 1900, Carlo Erba Instruments). All samples were degassed at a temperature of 100 °C for about 3 h prior to the measurements. The results have been presented in our previous work [8].

Atomic absorption spectroscopy (AAS) was used to determine the wt% of the metal incorporated into the support after impregnation. AAS was performed with a Thermo Scientific ICE 3000 series atomic absorption spectrometer using an air–acetylene flame. Samples for analysis were prepared by dissolving 200 mg of the dried catalyst in an aqua regia solution, followed by the addition of 500 ml deionized water to dilute the sample.

Temperature programmed desorption (TPD) was employed to investigate surface chemistry of carbon fibers in samples. The TPD tests were conducted in a set-up made of a U-shaped tubular reactor, placed inside an electrical furnace coupled to a Blazers Omnistar mass spectrometer for gas analysis. 200 mg of samples were heated up to 1000 °C with a constant heating rate of 50 °C/min. During the tests, He was passed through the reactor with the flow rate equal to 60 ml/min. The amounts of CO and CO_2 desorbed from samples were recorded by the mass spectrometer.

Ultra-High Resolution Field Emission Scanning Electron Microscope (UHRFESEM) was used to evaluate particle size, shape, surface morphology, and to monitor the agglomeration tendency of metal particles. The UHRFESEM and Energy Dispersive Spectroscopy (EDS) analysis were done by a Hitachi S-4800 microscope with an X-ray detector for micro-analytical X-ray mapping and

Please cite this article in press as: D. Gudarzi, et al., Factors affecting catalytic destruction of H_2O_2 by hydrogenation and decomposition over Pd catalysts supported on activated carbon cloth (ACC), Catal. Today (2014), http://dx.doi.org/10.1016/j.cattod.2013.12.050

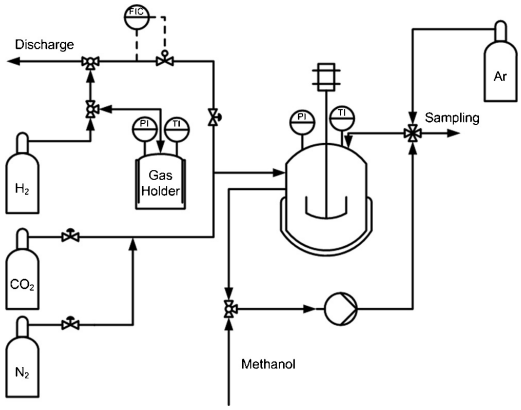

Fig. 2. Experimental set up for H_2O_2 hydrogenation/decomposition tests.

quantitative analysis. The active area of the X-ray detector for quantitative analysis was 10 mm^2.

The oxidized state of Pd in catalysts was examined by X-ray photoelectron spectroscopy (XPS). The spectra were obtained with a Perkin Elmer 5400 spectrometer, by using the Mg Ka (1253.6 eV) radiation of twin anode in the constant analyzer energy mode with pass energy of 37.75 eV. The pressure of the analysis chamber was maintained at 2×10^{-7} Pa. The binding energy scale was calibrated by setting the Au 4f7/2 transition to 84.0 eV. The spectra were analyzed by using Unifit peak-fitting program.

Thermal properties of the supports and the catalysts were characterized by simultaneous differential thermal analysis (DTA) and thermogravimetric (TGA) using a NETZSCH STA 449C Jupiter analyzer. Weight loss and heat flow during linear heating rate were measured in oxidized conditions. He was used as protective gas and O_2 as purge gas. The flow rates of He and O_2 were 40 ml/min and 20 ml/min, respectively. The furnace was heated up from 20 to 700 °C with heating rate 5 °C/min. Results of TGA/DTA were used in order to select a safe heat treatment region of the catalysts (e.g. calcination temperature). The details have been presented in our previous work [8].

2.3. Catalytic reactions

Decomposition and hydrogenation reactions of hydrogen peroxide was carried out in a stainless steel autoclave (Parr Instruments Ltd.) with a nominal volume of 450 ml and a maximum working pressure of 140 bar. The autoclave was equipped with an overhead stirrer (0–2000 rpm) and facilities to measure the temperature and pressure. The temperature was kept constant by a thermostat. In the case of hydrogenation reaction, hydrogen was fed into the reactor through a gas-holder with a volume of 33 ml and by the means of a mass flow controller. A recirculation line equipped with a multi-way valve was installed for sampling at different times (Fig. 2). The sampling line was designed to prevent pressure changes (and consequently, loss of gases) in the reactor during sampling. Catalysts were fixed in the reactor by the means of a metal stand [8]. Typically, the reactor was charged with about 60 mg of catalyst and successively with 200 g of 1 wt% hydrogen peroxide solution in methanol. In the case of decomposition tests, the air in the reactor was displaced by N_2. For hydrogenation reaction, first the air in the reactor was replaced with H_2 and then the reactor was filled with H_2 up to 4 bar. Stirring (1250 rpm) was begun immediately after H_2 feeding and the reaction time was started. Therefore, the possible decomposition of H_2O_2 during the H_2 feed does not matter. The gas–liquid and liquid–gas mass transfer effects were eliminated by adjusting the stirring speed. Adequate stirring speed for activity measurements was ensured beforehand by carrying out a series of hydrogenation tests varying the stirring rate. 1250 rpm provided sufficient mixing to eliminate the effect of mass transfer phenomena.

The concentration of H_2O_2 in the reaction (versus time) was measured quantitatively by a volumetric iodometry titration method. The water content was determined by coulometric Karl–Fischer titration using a Mettler DL35 Karl-Fischer Titrator. Research grade hydrogen and nitrogen were purchased from AGA. Methanol with purity of 99.9% was used as solvent (Merck). $PdCl_2$ with purity 99.999% (Sigma–Aldrich) was used as metal precursor. Nitric acid (65%, Merck) and acetic (Purity 100%, Merck) were used for acid pretreatment of the support. KI (Merck), acetic acid (Purity 100%, Merck), $K_2Cr_2O_7$ (purity 99.99%, Aldrich) and $Na_2S_2O_3{\cdot}5H_2O$ (Merck) were used for iodometric titration of hydrogen peroxide. Water content was determined by Karl-Fischer titration using Hydranal reagents (Fluka).

3. Results and discussions

3.1. Catalytic H_2O_2 hydrogenation

3.1.1. The effects of pretreatment of ACC with different acids

H_2O_2 hydrogenation activity of 3% Pd catalysts supported on non-oxidized ACC, ACC oxidized with nitric acid, and ACC oxidized with acetic acid versus time are presented in Fig. 3. This figure shows that hydrogenation activity of the catalyst supported on ACC oxidized with nitric acid is substantially less than of the other ones. Activity of the catalysts supported on non-oxidized ACC (NACC) and ACC oxidized with acetic acid ($OACC_A$) are almost the same. The main differences between these three catalysts which have the same Pd content are originated from the surface chemistry of their supports which can affect directly on their final catalytic activities. It also affects the other physicochemical properties of the catalysts (e.g. size, distribution, and morphology of the Pd particles). These parameters along with the surface chemistry of the support determine the final activity of the catalysts.

Surface chemistry of carbon supports is defined by the nature and amount of the functional groups present on the surface. Acid pretreatment of activated carbon cloth leads to formation of different oxygen-containing surface groups [8,46]. Strong acids (like nitric acid) create stronger acidic oxygen-containing surface groups

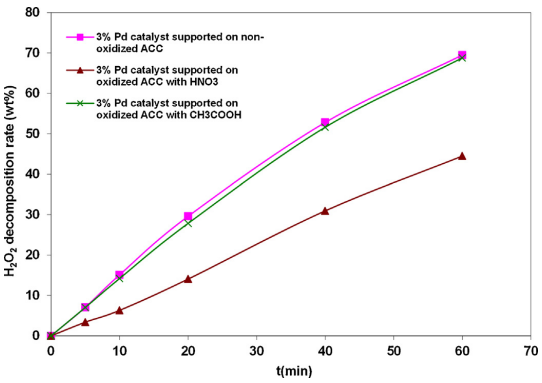

Fig. 3. Hydrogenation of H_2O_2 over 3%Pd catalysts supported on different ACC and calcined in air at 185 °C; $T_{reaction}$ = 21 °C, $m_{catalyst}$ = 60 mg, P_{H_2} = 4 bar.

Please cite this article in press as: D. Gudarzi, et al., Factors affecting catalytic destruction of H_2O_2 by hydrogenation and decomposition over Pd catalysts supported on activated carbon cloth (ACC), Catal. Today (2014), http://dx.doi.org/10.1016/j.cattod.2013.12.050

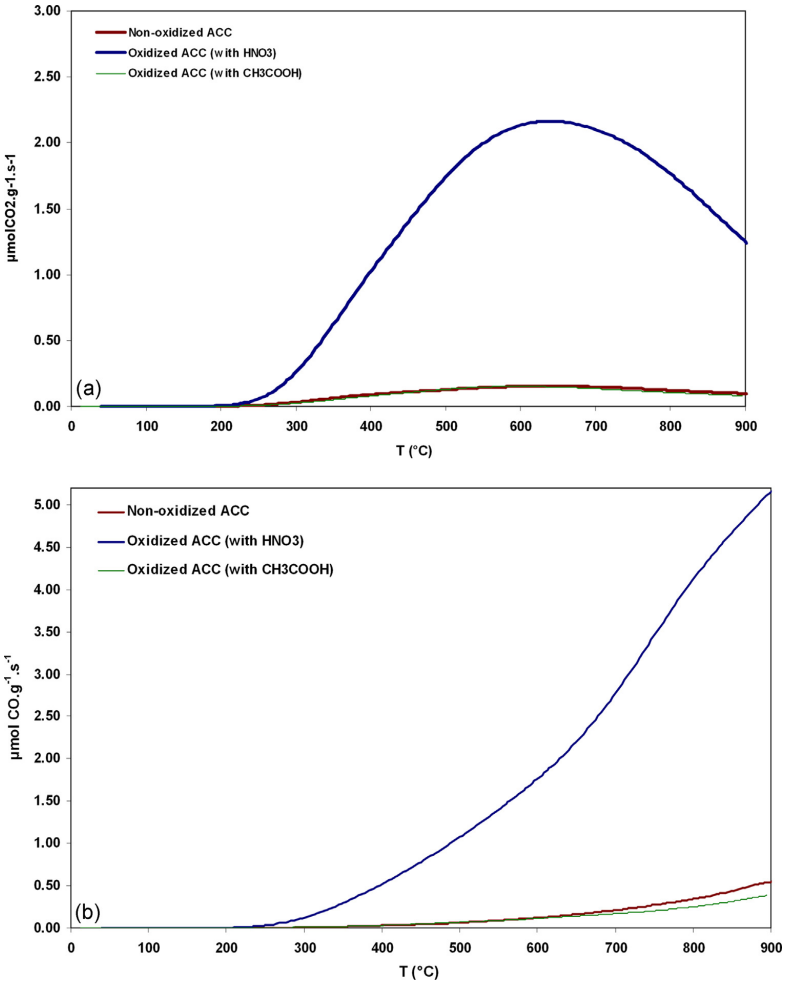

Fig. 4. The CO_2 (a), and CO (b) temperature programmed desorption profiles of the non-oxidized ACC, oxidized ACC (with HNO_3), and oxidized ACC (with CH_3COOH).

(like carboxylic and phenolic) and weak acids lead to formation of weaker ones [40–45]. These surface functional groups can be determined by thermal programmed desorption (TPD) tests [8,40,41,43]. The stronger acidic groups lead to CO_2-desorption at lower temperatures, while the weaker ones produce CO-desorption zone at higher temperatures.

The CO_2- and CO-TPD desorption profiles of the different oxidized and the non-oxidized activated carbon cloths are shown in Fig. 4. It can be observed that the oxidation treatment of the ACC with nitric acid introduces substantial amount of oxygen-containing functional groups, consisting of strong and weak acid groups, on the surface of ACC fibers. In contrast, acetic acid does not change the surface chemistry of ACC. Therefore, the TPD profiles of ACC oxidized with acetic acid are almost the same as non-oxidized ones.

Acidic oxygen-containing functional groups negatively charge the surface of ACC fibers [8] and decrease the surface hydrophobicity [42]. Less hydrophobic surface seems to have a low affinity to release the produced water molecules of the H_2O_2 hydrogenation reaction (Fig. 1, reaction iii). Therefore, it disturbs and slows down the transfer rate of the reactant molecules (H_2O_2, H_2) to the surface where the reaction takes place. These phenomena can result in less H_2O_2 hydrogenation/decomposition activity of the catalyst.

High resolution SEM images (Fig. 5) of the different 3% Pd catalysts supported on non-oxidized ACC, oxidized ACC (with acetic acid), and oxidized ACC (with nitric acid) demonstrate that:

- In non-oxidized ACC and ACC oxidized with acetic acid, Pd particles mostly formed on the outer surface of the fibers. The big and closed particles look like to cover almost the whole outer surface. Even the metallization of the outer surface of ACC fibers can be observed visually. The outer surface of the black ACC turned gray which is typical for palladium; while their inside remained black, as can be seen after cleavage of the fibers.
- In the case of ACC oxidized with nitric acid: firstly, the number of Pd particles on the outer surface of the fibers is dramatically less than the corresponding particles supported on non-oxidized

Please cite this article in press as: D. Gudarzi, et al., Factors affecting catalytic destruction of H_2O_2 by hydrogenation and decomposition over Pd catalysts supported on activated carbon cloth (ACC), Catal. Today (2014), http://dx.doi.org/10.1016/j.cattod.2013.12.050

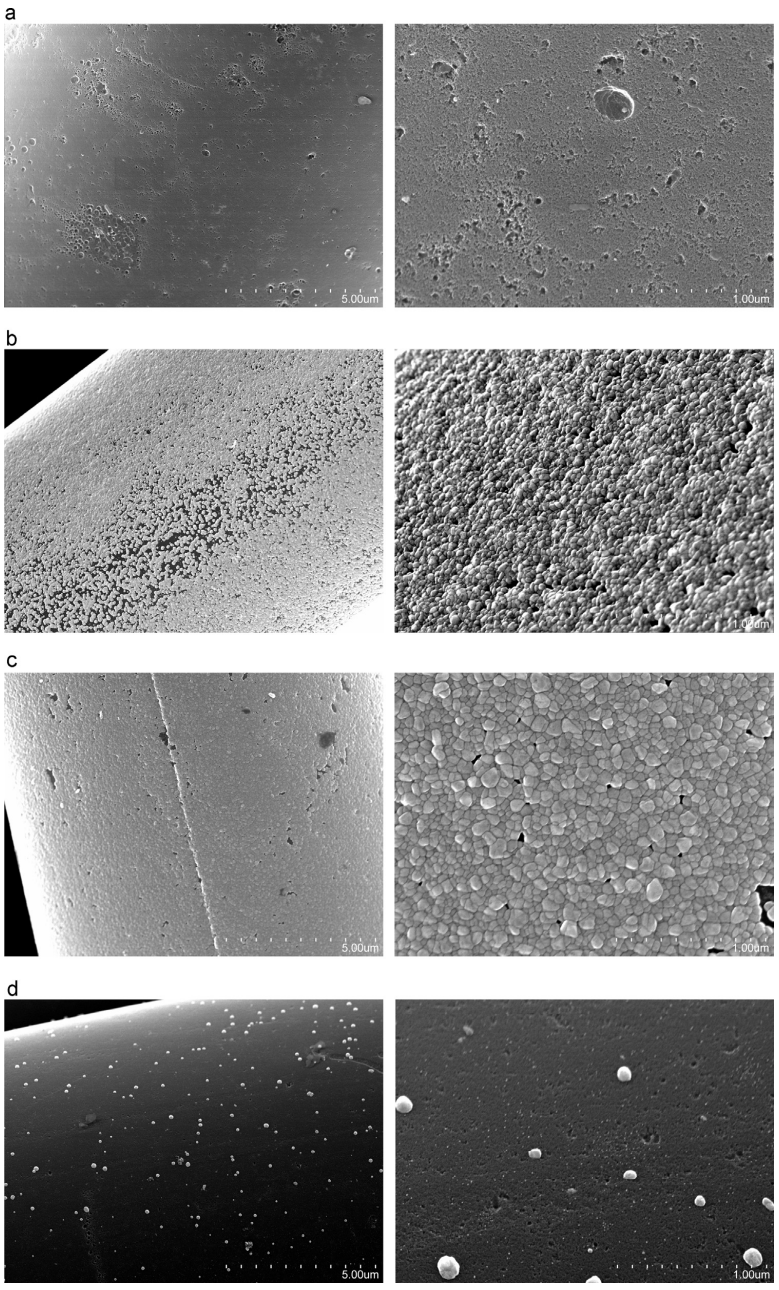

Fig. 5. High resolution SEM images of (a) virgin ACC and 3% Pd catalysts supported on: (b) non-oxidized ACC, (c) oxidized ACC with acetic acid (d), oxidized ACC with nitric acid.

ACC and ACC oxidized with acetic acid; secondly, their size is also much smaller.

- Low number of small Pd particles on the outer surface of the ACC fibers, in ACC oxidized with nitric acid, implies that considerable amount of Pd formed small particles in the pores of the fibers. The specific surface area and pore size distribution of the non-oxidized and oxidized ACC have been presented in our previous work [8].

Please cite this article in press as: D. Gudarzi, et al., Factors affecting catalytic destruction of H_2O_2 by hydrogenation and decomposition over Pd catalysts supported on activated carbon cloth (ACC), Catal. Today (2014), http://dx.doi.org/10.1016/j.cattod.2013.12.050

Access to the tiny particles in the pores is more difficult than to the particles on the outer surface of the ACC fiber. Therefore, H_2O_2 hydrogenation activity of the catalysts supported on ACC oxidized with nitric acid is less than the others.

Ionic palladium (Pd^{2+}) in acidic solution of palladium dichloride ($PdCl_2$) is mainly as tetrachloropalladic ion complex [46]. During the impregnation of non-oxidized ACC and ACC oxidized with acetic acid ($OACC_A$), the electrostatic attraction between the positively charged surface and the catalyst precursor anions $PdCl_4^{2-}$ facilitate the adsorption of Pd anions $PdCl_4^{2-}$ on the surface of the ACC fibers. Because, the outer surface of the fibers are directly exposed to the Pd precursor, the adsorption of $PdCl_4^{2-}$ occur rapidly on the outer surface of the fibers and lead to form the curst-like distribution of the big Pd particles on the outer surface of the ACC (Fig. 5b and c). Moreover, since carbon is essentially hydrophobic in nature, it has a very low affinity for solvents of polar character such as water [42]. Therefore, the metal precursor will be mostly located at the external surface of the ACC fibers when using water.

It was mentioned earlier that oxygen-containing functional groups negatively charge the surface of the ACC fibers oxidized with nitric acid ($OACC_N$). Repulsive forces between the Pd anions $PdCl_4^{2-}$ and the negatively charged surface of the $OACC_N$ fibers, prevent from fast and massive deposition and formation of the Pd particles on the outer surface of the ACC fibers. From the other side, Acidic surface functional groups introduced by treatment with HNO_3 decreased the hydrophobicity of the carbon thus making the interior of the microporosity more accessible to the aqueous solution of the metal precursor during impregnation [8]. Moreover, It can be observed virtually that the pale yellow color of the precursor disappear after a short contact of non-oxidized ACC and $OACC_A$ with precursor. Indeed, the adsorption equilibrium was found to be established in ca. 20 min on the non-oxidize ACC and $OACC_A$ and in about 3 h on the ACC oxidized with nitric acid (for more detailed explanation see our previous work [8]).

3.1.2. The effects of heat treatment in air and H_2

H_2O_2 hydrogenation activity of the different 3% Pd catalysts supported on non-oxidized and oxidized ACC (with nitric acid) are shown in Fig. 6. It can be observed that:

- For catalysts supported on non-oxidized ACC, the activities of all different catalysts are almost the same. Especially the reduced catalyst is almost as active as the calcined ones (see maximum H_2O_2 decomposition and average H_2O_2 decomposition rates in Table 4).
- In the case of the catalysts supported on oxidized ACC, the calcined catalysts almost showed the same H_2O_2 destructive activities. However, the catalyst which was calcined at 185 °C still demonstrates the lower activity. The catalyst reduced by H_2 at 185 °C is substantially more active than the other calcined catalysts (see maximum H_2O_2 decomposition and average H_2O_2 decomposition rates in Table 4).
- The calcined catalysts supported on oxidized ACC are less H_2O_2 destructive than the corresponding ones on non-oxidized ACC (Table 4).

The heat treatment (in H_2 at 185 °C and in air up to 235 °C) of the 3% Pd catalyst supported on oxidized ACC (with nitric acid), can affect the surface chemistry of the support and the physicochemical properties of the catalyst.

3.1.2.1. Surface chemistry of the support. In our previous work [8], it was shown that the heat treatment of the oxidized ACC, especially in the presence of palladium, leads to damage of the oxygen-containing surface functional groups. In the case of calcined catalysts, increasing the calcination temperature increases the damage, especially to the stronger acidic surface functional groups. These groups are responsible for CO_2 releasing in TPD test (Table 1). Reduction of Pd catalysts supported on oxidized ACC (with nitric acid) by H_2 at 185 °C causes maximum damage to the stronger acidic oxygen functional groups (Table 1).

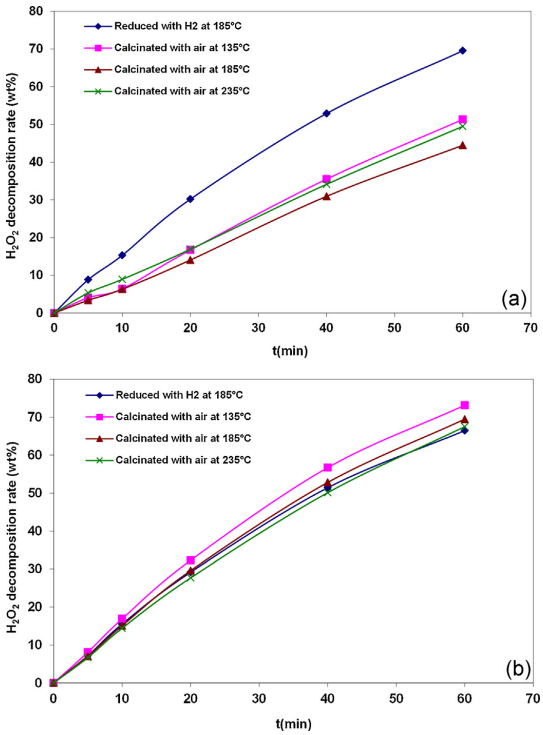

Fig. 6. Hydrogenation of H_2O_2 over 3 wt% Pd catalysts supported on (a) ACC oxidized with nitric acid and (b) non-oxidized ACC; $T_{reaction}$ = 21 °C, $m_{catalyst}$ = 60 mg, P_{H_2} = 4 bar.

3.1.2.2. Oxidation state of palladium in the catalyst. Palladium in the virgin impregnated catalysts is mostly in the metallic state (zero valences) [8]. The appearance of Pd^0 species in the virgin could be due to a reducing effect of the carbon during the impregnation step [46]. Therefore, reduction of the catalysts by H_2 has no considerable effect on the oxidation state of palladium in the catalysts. According to the X-ray photo electron spectroscopy (XPS) results, oxidation (calcination) of the virgin Pd catalyst resulted in production of oxidized state of palladium (PdO). Increasing the calcination temperature increased the amount of PdO in the final catalyst (Table 2). The amount of PdO was jumped substantially in

Table 1
Total reduction (mol%) in desorption of CO_2 (according to TPD curves), as a result of heat treatment of 3 wt% Pd supported on oxidized ACC (with nitric acid).

Sample	mol%
3%Pd/OACC ($T_{reduction}$ = 185 °C)	63.71
3%Pd/OACC ($T_{calcination}$ = 135 °C)	12.40
3%Pd/OACC ($T_{calcination}$ = 185 °C)	27.24
3%Pd/OACC ($T_{calcination}$ = 235 °C)	43.36

Please cite this article in press as: D. Gudarzi, et al., Factors affecting catalytic destruction of H_2O_2 by hydrogenation and decomposition over Pd catalysts supported on activated carbon cloth (ACC), Catal. Today (2014), http://dx.doi.org/10.1016/j.cattod.2013.12.050

Table 2
Total amount (wt%) of palladium in the form of palladium oxide (PdO) in different 3% Pd catalysts were supported on ACC oxidized with nitric acid, according to the results of x-ray photoelectron spectroscopy.

Sample	PdO (wt%)
3%Pd/OACC ($T_{reduction}$ = 185 °C)	0
3%Pd/OACC ($T_{calcination}$ = 135 °C)	5.56
3%Pd/OACC ($T_{calcination}$ = 185 °C)	10.21
3%Pd/OACC ($T_{calcination}$ = 235 °C)	69.12

the calcined catalyst at 235 °C (about 70% of the total amount of Pd in the catalyst). However, the Pd3d XPS spectra of the Pd catalysts which were undergone H_2O_2 hydrogenation reaction revealed that the oxidation state of palladium was dramatically influenced by H_2 during H_2O_2 hydrogenation reaction (Fig. 7a–g). In XPS spectra, the two peaks with binding energy at around 335.3 and 340.5 eV correspond to zero valances of Pd (Pd^0). The two peaks with binding energy at around 337.3 and 342.5 eV belong to palla-

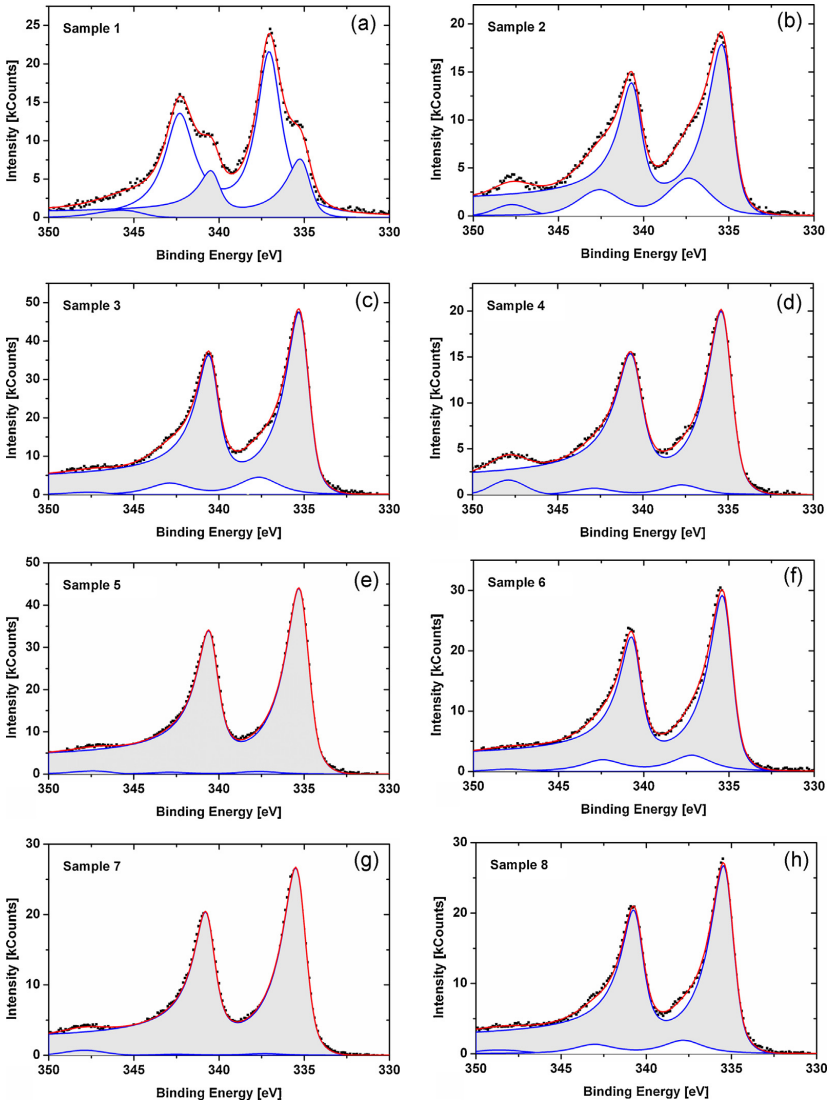

Fig. 7. The Pd3d XPS spectra of: (a) Sample 1: 3 wt% Pd/OACC calcined at 235 °C; (b) Sample 2: 3 wt% Pd/OACC and calcined at 235 °C; after H_2O_2 hydrogenation reaction (p_{H_2} = 4 bar, $T_{reaction}$ = 21 °C, $t_{reaction}$ = 5 min); (c) Sample 3: 3 wt% Pd/OACC and calcined at 235 °C; after H_2O_2 hydrogenation reaction (p_{H_2} = 4 bar, $T_{reaction}$ = 21 °C, $t_{reaction}$ = 15 min); (d) Sample 4: 3 wt% Pd/OACC and calcined at 235 °C; after H_2O_2 hydrogenation reaction (p_{H_2} = 4 bar, $T_{reaction}$ = 21 °C, $t_{reaction}$ = 30 min); (e) Sample 5: 3 wt% Pd/OACC and calcined at 235 °C; after H_2O_2 hydrogenation reaction (p_{H_2} = 4 bar, $T_{reaction}$ = 21 °C, $t_{reaction}$ = 60 min); (f) Sample 6: 3 wt% Pd/OACC and calcined at 185 °C; (g) Sample 7: 3 wt% Pd/OACC and calcined at 185 °C; after H_2O_2 hydrogenation reaction (p_{H_2} = 4 bar, $T_{reaction}$ = 21 °C, $t_{reaction}$ = 5 min); (h) Sample 8: 3 wt% Pd/OACC and calcined at 185 °C; after H_2O_2 decomposition reaction (p_{H_2} = 0 bar, $T_{reaction}$ = 21 °C, $t_{reaction}$ = 60 min); The two peaks with binding energy at around 335.3 and 340.5 eV correspond to zero valances of Pd (Pd^0). The two peaks with binding energy at around 337.3 and 342.5 eV belong to palladium oxide (PdO).

Please cite this article in press as: D. Gudarzi, et al., Factors affecting catalytic destruction of H_2O_2 by hydrogenation and decomposition over Pd catalysts supported on activated carbon cloth (ACC), Catal. Today (2014), http://dx.doi.org/10.1016/j.cattod.2013.12.050

Table 3
Total amount (wt%) of palladium in the form of palladium oxide (PdO) in the samples are introduced in Fig. 9, according to the results of x-ray photoelectron spectroscopy.

Sample	PdO (wt%)
3%Pd/OACC$_N$ ($T_{calcination}$ = 235 °C)	69.12
3%Pd/OACC$_N$ ($T_{calcination}$ = 235 °C); after H_2O_2 hydrogenation reaction ($t_{reaction}$ = 5 min)	19
3%Pd/OACC$_N$ ($T_{calcination}$ = 235 °C); after H_2O_2 hydrogenation reaction ($t_{reaction}$ = 15 min)	9
3%Pd/OACC$_N$ ($T_{calcination}$ = 235 °C); after H_2O_2 hydrogenation reaction ($t_{reaction}$ = 30 min)	5
3%Pd/OACC$_N$ ($T_{calcination}$ = 235 °C); after H_2O_2 hydrogenation reaction ($t_{reaction}$ = 60 min)	2
3%Pd/OACC$_N$ ($T_{calcination}$ = 185 °C)	10.21
3%Pd/OACC$_N$ ($T_{calcination}$ = 185 °C); after H_2O_2 hydrogenation reaction ($t_{reaction}$ = 5 min)	1
3%Pd/OACC$_N$ ($T_{calcination}$ = 185 °C); after H_2O_2 decomposition reaction ($t_{reaction}$ = 60 min)	10

dium oxide (PdO). According to results presented in Fig. 9, it can be stated:

- In the case of calcined catalyst at 235 °C, after 5 min of H_2O_2 hydrogenation reaction, the amount of palladium oxide (PdO) in the catalyst was slumped to 19% (wt%) from about 70%. With continuing the reaction up to half an hour, the amount of the PdO was dropped to 5%. Almost all PdO were reduced to zero valances (Pd^0) after the reaction time of nearly 1 h (Table 3).
- In calcined catalyst at 185 °C, the amount of oxidized palladium was only about 10% of the total amount of Pd (Fig. 7f). Almost all of the palladium oxide (PdO) was reduced to zero valences (Pd^0) after 5 min of the H_2O_2 hydrogenation reaction (Fig. 7g, Table 3).

In fact, the oxidation state of all palladium in the calcined catalysts at 135 and 185 °C became the same as in the reduced one (zero valances), after 5 min of the H_2O_2 hydrogenation reaction (Fig. 1, reaction iii). Therefore, it can be concluded that the oxidation state of palladium could not have an important role in causing the observed difference in their activities (Table 4). In calcined catalyst at 235 °C, there was still some PdO left even after half an hour of the reaction time. Even though the amount of remaining PdO in the catalyst is not too much, it still could weakly affect H_2O_2 hydrogenation activity of the catalyst.

According to the discussion above, the main reason that caused different activities of the different 3% Pd catalysts on oxidized ACC is the permanent change in surface chemistry of the support because of the heat treatments.

Table 4
Average decomposition rate (wt%/min) and maximum decomposition of H_2O_2 via hydrogenation over different 3 wt% Pd catalysts supported on non-oxidized ACC (NACC) and ACC oxidized with nitric acid (OACC$_N$).

Catalyst	Average decomposition rate (wt%/min)	Maximum decomposition (wt%)
3 wt% Pd/OACC$_N$ (reduced by H_2 at 185 °C)	1.16	69.54
3 wt% Pd/OACC$_N$ (calcined in air at 135 °C)	0.86	51.33
3 wt% Pd/OACC$_N$ (calcined in air at 185 °C)	0.73	43.96
3 wt% Pd/OACC$_N$ (calcined in air at 235 °C)	0.82	49.49
3 wt% Pd/NACC (reduced by H_2 at 185 °C)	1.11	66.50
3 wt% Pd/NACC (calcined in air at 135 °C)	1.22	73.13
3 wt% Pd/NACC (calcined in air at 185 °C)	1.16	69.47
3 wt% Pd/NACC (calcined in air at 235 °C)	1.12	67.49

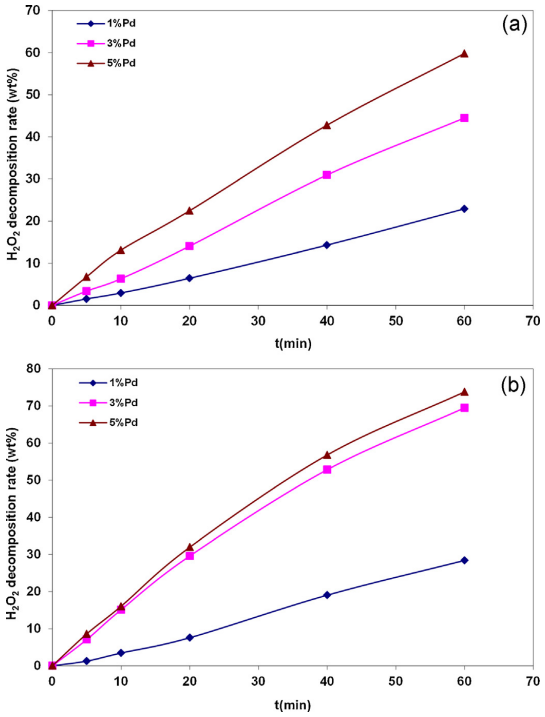

Fig. 8. H_2O_2 hydrogenation activity of 1, 3, 5 wt% Pd on (a) oxidized ACC with nitric acid and (b) non-oxidized ACC.

Non-oxidized ACC does not have considerable amount of oxygen-containing functional groups (Fig. 4). Therefore, the heat treatment of the 3% Pd catalyst supported on non-oxidized ACC causes no noticeable changes on the surface chemistry of the support. This fact is proven by the results shown in Fig. 6b. There all the different 3% Pd catalysts demonstrate almost the same H_2O_2 hydrogenation activities. However, heat treatment of carbon materials under H_2 at very high temperatures could cause changes in their surface chemistry [43,44].

3.1.3. *The effects of Pd content (wt%)*

The effects of Pd content (wt%) on the H_2O_2 hydrogenation activity of catalysts on non-oxidized and oxidized ACC (with nitric acid) are presented in Fig. 8. It can be perceived that:

- In both cases, with increasing the wt% of Pd from 1 to 3%, the activity of the catalysts was increased. This could be expected, because increasing the amount of Pd in the catalyst will increase the number of the Pd active sites.
- In the case of non-oxidized ACC, increasing wt% of Pd from 1 to 3% resulted in a big jump in the H_2O_2 destruction activity. However, above 3%, the catalytic activity was not considerably affected by wt% of Pd (Table 5). Therefore, increasing wt% of Pd from 3 to 5% resulted only in small changes in activity.
- In catalysts supported on oxidized ACC, the effect of the Pd content is not completely the same as non-oxidized one. In fact, increasing Pd content from 1 to 5% enhanced the catalytic activity almost with a constant rate (Table 5).
- Comparing the results with the catalysts on non-oxidized ACC to corresponding ones on oxidized ACC, reveals big activity

Please cite this article in press as: D. Gudarzi, et al., Factors affecting catalytic destruction of H_2O_2 by hydrogenation and decomposition over Pd catalysts supported on activated carbon cloth (ACC), Catal. Today (2014), http://dx.doi.org/10.1016/j.cattod.2013.12.050

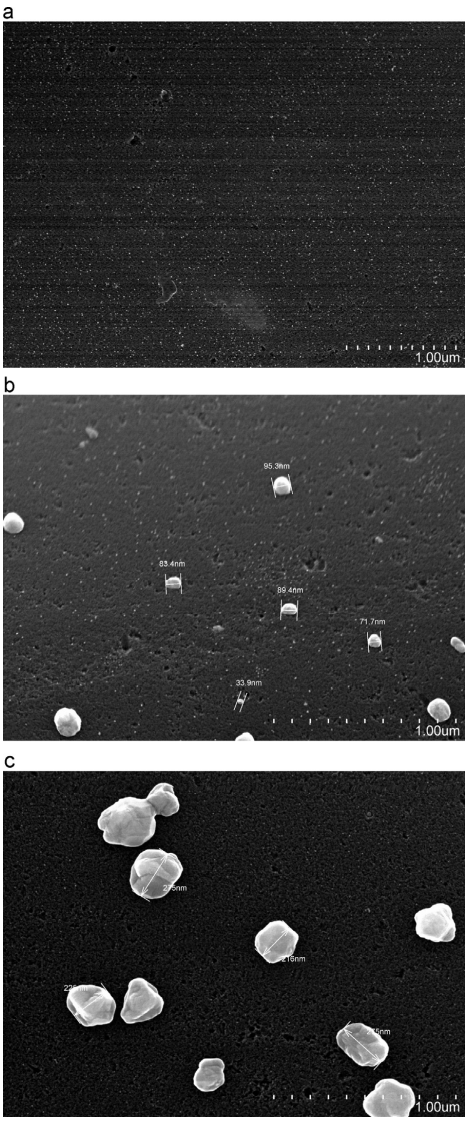

Fig. 9. High resolution SEM images of (a) 1%, (b) 3% and, (c) 5% Pd catalysts supported on ACC oxidized with nitric acid.

Table 5
Average decomposition rate (wt%/min), decomposition rate at the first 5 minute of the reaction time and (wt%/min), and maximum decomposition of H_2O_2 via hydrogenation over different Pd catalysts supported on non-oxidized ACC (NACC) and ACC oxidized with nitric acid ($OACC_N$).

Catalyst	Initial decomposition rate (wt%/min)	Average decomposition rate (wt%/min)	Maximum decomposition (wt%)
1 wt% Pd/$OACC_N$	0.31	0.38	22.93
3 wt% Pd/$OACC_N$	0.50	0.73	43.96
5 wt% Pd/$OACC_N$	1.36	1.00	59.81
1 wt% Pd/NACC	0.25	0.47	28.40
3 wt% Pd/NACC	1.41	1.16	69.47
5 wt% Pd/NACC	1.72	1.23	73.78

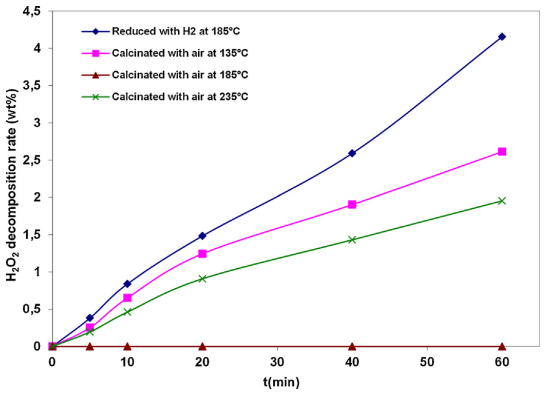

Fig. 10. Destruction of H_2O_2 by its decomposition over 3%Pd catalysts supported on ACC oxidized with nitric acid.

difference between 3% Pd catalysts. 3% Pd on non-oxidized ACC caused about 70% decomposition of H_2O_2 after 1 h while H_2O_2 was decomposed only 45% by the corresponding catalyst on oxidized ACC (Table 5).

The results in Fig. 10 are in agreement with the results of high resolution scanning electron microscopy (Figs. 5 and 9):

- It was shown and discussed (Section 3.1.1) that impregnation of non-oxidized ACC with palladium precursor leaded to form big Pd particles on the outer surface of the ACC fibers. Fig. 5b demonstrates with increasing the Pd content to 3 wt%, almost the whole outer surfaces of the ACC fibers were covered with the Pd particles and there was not any free surface for more additional new probable Pd particles. Additional increase in Pd content from 3 to 5 wt% resulted in denser and thicker Pd layer on the outer surface of the ACC fibers. Therefore, additional increase of Pd content does not change considerably the number of the Pd active sites and consequently the activity of the catalyst. However, in the 1 wt% Pd catalyst, there was still enough free area for more Pd particles on the ACC fibers [8]. Therefore, increasing the Pd content from 1 to 3% could lead to form more Pd particles and increase the catalytic activity.
- A possible explanation for the behavior of the Pd catalysts supported on ACC oxidized with nitric acid ($OACC_N$) could be that, with increasing the Pd content from 1 to 3 wt%, the big Pd particles form on the outer surface of the ACC fibers but, still a huge free surface for more additional new probable Pd particles is available (Fig. 9b). Therefore, additional increase of Pd content from 3 to 5 wt% can lead to form more new Pd particles which they could be considered as new active site for the reaction. Therefore the H_2O_2 destruction activity of the catalyst kept continuing to increase with increasing the Pd content from 3 to 5 wt%. To confirm this theory, it would be necessary to measure the exact number of active sites by chemisorption.

3.2. Destruction of H_2O_2 by its decomposition

H_2O_2 decomposition (Fig. 1, reaction iv) tests were done in the same experimental setup and conditions as hydrogenation tests. N_2 was used in order to replace air from the reactor. The results of destruction of H_2O_2 by its decomposition over different 3% Pd catalysts supported on oxidized ACC are presented in Fig. 10. It can be observed that:

Please cite this article in press as: D. Gudarzi, et al., Factors affecting catalytic destruction of H_2O_2 by hydrogenation and decomposition over Pd catalysts supported on activated carbon cloth (ACC), Catal. Today (2014), http://dx.doi.org/10.1016/j.cattod.2013.12.050

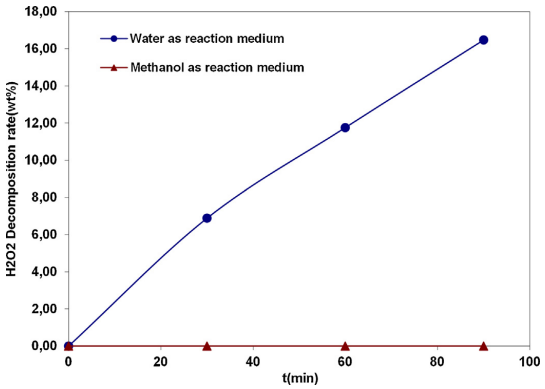

Fig. 11. The effect of reaction medium on destruction of H_2O_2 by its decomposition over 1%Pd catalyst supported on ACC oxidized with nitric acid and calcined at 185 °C; $T_{reaction}$ = 21 °C, $m_{catalyst}$ = 60 mg.

- H_2O_2 decomposition activity of the catalyst calcined at 185 °C was almost zero.
- The catalyst reduced by H_2 at 185 °C had maximum H_2O_2 destruction activity.
- The calcined catalyst at 235 °C is less active than the corresponding one which was calcined at 135 °C.
- A comparison between the results were presented in Fig. 6a with Fig. 10 reveals that destruction of H_2O_2 by its decomposition is really low and negligible as compared to the H_2O_2 destruction by hydrogenation (Fig. 1, reaction iii).
- The same results were observed for the corresponding 1 and 5% Pd catalysts.

H_2O_2 decomposition activity of the 3% Pd catalysts supported on oxidized ACC is influenced by the same factors as the H_2O_2 hydrogenation reaction (Section 3.1). The main difference in decomposition test is the lack of H_2 in the reaction medium and atmosphere. Therefore, oxidation state of Pd can have stronger and long term effect in the final activity of the catalysts. In fact, unlike the hydrogenation tests, the XPS results indicate that the oxidation state of palladium in the catalyst did not change during the decomposition test (Fig. 7h). Therefore, surface chemistry of the supports along with the oxidation state of palladium are the two main factors leading to different activities of the different 3% Pd catalysts. In the case of the calcined catalysts, the one calcined at 235 °C had maximum amount of oxidized palladium, around 70 wt% of the total Pd (Table 2). However, calcination of catalyst at 235 °C damaged the oxygen-containing functional groups more than the same procedure at lower temperatures. Smaller decomposition activity of the calcined catalyst at 235 °C than at 135 °C implies that the existence of oxidized state of Pd (PdO) makes the catalyst to decompose H_2O_2 less than the corresponding zero valances Pd (Pd^0).

Maximum damage in oxygen functional groups (Table 1) and lack of palladium oxide (PdO) in the catalyst reduced by H_2, maximized the decomposition of H_2O_2.

It can be concluded that a combination of these two factors (the amount of oxygen-containing functional groups and the presence of palladium oxide in the catalyst) determined the final differences in H_2O_2 decomposition activity of the 3% Pd catalysts.

3.3. The role of the reaction medium

The results of H_2O_2 decomposition over 1% Pd supported on oxidized (with nitric acid) ACC indicate that (see Fig. 11) methanol significantly stabilizes H_2O_2. As it can be observed, decomposition of H_2O_2 in water is much faster than in methanol. According to Melada et al. [18], the most reactive Pd sites could be blocked by formate compounds prohibiting HO—OH bond cleavage.

4. Conclusions

Pretreatment of the activated carbon cloth (ACC) with nitric acid creates strong and weak acidic oxygen-containing functional groups on the surface of ACC fibers. These surface functional groups influence a lot on the physicochemical properties of the final catalysts, e.g. size, distribution, and morphology of Pd particles. Pd catalysts on ACC, oxidized with nitric acid, are considerably less active in catalytic decomposition ($H_2O_2 \rightarrow H_2O + (1/2)O_2$) and hydrogenation ($H_2O_2 + H_2 \rightarrow 2H_2O$) of hydrogen peroxide than the corresponding ones on non-oxidized ACC.

Heat treatment (reduction by H_2 at 185 °C and calcination in air at 135–235 °C) of the Pd catalyst on ACC oxidized with nitric acid, affected the surface functional groups. In the case of calcined catalysts, increasing the calcination temperature increases the damage, especially to the stronger acidic functional groups. Heat treatment of Pd catalysts on ACC oxidized with nitric acid by H_2 at 185 °C (reduction process) maximizes the damage on the stronger acidic oxygen functional groups. Therefore, in a series of Pd catalysts supported on oxidized ACC with the same Pd content, the reduced one was substantially more active in H_2O_2 decomposition and hydrogenation.

Oxidation (calcination) of the virgin Pd catalysts in air leads to production of oxidized palladium (PdO). The presence of the oxidized Pd (PdO) makes the catalyst less active in H_2O_2 decomposition than the corresponding zero valances (Pd^0). During the hydrogenation reaction, H_2 reduced palladium oxide (PdO) to the metallic state (Pd^0). Therefore, in the PdO containing catalysts, PdO could not have strong and long term effect on the H_2O_2 hydrogenation activity.

Finally, the results demonstrated that methanol, as a reaction medium, significantly stabilizes H_2O_2 as compared to water.

Acknowledgement

The authors thank Dr. Kari Eranen for helping with the TPD and SSA measurements.

References

[1] C. Samanta, Appl. Catal. A: Gen. 350 (2008) 133–149.
[2] R. Burch, P.R. Ellis, Appl. Catal. B 42 (2003) 203–211.
[3] V.R. Choudhary, C. Samanta, T.V. Choudhary, Appl. Catal. A: Gen. 308 (2006) 128–133.
[4] V.R. Choudhary, C. Samanta, A.G. Gaikwad, Chem. Commun. (18) (2004) 2054–2055.
[5] A.G. Gaikwad, S.D. Sansare, V.R. Choudhary, J. Mol. Catal. A: Chem. 181 (2002) 143–149.
[6] V.R. Choudhary, A.G. Gaikwad, S.D. Sansare, Catal. Lett. 83 (2002) 235–239.
[7] V.R. Choudhary, S.D. Sansare, A.G. Gaikwad, Catal. Lett. 84 (2002) 81–87.
[8] D. Gudarzi, W. Ratchananusorn, I. Turunen, T. salmi, M. Heinonen, Top. Catal. 56 (2013) 527–539.
[9] M. Piccinini, J.K. Edwards, J.A. Moulijn, G.J. Hutchings, Catal. Sci. Technol. 2 (2012) 1908–1913.
[10] C.E. Baukal, Oxygen-Enhanced Combustion, 2nd ed., CRC, Boca Raton, 1998.
[11] J.K. Edwards, G.J. Hutchings, Angew. Chem. Int. Ed. 47 (2008) 9192–9198.
[12] B.E. Solsona, J.K. Edwards, P. Landon, A.F. Carley, A. Herzing, C.J. Kiely, G.J. Hutchings, Chem. Mater. 18 (2006) 2689–2695.
[13] W.T. Hess, J.J. Kroschwitz, M. Howe-Grant (Eds.), Kirk-Othmer Encyclopedia of Chemical Technology, 13, 4th ed., Wiley, New York, 1995, p. 961.
[14] V.V. Krishnan, A.G. Dokoutchaev, M.E. Thompson, J. Catal. 196 (2000) 366–374.
[15] D.P. Dissanayake, J.H. Lunsford, J. Catal. 214 (2003) 113–120.
[16] S. Abate, G. Centi, S. Melada, S. Perathoner, F. Pinna, G. Strukul, Catal. Today 104 (2005) 323–328.
[17] S. Melada, F. Pinna, G. Strukul, S. Perathoner, G. Centi, J. Catal. 235 (2005) 241–248.

Please cite this article in press as: D. Gudarzi, et al., Factors affecting catalytic destruction of H_2O_2 by hydrogenation and decomposition over Pd catalysts supported on activated carbon cloth (ACC), Catal. Today (2014), http://dx.doi.org/10.1016/j.cattod.2013.12.050

[18] S. Melada, F. Pinna, G. Strukul, S. Perathoner, G. Centi, J. Catal. 237 (2006) 213–219.
[19] T.A. Pospelova, N.I. Kobozev, E.N. Eremin, J. Phys. Chem. 35 (1961) 143–147.
[20] T.A. Pospelova, N.I. Kobozev, J. Phys. Chem. 35 (1961) 262–265.
[21] K.P. Reis, V.K. Joshi, M.E. Thompson, J. Catal. 161 (1996) 62–67.
[22] D.P. Dissanayake, J.H. Lunsford, J. Catal. 206 (2002) 173–176.
[23] S. Chinta, J.H. Lunsford, J. Catal. 225 (2004) 249.
[24] Y.-F. Han, J.H. Lunsford, J. Catal. 230 (2005) 313.
[25] Y.-F. Han, J.H. Lunsford, Catal. Lett. 99 (2005) 13.
[26] Q. Liu, J.H. Lunsford, J. Catal. 239 (2006) 237.
[27] Q. Liu, J.H. Lunsford, Appl. Catal. A: Gen. 314 (2006) 94–100.
[28] V.Z. Radkevich, T.L. Senko, K. Wilson, L.M. Grishenko, A.N. Zaderko, V.Y. Diyuk, Appl. Catal. A: Gen. 335 (2008) 241–251.
[29] L. Fu, K.T. Chuang, R. Fiedorow, Stud. Surf. Sci. Catal. 72 (1992) 33–41.
[30] S. Polizzi, A. Benedetti, G. Fagherazzi, C. Goatin, R. Stozzi, G. Talamini, L. Toniolo, J. Catal. 106 (1987) 494–499.
[31] R.A. Sheldom, J. Dakka, Catal. Today 19 (1994) 215–245.
[32] S. de Miguel, M.C. Román-Martínez, E. Jablonski, J.L.G. Fierro, D. Cazorla-Amorós, O.A. Scelza, J. Catal. 184 (1999) 514–525.
[33] J.B. Donnet, R.C. Bansal, F. Stoeckli, Carbon Fibers, Marcel Dekker, New York, 1990.
[34] Yu. Shindler, Yu. Matatov-Meytal, M. Sheintuch, Ind. Eng. Chem. Res. 40 (2001) 3301–3308.
[35] R.N. McNair, G.N. Arons, Sorptive Textile Systems Containing Active Carbon Fibers, Carbon Adsorption Handbook (Chapter 22), Ann Arbor Science, Ann Arbor, MI, 1980, pp. 819.
[36] U. Matatov-Meytal, M. Sheintuch, Catal. Today 102–103 (2005) 121–127.
[37] Roskill, The Economics of Activated Carbon, 3rd ed., Roskill Information Services, London, 1990.
[38] Z.M. Wang, N. Shindo, Y. Otake, K. Kaneko, Carbon 32 (1994) 515–521.
[39] W. Ratchananusorn, D. Simonov, D. Gudarzi, E. kolehmainen, I. Turunen, Chemical Engineering and processing, Process Int. 50 (2011) 1186–1192.
[40] C.M. Moreno-Castilla, V. López-Ramón, F. Carrasco-Marín, Carbon 38 (2000) 1995–2001.
[41] Sh. Wenzhong, L. Zhijieand, L. Yihong, Recent Pat. Chem. Eng. 1 (2008) 27–40.
[42] F. Rodríguez-reinoso, Carbon 36 (1998) 159–175.
[43] J.M. Rosas, J. Bedia, J. Rodríguez-Mirasol, T. Cordero, Fuel 88 (2009) 19–26.
[44] M.L. Toebes, J.A. van Dillen, K.P. de Jong, J. Mol. Catal. A: Chem. 173 (2001) 75–98.
[45] W.-C. Oh, M.-H. Yum, Bull. Korean Chem. Soc. 25 (2004) 1189–1194.
[46] P.A. Simonov, S. Troitskii Yu, V.A. Likholobov, Kinet. Catal. 41 (2000) 255–269.

Please cite this article in press as: D. Gudarzi, et al., Factors affecting catalytic destruction of H_2O_2 by hydrogenation and decomposition over Pd catalysts supported on activated carbon cloth (ACC), Catal. Today (2014), http://dx.doi.org/10.1016/j.cattod.2013.12.050

Publication III

D. Gudarzi, W. Ratchananusorn, I. Turunen, M. Heinonen, T. Salmi
Promotional effects of Au in Pd-Au bimetallic catalysts supported on activated carbon cloth (ACC) for direct synthesis of H_2O_2 from H_2 and O_2
Catalysis Today (2014)
Available online at http://dx.doi.org/10.1016/j.cattod.2014.04.011

G Model
CATTOD-9038; No. of Pages 11
ARTICLE IN PRESS

Catalysis Today xxx (2014) xxx–xxx

Contents lists available at ScienceDirect

Catalysis Today

journal homepage: www.elsevier.com/locate/cattod

Promotional effects of Au in Pd–Au bimetallic catalysts supported on activated carbon cloth (ACC) for direct synthesis of H_2O_2 from H_2 and O_2

Davood Gudarzi[a,*], Warin Ratchananusorn[a], Ilkka Turunen[a], Markku Heinonen[b], Tapio Salmi[c]

[a] Department of Chemical Technology, Lappeenranta University of Technology, Lappeenranta FI-53851, Finland
[b] Department of Physics and Astronomy, University of Turku, Turku FI-20014, Finland
[c] Laboratory of Industrial Chemistry and Reaction Engineering, Åbo Akademi University, Turku/Åbo FI-20500, Finland

ARTICLE INFO

Article history:
Received 10 December 2013
Received in revised form 3 April 2014
Accepted 14 April 2014
Available online xxx

Keywords:
Pd–Au bimetallic catalysts
Activated carbon cloth
Hydrogen peroxide
Wet oxidation

ABSTRACT

In this study, the promotional effects of gold in Pd–Au bimetallic catalysts supported on activated carbon cloth for direct synthesis of H_2O_2 has been investigated. The bimetallic catalysts were prepared by simultaneous co-impregnation approach. Direct synthesis was performed batch-wise in a stainless steel autoclave under high pressure (38 bar) at 0 °C and methanol (220 ml) was used as the reaction medium. A series of experiments were conducted to assess the effects of: (i) the surface chemistry of the support and (ii) the amount and ratio of palladium and gold on the surface morphology of the bimetallic catalysts and on their catalytic performances, and (iii) the oxidation state of the metallic components on the activity of the catalysts. Moreover, (iv) the effects of heat treatment of the catalysts in H_2 at 185 °C and in air at 185–275 °C on the surface chemistry of the support, surface morphology of the metallic component, and the performances of the final catalyst were investigated. Almost all of the Pd–Au bimetallic catalysts were more selective than the corresponding Pd monometallic catalysts. The results showed that the surface morphology of the Pd–Au bimetallic catalysts and their catalytic performance were highly influenced by the surface chemistry of the support and the amount and the ratio of Pd and Au in the catalyst. The presence of palladium oxide made the catalysts more selective and active than the corresponding zero-valent palladium (Pd^0) catalysts.

1. Introduction

Hydrogen peroxide (H2O2) is recognized as an important selective green oxidant since it contains a high fraction of active oxygen and the only by-product from oxidation is water. It has a wide range of applications in many large scale processes such as pulp bleaching, waste water treatment, cosmetic and pharmaceutical industries. In pulp and paper industry, hydrogen peroxide has partially replaced chlorine containing bleaching agents to address environmental issues. Industrially, H2O2 is produced by the cyclic sequential hydrogenation and oxidation of alkyl anthraquinones. This process is only economical at large scale and at high product concentrations [1]. However, H_2O_2 is often required in smaller scales and at lower concentrations. Direct synthesis would allow small scale on-site production of dilute H_2O_2 solutions in a green and economical manner. Moreover, the direct process may eliminate the need of transportation with substantial safety risks involved [2].

A process for the direct synthesis of hydrogen peroxide from hydrogen and oxygen represents considerable challenges in catalysis and process design. Firstly, mixtures of hydrogen and oxygen are explosive over a wide range of concentrations (4–94% H_2 in O_2) [3]. Secondly, the catalytic reaction of hydrogen and oxygen involves several reaction pathways, most of them result in the production of water [6] decreasing the selectivity.

Pd is the most common catalyst for this process. However, it suffers from low selectivity, as it catalyzes the decomposition/hydrogenation of H_2O_2 ($H_2O_2 \rightarrow H_2O + (1/2)O_2$; $H_2O_2 + H_2 \rightarrow 2H_2O$) and the non-selective water synthesis ($H_2 + (1/2)O_2 \rightarrow H_2O$). The performance of Pd catalysts is highly affected by the support material. Acidic support like SiO_2 results in more active and selective catalysts than basic ones (e.g. Al_2O_3) [4,5]. It has been shown that the existence of the oxidized state of

* Corresponding author. Tel.: +358 44 5177734.
E-mail addresses: davood.gudarzi@lut.fi, d.goudarzi@gmail.com (D. Gudarzi).

http://dx.doi.org/10.1016/j.cattod.2014.04.011
0920-5861/

Pd (PdO) makes Pd catalysts more selective and more active than the corresponding zero-valent state of Pd (Pd^0) [6–9]. Using of halide ions (especially Cl^- and Br^-) and protons (H^+) as promoters improve the selectivity of Pd catalysts in direct H_2O_2 synthesis [7–23].

Bimetallic catalysts have attracted considerable attention because their properties often differ remarkably from the corresponding monometallic ones. Among bimetallic catalysts, Pd–Au has received a great deal of attention because of its superior activity in a number of reactions, e.g. low-temperature CO oxidation, synthesis of vinyl acetate monomer, hydrogenation of hydrocarbons, cyclotrimerization of acetylene, and many others. Pure Au catalysts are not so active in direct H_2O_2 synthesis [2,24]. The addition of a second metal (e.g. Pt, Au, Ru, Rh) to Pd catalysts has been reported to affect catalytic activity and selectivity in direct H_2O_2 synthesis [5,25–34]. Addition of Au or Pt, at their optimum concentrations, to a Pd catalyst was reported to improve the catalyst selectivity, while the presence Rh or Ru exhibited an adverse effect [26].

The promotional effects of Au in Pd–Au bimetallic catalysts on direct H_2O_2 synthesis were firstly reported by G. J. Hutchings et al. [5,30,35,36]. It has also been found out that, unlike in the case of Pd monometallic catalysts, the addition of promoters, such as Br^- ions and H_3PO_4, were deleterious for the Au–Pd catalysts in this reaction [31]. Supported Pd–Au catalysts can be prepared using traditional impregnation or deposition–precipitation of Pd and Au salts, either concurrently or sequentially, followed by calcination and reduction. The major drawback is the lack of homogeneity of the formed catalysts in terms of particle size, composition and shape. For example, it is not uncommon to observe Au and Pd monometallic particles, and Pd–Au alloy particles with different sizes and compositions on the same support [5,30,35–37]. Au–Pd catalysts prepared by impregnation have been shown to be very active for the direct formation of hydrogen peroxide [33]. In contrast, the catalysts prepared by co-precipitation or deposition–precipitation gave a very low hydrogen peroxide production rate [33].

In our previous paper [6], we studied Pd catalysts supported on activated carbon cloth for direct synthesis of hydrogen peroxide. In this study, the promotional effects of gold in Pd–Au bimetallic catalysts supported on activated carbon cloth were investigated. The goal was to study the effects of the surface chemistry of the support, the amount and ratio of palladium and gold, and the heat treatment of the catalysts in either H_2 or air on the dispersion and morphology of metallic components, and on the performance of the Pd–Au bimetallic catalysts.

2. Experimental

2.1. Catalysts preparation

A commercial activated carbon cloth ACC-5092-20 (Kynol Europa GmbH), after cleaning and a chemical treatment, was employed as a support. Palladium (II) chloride ($PdCl_2$) and gold (III) chloride hydrate ($HAuCl_4$) were used for making metal precursors. Nitric acid was used for acid pretreatment of the support. The activated carbon cloth was first treated in an oven at 100 °C for about 12 h. Then it was cleaned with 50% solution of methanol at room temperature for 1 h, and finally washed with plenty of deionized water. For wet oxidation, the cleaned ACC was treated with 20% solution of nitric acid at room temperature for 40 h. After this oxidative treatment the samples were washed with deionized water until neutral conditions were reached, and then dried at 60 °C for 24 h. This sample is referred as oxidized ACC (OACC). Acid pre-treatment step was used to create oxygen-containing functional groups on the surface of activated carbon and to modify the surface as suggested by several authors [38–43].

The Pd catalysts were prepared using impregnation method as described previously [6]. The Pd–Au bimetallic catalysts on non-oxidized and oxidized activated carbon cloth were prepared by simultaneous co-impregnation of the supports with an aqueous acidic solution of $PdCl_2$ and $HAuCl_4$ at room temperature for 6–7 h. The impregnation was done in a glass reactor with stirring rate of 400–500 rpm. The rate of the stirring was adjusted to get uniform distribution of the metal particles in the catalysts. The ratio of the solution volume to catalyst mass was 500 ml/g. The amount of the precursor (Pd + Au) between 7.2 and 17.3 mg per 200 mg of the support in a 200 ml glass reactor gave metal loading (Pd + Au) in the range of 1–5 wt%. After impregnation, the catalysts were dried at room temperature for 3 h, and then at 60 °C for 12 h. The reduction process was done by treating the fresh dried catalysts with H_2 at 185 °C under 3.5 bar for about 12 h. A series of different calcined catalysts were prepared by oxidizing the fresh dried catalysts at temperatures 185, 235, and 275 °C in static air for 12 h. The calcination temperatures were selected based on the TGA/DTA results in order to be in the safe thermal treatment region of the supports and their surface functional groups (in the case of oxidized ACC) [6].

2.2. Catalysts characterization

The pore size distribution and specific surface area of the supports and the catalysts were measured via nitrogen adsorption/desorption isotherms at liquid nitrogen temperature (−350 °C) using an Automated Gas Sorption System, (Sorptomatic 1900, Carlo Erba Instruments). All the samples were degassed at a temperature of 100 °C for about 3 h prior to the measurements.

Metal (Au and Pd) contents of the catalysts were determined using flame Atomic Absorption Spectroscopy (AAS). AAS tests were performed with a Thermo Scientific ICE 3000 series atomic absorption spectrometer using an air-acetylene flame. Samples for analysis were prepared by dissolving 200 mg of the dried catalyst in an aqua regia solution followed by the addition of 500 ml of deionized water to dilute the solution. AAS was employed to determine the weight % of the metal incorporated in the support after impregnation. Moreover, it was used to determine the amount of Au or Pd leached out into the reaction medium during the direct synthesis test. The leached amount was calculated by comparing the Au and Pd content of the used catalyst and fresh catalyst.

Temperature programmed desorption (TPD) was employed to study different oxygen-containing surface functional groups in the supports and catalysts. The TPD tests were run in a set-up made of a U-shaped tubular reactor, placed inside an electrical furnace coupled to a Blazers Omnistar mass spectrometer for gas analyses. 200 mg of each sample was heated up to 1000 °C with a constant heating rate of 50 °C/min. During the tests, He was passed through the reactor with the flow rate of 60 ml/min. The amounts of CO and CO_2 desorbed from the samples were recorded by the mass spectrometer.

Ultra-high resolution field emission scanning electron microscopy (UHRFESEM) and scanning transmission electron microscopy (STEM) were hired to assess particle size, shape, surface morphology, and to monitor the agglomeration tendency of metal particles. The UHRFESEM, STEM, and energy dispersive spectroscopy (EDS) analyses were done by a Hitachi S-4800 microscope with an X-ray detector for micro-analytical X-ray mapping and quantitative analysis. The active area of the X-ray detector for quantitative analysis was 10 mm^2.

The oxidation states of the active components (Pd and Au) were determined by X-ray photoelectron spectroscopy (XPS). The spectra were obtained with a Perkin Elmer 5400 spectrometer, by using the Mg Ka (1253.6 eV) radiation of twin anode in the constant analyzer energy mode with pass energy of 37.75 eV. The pressure of

Please cite this article in press as: D. Gudarzi, et al., Promotional effects of Au in Pd–Au bimetallic catalysts supported on activated carbon cloth (ACC) for direct synthesis of H_2O_2 from H_2 and O_2, Catal. Today (2014), http://dx.doi.org/10.1016/j.cattod.2014.04.011

the analysis chamber was maintained at 2×10^{-7} Pa. The binding energy scale was calibrated by setting the Au 4f7/2 transition to 84.0 eV. The spectra were analyzed by using Unifit peak-fitting program.

2.3. Direct synthesis reaction

The synthesis was carried out in a stainless steel autoclave (Parr Instruments Ltd) with a nominal volume of 450 ml and a maximum working pressure of 140 bar. The autoclave was equipped with an overhead stirrer (0–2000 rpm) and facilities to measure the temperature and pressure. Hydrogen (18 mmol) was fed into the reactor through a gas-holder with a volume of 33 ml and through a flow controller. The gas-holder was used to measure the precise amount of hydrogen. A circulation line equipped with a multi-way valve was installed for sampling at different times (as shown in the previous paper [6]). The sampling line was designed to cause minimum pressure changes and gas losses during sampling. Typically, the reactor was charged with about 60 mg of catalyst and successively with carbon dioxide up to 15.2 bar at room temperature. The pressure was thereafter elevated to 20.2 bar with oxygen and further to 35.2 bar with carbon dioxide again at room temperature. Catalysts were fixed in the reactor by means of a metal stand as shown in the previous paper [6]. Methanol was employed as a reaction medium. 175 g of methanol was pumped in and the reactor was cooled down to about −1 °C. Stirring (1250 rpm) was begun after 2/3 of the methanol had been fed. When the desired temperature was reached, the partial pressure of hydrogen was raised up to 3.2 bar. The reaction time now began. The gas–liquid and liquid–solid mass transfer effects were eliminated by adjusting the stirring speed. This was done beforehand by carrying out a series of tests varying the stirring rate. It was found out that 1250 rpm was a sufficient stirring rate to eliminate the mass transfer limitations.

The concentration of H_2O_2 which was formed in the reaction was measured quantitatively by a volumetric iodometry titration using the following chemicals: KI (Merck), CH_3COOH (Purity 100%, Merck), $K_2Cr_2O_7$ (purity 99.99%, Aldrich) and $Na_2S_2O_3{\cdot}5H_2O$ (Merck). The produced water was determined by coulometric Karl–Fischer titration using a Mettler DL35 Karl–Fischer titrator and hydranal reagents (Fluka). The water content in the reaction medium before catalyst addition was determined prior to each experiment. Palladium (II) chloride ($PdCl_2$, purity 99.999%, Sigma–Aldrich) and gold (III) chloride hydrate ($HAuCl_4$, purity 99.999%, Aldrich) were used as metal precursors. Nitric acid 65% (Merck) was used for acid pretreatment of the support. Research grade oxygen, hydrogen and carbon dioxide were purchased from AGA. Methanol with a purity of 99.9% was used as a solvent (Merck).

3. Results and discussions

Catalytic performance was evaluated by the means of the following parameters: the final concentration of the produced hydrogen peroxide and water (wt%), selectivity (%), yield (%), and total H_2 conversion (%). The last three parameters are defined as follows:

$$\text{Selectivity}\ (\%) = \frac{\text{moles of produced } H_2O_2}{\text{moles of produced } H_2O_2 + \text{moles of produced } H_2O} \times 100 \quad (1)$$

$$\text{Yield}\ (\%) = \frac{\text{moles of produced } H_2O_2}{\text{moles of } H_2 \text{ fed}} \times 100 \quad (2)$$

$$\text{Conversion}\ (\%) = \frac{\text{moles of produced } H_2O_2 + \text{moles of produced } H_2O}{\text{moles of } H_2 \text{ fed}} \times 100 \quad (3)$$

Another parameter which can be used in order to take in to account the metal content of the catalysts in their activities is productivity:

$$\text{Productivity} = \frac{\text{moles of produced } H_2O_2\ (\text{mol})}{\text{reaction time (h)} \times \text{the metal content of the catalyst (kg)}} \quad (4)$$

3.1. The effects of Au/Pd ratio and metal content in the catalytic activity of Pd–Au bimetallic catalysts

3.1.1. Increasing the amount of gold with a constant amount of palladium

The catalytic performance of Pd–Au bimetallic catalysts with 1 wt% Pd and 1–5 wt% Au supported on the oxidized ACC are presented in Fig. 1. For comparison, also the results with 1 wt% Pd monometallic catalyst are shown. It can be observed that:

- All Pd–Au bimetallic catalysts are more selective than the Pd monometallic catalyst. Especially in the first 60 min of the reaction time, almost all of the Pd–Au bimetallic catalysts are considerably more selective than the Pd monometallic catalyst (Fig. 1).
- In the case of Pd–Au bimetallic catalysts, with increasing the amount of gold, the selectivity drops, especially during the first 60 min. However, at reaction times above 1.5 h, the differences between the selectivity of the different Pd–Au catalysts became smaller (see the exact values in Table 1).
- In the case of Pd–Au bimetallic catalysts, the activity (yield, productivity and H_2 conversion rates) was increased when increasing the amount of gold (Fig. 1, Table 1).
- The Pd–Au catalysts with less than 3 wt% Au are less active in water production than the 1 wt% Pd catalyst. Especially the catalysts with 1 and 2 wt% gold produced substantially lower amount of water (more than 50% less) when compared to the Pd monometallic catalyst (see the exact values in Table 1). However, increasing the Au content from 3 wt% to 4 wt% seemed to cause a sudden increase in water production (see the exact values in Table 1).
- Indeed the 1% Pd–4% Au catalyst was substantially more active than the other catalysts in both H_2O_2 and water production.
- Fig. 1 demonstrates that the selectivity of catalysts (at least in the case of Pd–Au bimetallic catalysts) could be changing with the reaction time. This is because of the direct synthesis of H_2O_2 has a complex mechanism and could be influenced by different parameters. Therefore, in comparison of the performance of different catalysts, it is needed to consider the results versus time.

In general and according to the results presented in Fig. 1 and Table 1, the Pd–Au catalysts are more selective but less active (have lower yield and productivity) than the Pd monometallic catalyst even with lower total metal content. The only exception is the catalyst with 4 wt% Au. This catalyst is substantially more active in H_2O_2 and water production than the other bimetallic and monometallic Pd catalysts. Its selectivity is almost constant and does not change with the reaction time. However, the selectivity of the other Pd–Au catalysts is strongly dependent on reaction time, especially up to 1 h.

3.1.2. Increasing the amount of palladium with a constant amount of gold

In order to study the effect(s) of increasing the amount of palladium in Pd–Au bimetallic catalysts, a series of Pd–Au catalysts with constant amount of gold (1 wt%) and maximum 4 wt% palladium

Please cite this article in press as: D. Gudarzi, et al., Promotional effects of Au in Pd–Au bimetallic catalysts supported on activated carbon cloth (ACC) for direct synthesis of H_2O_2 from H_2 and O_2, Catal. Today (2014), http://dx.doi.org/10.1016/j.cattod.2014.04.011

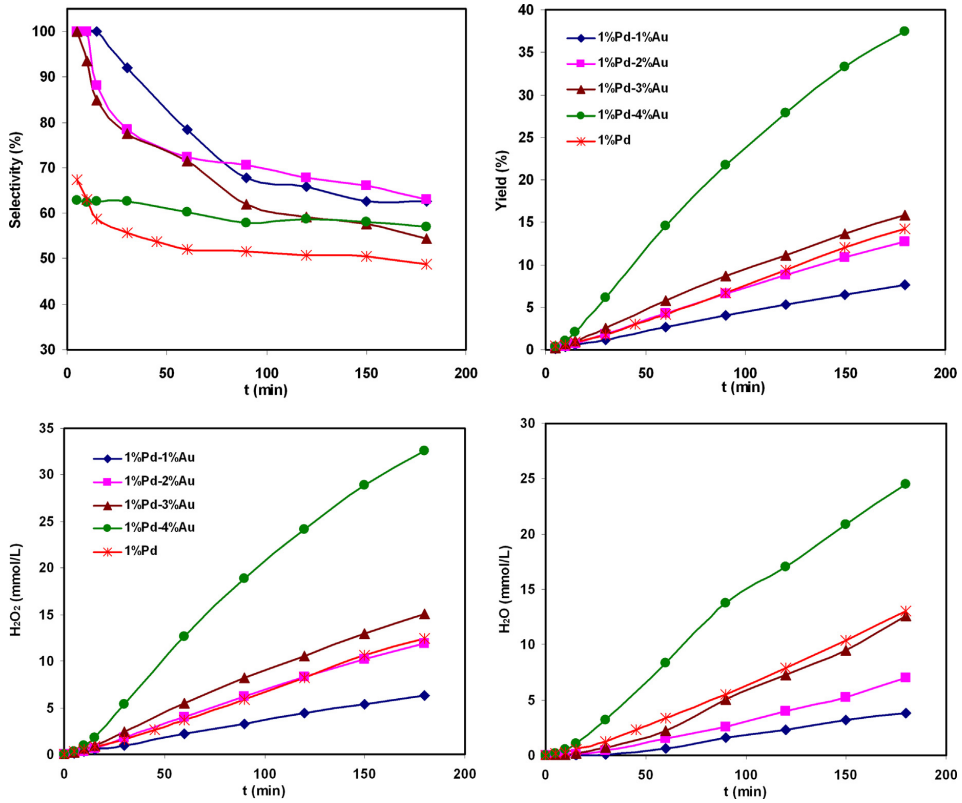

Fig. 1. The effect(s) of increasing the amount of gold on the catalytic activity of Pd_Au bimetalic catalysts supported on oxidized ACC; mass of catalyst = 56 mg, $T_{reaction}$ = 0 °C, and all catalysts calcined in air at 185 °C.

were prepared. The results of the performance of the catalysts are presented in Fig. 2. It can be observed that:

- When increasing the amount of palladium from 1 wt% to 2, 3, and 4 wt%, the selectivity of the Pd–Au bimetallic catalysts dropped a lot, especially in the first hour of the reaction time. It dropped more than 37% during the first 15 min. At the reaction times above 1.5 h, the differences between the selectivity of the different Pd–Au catalysts became smaller (less than 15% in the worst cases; see Table 1).
- The Pd–Au bimetallic catalysts with 1 wt% gold and more than 1 wt% Pd almost demonstrated constant selectivity versus time (Fig. 2), otherwise than the corresponding catalysts presented in Fig. 1.
- When increasing the amount of palladium in the Pd–Au catalysts, the rate of H_2O_2 production, yield, and H_2 conversion were increased almost with similar trends (Fig. 2, Table 1). When

Table 1
The catalytic activity of the Pd and Au mono metallic, and Pd_Au bimetallic catalysts supported on oxidized ACC after 3 h of the reaction time (in H_2O_2 direct synthesis). All catalysts were calcined in air at 185 °C.

Catalyst	H_2O_2 (mmol/L)	H_2O (mmol/L)	Selectivity (%)	Yield (%)	Productivity $\left(\frac{mol_{H_2O_2}}{h_{reaction}\, kg_{cat}}\right)$	H_2 conversion (%)
1% Pd	12.47	13.04	48.88	14.20	1467	29.05
3% Pd	24.45	28.13	46.49	27.63	985	59.42
5% Pd	19.72	24.75	44.34	24.87	520	56.09
1% Pd_1% Au	6.33	3.77	62.63	7.67	408	12.24
1% Pd_2% Au	11.96	7.02	63.00	12.66	514	20.10
1% Pd_3% Au	15.03	12.60	54.40	15.81	522	29.05
1% Pd_4% Au	32.56	24.49	57.08	37.51	846	65.71
2% Pd_1% Au	22.85	21.77	51.22	25.68	984	50.15
3% Pd_1% Au	35.28	27.08	56.58	44.62	1141	78.88
4% Pd_1% Au	39.51	43.32	47.70	45.34	1025	95.07
3% Pd_2% Au	26.88	26.03	50.81	28.52	693	56.13
2% Pd_3% Au	21.98	16.99	56.41	24.36	570	43.18
2.5% Pd_2.5% Au	30.41	23.57	56.34	32.45	791	57.59

Please cite this article in press as: D. Gudarzi, et al., Promotional effects of Au in Pd–Au bimetallic catalysts supported on activated carbon cloth (ACC) for direct synthesis of H_2O_2 from H_2 and O_2, Catal. Today (2014), http://dx.doi.org/10.1016/j.cattod.2014.04.011

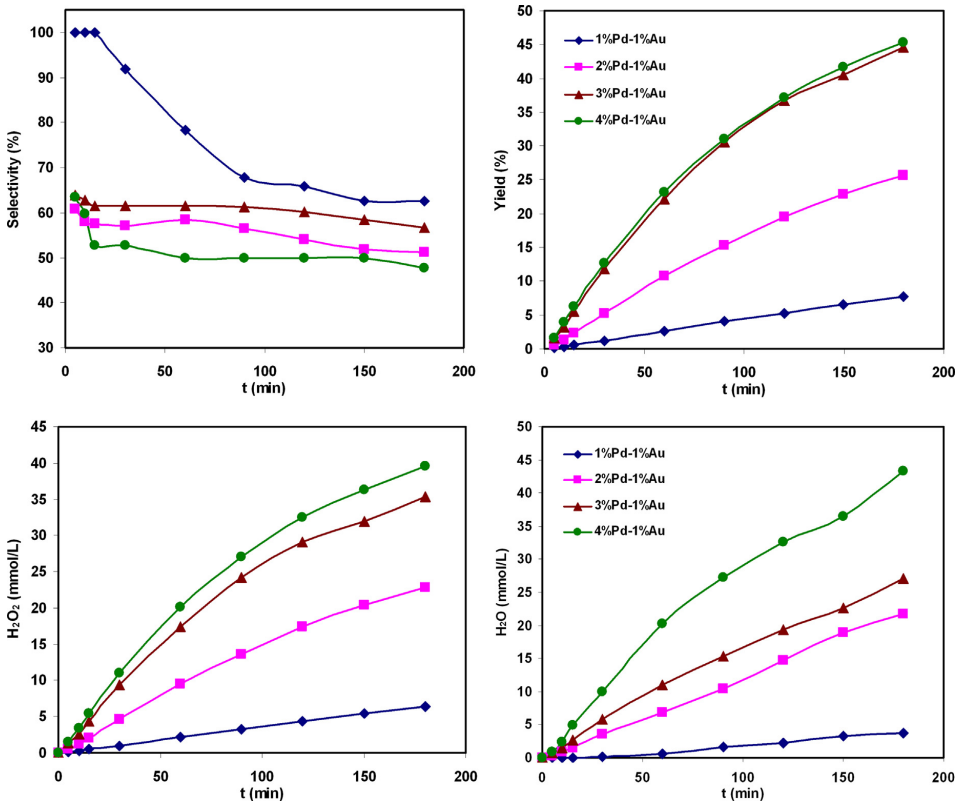

Fig. 2. The effect(s) of increasing the amount of palladium on the catalytic activity of Pd_Au bimetalic catalysts supported on oxidized ACC; mass of catalyst = 56 mg, $T_{reaction}$ = 0 °C, and all catalysts calcined in air at 185 °C.

increasing palladium from 1 to 2 wt% and from 2 to 3 wt%, the rate of H_2O_2 production, yield, productivity, and H_2 conversion jumped a lot (see exact values in Table 1). However, when increasing palladium from 3 to 4 wt%, these quantities did not change considerably. Indeed, the catalyst with 3 and 4 wt%Pd produced almost the same yields (see exact values in Table 1).

- When increasing the amount of palladium, the production rate of H_2O with the Pd–Au catalyst was also increased. However, when increasing palladium from 2 to 3 wt%, the rate did not change so much.
- Based on the results presented in Figs. 1–2 and Table 1, it can be said that the bimetallic catalysts with 1 wt% Au and ≥2 wt% Pd are more active (have higher yield and productivity) than the corresponding bimetallic catalysts with 1 wt% Pd and ≥2 wt% Au and Pd monometallic catalysts with same metal content.

In general, it can be concluded that increasing the amount of palladium in the Pd–Au bimetallic catalysts resulted in better activity but worse selectivity. Moreover, it should be mentioned that gold monometallic catalysts did not show any noticeable activity in direct synthesis of H_2O_2.

3.1.3. Changing Au/Pd ratio with a constant total metal content

The effects of the Au/Pd ratio on the final performance of the Pd–Au bimetallic catalysts with constant total metal content (Pd + Au = 5 wt%) are presented in Fig. 3. It can be observed that:

- All Pd–Au catalysts with Au/Pd ≥ 1 were more selective when compared to the 5 wt% Pd monometallic catalyst and the other bimetallic catalysts with Au/Pd < 1 (see exact values in Table 1).
- All Pd–Au bimetallic catalysts were more selective than the 5 wt% Pd monometallic catalyst when the reaction time was above 1.5 h.
- The bimetallic catalysts with Au/Pd < 1 were less selective when compared to the 5 wt% Pd monometallic catalyst when the reaction time was less than 1.5 h.
- The most selective one is the 2% Pd_3% Au bimetallic catalyst. However, it is also the least active catalyst. The rate of water production and H_2 conversion with this catalyst was considerably low when compared to the others (see exact values in Table 1).
- In the case of bimetallic catalysts, the 4% Pd_1% Au was substantially more active than the others (see exact values in Table 1). The rate of H_2O_2 and water production and consequently yield and H_2 conversion rate with this catalyst were considerably higher than with the others. However, it was the least selective one, especially when the reaction time was below 1.5 h.
- The second active catalyst was the one with 1 wt% of Pd and 4 wt% of Au. It was also one of the most selective ones. However, its activity was considerably less than the most active catalyst (4% Pd_1% Au).
- The third active catalyst was the one with 2.5 wt% of Pd and 2.5 wt% of Au. It was also one the most selective ones. Indeed, its selectivity was a little smaller than with the most selective catalyst (2% Pd_3% Au).

Please cite this article in press as: D. Gudarzi, et al., Promotional effects of Au in Pd–Au bimetallic catalysts supported on activated carbon cloth (ACC) for direct synthesis of H_2O_2 from H_2 and O_2, Catal. Today (2014), http://dx.doi.org/10.1016/j.cattod.2014.04.011

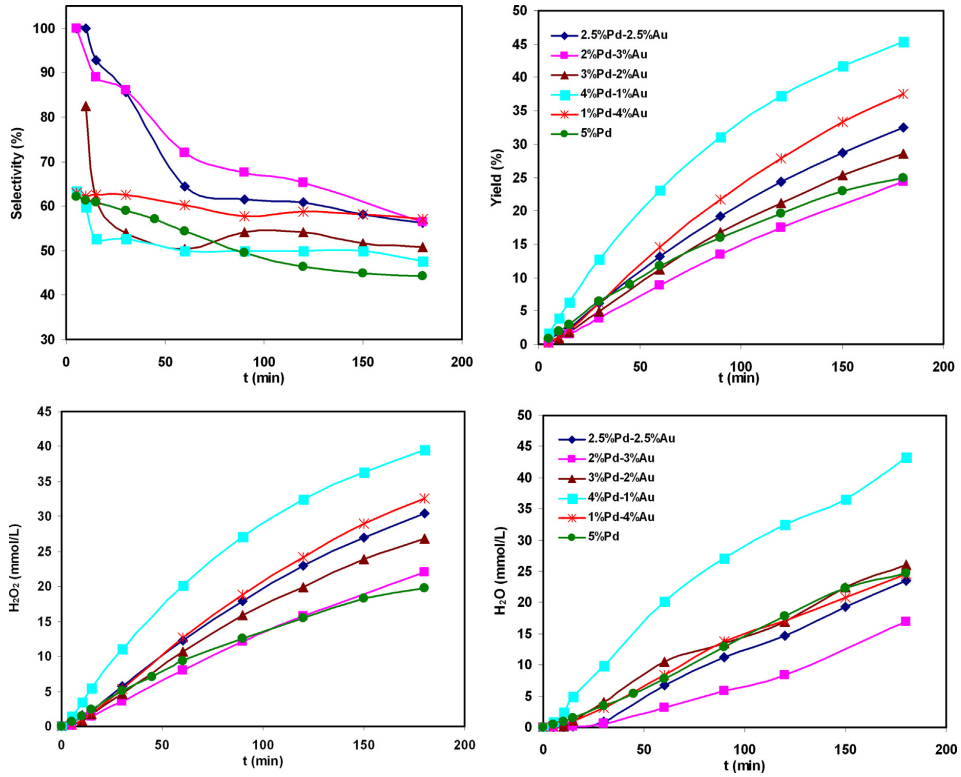

Fig. 3. The effect(s) of the Pd/Au ratio on the catalytic activity of Pd_Au bimetallic catalysts supported on oxidized ACC with constant amount of metal content (Pd + Au = 5 wt%); mass of catalyst = 56 mg, $T_{reaction}$ = 0 °C and all catalysts calcined in air at 185 °C.

– The rate of water production and H_2 conversion of the all the catalysts were almost the same, except with catalysts 4% Pd_1% Au and 2% Pd_3% Au.

3.1.4. Discussion

All of the catalysts presented in Figs. 1–3 were supported on the same carrier (oxidized ACC). Therefore, surface chemistry of the support is the same for all of them. However, different amount of the loaded metal could slightly affect the free available surface area of the support in the final catalyst (Table 2). Therefore, it can be concluded that the surface chemistry of the support cannot be main reason for the observed differences in the performance of different catalysts in Figs. 1–3.

Oxidation state of palladium and gold in the catalysts were determined by X-ray photo electron microscopy (XPS). XPS spectra of the presented bimetallic catalysts revealed that almost all of the palladium and gold were in zero-valent state or in metallic form (Pd^0). However, traces of palladium were in the ionic form (Pd^{+2}).

Ultra-High Resolution Field Emission Scanning Electron Microscope (UHRFESEM) images of the bimetallic catalysts with 1 wt% Pd and 1 wt% Au are presented in Fig. 4 (supplementary UHRFESEM images of different bimetallic catalysts were presented in the Supporting information (Figs. 3–5)). Based on the UHRFESEM images, the bimetallic catalysts consist of mainly small metal particles (Fig. 4b) with the size mostly 5–15 nm and also relatively big ones with different sizes in the order of 100 nm (Fig. 4a and c). All of them (small and big particles) are well dispersed in the support. Concerning the small metal particles, it can be said that:

Table 2
The effect of impregnation of oxidized ACC with different amount of gold and palladium, on the specific surface area of the final bimetallic catalysts.

Sample	S_{N_2} ($m^2\,g^{-1}$)
Oxidized ACC (OACC)	1550
(1% Pd_1% Au)/OACC	1521
(1% Pd_2% Au)/OACC	1480
(1% Pd_3% Au)/OACC	1468
(3% Pd_1% Au)/OACC	1424
(2.5% Pd_2.5% Au)/OACC	1397

– In the case of catalyst with 1 wt% Pd and 1 wt% Au, the size of small particles was mainly around 5 nm (Fig. 3a of Supporting information).
– When the amount of Pd was increased to 3 wt%, the size of the small particles was also increased to 10–15 nm. However, some particles with size 20–50 nm can be found (Fig. 4c and d of Supporting information).
– The catalyst with 1 wt% Pd and 3 wt% Au consist of considerable number of gold particles with different shape and the size mainly 20–50 nm (Fig. 5c and d of Supporting information). However, similar to the catalyst with 3 wt% Pd and 1 wt% Au, the small Pd particles were mostly 10–15 nm (Fig. 5e of Supporting information).

Please cite this article in press as: D. Gudarzi, et al., Promotional effects of Au in Pd–Au bimetallic catalysts supported on activated carbon cloth (ACC) for direct synthesis of H_2O_2 from H_2 and O_2, Catal. Today (2014), http://dx.doi.org/10.1016/j.cattod.2014.04.011

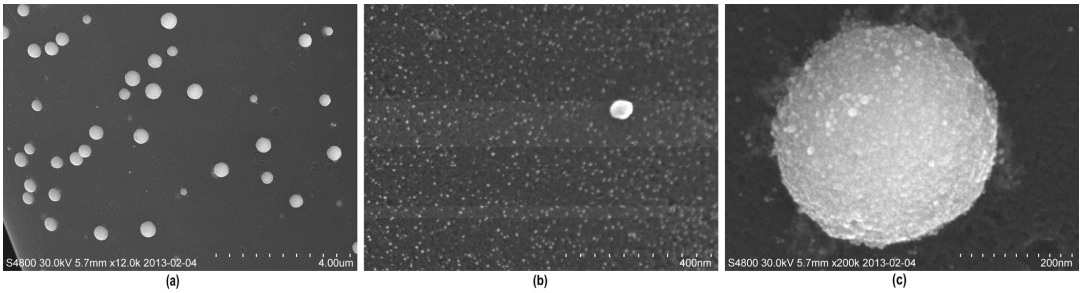

Fig. 4. The ultra-high resolution field emission scanning electron microscopy (UHRFESEM) images (with different magnifications) of 1 wt% Pd_1 wt% Au catalyst supported on oxidized ACC with different magnification.

- Based on EDS analysis of UHRFESEM images, small particles consist of monometallic palladium and gold along with Pd–Au alloy particles.
- In the case of catalyst with 3 wt% Pd and 1 wt% Au, small particles mostly consist of monometallic Pd particles. However, in the case of catalyst with 1 wt% Pd and 3 wt% Au, the number of Au monometallic particles was considerable.

Dispersion of the metal particles could be related to surface chemistry of the oxidized ACC and the electrostatic interaction between the surface of ACC fibers and ionic gold and palladium in the precursors. Ionic gold (Au^{3+}) in chloroauric acid ($HAuCl_4$) solution is mainly in the form of ($AuCl_4^-$) [44]. Ionic palladium (Pd^{2+}) in acidic solution of palladium dichloride ($PdCl_2$) appears mainly as tetrachloropalladic ion complex ($PdCl_4^{2-}$) [45]. Wet oxidation of activated carbon cloth (ACC) with nitric acid leads to formation of oxygen-containing functional groups on the surface of ACC fibers (see Section 3.3 for more detailed discussion). These acidic groups charged negatively the surface of ACC fibers. The electrostatic interaction (repulsion) between the metal precursors ($AuCl_4^-$, $PdCl_4^{2-}$) and the negatively charged surface of the oxidized ACC could result in good dispersion of metal precursors on the support surface. However, largely aggregated metallic particles (specially Au) were obtained principally due to the redox properties of activated carbon [46,47] In fact, the higher variety of activated carbon functionalities than those present on oxides (like silica and alumina) can promote other electrostatic interactions [46]. Concerning the big metal particles, it can be observed that:

- In the case of the catalyst with 1 wt% Pd and 1 wt% Au, the images with higher magnification of a big metal particle (Figs. 4c and 3b of Supporting information) and the Energy Dispersive X-ray Spectroscopy (EDS) analysis of STEM image of a Pd–Au particle (Fig. 5) reveal that these relatively round and big particles consist of a gold-rich core which was surrounded by a lot of small palladium particles. As a result, the outer surface of activated carbon cloth in 1% Pd_1% Au catalyst was changed to dark gray which is slightly lighter than the black color of the ACC. This pale gray color could possibly be assigned to the natural color of palladium.
- When increasing the amount of palladium, like in 3 wt% Pd_1 wt% Au bimetallic catalyst, the small Pd particles seemed to form a thicker and denser layer around the golden core. Therefore the Pd–Au particles on the outer surface of ACC fibers grew bigger (Fig. 4a and b of Supporting information).
- When the amount of gold was increased, like in 1 wt% Pd_3 wt% Au bimetallic catalyst, the round core–shell morphological Pd–Au particles were formed over bigger thin spots of gold (Fig. 5a and b of Supporting information). The round Pd–Au particles had almost the same morphology as the particles in 1% Pd_1% Au catalyst. The new morphology of Pd–Au particles was supported by EDS analysis of UHRFESEM images (Fig. 6). However, the changes of the color of the surface of the activated carbon cloth to pale yellow in the bimetallic catalysts with higher amount of gold can be seen.
- The morphology of the Pd–Au particles on the outer surface of ACC fibers in the 2.5 wt% Pd_2.5 wt% Au bimetallic catalyst looked almost the same as in 1 wt% Pd_3 wt% Au catalyst.
- The big Pd–Au particles formed on the outer surface of ACC fibers mainly consist of gold-rich core covered by small Pd particles with the size mostly less than 10 nm (Figs. 4c and 3b of Supporting information). Therefore, they could not be inactive. Indeed, it is assumed that Au acts as an electronic promoter for the Pd-rich shell [5,30,31].

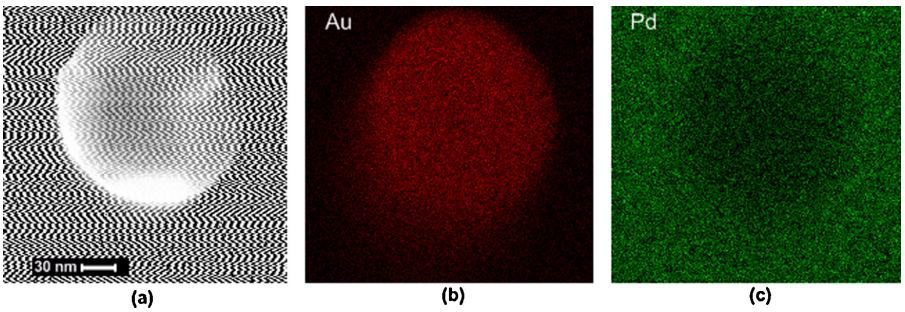

Fig. 5. STEM-EDS mapping and analysis of a separated Pd_Au particle in the 1 wt%_1 wt% Au bimetallic catalyst; (a) STEM image, (b) Au map, and (c) Pd map.

Please cite this article in press as: D. Gudarzi, et al., Promotional effects of Au in Pd–Au bimetallic catalysts supported on activated carbon cloth (ACC) for direct synthesis of H_2O_2 from H_2 and O_2, Catal. Today (2014), http://dx.doi.org/10.1016/j.cattod.2014.04.011

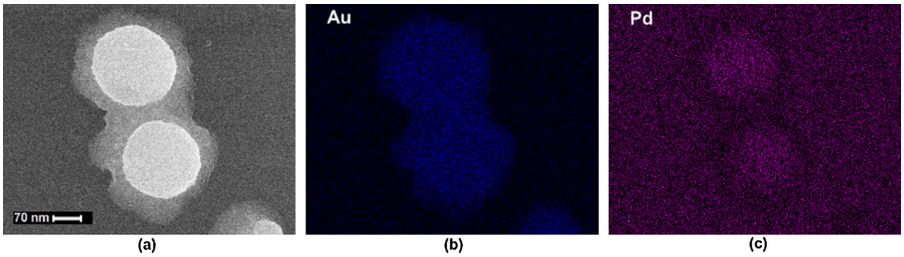

Fig. 6. STEM-EDS mapping and analysis of the 1 wt%_3 wt% Au bimetallic catalyst; (a) STEM image, (b) Au map, and (c) Pd map.

Based on the discussion above, it can be concluded that the morphology and size of the metal particles in the bimetallic catalysts are determined by the amount of palladium and gold and their ratio. Consequently, the different selectivities and activities of the Pd–Au catalysts presented in Figs. 1–3 could mostly be related to the different morphology and size of the metal particles.

3.2. The effects of the oxidation state of the loaded metal

In order to investigate the effects of the oxidation state of the metal components (Pd and Au), the catalysts supported on non-oxidized ACC were selected. In the case of oxidized ACC, the presence of the oxygen-containing surface functional groups also affected the final catalytic performance. Therefore, the results would reflect combined effect of different factors (surface chemistry of the support, oxidation state of the metal part . . .). In the case of the non-oxidized ACC, lack of the oxygen-containing surface functional groups makes it possible to investigate merely the effects of the oxidation state of the metallic part of the catalysts.

The results of the catalytic activities of the different 3% Pd_1% Au bimetallic catalysts supported on non-oxidized ACC are presented in Table 3. One of the catalysts was calcined in air at 185 °C and, the other one at 275 °C. It can be observed that:

- The yield and H_2O_2 production rates demonstrate that the catalyst calcined at 275 °C is more active in H_2O_2 production than the other.
- However, the H_2 conversion and water production rates reveal that the catalyst calcined at 185 °C is more active in water production than the other.
- Therefore, the catalyst calcined at 275 °C is more selective (about 50%) than the other.

The X-ray photo electron microscopy spectra of the calcined 3% Pd_1% Au catalysts (Fig. 7 of Supporting information) revealed that:

- Palladium in the catalyst calcined at 185 °C was almost in zero-valent or in metallic state (Pd^0) and only traces of the palladium were in the form of Pd^{+2} originated from palladium dichloride $PdCl_2$.
- When increasing the calcination temperature to 235 °C almost 8 wt% of the total amount of the palladium was oxidized to palladium oxide (PdO).
- In the catalyst calcined at 275 °C, almost 63 wt% of the total amount of palladium is in the form of palladium oxide. Therefore, increasing the calcination temperature increases the amount of palladium oxide.
- In the case of 1% Pd-4% Au bimetallic catalyst, when increasing the calcination temperature, the amount of PdO was substantially low compare to the corresponding calcined catalysts with 3% Pd and 1% Au. Indeed, in the 1% Pd_4% Au catalyst calcined at 275 °C, only 8% of the total amount of palladium was in the form of palladium oxide.
- In general, in the case of Pd–Au bimetallic catalysts with Au/Pd > 1, calcination at 235–275 °C resulted in smaller amount of palladium oxide than with Au/Pd ≤ 1.
- Gold in all calcined catalyst was still in metallic or zero-valent state.

Based on the results and discussions above, it could be concluded that the presence of palladium oxide (PdO) made the Pd–Au bimetallic catalysts more selective and more active than the corresponding catalysts with Pd^0.

Low amount of PdO in 1% Pd_4% Au catalyst calcined at 275 °C resulted in smaller differences in catalytic performance of the two catalysts calcined at 185 °C and 275 °C when compared to the corresponding differences observed for the 3% Pd_1% Au catalysts (Table 3).

3.3. The effects of the surface chemistry of the ACC fibers on the final catalytic performance and surface morphology of the Pd–Au bimetallic catalysts

The results of the catalytic performance of two bimetallic catalysts with different amounts of palladium and gold supported on

Table 3
The catalytic activity of the Pd–Au bimetallic catalysts supported on non-oxidized ACC and ACC oxidized with nitric acid after 2 h of the reaction time (in H_2O_2 direct synthesis). The catalysts calcined in air at 185–275 °C.

Catalyst	H_2O_2 (mmol/L)	H_2O (mmol/L)	Selectivity (%)	Yield (%)	H_2 Conversion (%)
Catalysts supported on non-oxidized ACC					
3% Pd_1% Au, T_{cal} = 185 °C	23.49	57.41	29.04	26.64	91.73
3% Pd_1% Au, T_{cal} = 275 °C	30.77	40.69	43.06	36.82	85.52
1% Pd_4% Au, T_{cal} = 185 °C	20.45	37.00	35.72	23.15	65.11
1% Pd_4% Au, T_{cal} = 275 °C	20.49	32.87	38.40	23.13	60.24
Catalysts supported on oxidized ACC					
3% Pd_1% Au, T_{cal} = 185 °C	29.09	19.31	60.10	36.79	61.22
1% Pd_4% Au, T_{cal} = 185 °C	24.19	17.03	58.69	33.30	47.47

Please cite this article in press as: D. Gudarzi, et al., Promotional effects of Au in Pd–Au bimetallic catalysts supported on activated carbon cloth (ACC) for direct synthesis of H_2O_2 from H_2 and O_2, Catal. Today (2014), http://dx.doi.org/10.1016/j.cattod.2014.04.011

Table 4
Total amount of CO and CO_2 desorbed according to temperature programmed desorption test.

Sample	CO (μmol/g)	CO_2 (μmol/g)
Non-oxidized ACC	115.13	82.73
Oxidized ACC (OACC)	1147.52	1290.44
3%Pd_1% Au/OACC (T_{red} = 185 °C)	1015.26	445.81
3%Pd_1% Au/OACC (T_{cal} = 185 °C)	1390.23	935.57
3%Pd_1% Au/OACC (T_{cal} = 235 °C)	1483.51	742.43
3%Pd_1% Au/OACC (T_{cal} = 270 °C)	1569.35	529.53

non-oxidized ACC and ACC oxidized with nitric acid are presented in Table 3. It can be observed that:

- The catalysts supported on oxidized ACC were substantially more selective than the corresponding ones supported on non-oxidized ACC. In the case of the catalyst with 3 wt% Pd and 1 wt% Au, the catalyst supported on oxidized ACC was almost 2 times more selective than the corresponding one on non-oxidized ACC.
- According to the results of yield and rate of H_2O_2 production, the catalysts supported on oxidized ACC were also more active than the corresponding catalysts on non-oxidized ACC.
- H_2 conversion results and the rate of water production demonstrated that the catalysts supported on non-oxidized ACC were considerably more active in water production than the corresponding ones on the oxidized ACC.
- Almost similar results were observed for the other bimetallic catalysts presented in this paper. The only difference is that in the case of bimetallic catalysts with Au/Pd ≥ 1, the differences between performances of the catalysts supported on oxidized ACC and non-oxidized ACC is smaller than the catalysts with Au/Pd < 1. This can be explained as, in general, with increasing the amount of Au, bimetallic catalysts become more selective and less active.

In our previous work [6], it was demonstrated that the oxidation pretreatment of activated carbon cloth (ACC) with nitric acid introduce considerable amounts of oxygen-containing functional groups on the surface of ACC fibers. These functional groups can be classified as strong acidic oxygen-containing groups (like carboxylic and anhydride groups) and weak acid ones (like lactones, phenols and carbonyl groups) [38–43]. These acidic functional groups affect a lot the activity and physicochemical properties of final catalysts [6]. The oxygen-containing functional groups can be characterized by thermal programmed desorption (TPD) test [6,38–41]. Strong and weak acidic oxygen-containing groups are responsible for CO_2 and CO desorption in TPD, respectively (Table 4). Different surface chemistry of the supports (Table 4) leads to different morphology in Pd–Au bimetallic catalysts supported on non-oxidize and oxidized ACC. The morphology of Pd–Au particles in the catalysts supported on oxidized ACC has been discussed in Section 3.1.4 In the case of non-oxidized ACC, palladium and gold form really big and joined particles at the outer surface of ACC fibers (Fig. 6 of Supporting information). In most areas, the metal particles almost cover the outer surface of the ACC fibers. These completely different surface morphologies result in different catalytic performance. The considerable surface morphology changes in the non-oxidized could be explained as follow.

It was mention earlier (Section 3.1.4) that the ionic gold (Au^{3+}) and palladium (Pd^{2+}) in acidic solution of hydrogen tetrachloroaurate ($HAuCl_4$) and palladium dichloride ($PdCl_2$) appear mainly as ion complexes ($AuCl_4^-$ and $PdCl_4^{2-}$). The pH of the precursors during the impregnation of the ACC was in the range of 3.5–4. According to isoelectric point measurements [6], the pH_{IEP} of the oxidized and non-oxidized ACC were 3.5 and 5, respectively. At pH below the pH_{IEP} the surface is negatively charged while at pH over the pH_{IEP}, the surface is positively charged. During the impregnation of non-oxidized ACC with gold and palladium precursor, the pH of the precursor is considerably less than pH_{IEP} of the surface of the ACC fibers. Therefore, the electrostatic attraction between the positively charged surface ($pH < pH_{IEP}$) and the catalyst precursor anions ($AuCl_4^-$ and $PdCl_4^{2-}$) facilitate the adsorption of ionic gold and palladium species ($AuCl_4^-$ and $PdCl_4^{2-}$) on the surface of the ACC fibers. Moreover, carbon is essentially not hydrophilic in nature and it has a very low affinity for solvents of polar character such as water [40]. Therefore, the metal precursors will be mostly exposed to the outer surface of the ACC fibers when using water. This factor together with electrostatic attraction between the surface of non-oxidized ACC and the catalyst precursor anions ($AuCl_4^-$ and $PdCl_4^{2-}$) leads to a rapid massive deposition of Au and Pd on the outer surface of ACC fibers.

Moreover, in the case of oxidized ACC, oxygen-containing surface functional groups might also affect directly the final performance of the catalysts. These acidic groups negatively charge the surface of activated carbon cloth [6] and decrease the hydrophobicity of the surface [40]. Therefore, the concentration of water on the surface of ACC's fibers and pores is higher in the oxidized ACC than in non-oxidized one. The affinity of the surface of oxidized ACC holding water molecules might also affect the final rate of water production by H_2O_2 decomposition/hydrogenation ($H_2O_2 \rightarrow H_2O + (1/2)O_2$; $H_2O_2 + H_2 \rightarrow 2H_2O$) and non-selective H_2O synthesis ($H_2 + (1/2)O_2 \rightarrow H_2O$), according to the Le Chatelier's principle.

3.4. The effects of heat treatment of the catalysts in H_2 and air at different temperatures

The results of the catalytic performance of the different 3% Pd_1% Au catalysts supported on oxidized ACC are presented in Fig. 7. It can be observed that:

- The catalysts calcined in the air at 185–275 °C were almost 3 times more selective than the catalyst reduced by H_2 at 185 °C.
- According to the results of yield and H_2O_2 production rate, the calcined catalysts were substantially more active in H_2O_2 production than the corresponding reduced one.
- The catalyst reduced by H_2 was dramatically more active in water production than the calcined catalysts.
- The catalyst calcined at 235 °C was considerably more active in H_2O_2 and also in water production than the other calcined catalysts.
- In the case of calcined catalysts, the catalyst calcined at 185 °C had the highest selectivity and, the one calcined at 235 °C had the lowest selectivity. However, the selectivities of the different calcined catalysts were quite close to each other.
- In the case of calcined catalysts, the catalyst calcined at 275 °C showed lower activity in H_2O_2 and water production than the other ones.
- Almost similar results were observed for the other bimetallic catalysts supported on oxidized ACC.

The ultra-high resolution field emission scanning electron microscope (UHRFESEM) images and EDS analysis confirmed that the heat treatment in H_2 at 185 °C and the calcination in air up to 275 °C had no noticeable effects on the morphology of the Pd–Au particles in the catalyst. However, the heat treatment of the oxidized ACC damages the oxygen-containing surface functional groups (Table 4). In the case of calcined catalysts, increasing the calcination temperature increased the damage, especially to the stronger acidic surface functional groups. These groups are responsible for CO_2 releasing in temperature programmed desorption (TPD) test (Table 4). Heat treatment of Pd–Au catalysts supported

Please cite this article in press as: D. Gudarzi, et al., Promotional effects of Au in Pd–Au bimetallic catalysts supported on activated carbon cloth (ACC) for direct synthesis of H_2O_2 from H_2 and O_2, Catal. Today (2014), http://dx.doi.org/10.1016/j.cattod.2014.04.011

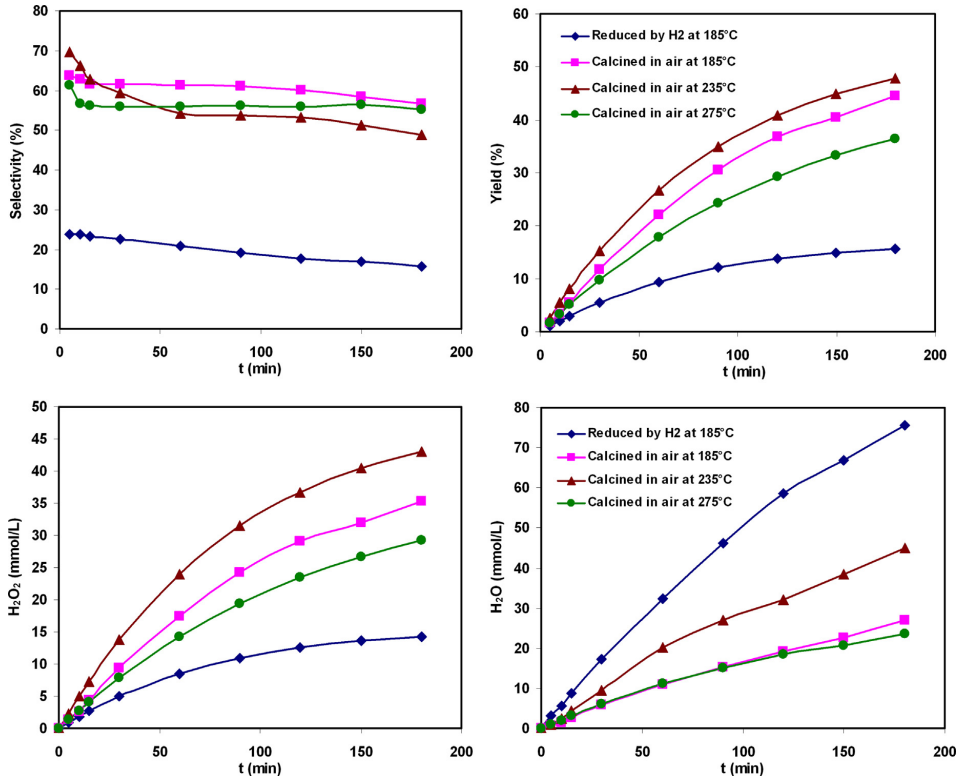

Fig. 7. The catalytic activity of the different 3 wt% Pd_1 wt% Au bimetallic catalysts on oxidized ACC; mass of catalyst = 56 mg, $T_{reaction}$ = 0 °C.

on oxidized ACC by H_2 at 185 °C causes maximum damage to the stronger acidic oxygen functional groups (Table 4).

From the other side, increasing the calcination temperature increases the amount of PdO in the final catalyst (see Section 3.2). Based on the results and discussions in Sections 3.2 and 3.3, higher amount of palladium oxide in the catalyst and fewer damages to the surface functional groups (in the case of ACC oxidized with nitric acid) are favored for direct catalytic synthesis of H_2O_2. Therefore, increasing the calcination temperature has two opposite effects, namely the damage to the oxygen-containing surface functional groups (Table 4) and increasing the amount of palladium oxide, and the resultant of these two effects mainly determine the different activities observed in Fig. 7.

In the case of the catalyst reduced by H_2 at 185 °C, it seems that the lack of palladium oxide and maximum damages to the oxygen-containing surface functional groups (Table 4) caused the catalyst to be considerably less selective and less active in H_2O_2 production and substantially more active in water production than the calcined catalysts.

4. Conclusions

The results showed that the surface morphology of the Pd–Au bimetallic catalysts and their catalytic performance in direct synthesis of H_2O_2 were highly influenced by the surface chemistry of the support and the amount and the ratio of Pd and Au in the catalyst.

Wet oxidation of activated carbon cloth (ACC) resulted in formation of oxygen-containing functional groups on the surfaces of ACC's fibers. These functional groups mainly control surface morphology, and consequently the selectivity and activity of the bimetallic catalysts in direct synthesis of H_2O_2. The bimetallic catalysts supported on the oxidized ACC were substantially more selective and also more active in H_2O_2 production than the corresponding ones supported on non-oxidized ACC. However, the catalysts supported on non-oxidized ACC had high H_2 conversion since they were considerably more active in water production than the corresponding catalysts on oxidized ACC.

Almost all of the Pd–Au bimetallic catalysts were more selective than Pd monometallic catalysts. In the case of bimetallic catalysts:

- Increasing the amount of Au resulted in more selective but less active catalysts.
- Increasing the amount of Pd resulted in more active but less selective catalysts.
- Moreover, morphology of Pd–Au particles was also affected with the amount and ratio of gold and palladium in the catalysts.

The presence of palladium oxide made the catalysts more selective and active in H_2O_2 production but less active in water production than the corresponding catalysts consisting of zero-valent palladium (Pd^0).

Please cite this article in press as: D. Gudarzi, et al., Promotional effects of Au in Pd–Au bimetallic catalysts supported on activated carbon cloth (ACC) for direct synthesis of H_2O_2 from H_2 and O_2, Catal. Today (2014), http://dx.doi.org/10.1016/j.cattod.2014.04.011

Acknowledgement

The authors thank Dr. Kari Eranen for helping with the TPD and SSA measurements.

Appendix A. Supplementary data

Supplementary data associated with this article can be found, in the online version, at http://dx.doi.org/10.1016/j.cattod.2014.04.011.

References

[1] M. Piccinini, J.K. Edwards, J.A. Moulijn, G.J. Hutchings, Catal. Sci. Technol. 2 (2012) 1908–1913.
[2] G.J. Hutchings, Catal. Today 138 (2008) 9–14.
[3] C.E. Baukal, Oxygen-Enhanced Combustion, CRC Press LLC, Boca Raton, Florida, 1998.
[4] J.K. Edwards, G.J. Hutchings, Angew. Chem. Int. Ed. 47 (2008) 9192.
[5] B.E. Solsona, J.K. Edwards, P. Landon, A.F. Carley, A. Herzing, C.J. Kiely, G.J. Hutchings, Chem. Mater. 18 (2006) 2689.
[6] D. Gudarzi, W. Ratchananusorn, I. Turunen, M. Heinonen, T. salmi, Top. Catal. 56 (2013) 527.
[7] A.G. Gaikwad, S.D. Sansare, V.R. Choudhary, J. Mol. Catal. A Chem. 181 (2002) 143.
[8] V.R. Choudhary, A.G. Gaikwad, S.D. Sansare, Catal. Lett. 83 (2002) 235.
[9] V.R. Choudhary, S.D. Sansare, A.G. Gaikwad, Catal. Lett. 84 (2002) 81.
[10] V.V. Krishnan, A.G. Dokoutchaev, M.E. Thompson, J. Catal. 196 (2000) 366.
[11] D.P. Dissanayake, J.H. Lunsford, J. Catal. 214 (2003) 113.
[12] R. Burch, P.R. Ellis, Appl. Catal. B: Environ. 42 (2003) 203.
[13] S. Abate, G. Centi, S. Melada, S. Perathoner, F. Pinna, G. Strukul, Catal. Today. 104 (2005) 323.
[14] S. Melada, F. Pinna, G. Strukul, S. Perathoner, G. Centi, J. Catal. 235 (2005) 241.
[15] S. Melada, F. Pinna, G. Strukul, S. Perathoner, G. Centi, J. Catal. 237 (2006) 213.
[16] T.A. Pospelova, N.I. Kobozev, E.N. Eremin, J. Phys. Chem. (Trans.) 35 (1961) 143.
[17] T.A. Pospelova, N.I. Kobozev, J. Phys. Chem. (Trans.) 35 (1961) 262.
[18] K.P. Reis, V.K. Joshi, M.E. Thompson, J. Catal. 161 (1996) 62.
[19] D.P. Dissanayake, J.H. Lunsford, J. Catal. 206 (2002) 173.
[20] S. Chinta, J.H. Lunsford, J. Catal. 225 (2004) 249.
[21] Y.-F. Han, J.H. Lunsford, J. Catal. 230 (2005) 313.
[22] Q. Liu, J.H. Lunsford, J. Catal. 239 (2006) 237.
[23] Q. Liu, J.H. Lunsford, Appl. Catal. A: Gen. 314 (2006) 94.
[24] D. Gudarzi, O.A. Simakova, J.R. Hernández Carucci, P.D. Biasi, K. Eränen, E. Kolehmainen1, I. Turunen, D.Y. Murzin, T. Salmi, Chem. Eng. Trans. 21 (2010) 925.
[25] T. Danciu, E.J. Beckmann, T. Hancu, R.N. Cochran, R. Grey, D.M. Hajnik, J. Jewson, Angew Chem. Int. Ed. 2 (2003) 1140.
[26] V.R. Choudhary, C. Samanta, T.V. Choudhary, Appl. Catal. A: Gen. 308 (2006) 128.
[27] C. Samanta, V.R. Choudhary, Appl. Catal. A: Gen. 326 (2007) 28.
[28] P. Landon, P.J. Papworth, C.J. Kiely, G.J. Hutchings, Chem. Commun. (2002) 2058.
[29] P. Landon, P.J. Collier, A.F. Carley, D. Chadwick, A.J. Papworth, A. Burrows, C.J. Kiely, G.J. Hutchings, Phys. Chem. Chem. Phys. 5 (2003) 1917.
[30] J.K. Edwards, B.E. Solsona, P. Landon, A.F. Carley, A. Herzing, C.J. Kiely, G.J. Hutchings, J. Catal. 236 (2005) 69.
[31] J.K. Edwards, B. Solsona, P. Landon, A.F. Carley, A. Herzing, M. Watanabe, C.J. Kiely, G.J. Hutchings, J. Mater. Chem. 15 (2005) 4595.
[32] G. Li, J. Edwards, A.F. Carley, G.J. Hutchings, Catal. Today 122 (2007) 361.
[33] J.K. Edwards, A. Thomas, B.E. Solsona, P. Landon, A.F. Carley, G.J. Hutchings, Catal. Today 122 (2007) 397.
[34] G. Li, J. Edwards, A.F. Carley, G.J. Hutchings, Catal. Today 114 (2006) 369.
[35] J.K. Edwards, A.F. Carley, A.A. Herzing, C.J. Kiely, G.J. Hutchings, Faraday Discuss. 138 (2008) 225.
[36] J.K. Edwards, E. Ntainjua, A.F. Carley, A.A. Herzing, C.J. Kiely, G.J. Hutchings, Angew. Chem., Int. Ed. 48 (2009) 8512.
[37] A.M. Venezia, V. La Parola, G. Deganello, B. Pawelec, J.L.G. Fierro, J. Catal. 215 (2003) 317.
[38] C. Moreno-Castilla, M.V. López-Ramón, F. Carrasco-Marín, Carbon 38 (2000) 1995–2001.
[39] Sh. Wenzhong, Li. Zhijieand, Liu Yihong, Recent Patents Chem. Eng. 1 (2008) 27–40.
[40] F. Rodríguez-reinoso, Carbon 36 (1998) 159–175.
[41] J.M. Rosas, J. Bedia, J. Rodríguez-Mirasol, T. Cordero, Fuel 88 (2009) 19–26.
[42] M.L. Toebes, J.A. van Dillen, K.P. de Jong, J. Mol. Catal. A: Chem. 173 (2001) 75–98.
[43] W.C. Oh, M.H. Yum, Bull. Korean Chem. Soc. 25 (2004) 1189–1194.
[44] M. Haruta, Catal. Today 36 (1997) 153–166.
[45] P.A. Simonov, A.V. Romanenko, I.P. Prosvirin, E.M. Moroz, A.I. Boronin, A.L. Chuvilin, V.A. Likholobov, Carbon 35 (1997) 73–82.
[46] L. Prati, A. Villa, Catalysts 2 (2012) 24–37.
[47] L. Prati, Gold Bull. 32 (1999) 96–101.

Please cite this article in press as: D. Gudarzi, et al., Promotional effects of Au in Pd–Au bimetallic catalysts supported on activated carbon cloth (ACC) for direct synthesis of H_2O_2 from H_2 and O_2, Catal. Today (2014), http://dx.doi.org/10.1016/j.cattod.2014.04.011

Publication IV

D. Gudarzi, W. Ratchananusorn, I. Turunen, M. Heinonen, T. Salmi
Factors influencing hydrogenation and decomposition of H_2O_2 over Pd-Au catalysts supported on activated carbon cloth (ACC)
Submitted to Topics in Catalysis

Factors influencing hydrogenation and decomposition of H_2O_2 over Pd-Au catalysts supported on activated carbon cloth (ACC)

Davood Gudarzi *[a], Ilkka Turunen [a], Markku Heinonen [b], Tapio Salmi [c],

[a] Department of Chemical Technology, Lappeenranta University of Technology, Lappeenranta, FI-53851 Finland

[b] Department of Physics and Astronomy, University of Turku, Turku, FI-20014 Finland

[c] Laboratory of Industrial Chemistry and Reaction Engineering, Åbo Akademi University, Turku/Åbo, FI-20500 Finland

[*] Corresponding author. E-mail: davood.gudarzi@lut.fi; Tel: +358 44 5177734;

Abstract

The bimetallic Pd-Au catalysts were prepared by simultaneous co-impregnation or consequent impregnation of supports by palladium and gold precursors. The catalytic reactions were performed batch-wise in a Parr stainless steel autoclave and methanol (220 ml) was used as solvent. A series of experiments were conducted to study effects of several variables and conditions on the final H_2O_2 destruction activity of the catalysts. The factors studied where : the surface chemistry of the support, the amount and ratio of palladium and gold, the catalyst preparation method, the heat treatment of the catalysts in H_2 and air, the reaction medium, and reaction temperature. As a conclusion, H_2O_2 destruction activities of the catalysts were strongly affected by the surface chemistry of the support and the amount and ratio of palladium and gold. Bimetallic catalysts prepared by co-impregnation of Pd and Au were less destructive than the corresponding ones prepared by consequent impregnation. The catalysts supported on ACC oxidized by nitric acid were considerably less destructive than the corresponding ones on non-oxidized ACC. H_2O_2 destruction activity of the catalysts on oxidized ACC were highly affected by the heat treatment in H_2 and air at different temperatures. Using water instead of methanol as reaction medium substantially speeded up H_2O_2 destruction. Furthermore, increasing the reaction temperature accelerated destruction of H_2O_2. Catalytic destruction of H_2O_2 via its decomposition was considerably low as compared to hydrogenation.

1. Introduction

Hydrogen peroxide (H_2O_2) is an environmentally friendly strong oxidizing agent with a global production of over two million tons per year, and increasing annually by 10% [1]. It is mainly used as a bleaching agent or disinfectant and also as a green oxidant for chemical synthesis. Commercially, hydrogen peroxide is manufactured by the sequential hydrogenation and oxidation of an alkyl anthraquinones. This method has several drawbacks, including the use of a complex solvent system, deactivation of hydrogenation catalysts, relatively high numbers of process equipment leading to high investment cost. Direct synthesis from H_2 and O_2 provides a promising process alternative. Therefore, it has received considerable attention in recent years. Palladium has mainly been used as a catalyst in this process. In the direct synthesis of H_2 and O_2 to H_2O_2 over Pd catalysts, also water is obtained in addition to H_2O_2 (Fig. 1 reactions i, ii).

Furthermore, the produced H_2O_2 is unstable in the presence of the catalyst which facilitates its conversion to water (Fig. 1 reactions iii, iv). Therefore, selectivity is a key issue. Moreover, mixtures of hydrogen and oxygen are explosive over a wide range of concentrations (4-94% H_2 in O_2) [2]. These challenges have prohibited the commercial application of the direct synthesis so far.

Activity and selectivity of Pd catalysts are strongly affected by the support materials. Pd catalysts on acidic support, e.g. Pd on SiO_2, were reported to be more active than basic supports (Pd on γAl_2O_3) [2-4]. Majority of researches have focused on the factors which maximize the rate of reaction i (Fig. 1) while suppressing reactions ii–iv (Fig. 1). V.R. Choudhary et al [5-7] have reported that the H_2O_2 destruction activity (Fig. 1, reactions iii and iv) of Pd catalysts was highly influenced by the oxidation state of Pd particles. They showed that palladium oxide (PdO) is substantially less destructive than zero valent state of palladium (Pd^0). Indeed, it was demonstrated that supported PdO catalysts are more selective but less active than the corresponding Pd^0 catalysts [4, 8-14]. Several promoters have been examined to enhance the selectivity of Pd catalysts. Using of halide ions (especially Br^-) in reaction medium and/or directly in the catalyst along with protons (H^+) can raise selectivity [5-7, 15-29]. The halide ions together with protons (H^+) ions promote the selectivity mainly by reducing the non-selective oxidation of H_2 to water. It happens by inhibiting the dissociative chemisorption of oxygen on the catalyst surface and also by decreasing the decomposition and hydrogenation of H_2O_2 [30]. Fu et al [31] have demonstrated that the H_2O_2 yield and selectivity depend more on the surface chemistry of the support than on the metal particle size and specific surface area. In the case of carbon material as support, Gudarzi et al [4, 8, and 32] have shown that the selectivity and H_2O_2 destruction activity of Pd catalysts were highly affected by the amount and nature of surface functional groups.

The addition of a second metal (e.g. Pt, Au, Ru, Rh) to Pd catalysts has been reported to affect activity and selectivity in direct H_2O_2 synthesis [3, 33–41]. The addition of Au or Pt (at an optimum concentration) to a Pd catalyst has been reported to enhance the selectivity, while the presence Rh or Ru exhibited an adverse effect [42]. The observation that Au–Pd bimetallic catalysts were more active in direct H_2O_2 synthesis than either Pd or Au monometallic catalysts was initially reported by Hutchings et al. [3, 37, 43-44]. It was also found that, on the contrary to Pd monometallic catalysts, the addition of stabilizers, such as Br^- ions and protons (H^+) were deleterious for the Au–Pd catalysts [38]. Edwards et al. [44] showed that acid pretreatment of carbon support for a gold-palladium alloy catalyst eliminates the decomposition of H_2O_2. Supports can highly affect the performance of Pd-Au bimetallic catalysts, in the same way as to Pd monometallic catalysts. Hutching et al [40] reported the performance of different supports decreases in the following order: carbon>TiO_2>SiO_2>Al_2O_3>Fe_2O_3. Structured forms of activated carbon materials, such as activated carbon felts and activated carbon cloths (ACCs) represent promising alternatives due to their excellent characteristics and properties [45]. However, the use of the textural form of activated carbons (ACC and ACF) as catalyst supports is not yet well covered in scientific literature.

Previously [4, 8], direct synthesis and catalytic destruction of H_2O_2 over Pd catalysts supported on activated carbon cloth (ACC) were thoroughly studied. Promotional effects of Au in Pd-Au bimetallic catalysts supported on activated carbon cloth (ACC) have been investigated by Gudarzi et al [46]. Since H_2O_2 destruction can highly affect the selectivity and yield, it is important to have a deep understanding of the catalytic factors affecting the H_2O_2 decomposition

reactions (Fig. 1, reactions iii, iv). In the present work, the destruction of H_2O_2 by its decomposition (Fig. 1, reaction iv) and hydrogenation (Fig. 1, reaction iii) over Pd-Au bimetallic catalysts supported on activated carbon cloth were considered. The effects of the surface chemistry of the support, the amount and ratio of palladium and gold, the preparation method, the oxidation state of the metallic components, heat pre-treatment of the catalysts in air and H_2 at different temperatures, and reaction conditions on the final H_2O_2 destruction activity of the catalysts were investigated.

2. Experimentation

2.1. Catalysts preparation

A commercial activated carbon cloth ACC-5092-20 (Kynol Europa GmbH), after cleaning and a chemical treatment, was employed as a support. Acidic solution of palladium (II) chloride ($PdCl_2$) and gold (III) chloride hydrate ($HAuCl_4$) were used as metal precursors. The activated carbon cloth was first treated in an oven at 100 °C for about 12 h. Then it was cleaned with 50 wt% solution of methanol at room temperature for 1 h, and finally washed with plenty of deionized water. For wet oxidation, the cleaned ACC was treated with 20 wt% solution of nitric acid at room temperature for 40 h. After the oxidative treatment, the ACC samples were washed with deionized water until neutral conditions were reached, and then dried at 60 °C for 24 h. This sample is referred as oxidized ACC (OACC). Acid pre-treatment step was used to create oxygen-containing functional groups on the surface of activated carbon fibers and to modify the surface as suggested by several authors [47-52].

The Pd catalysts were prepared using impregnation method as described by Gudarzi et al [4]. The Pd-Au bimetallic catalysts on non-oxidized and oxidized activated carbon cloth were prepared by simultaneous co-impregnation of the supports with an aqueous acidic solution of $PdCl_2$ and $HAuCl_4$ at room temperature for 6-7 h. The impregnation was done in a 200 ml glass reactor with stirring rate of 400-500 rpm. The ratio of the solution volume to catalyst mass was 500 ml/g. The amount of the precursor (Pd + Au) between 7.2-17.3 mg per 200 mg of the support in a 200 ml glass reactor gave metal loading (Pd + Au) in the range of 1–5 wt%. This is the main method used to make the Pd-Au bimetallic catalysts in this work, unless specified otherwise. Moreover, in order to study the effects of catalyst preparation method, a series of bimetallic catalysts were also prepared by consequent impregnation of supports by Pd and Au precursors. After impregnation, the catalysts were dried at room temperature for 3 h, and then at 60 °C for 12 h. The reduction process was done by treating the fresh dried catalysts with H_2 at 185 °C under 3.5 bar for about 12 h. A series of different calcined catalysts were prepared by oxidizing the fresh dried catalysts at temperatures 185, 235, and 275 °C in air for 12 h. The calcination temperatures were selected based on the TGA/DTA results in order to be in the safe thermal treatment region of the supports and their surface functional groups (in the case of oxidized ACC) [4].

2.2. Catalysts characterization

The supports and the catalysts were characterized by means of the pore size distribution and specific surface area measurements, Atomic Absorption Spectroscopy (AAS), Temperature Programmed Desorption (TPD), Ultra-high Resolution Field Emission Scanning Electron Microscopy (UHRFESEM) and Scanning Transmission Electron Microscopy (STEM), and X-

ray Photoelectron Spectroscopy (XPS). The details of the characterization methods have been described by Gudarzi et al [4, 46].

2.3. Hydrogenation and decomposition tests

Catalytic decomposition and hydrogenation reactions of hydrogen peroxide were carried out in a stainless steel autoclave (Parr Instruments Ltd) with a nominal volume of 450 ml and a maximum working pressure of 140 bar. The autoclave was equipped with an overhead stirrer (0–2000 rpm) and facilities to measure the temperature and pressure. The temperature was kept constant by a thermostat. Hydrogen was fed into the reactor through a gas-holder with a volume of 33 ml and by the means of a mass flow controller. A recirculation line equipped with a multi-way valve was installed for sampling at different times (Fig. 2). The sampling line was designed to prevent pressure changes (and consequently, loss of gases) in the reactor during sampling. Catalysts were fixed in the reactor by the means of a metal stand as described elsewhere [4]. Typically, the reactor was charged with about 60 mg of catalyst and successively with 200 g of 1wt % hydrogen peroxide solution in methanol. In the case of decomposition tests, the air in the reactor was displaced by N_2. For hydrogenation reaction, first the air in the reactor was replaced with H_2 and then the reactor was filled with H_2 up to 4 bar. Stirring (1250 rpm) was begun immediately after H_2 feeding and the reaction time was started. Therefore, the possible decomposition of H_2O_2 during the H_2 feed does not matter. The gas-liquid and liquid-gas mass transfer effects were eliminated by maintaining the sufficient stirring speed (1250 rpm).

The concentration of H_2O_2 was measured quantitatively by a volumetric iodometry titration method. The water content was determined by using a Mettler DL35 Karl-Fischer Titrator. Research grade hydrogen and nitrogen were purchased from AGA. Methanol (Merck) with purity of 99.9 % was used as solvent. $PdCl_2$ with purity 99.999 % (Sigma-Aldrich) and gold (III) chloride hydrate ($HAuCl_4$, purity 99.999 %, Aldrich) were used as metal precursors. Nitric acid (65%, Merck) was used for acid pretreatment of the support. KI (Merck), acetic acid (purity 100 %, Merck), $K_2Cr_2O_7$ (purity 99.99 %, Aldrich) and $Na_2S_2O_3{\cdot}5H_2O$ (Merck) were used for iodometric titration of hydrogen peroxide. Water content was determined by Karl-Fischer titration using Hydranal reagents (Fluka).

3. Results and discussion

3.1. Hydrogenation of H_2O_2

3.1.1. The effects of Au/Pd ratio and metal content in the catalytic activity of Pd-Au bimetallic catalysts

3.1.1.1. Increasing the amount of gold with a constant amount of palladium

The results of hydrogenation of H_2O_2 over Pd-Au bimetallic catalysts with 1 wt % Pd and 1-4 wt % Au supported on the oxidized ACC (OACC) are presented in Fig. 3. For comparison, also the result with 1 wt % Pd monometallic catalyst is shown. It can be observed that:

- All Pd-Au bimetallic catalysts are substantially less destructive than the Pd monometallic catalyst. In other words, adding Au to Pd monometallic catalyst dramatically diminished its activity in hydrogenation of H_2O_2. Especially the catalyst with 1 wt% Pd and 1 wt% Au is

almost 5 times less destructive than the corresponding 1 wt% Pd monometallic catalyst (see the exact values in Table 1).

– In the case of Pd-Au bimetallic catalysts, with increasing the amount of gold from 1 wt% to 2 wt% the activity of the catalyst in hydrogenation of H_2O_2 increased about 1.8 times (see the exact values in Table 1). Further increase of Au from 2 to 3 and then to 4 wt% did not change so much the activity of the catalyst. In other words, the bimetallic catalysts with 2, 3 and 4 wt% of Au resulted almost in the same hydrogenation activities, especially during the first half an hour of the reaction time (see Fig. 3).

3.1.1.2. Increasing the amount of palladium with a constant amount of gold

In order to study the effect of increasing palladium, a series of Pd-Au catalysts with constant amount of gold (1 wt %) and 1-4 wt % palladium were prepared. The results of the hydrogenation tests are presented in Fig. 4. For comparison, also the results with 1, 3, and 5 wt % Pd monometallic catalysts are shown. It can be observed that:

– In the case of Pd-Au bimetallic catalysts (Fig. 4a), with increasing the amount of palladium from 1 wt% to 2 wt%, the H_2O_2 hydrogenation activity of the catalyst was substantially increased. Indeed, the catalyst with 2 wt% Pd is about 6.5 times more active than the corresponding one with 1 wt% Pd (see the exact values in Table 1).

– In the case of Pd-Au bimetallic catalysts (Fig. 4a), increasing the amount of Pd from 2 to 3 wt%, slightly decreased the hydrogenation activity. However, increasing the amount of palladium more from 3 to 4 wt% again resulted in more active catalyst (see the exact values in Table 1).

– In general and based on the results in Figs 4b-d, it can be concluded that in the case of Pd-Au bimetallic catalysts with the same total metal content (Pd+Au), catalysts with higher amount of gold are less H_2O_2 destructive than the corresponding ones with higher amount of palladium.

– All the Pd-Au bimetallic catalysts are less H_2O_2 destructive than the corresponding monometallic Pd catalysts (Figs 4b-d).

3.1.1.3. Changing Au/Pd ratio with a constant total metal content

The influence of varying the Au/Pd ratio on the hydrogenation activity of the Pd-Au bimetallic catalysts with constant total metal content (Pd + Au = 5 wt %) are presented in Fig. 5. It can be observed that:

– All Pd-Au bimetallic catalysts were less H_2O_2 destructive than the 5 wt % Pd monometallic catalyst.

– All Pd-Au catalysts with $\frac{Au}{Pd} \geq 1$ were less active in hydrogenation of H_2O_2 when compared to the other bimetallic catalysts with $\frac{Au}{Pd} < 1$ (see exact values in Table 1).

– In the case of Pd-Au bimetallic catalysts, the catalyst with 1 wt% Pd and 4 wt% Au is substantially less active than the others (see exact values in Table 1).

3.1.1.4. Discussion

All of the catalysts presented in Figs. 3-5 were supported on the same carrier (ACC oxidized with nitric acid). Therefore, surface chemistry of the support is the same for all of them and, it

can be concluded that the surface chemistry of the support cannot be main reason for the observed differences in the H_2O_2 hydrogenation activity of the catalysts.

All of the catalysts presented in Figs. 3-5 were calcined in air at 185 °C. Oxidation state of palladium and gold in the catalysts were determined by x-ray photo electron microscopy (XPS). XPS spectra of the presented bimetallic catalysts revealed that almost all of the palladium and gold were in zero-valent state or in metallic form. However, traces of palladium were in the ionic form (Pd^{+2}) (see Table 3). Therefore, the oxidation state of the metallic part could not cause the observed differences.

Ultra-High Resolution Field Emission Scanning Electron Microscope (UHRFESEM) images of different Pd-Au bimetallic catalysts revealed considerable changes in the morphology of the metal particles with changing the amounts and ratio of palladium and gold. The UHRFESEM images of different Pd-Au bimetallic catalysts, and the explanations concerning the morphology of metal particles, have already been discussed in detail in our previous paper [46]. In order to avoid duplication, just the main results are summarized below:

- The bimetallic catalysts supported on oxidized ACC mainly consist of small metal particles with the size mostly 5-15 nm and also relatively big ones (with different sizes in the order of 100 nm). All of them are well dispersed in the support.
- Based on EDS analysis of UHRFESEM images, small particles consist of monometallic palladium and gold along with Pd-Au alloy particles.
- Increasing the amount of Pd and/or gold increased the size of the particles.
- Catalysts with higher amount of gold (>2 wt %) consisted of considerable number of gold monometallic particles with different shape and size (20-50 nm).

Concerning the big metal particles, it was observed [46] that:

- In the case of the catalyst with 1 wt% Pd and 1 wt% Au, these relatively round and big particles consist of a gold-rich core which was surrounded by a lot of small (less than 10 nm) palladium particles.
- When increasing the amount of palladium, like the catalyst with 3 wt% Pd and 1 wt% Au bimetallic catalyst, the small Pd particles seemed to form a thicker and denser layer around the golden core. Therefore the Pd-Au particles on the outer surface of ACC fibers grew bigger.
- When the amount of gold was increased, like in the case of the catalyst with 1 wt% Pd and 3 wt% Au, the round core-shell morphological Pd-Au particles were formed over bigger thin spots of gold. As a result of the new morphology, the color of the surface of the activated carbon cloth changed to pale yellow.

Based on the discussion above, it can be concluded that the different hydrogenation activity of the catalysts presented in Figs. 3-5 could mostly be related to the different morphology and size of their metal particles. Meanwhile, the size and morphology were governed by the amounts and ratio of palladium and gold.

3.1.2. The effects of the catalyst preparation method

The results of the hydrogenation of H_2O_2 over three different Pd-Au bimetallic catalysts supported on oxidized ACC (OACC) and prepared with different methods (see Section 2.1) are presented in Fig. 6. It can be observed that:

- The catalysts prepared by co-impregnation method were less active than the corresponding ones prepared by the consequent impregnation with Pd and Au.

– In the case of the catalysts with $\frac{Au}{Pd} \geq 1$, the catalysts prepared by first impregnating with Au and then with Pd were less active than the corresponding ones which were prepared by impregnating with Pd and then with Au.
– However, in the case of the catalysts with $\frac{Au}{Pd} < 1$, the catalysts prepared by impregnating with Pd and then with Au were slightly less active than the corresponding ones prepared vice versa (first with gold and then with palladium).
– The differences between hydrogenation activities of the catalysts prepared with the different methods are larger in the catalysts with $\frac{Au}{Pd} > 1$ (e.g. catalyst with 1 wt% Pd and 3 wt% Au) when compared to the catalysts with $\frac{Au}{Pd} \leq 1$. This means that the hydrogenation activity of the bimetallic catalysts is more affected by the catalyst preparation method if $\frac{Au}{Pd} > 1$

The UHRFESEM images of some Pd-Au bimetallic catalysts prepared by consequent impregnation methods are presented in Figs. 7-8. It can be seen that:
– In the case of bimetallic catalyst with 1 wt% Pd and 3 wt% Au, impregnation with Pd and then with Au resulted in the formation of big particles jointed together and almost formed a metal layer on the other surface of the ACC fibers (Fig. 7a)
– In the case of bimetallic catalyst with 1 wt% Pd and 3 wt% Au, impregnation with Pd and then with Au resulted in formation of big but separate metal particles (Fig. 7b). Based on the EDS analysis, these big particles are mainly gold monometallic particles. However, palladium formed mainly small particles (Fig. 7c).
– In the case of catalyst with 3 wt% Pd and 1 wt% Au, consequent impregnation resulted in the formation of big and almost separate metal particles (Fig. 8). However, impregnation with Pd and then with Au resulted in the formation smaller metal particles than the approach vice versa (first with Au and then Pd, Fig. 8c). Almost similar morphology of the metal particles with these two preparation methods resulted in hydrogenation activities quite close to each other (Fig. 6c).

Based on the discussion above, the surface morphology of the Pd-Au bimetallic catalysts was affected strongly by the preparation method (see Section 3.1.1.4 for co-impregnation). These different surface morphologies lead to different hydrogention activities.

3.1.3. The effects of the surface chemistry of the ACC fibers

The results of the hydrogenation of H_2O_2 over three different bimetallic catalysts supported on non-oxidized ACC and on ACC oxidized with nitric acid are presented in Fig 9. It can be observed that the catalysts supported on oxidized ACC were substantially less H_2O_2 destructive than the corresponding ones on non-oxidized ACC. Especially the catalyst with 1 wt% Pd and 1 wt% Au supported on non-oxidized ACC is about 10 times more destructive than the corresponding one supported on oxidized ACC.

Pretreatment of activated carbon cloth with nitric acid leads to formation of different oxygen-containing functional groups on the surface of ACC fibers [4]. These functional groups can be

classified as strong acidic oxygen-containing groups (like carboxylic and anhydride) and weak acid ones (like lactones, phenols and carbonyl). These oxygen-containing surface functional groups can be determined by thermal programmed desorption (TPD) test [4]. Strong and weak acidic oxygen-containing groups are responsible for CO_2 and CO desorption in TPD, respectively [4]. The TPD results of non-oxidized ACC and ACC oxidized with nitric acid along with some Pd-Au catalysts supported on oxidized ACC are presented in Table 2.

Different surface chemistry of the ACC fibers in the non-oxidized and oxidized ACC (with nitric acid) led to a huge differences in morphology of Pd-Au particles. The UHRFESEM images and the corresponding explanations about the surface morphology of the Pd-Au bimetallic catalysts supported on non-oxidized ACC were already discussed in details in our previous paper [46]. In order to avoid duplication, it can be briefly mentioned here that in the case of non-oxidized ACC, palladium and gold form really big and joined particles at the outer surface of ACC fibers [46]. In most areas, the metal particles almost cover the outer surface of the ACC fibers. The completely different surface morphology of Pd-Au catalysts supported non-oxidized and oxidize ACC could be the main reason of different catalytic hydrogenation activities.

Furthermore, in the case of oxidized ACC, oxygen-containing surface functional groups might also affect directly the final activity of the catalysts. These acidic groups negatively charge the surface of the carbon fibers [4] and decrease the hydrophobicity of the surface [49]. Therefore, the concentration of water in pores and on the surface of ACC's fibers is higher in the oxidized ACC than in the non-oxidized one. The affinity of the surface of oxidized ACC holding water molecules might also affect the final rate of water production (Fig. 1, iii) according to the Le Chatelier's principle**.**

3.1.4. The effects of heat treatment of the catalysts in H_2 and air at different temperatures

The results of the hydrogenation of H_2O_2 overthree different sets of bimetallic catalysts supported on oxidized ACC (OACC) are presented in Fig. 10. Each set consists of the same catalysts which three of them calcined in air at 185, 235, and 275 °C and one of them reduced by H_2 at 185 °C. It can be observed that:

- The catalysts calcined in air at 185-275 °C were less active than the corresponding catalysts reduced by H_2 at 185 °C. Especially in the case of catalyst with 1 wt% Pd and 1 wt% Au, the one reduced by H_2 is about 10 times more destructive than the corresponding calcined catalysts.
- In the case of catalysts calcined in air, the ones calcined at 185 °C were less H_2O_2 destructive than the others. Especially this is clearly visible in the case of the catalyst with 1 wt% Pd and 3 wt% Au and the catalyst with 3 wt% Pd and 1 wt% Au.
- It looks that in the case of catalysts with $\frac{Au}{Pd}>1$, calcination at different temperatures affected more on hydrogenation activity of the final catalysts when compared to the catalysts with $\frac{Au}{Pd}\leq 1$.
- In the case of catalysts calcined in air, increasing the calcination temperature from 185 °C to 275 °C resulted in more H_2O_2 destructive catalysts. Especially this can be seen in the case of the catalyst with 1 wt% Pd and 3 wt% Au and the catalyst with 3 wt% Pd and 1 wt% Au.

The heat treatment of the oxidized ACC damages the oxygen-containing surface functional groups (Table 2). In the case of calcined catalysts, increasing the calcination temperature caused more damages, especially to the stronger acidic surface functional groups. These groups are responsible for CO_2 releasing in the temperature programmed desorption (TPD) test (Table 2). Heat treatment of the catalysts supported on oxidized ACC by H_2 at 185 °C causes substantial damage to the stronger acidic oxygen-containing functional groups (Table 2).
Furthermore, and based on the X-ray photo electron microscopy (XPS) results, oxidation (calcination) of the fresh catalysts could result in production of oxidized state of metallic components in the catalyst. Higher calcination temperature could oxidize larger amount of active (metallic) part of the catalysts. The main results of the XPS test of the Pd-Au bimetallic catalysts with different amount of Pd and Au are presented in Table 3. It can be mentioned that:

- Despite of the calcination temperature, gold was in the metallic or zero valance state (Au^0) in all bimetallic samples.
- Palladium in the catalyst calcined at 185 °C was almost in zero-valent or in metallic state (Pd^0) and only traces of the palladium was in the form of Pd^{+2} originated from palladium dichloride $PdCl_2$.
- Almost 8.5 wt % of the total amount of the palladium was oxidized to palladium oxide (PdO) when increasing the calcination temperature to 235 °C in the case of the catalyst with 3 wt% Pd and 1 wt% Au. Almost 63 wt % of the total amount of palladium was in the form of palladium oxide in the catalyst calcined at 275 °C. Therefore, increasing the calcination temperature dramatically increases the amount of palladium oxide.
- Calcination resulted in smaller amount of PdO in the catalyst with 1 wt% Pd and 3 wt% Au than in the catalyst with 3 wt% Pd and 1 wt% Au (Table 3). Indeed, when the latter catalyst was calcined at 275 °C, only 11.2 wt% of the total amount of palladium was oxidized to palladium oxide.
- In the case of bimetallic catalysts with $\frac{Au}{Pd}>1$, calcination at 235-275 °C resulted in lower amount of palladium oxide than with $\frac{Au}{Pd}\leq 1$.

However, the Pd3d XPS spectra revealed that the oxidation state of palladium was considerably influenced by H_2 during hydrogenation reaction (Fig. 11, Table 4). In XPS spectra, the two peaks with binding energy at around 335.3 and 340.5 eV correspond to zero valances of Pd (Pd^0). The two peaks with binding energy at around 336.5 and 341.5 eV belong to palladium oxide (PdO). The two peaks with binding energy at around 338 and 343 eV belong to Pd^{+2} in palladium dichloride ($PdCl_2$). According to these XPS results, it can be stated:

- In the case of the catalyst with 3 wt% Pd and 1 wt% Au calcined at 275 °C, after 5 min of hydrogenation reaction, the amount of palladium oxide (PdO) in the catalyst was dropped to 21% (wt %) from about 63%. After half an hour, the amount of the PdO was dropped further to 17%. Almost 80% of Pd in PdO was reduced to zero valent state (Pd^0) after 1h reaction time (Table 4).
- In the case of the catalyst with 1 wt% Pd and 1 wt% Au calcined at 275 °C, after 5 min of hydrogenation reaction, the amount of palladium oxide (PdO) in the catalyst was decreased to 16% (wt %) from about 39%. after half an hour, the amount of the PdO was

decreased further to 14%. Almost 70% Pd in PdO were reduced to zero valent state (Pd^0) after 1h reaction time (Table 4).

In fact, considerable amount palladium in palladium oxide (PdO) was almost reduced to the zero valent state (Pd^0) during the hydrogenation reaction (Fig. 1, reaction iii). Therefore, it can be concluded that the oxidation state of palladium could not have the main role in causing the observed difference in hydrogenation activity.

Summarizing the discussion above, the damages in the oxygen-containing surface functional groups of the oxidized ACC (support) are the main reason for different hydrogenation activities of the catalysts with equal amounts of Pd and Au. These damages were caused by heat treatment.

3.1.5. The effect of the reaction temperature

The results in Fig. 12 demonstrate that the hydrogenation of H_2O_2 was strongly affected by the reaction temperature. The results show that:

- Increasing the reaction temperature resulted in more H_2O_2 destruction. Maximum destruction was observed at 21 °C
- The outstanding result is that in the case of the catalyst with 1 wt% Pd and 1 wt% Au and at reaction temperature equal to 0 °C, the hydrogenation of H_2O_2 was negligible. The hydrogenation of H_2O_2 at 0 °C and after 1h reaction time was about 0.78 wt% which it is really negligible.
- In the case of catalyst with 1 wt% Pd and 3 wt% Au, hydrogenation activity of the catalyst at 21 °C was at least 3 times more than at 0 °C (see exact values in Table 2).

Temperature affects, of course, also the hydrogenation rate by changing the activation energy of the reaction and the solubility of hydrogen in methanol.

3.1.6. The effect of the solvent

Hydrogenation decomposition of H_2O_2 in water and methanol are shown in Fig. 13. The results demonstrate that hydrogenation of H_2O_2 was highly affected by the reaction medium. It indicates that methanol significantly stabilized H_2O_2. Despite of higher solubility of H_2 in methanol, hydrogenation of H_2O_2 in water was much faster than in methanol. According to S. Melada *et al.* [19], the most reactive sites of the catalyst could be blocked by formate compounds prohibiting HO-OH bond cleavage.

3.2. Destruction of H_2O_2 by its decomposition

In this section decomposition of H_2O_2 means destruction of H_2O_2 by its decomposition (Fig.1, reaction iv) over the Pd-Au bimetallic catalysts. Decomposition tests were run under the same pressure as the hydrogenation tests. The only difference was using N_2 instead of H_2.

3.2.1. Catalysts supported on ACC oxidized with nitric acid

Based on the results of the bimetallic catalysts supported on oxidized ACC, it can be mentioned that:

- In the case of the catalysts with 1 wt% of palladium and calcined in air at 185 °C, decomposition of H_2O_2 was almost zero.
- In the case of catalysts with 2 wt% palladium or more and calcined in air at 185 °C, decomposition of H_2O_2 was still negligible (less than 0.60 wt% after 1.5h of the reaction time).

– Increasing the calcination temperature to 235 °C and 275 °C increased H_2O_2 decomposition. For the catalysts with 1 wt% palladium, the decomposition rate was still negligible (less than 0.55 wt% after 1.5h of the reaction time). For the catalysts with 2 wt% palladium or more, the decomposition rate was slightly higher (less than 1.5 wt % after 1.5 h of the reaction time) when compared to the catalysts with 1 wt% Pd. However, it is still much lower than the hydrogenation rate. (see the hydrogenation results in Table 1).
– Maximum H_2O_2 decomposition rate was obtained with the catalysts reduced by H_2 at 185 °C (Fig. 14). For the catalysts with 1 wt% Pd, the decomposition rate was about 5 wt % after 1.5 h of the reaction time. The decomposition rate for the reduced catalysts with 2 wt% palladium or more was considerably more (about 15 wt% after 1.5 h of the reaction time) when compared to the catalyst with 1 wt% Pd (see exact values in Table 5).

Wet oxidation of activated carbon cloth with nitric acid resulted in different oxygen-containing functional groups on the surface of ACC fibers (section 3.1.3). As it was already discussed in section 3.1.4, heat treatment of the catalysts supported on oxidized ACC caused considerable damages on these functional groups. These damages increase the rate of H_2O_2 decomposition.

3.2.2. Catalysts supported on non-oxidized ACC

In the case of the catalysts supported on non-oxidized ACC, the H_2O_2 decomposition rate depended on the amount and ratio of palladium and gold and is almost independent of the heat treatment, changed between 1 to 5 wt% after 1.5 h of the reaction time (see exact value in Table 5). However, it is quite low when compared to the hydrogenation rate of H_2O_2 (see the hydrogenation results in Table 1).

4. Conclusions

The results showed that the surface morphology, and consequently the H_2O_2 destruction activity of Pd-Au bimetallic catalysts, was highly influenced by the surface chemistry of the support and the amount and the ratio of Pd and Au in the catalyst

Wet oxidation of activated carbon cloth (ACC) resulted in formation of oxygen-containing functional groups on the surfaces of ACC fibers. The surface chemistry of the ACC fibers was highly affected by these functional groups. The bimetallic catalysts supported on the oxidized ACC were substantially less destructive than the corresponding ones supported on non-oxidized ACC.

Almost all of the Pd-Au bimetallic catalysts were less H_2O_2 destructive than the Pd monometallic catalysts with the same amount of Pd. In the case of bimetallic catalysts, increasing the amount of gold and decreasing the amount of Pd resulted in low H_2O_2 destruction activity. Moreover, the bimetallic catalysts prepared by co-impregnation of Pd and Au were less destructive than the corresponding catalysts prepared by consequent impregnation approaches.

In the case of oxidized ACC as support, the bimetallic catalysts calcined in air at 185 °C were the least destructive and the catalysts reduced by H_2 at 185 °C were the most destructive.

Using water instead of methanol as reaction medium substantially speeded up H_2O_2 destruction. Furthermore, increasing the reaction temperature accelerated destruction of H_2O_2. Finally, catalytic destruction of H_2O_2 via its direct decomposition was considerably low compare to H_2O_2 hydrogenation.

References

[1] E. N. Ntainjua, M. Piccinini, S. J. Freakley, J. C. Pritchard, J. K. Edwards, A. F. Carley, G. J. Hutchings, Green Chem. 14 (2012) 170-181.
[2] J.K. Edwards, G.J. Hutchings, Angew. Chem. Int. Ed. 47 (2008) 9192
[3] B. E. Solsona, J.K. Edwards, P. Landon, A.F. Carley, A. Herzing, C.J. Kiely, G.J. Hutchings, Chem. Mater. 18 (2006) 2689.
[4] D. Gudarzi, W. Ratchananusorn, I. Turunen, M. Heinonen, T. salmi, Top. Catal. 56 (2013) 527.
[5] A.G. Gaikwad, S.D. Sansare, V.R. Choudhary, J. Mol. Catal. A Chem. 181 (2002) 143-149.
[6] V.R. Choudhary, A.G. Gaikwad, S.D. Sansare, Catal. Lett. 83 (2002) 235-239.
[7] V.R. Choudhary, S.D. Sansare, A.G. Gaikwad, Catal. Lett. 84 (2002) 81-87.
[8] maghaleh sevome khodam
[9] C. Samanta, V.R. Choudhary, Catal. Commun. 8 (2007) 73.
[10] V.R. Choudhary, C. Samanta, T.V. Choudhary, Catal. Commun. 8 (2007) 1310.
[11] C. Samanta, V.R. Choudhary, Appl. Catal. A: Gen. 326 (2007) 28.
[12] C. Samanta, V.R. Choudhary, Catal. Commun. 8 (2007) 2221.
[13] C. Samanta, V.R. Choudhary, Chem. Eng. J. 136 (2008) 126.
[14] C. Samanta, V.R. Choudhary, Appl. Catal. A: Gen. 330 (2007) 23.
[15] V.V. Krishnan, A.G. Dokoutchaev, M.E. Thompson, J. Catal. 196 (2000) 366–374.
[16] D.P. Dissanayake, J.H. Lunsford, J. Catal. 214 (2003) 113-120.
[17] S. Abate, G. Centi, S. Melada, S. Perathoner, F. Pinna, G. Strukul, Catal. Today 104 (2005) 323-328.
[18] S. Melada, F. Pinna, G. Strukul, S. Perathoner, G. Centi, J. Catal. 235 (2005) 241-248.
[19] S. Melada, F. Pinna, G. Strukul, S. Perathoner, G. Centi, J. Catal. 237 (2006) 213-219.
[20] T.A. Pospelova, N.I. Kobozev, E.N. Eremin, J. Phys. Chem. 35 (1961) 143-147.
[21] T.A. Pospelova, N.I. Kobozev, J. Phys. Chem. 35 (1961) 262-265.
[22] K.P. Reis, V.K. Joshi, M.E. Thompson, J. Catal. 161 (1996) 62–67.
[23] D.P. Dissanayake, J.H. Lunsford, J. Catal. 206 (2002) 173-176.
[24] S. Chinta, J.H. Lunsford, J. Catal. 225 (2004) 249.
[25] Y-F. Han, J.H. Lunsford, J. Catal. 230 (2005) 313.
[26] Y-F. Han, J.H. Lunsford, Catal. Lett. 99 (2005) 13.
[27] Q. Liu, J.H. Lunsford, J. Catal. 239 (2006) 237.
[28] Q. Liu, J.H. Lunsford, Appl. Catal. A: Gen. 314 (2006) 94-100.
[29] V.Z. Radkevich, T.L. Senko, K. Wilson, L.M. Grishenko, A.N. Zaderko, V.Y. Diyuk, Appl. Catal. A: Gen. 335 (2008) 241-251.
[30] C. Samanta, Appl. Catal. A: Gen. 350 (2008) 133-149.
[31] L. Fu, K. T. Chuang, R. Fiedorow, Stud. Surf. Sci. Catal. 72 *(*1992) 33-41.
[32] D. Gudarzi, O. A. Simakova, J. R. H. Carucci, P. D. Biasi, K. Eränen, E. Kolehmainen, I. Turunen, D. Y. Murzin, T. Salmi, Chem. Eng. Tran. 21 (2010) 925-930.
[33] T. Danciu, E.J. Beckmann, T. Hancu, R.N. Cochran, R. Grey, D.M. Hajnik, J. Jewson, Angew. Chem. Int. Ed. 2 (2003) 1140-1142.
[34] E. N. Ntainjua, M. Piccinini, J. C. Pritchard, J K. Edwards, A. F. Carley, Ch. J. Kiely, G. J. Hutchings, Catal. Today 178(2011) 47-50
[35] P. Landon, P.J. Papworth, C.J. Kiely, G.J. Hutchings, Chem. Commun. (2002) 2058-2059.

[36] P. Landon, P.J. Collier, A.F. Carley, D. Chadwick, A.J. Papworth, A. Burrows, C.J. Kiely, G.J. Hutchings, Phys. Chem. Chem. Phys. 5 (2003) 1917-1923.
[37] J.K. Edwards, B.E. Solsona, P. Landon, A.F. Carley, A. Herzing, C.J. Kiely, G.J. Hutchings, J. Catal. 236 (2005) 69-79.
[38] J.K. Edwards, B. Solsona, P. Landon, A.F. Carley, A. Herzing, M. Watanabe, C.J. Kiely, G.J. Hutchings, J. Mater. Chem. 15 (2005) 4595-4600.
[39] G. Li, J. Edwards, A.F. Carley, G.J. Hutchings, Catal. Today 122 (2007) 361-364.
[40] J.K. Edwards, A. Thomas, B.E. Solsona, P. Landon, A.F. Carley, G.J. Hutchings, Catal. Today 122 (2007) 397-402.
[41] G. Li, J. Edwards, A.F. Carley, G.J. Hutchings, Catal. Today 114 (2006) 369-371.
[42] V.R. Choudhary, C. Samanta, T.V. Choudhary, Appl. Catal. A: Gen. 308 (2006) 128-133.
[43] J. K. Edwards, A. F. Carley, A. A. Herzing, C. J. Kiely and G. J. Hutchings, Faraday Discuss. 138(2008) 225-239.
[44] J. K. Edwards, E. Ntainjua, A. F. Carley, A. A. Herzing, C. J. Kiely and G. J. Hutchings, Angew. Chem., Int. Ed. 48(2009) 8512-8515.
[45] J.B. Donnet, R.C. Bansal, F. Stoeckli, Carbon Fibers, Marcel Dekker, New York, 1990.
[46] D. Gudarzi, W. Ratchananusorn, I. Turunen, M. Heinonen, T. salmi, Catal. Today (2014) CATTOD-9038.
[47] C. Moreno-Castilla, M.V López-Ramón, F. Carrasco-Marín, Carbon 38 (2000) 1995-2001.
[48] Sh. Wenzhong, Li. Zhijieand, Liu Yihong, Recent Patents on Chemical Engineering 1 (2008) 27-40.
[49] F. Rodríguez-reinoso, Carbon 36 (1998) 159-175.
[50] J.M. Rosas, J. Bedia, J. Rodríguez-Mirasol, T. Cordero, Fuel 88 (2009) 19-26.
[51] M. L. Toebes, J. A. van Dillen, K. P. de Jong, J. Mol. Catal. A: Chem. 173 (2001) 75-98.
[52] Won-Chun Oh, Min-Hyung Yum, Bull. Korean Chem. Soc. 25 (2004) 1189-1194.

Table 1

Destruction of H_2O_2 by hydrogenation over the Pd and Pd-Au bimetallic catalysts after 1h. All catalysts supported on oxidized ACC and calcined in air at 185 °C.

Sample	H_2O_2 decomposition (wt%)
1 wt% Pd	22.93
3 wt% Pd	43.96
5 wt% Pd	59.81
1 wt% Pd_1 wt% Au	5.34
1 wt% Pd_2 wt% Au	10.24
1 wt% Pd_3 wt% Au	9.59
1 wt% Pd_4 wt% Au	10.71
2 wt% Pd_1 wt% Au	34.47
3 wt% Pd_1 wt% Au	28.75
4 wt% Pd_1 wt% Au	37.67
2.5 wt% Pd_2.5 wt% Au	31.62
2 wt% Pd_3 wt% Au	33.41
3 wt% Pd_2 wt% Au	42.41

Table 2

Total amount of CO and CO_2 desorbed according to the temperature programmed desorption (TPD) tests.

Sample	CO (μmol/g)	CO_2 (μmol/g)
Non-oxidized ACC	115.13	82.73
Oxidized ACC (OACC)	1147.52	1290.44
3%Pd_1% Au/OACC (T_{red}=185 °C)	1015.26	445.81
3%Pd_1% Au/OACC (T_{cal}=185 °C)	1390.23	935.57
3%Pd_1% Au/OACC (T_{cal}=235 °C)	1483.51	742.43
3%Pd_1% Au/OACC (T_{cal}=270 °C)	1569.35	529.53
1%Pd_3% Au/OACC (T_{red}=185 °C)	1091.29	480.72
1%Pd_3% Au/OACC (T_{cal}=185 °C)	1378.45	910.45
1%Pd_3% Au/OACC (T_{cal}=235 °C)	1432.52	795.14
1%Pd_3% Au/OACC (T_{cal}=275 °C)	1508.26	581.38

Table 3

Total amount (wt %) of palladium in the form of metallic state (Pd^0), palladium chloride (Pd^{+2}), and palladium oxide (PdO) in some Pd-Au bimetallic catalysts with different amount of palladium and gold, Based on the results of x-ray photoelectron spectroscopy. All were supported on ACC oxidized with nitric acid and calcined in air at different temperatures.

Catalyst	Pd^0 (wt%)	Pd^{+2} (wt%)	PdO (wt%)
1 wt% Pd_3 wt% Au, Tcal=185 °C	94.20	5.80	0.00
1 wt% Pd-3 wt% Au, Tcal=235 °C	90.94	5.65	3.42
1 wt% Pd-3 wt% Au, Tcal=275 °C	83.86	4.90	11.24
3 wt% Pd-1 wt% Au, Tcal=185 °C	93.54	5.79	0.67
3 wt% Pd-1 wt% Au, Tcal=235 °C	86.04	5.48	8.48
3 wt% Pd-1 wt% Au, Tcal=275 °C	36.86	0.00	63.14
2.5 wt% Pd-2.5 wt% Au, Tcal=185 °C	96.39	3.61	0.00
2.5 wt% Pd-2.5 wt% Au, Tcal=235 °C	97.06	2.80	3.26
2.5 wt% Pd-2.5 wt% Au, Tcal=275 °C	83.06	2.18	14.76
1 wt% Pd-1 wt% Au, Tcal=275 °C	60.11	0.56	39.33
2 wt% Pd-3 wt% Au, Tcal=275 °C	71.26	0.48	28.26
3 wt% Pd-2 wt% Au, Tcal=275 °C	67.16	0.68	32.16

Table 4

Total amount (wt %) of palladium in the form of palladium oxide (PdO) in the different samples of the catalyst with 3 wt% Pd and 1 wt% Au, and with 3 wt% Pd and 1 wt% Au supported on ACC oxidized with nitric acid and calcined in air at 275 ºC, based on the results of x-ray photoelectron spectroscopy.

Sample	PdO (wt %)
3% Pd – 1% Au ($T_{calcination}$=275 °C)	63
3% Pd – 1% Au ($T_{calcination}$=275 °C); after H_2O_2 hydrogenation reaction (P_{H2}=4.1 bar, $T_{reaction}$= 298.15 K, $t_{reaction}$=5 min)	21
3% Pd – 1% Au ($T_{calcination}$=275 °C); after H_2O_2 hydrogenation reaction (P_{H2}=4.1 bar, $T_{reaction}$= 298.15 K, $t_{reaction}$=15 min)	20
3% Pd – 1% Au ($T_{calcination}$=275 °C); after H_2O_2 hydrogenation reaction (P_{H2}=4.1 bar, $T_{reaction}$= 298.15 K, $t_{reaction}$=30 min)	17
3% Pd – 1% Au ($T_{calcination}$=275 °C); after H_2O_2 hydrogenation reaction (P_{H2}=4.1 bar, $T_{reaction}$= 298.15 K, $t_{reaction}$=60 min)	14
1% Pd – 1% Au ($T_{calcination}$=275 °C)	39
1% Pd – 1% Au ($T_{calcination}$=275 °C); after H_2O_2 hydrogenation reaction (P_{H2}=4.1 bar, $T_{reaction}$= 298.15 K, $t_{reaction}$=5 min)	16
1% Pd – 1% Au ($T_{calcination}$=275 °C); after H_2O_2 hydrogenation reaction (P_{H2}=4.1 bar, $T_{reaction}$= 298.15 K, $t_{reaction}$=15 min)	15
1% Pd – 1% Au ($T_{calcination}$=275 °C); after H_2O_2 hydrogenation reaction (P_{H2}=4.1 bar, $T_{reaction}$= 298.15 K, $t_{reaction}$=30 min)	14
1% Pd – 1% Au ($T_{calcination}$=275 °C); after H_2O_2 hydrogenation reaction (P_{H2}=4.1 bar, $T_{reaction}$= 298.15 K, $t_{reaction}$=60 min)	12

Table 5
Destruction of H_2O_2 by its decomposition over the Pd-Au bimetallic catalysts after 1.5 h.

Sample	H_2O_2 decomposition (wt%)
Catalysts supported on oxidized ACC	
(1% Pd_1% Au)/ OACC, Reduced by H_2 at 185 °C	5.02
(1% Pd_3% Au)/ OACC, Reduced by H_2 at 185 °C	5.86
(3% Pd_3% Au)/ OACC, Reduced by H_2 at 185 °C	13.30
(2.5% Pd_2.5% Au)/ OACC, Reduced by H_2 at 185 °C	14,67
Catalysts supported on non-oxidized ACC	
(1% Pd_1% Au)/ NACC, calcined in air at 185 °C	1.28
(1% Pd_1% Au)/ NACC, calcined in air at 275 °C	1.21
(1% Pd_1% Au)/ NACC, Reduced by H_2 at 185 °C	1.18
(1% Pd_3% Au)/ NACC, calcined in air at 185 °C	2.94
(1% Pd_3% Au)/ NACC, calcined in air at 275 °C	3.11
(1% Pd_3% Au)/ NACC, Reduced by H_2 at 185 °C	3.01
(3% Pd_1% Au)/ NACC, calcined in air at 185 °C	4.92
(3% Pd_1% Au)/ NACC, calcined in air at 275 °C	4.85
(3% Pd_1% Au)/ NACC, Reduced by H_2 at 185 °C	5.01

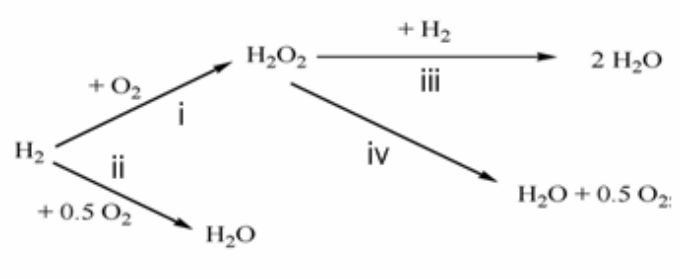

Fig. 1 Reactions involved in the direct reaction of H_2 and O_2.

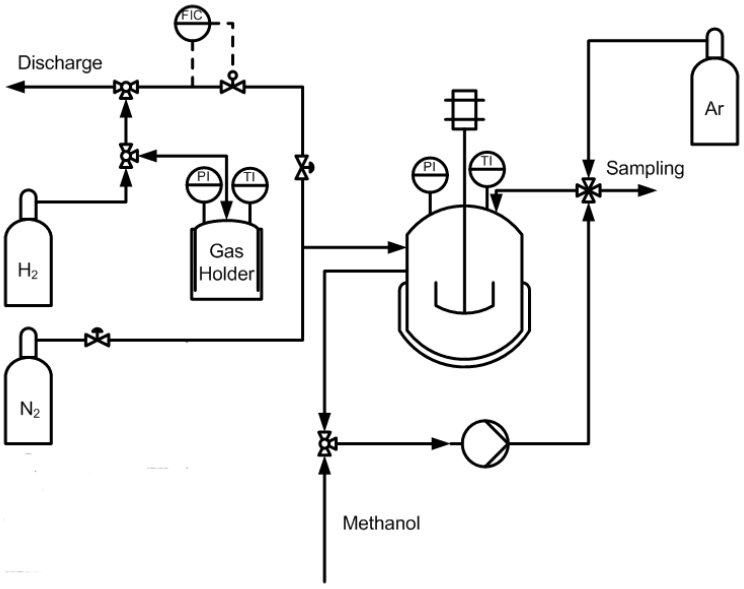

Fig. 2 Experimental set up for H_2O_2 direct synthesis.

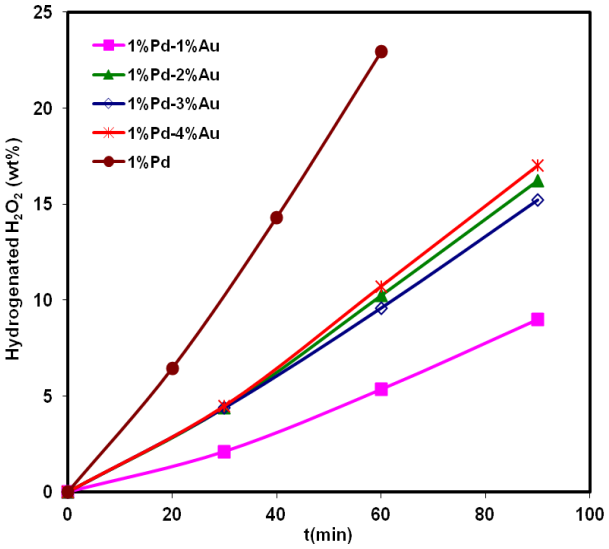

Fig. 3 The effect of increasing the amount of gold on the H_2O_2 hydrogenation activity of the Pd_Au bimetalic catalysts supported on oxidized ACC. Mass of catalyst = 56 mg, $T_{reaction}$= 21 °C, P_{H2}= 4 bar and all catalysts calcined in air at 185 °C.

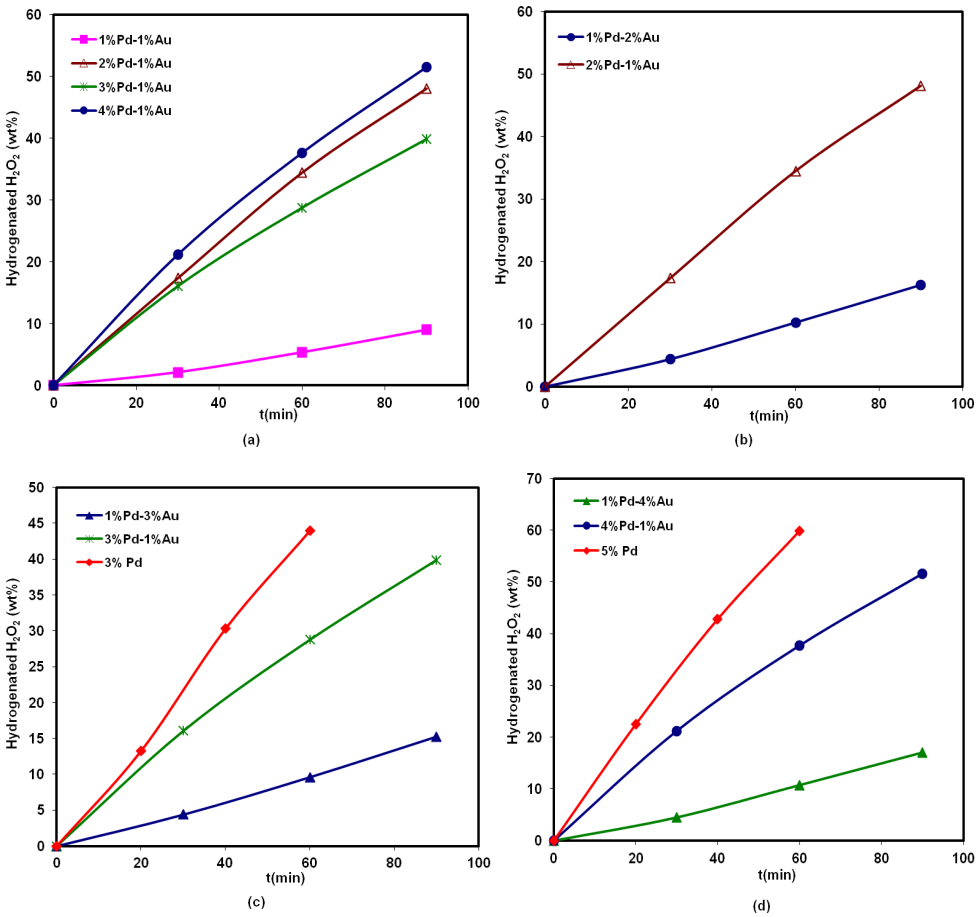

Fig. 4 The effect of increasing palladium on the H_2O_2 hydrogenation activity of the Pd-Au bimetalic catalysts supported on oxidized ACC. Mass of catalyst = 56 mg, $T_{reaction}$= 21 °C, P_{H2}= 4 bar and all catalysts calcined in air at 185 °C.

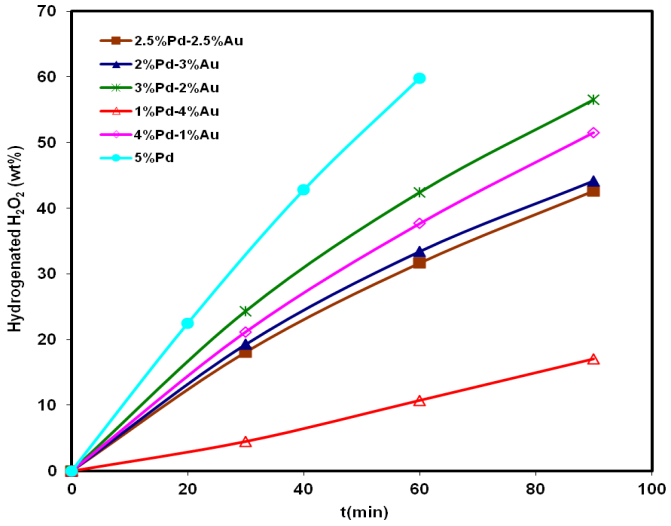

Fig. 5 The effect of the Pd/Au ratio on the H_2O_2 hydrogenation activity of the Pd-Au bimetallic catalysts supported on oxidized ACC with constant amount of metal content (Pd+Au= 5wt%). Mass of catalyst = 56 mg, $T_{reaction}$= 21 °C, P_{H2}= 4 bar and all catalysts calcined in air at 185 °C.

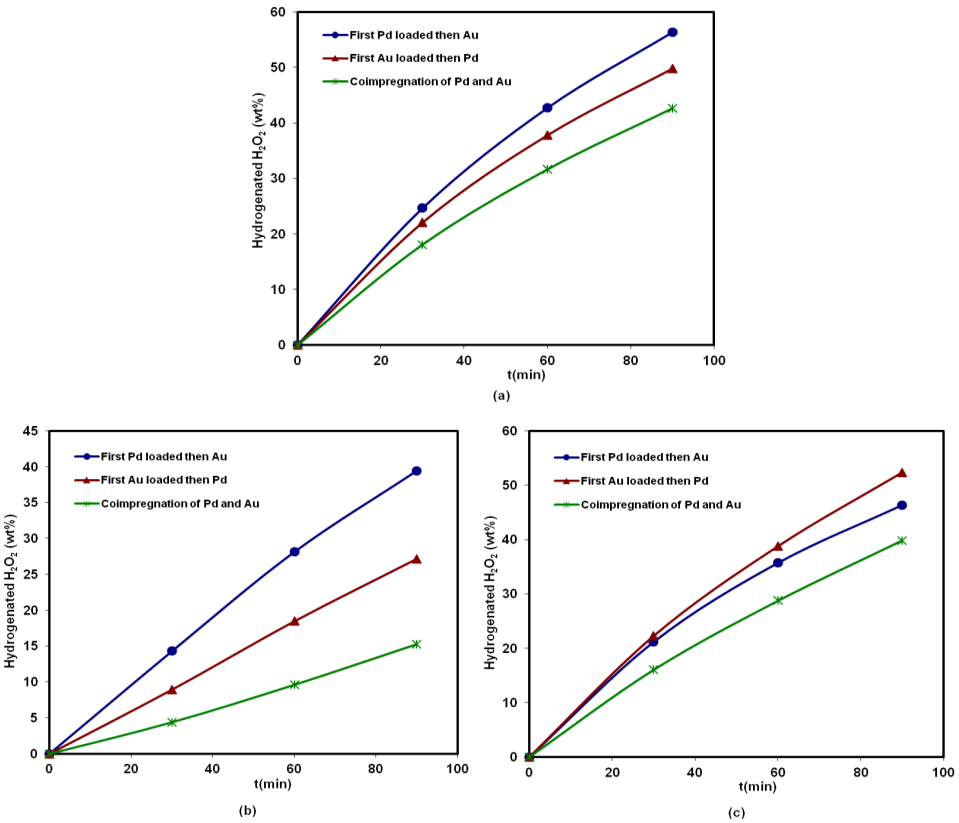

Fig. 6 The effect of the catalyst preparation method on the final H_2O_2 hydrogenation activity of the Pd-Au bimetallic catalysts: (a) the catalyst with 2.5 wt% Pd and 2.5 wt% Au, (b) the catalyst with 1 wt% Pd and 3 wt% Au, (c) the catalyst with 3 wt% Pd and 1 wt% Au. Mass of catalyst = 56 mg, $T_{reaction}$= 21 °C, P_{H2}= 4 bar and all catalysts supported on oxidized ACC (OACC) and calcined in air at 185 °C.

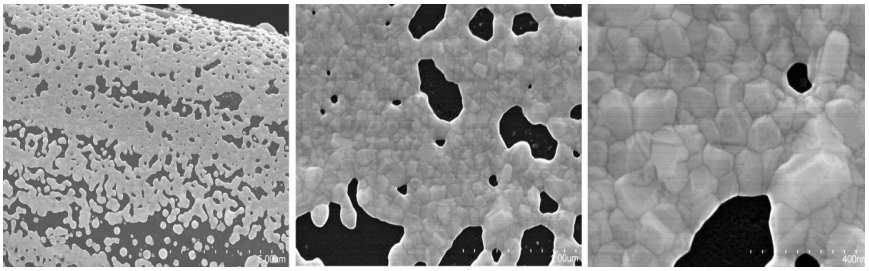

(a)

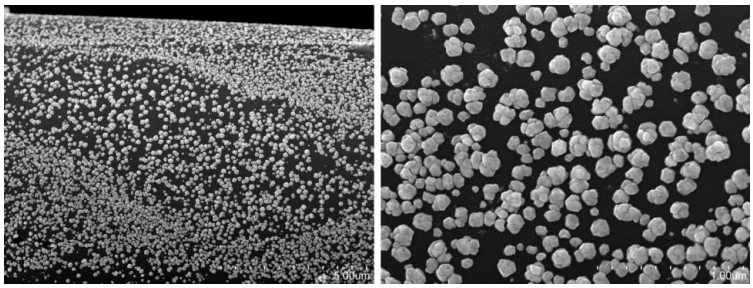

(b)

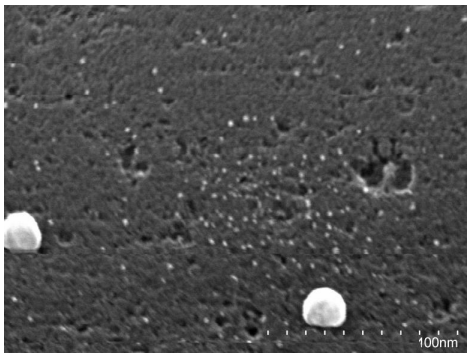

(c)

Fig. 7 The ultra-high resolution field emission scanning electron microscopy (UHRFESEM) images with different magnification of the catalyst with 1 wt % Pd and 3 wt % Au supported on oxidized ACC (OACC) and prepared by consequent impregnation of the support: (a) first with gold and then with palladium, (b) first with palladium and then with gold; (c) and also after impregnation with palladium and before consequent impregnation with gold.

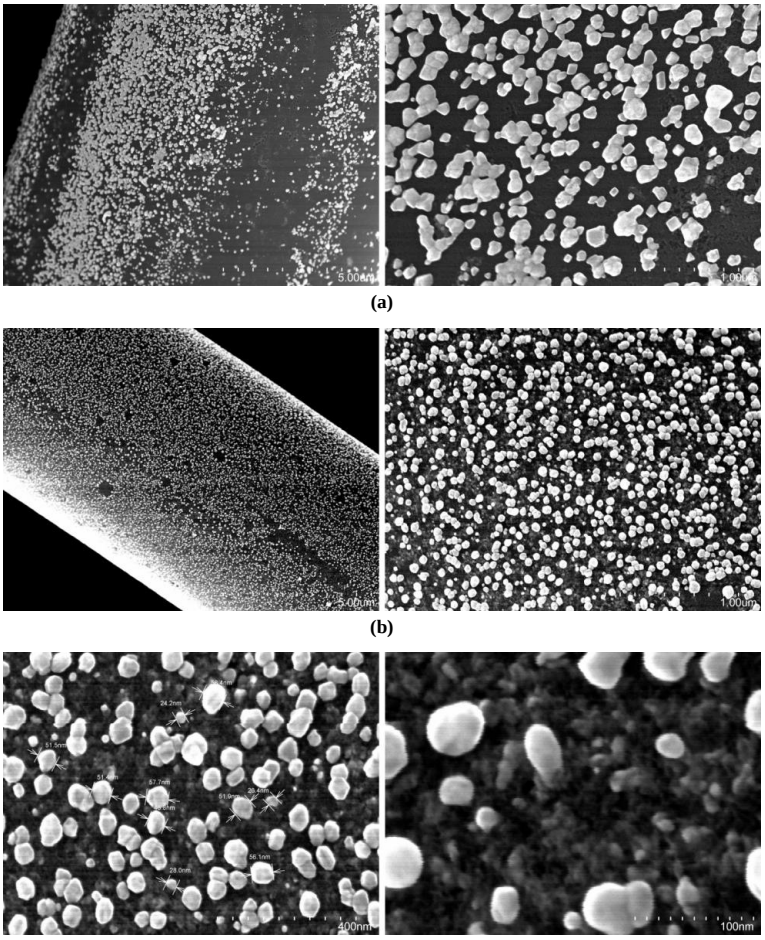

Fig. 8 The ultra-high resolution field emission scanning electron microscopy (UHRFESEM) images with different magnifications of the catalyst with 3 wt % Pd and 1 wt % Au supported on oxidized ACC (OACC) and prepared by consequent impregnation of the support: (a) first with gold and then with palladium, (b-c) first with palladium and then with gold.

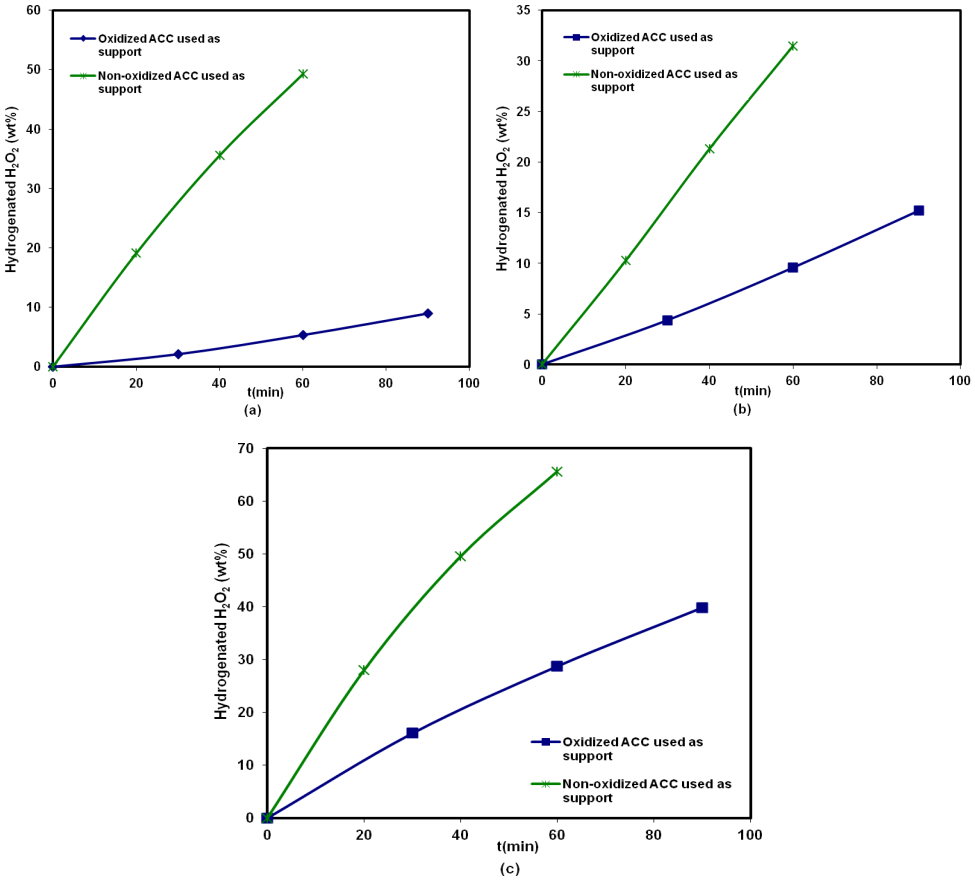

Fig. 9 The H_2O_2 hydrogenation activity of Pd-Au bimetallic catalysts supported on non-oxidized and oxidized ACC (with nitric acid): (a) the catalyst with 1 wt% Pd and 1 wt% Au, (b) the catalyst with 1 wt% Pd and 3 wt% Au, (c) the catalyst with 3 wt% Pd and 1 wt% Au. All catalysts were calcined in the air at 185 °C. Mass of catalyst = 56 mg, $T_{reaction}$= 21°C, P_{H2}= 4 bar.

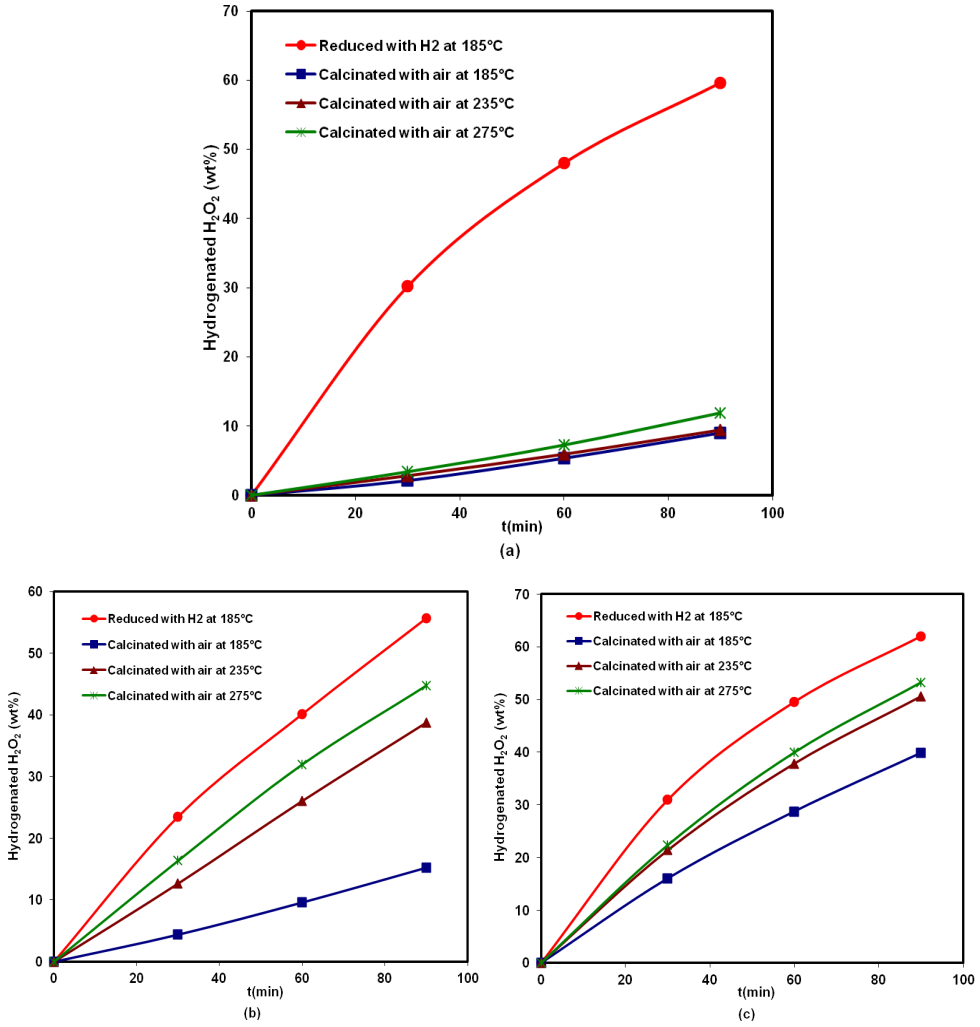

Fig. 10 The H_2O_2 hydrogenation activity of Pd-Au bimetallic catalysts supported on oxidized ACC and reduced by H_2 at 185 °C or calcined in air at different temperatures: (a) the catalyst with 1 wt% Pd and 1 wt% Au, (b) the catalyst with 1 wt% Pd and 3 wt% Au, (c) the catalyst with 3 wt% Pd and 1 wt% Au. Mass of catalyst = 56 mg, $T_{reaction}$= 21°C, P_{H2}= 4 bar.

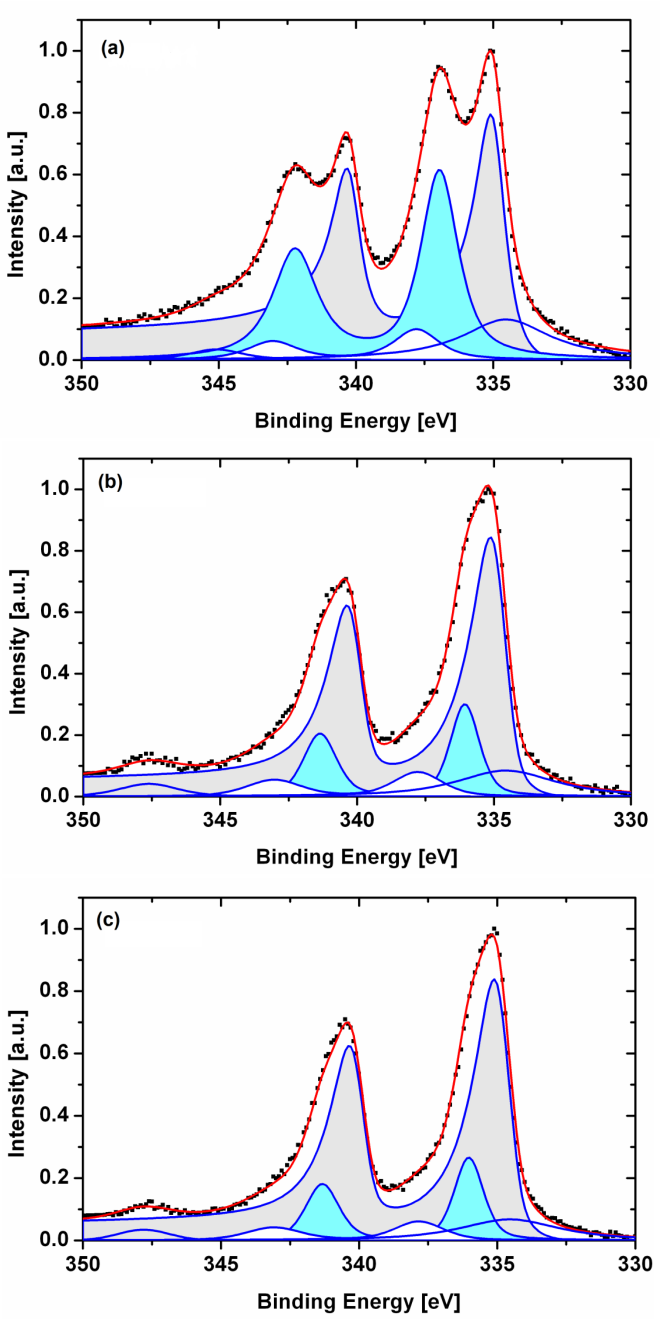
(a)
(b)
(c)
Intensity [a.u.]
Binding Energy [eV]
1.0
0.8
0.6
0.4
0.2
0.0
350
345
340
335
330

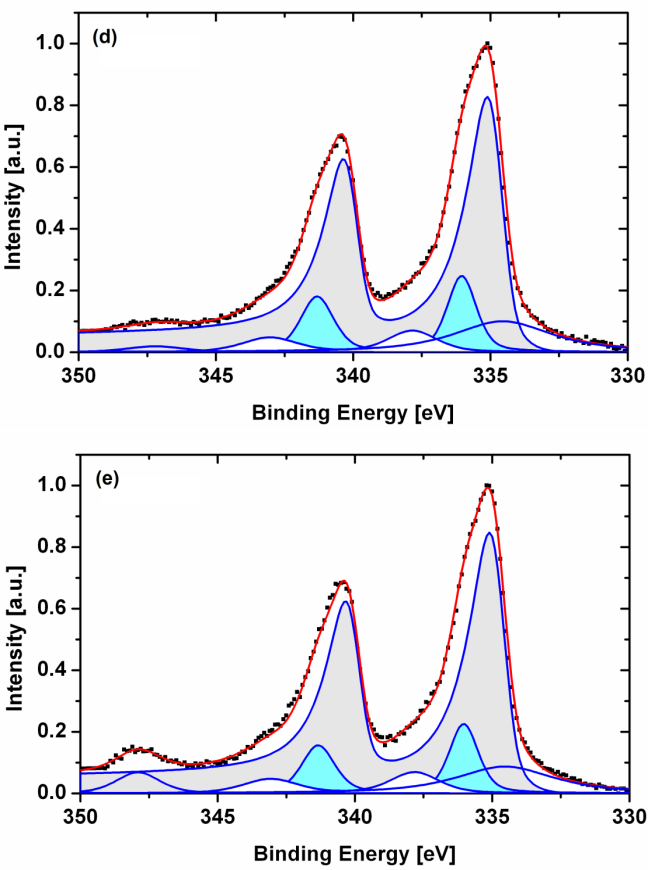

Fig. 11 The Pd 3d XPS spectra of 1 wt % Pd_1 wt % Au bimetallic catalysts supported oxidized ACC and calcined in air at 275 °C: (a) just before hydrogenation reaction, (b) after H_2O_2 hydrogenation reaction ($t_{reaction}$= 5 min), (c) after H_2O_2 hydrogenation reaction ($t_{reaction}$= 15 min), (d) after H_2O_2 hydrogenation reaction ($t_{reaction}$= 30 min), and (e) after H_2O_2 hydrogenation reaction ($t_{reaction}$= 60 min); Mass of catalyst = 56 mg, $T_{reaction}$= 21°C, and P_{H2}= 4 bar.

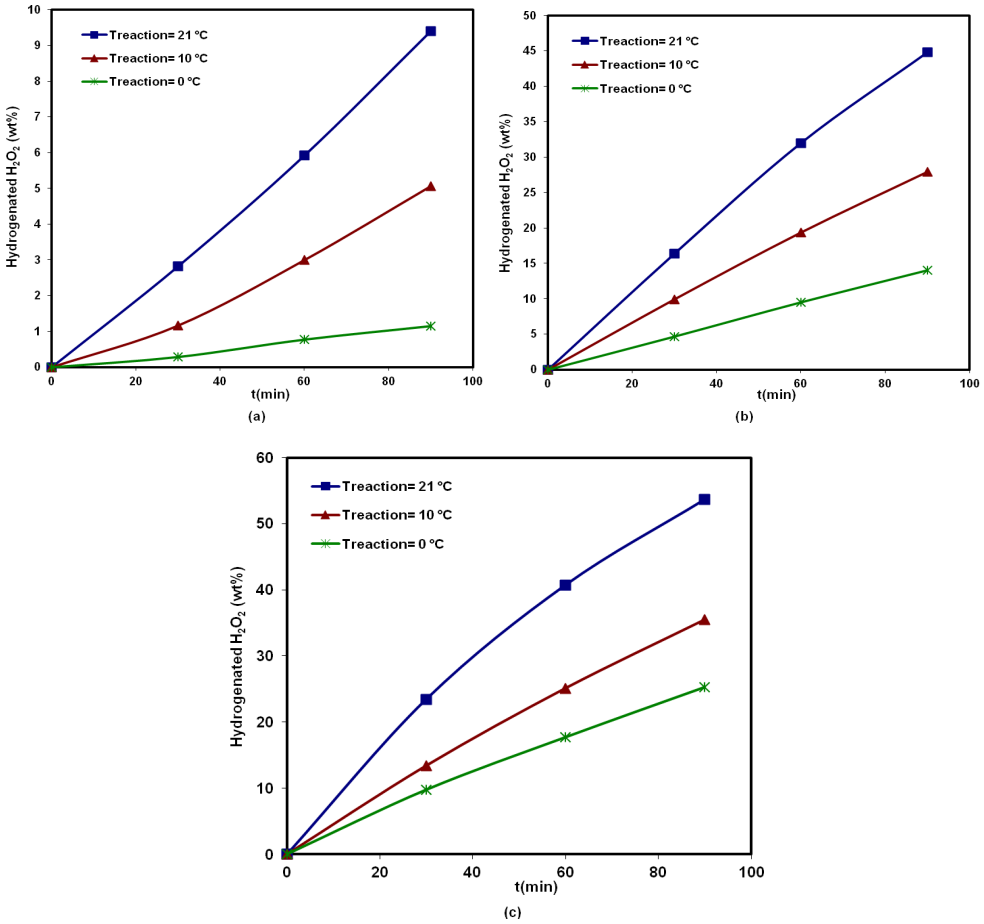

Fig. 12 The effect of the reaction temperature on the final H_2O_2 hydrogenation activity of the Pd-Au bimetallic catalysts: (a) the catalyst with 1 wt% Pd and 1 wt% Au, (b) the catalyst with 1 wt% Pd and 3 wt% Au, (c) the catalyst with 4 wt% Pd and 1 wt% Au. Mass of catalyst = 56 mg and P_{H2}= 4 bar.

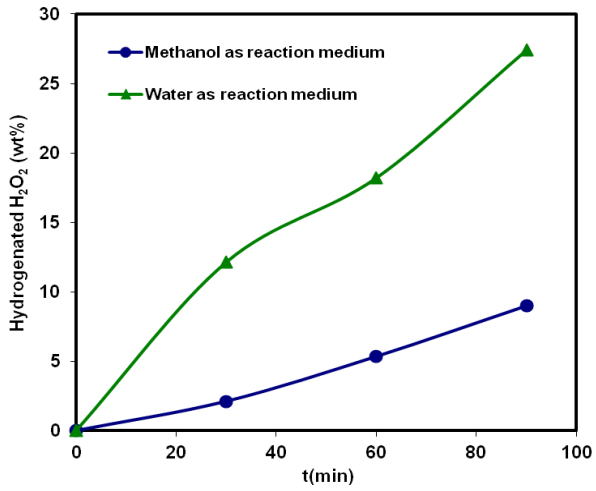

Fig. 13 The effect of the reaction medium on the final H_2O_2 hydrogenation activity of the catalyst with 1 wt% Pd and 1 wt% Au supported on oxidized ACC and calcined in air at 185 °C. Mass of catalyst = 56 mg, $T_{reaction}$= 21°C, and P_{H2}= 4 bar.

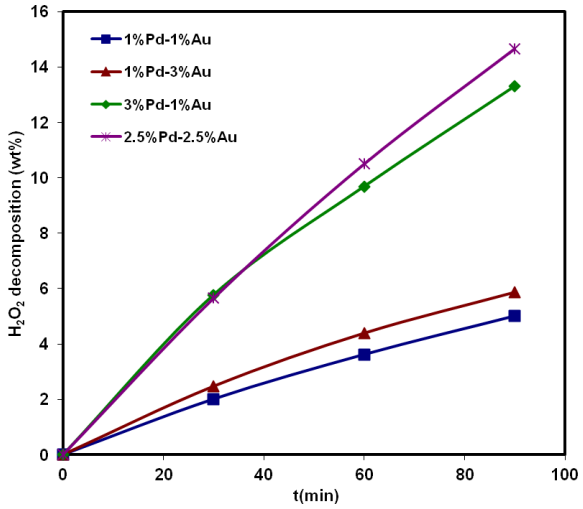

Fig. 14 Destruction of H_2O_2 by its decomposition over the Pd-Au bimetallic catalysts supported on oxidized ACC and reduced by H_2 at 185 °C. Mass of catalyst = 56 mg, $T_{reaction}$= 21°C, and P_{N2}= 4 bar.

Publication V

D. Gudarzi, O. A. Simakova, J. R. Hernández Carucci, P. D. Biasi, K. Eränen, E. Kolehmainen, I. Turunen, D. Y. Murzin, T. Salmi
Direct synthesis of H_2O_2 from H_2 and O_2 over carbon supported Au, Pd and Au-Pd/C bimetallic catalysts
Chemical Engineering Transaction 21 (2010) 925-930

CHEMICAL ENGINEERING TRANSACTIONS Volume 21, 2010
Editor J. J. Klemeš, H. L. Lam, P. S. Varbanov
 ISBN 978-88-95608-05-1 ISSN 1974-9791
DOI: 10.3303/CET1021155

Direct Synthesis of H_2O_2 from H_2 and O_2 over Carbon Supported Au, Pd and Au-Pd/C Bimetallic Catalysts

Davood Gudarzi[1]*, Olga A. Simakova , Jose R. Hernández Carucci[2], Pier D. Biasi[2], Kari Eränen[2], Eero Kolehmainen[1], Ilkka Turunen[1], Dmitry Y. Murzin[2], Tapio Salmi[2]
[1]Department of Chemical Technology, Lappeenranta University of Technology, Lappeenranta, P.O. Box 53851 Finland
[2]Laboratory of Industrial Chemistry and Reaction Engineering, Åbo Akademi University, Turku/Åbo, P.O. Box 20500, Finland
davood.gudarzi@lut.fi

The direct synthesis of hydrogen peroxide from hydrogen and oxygen using Pd/C, Au/C and bimetallic Au-Pd/C in a batch reactor was investigated and the kinetic curves have been obtained. Mesoporous carbon (Sibunit) was used as a support in the forms of oxidized and non-oxidized states. The presence of two metals (Pd, Au) on the carbon support enhances the catalytic performance compared to both Pd/C and Au/C catalysts in the case of non-oxidized and oxidized Sibunit. The enhancements become more apparent as the reaction time increases. Pre-oxidizing of the catalytic support also affects the catalytic performance of both the bimetallic Au-Pd/C and monometallic Pd/C catalysts for the direct synthesis of hydrogen peroxide. In the case of the monometallic Pd/C catalyst, when a pre-oxidized support, was used, the catalytic activities of the production of hydrogen peroxide and water increase in the same order of magnitude. Additionally, the pre-oxidized sibunit enhances the yield considerably. Nonetheless, the selectivity changes were found to be minimal. For the bimetallic Au-Pd/C catalysts, the behaviour was the opposite: the use of a pre-oxidized support increases the selectivity and consequently the catalytic performance for the synthesis of hydrogen peroxide, by reducing the production of water.

1. Introduction

Hydrogen peroxide (H_2O_2) is one of the most powerful and environmentally friendly known oxidizers with a wide range of applications in pulp bleaching, waste water treatment, cosmetic and pharmaceutical industries. The main commercial method to produce hydrogen peroxide is the athraquinone auto-oxidation method. This method is economically viable only for large-scale production and high concentrations of hydrogen peroxide (Edwards and Hutchings, 2008). Because of high investment and operating costs, it is not economically rational to produce hydrogen peroxide on-site at the end users sites. The simplest method to produce hydrogen peroxide and main competitor for the anthraquinone method is the direct catalytic synthesis of hydrogen peroxide from elemental hydrogen and oxygen. The direct method suffers from two

Please cite this article as: Gudarzi D, OSimakova O.A., Hernández Carucci J.R., Biasi P.D., Eränen K., Kolehmainen E., Turunen I., Murzin D.Y. and Salmi T. (2010), Direct synthesis of H_2O_2 from H_2 and O_2 over carbon supported Au, Pd and Au-Pd/C bimetallic catalysts, Chemical Engineering Transactions, 21, 925-930 DOI: 10.3303/CET1021155

serious technical challenges. Firstly, the safety problem: mixtures of hydrogen and oxygen are explosive over a wide range of concentrations (4-94 % H_2 in O_2) (Edwards and Hutchings, 2008). Secondly, the selectivity problem: supported Pd catalyst is the main catalyst for this reaction but it is also active for the other undesired reactions (see Scheme 1) - Samanta, 2008. Therefore, water is also produced in addition of hydrogen peroxide. Because of these two reasons, the direct method has not been commercialized yet even though it has been widely studied (Edwards and Hutchings, 2008).

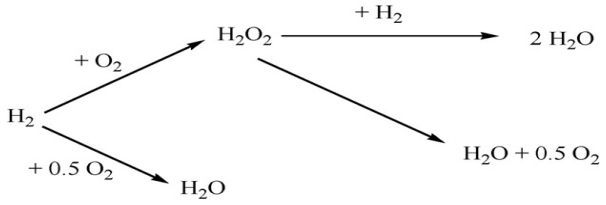

Scheme 1: Reactions involved in the direct synthesis of H_2O_2 [2]

The first problem may be avoided by working below the explosion limit or by using catalytic membranes to separate the gases. Microreactors might offer another way to eliminate the safety problem. The selectivity could be increased by using bimetallic catalysts or proper promoters, e.g. acidic solution and halide ions. Adding halide ions to an acidic reaction medium or directly to the catalyst has been shown to enhance H_2O_2 selectivity and yield over supported Pd catalysts (Samanta, 2008; Samanta and Choudhary, 2007a; Samanta and Choudhary, 2007b) and less active supported Au-Pd catalysts (Ntainjua et al, 2009). It has been reported that supported Au-Pd bimetallic catalysts are more active than Pd and Au monometallic catalysts for direct synthesis of hydrogen peroxide from H_2 and O_2 (Edwards and Hutchings, 2008).
Direct synthesis of hydrogen peroxide using gold and gold –palladium on a carbon support (Sibunit) is studied in this paper. The results are also compared with carbon supported palladium catalyst.

2. Experimental

2.1 Materials and Catalyst Preparation

Sibunit was used as the catalyst support in this study. It is a new class of porous carbon-carbon composite materials combining advantages of graphite (chemical stability and electric conductivity) and active carbons (high specific surface area and adsorption capacity) - Simakova et al, 2008. These composites are characterized by high mesopore volume and specific surface area (S_{BET} = 450 m^2/g). Catalysts on both non-oxidized and pre-oxidized carbon were prepared almost with the same procedure. The only difference was that when pre-oxidized Sibunit was used, the support was inmersed in 5 wt.% nitric acid at room temperature and let to stay overnight.
Preparation of Au on carbon was started by dissolving $HAuCl_4$ (ABCR, Darmstad, 49% Au) in deionized water, then polyvinylalcohol was added to form gold sol (Prati and Porta, 2005). After a few minutes of mixing, gold sols were reduced by freshly prepared 0.1 M $NaBH_4$ solution. The ruby red Au(0) sols were immobilized immediately by

adding the carbon support (Sibunit) under vigorous stirring in the amount corresponding to 2.5 wt.% Au/C. After 2 h the slurry was filtered and washed with deionized water. The catalyst was dried overnight at 60 °C.

Preparation of Pd on carbon was started by mixing with alkali solution of Na_2CO_3 at pH 8 (Simakova et al., 2008) After that aqueous solution of H_2PdCl_4 was added in the amount corresponding to 2.5 wt.% Pd/C. The slurry was mixed overnight at room temperature, then filtered and washed with deionized water. The catalyst was reduced in hydrogen flow at 150°C.

Au-Pd-catalyst on carbon was prepared by a two-steps procedure (Prati et al, 2007). First, $HAuCl_4$ (ABCR, Darmstad, 49% Au) was dissolved in deionized water was mixed with polyvinylalcohol to form a gold sol, then after a few minutes of mixing, the sol was reduced by freshly prepared 0.1 M $NaBH_4$ solution and immobilized immediately by adding carbon support under vigorous stirring in the amount corresponding to 2.5 wt. % Au/C. After 2 h of mixing at room temperature the slurry was filtered and washed with deionized water. The obtained slurry was mixed with a palladium sol, formed by mixing aqueous solution of H_2PdCl_4 with polyvinylalcohol and hydrogen bubbled at room temperature (50 mL/min) for 2 h. Then the slurry was mixed in air atmosphere overnight, filtered and washed with water. The catalyst was dried at 60°C. The catalysts were after each step of deposition (Au, Pd) by $NaBH_4$ and by bubbling H_2.

2.2 Experimental set-up

The direct synthesis of hydrogen peroxide was carried out in a stainless steel autoclave (Parr Instruments Ltd) with a nominal volume of 600 ml and a maximum working pressure of 140 bar. The autoclave was equipped with an overhead stirrer (0–2000 rpm) and facilities to measure the temperature and pressure. Hydrogen was fed into the main reactor through a pre-reactor with a volume of 35 ml and by means of a mass flow controller. The pre-reactor was used to measure the precise amount of hydrogen fed to the system. A recirculation line containing a six-way valve was used for sampling. Typically, the reactor was charged with 31-32 mg of catalyst and successively with carbon dioxide up to 15.2 bars. The pressure was thereafter elevated to 20.2 bar with oxygen and further to 35.2 bar with carbon dioxide again. 175 g of methanol were pumped in and the reactor was cooled down to -1 °C. Stirring (1250 rpm) began after 2/3 of the methanol was fed. When the desired temperature was reached, hydrogen was charged and the reaction time was started.

3. Results and Discussion

In order to evaluate the activity of the catalysts, the following two parameters were calculated:

$$Yield\,(\%) = \frac{\text{Moles of produced } H_2O_2}{\text{Moles of } H_2 \text{ fed}} \times 100$$

$$Selectivity(\%) = \frac{\text{Moles of produced } H_2O_2}{\text{Moles of produced } H_2O_2 + \text{Moles of produced } H_2O} \times 100$$

3.1 The effect of adding Pd to carbon supported Au catalyst:

Fig.1 shows the selectivity and yield of the catalysts versus reaction time when non-oxidized Sibunit is used as a support. Selectivity of the bimetallic Au-Pd/C catalyst is higher than the pure Pd/C catalyst, especially when the reaction time is between 15 to 90 min. Au/C catalyst is much more selective than the bimetallic Au-Pd/C and Pd/C catalysts as it produces less water. On the basis of the yield, the catalysts perform differently. The yield for the bimetallic Au-Pd/C catalyst is much higher than for both monometallic catalysts, especially at higher reaction times.

Fig.2 displays the selectivity and yield when pre-oxidized Sibunit is used as a support. Adding Pd to the Au/C catalyst increases selectivity and yield significantly. The enhancements in selectivity and yield for bimetallic Au-Pd/C compared to Pd/C were higher than when non-oxidized carbon was used. In the other words, in the case of the oxidized carbon, the bimetallic Au-Pd/C catalyst is much more selective than monometallic Pd/C catalyst.

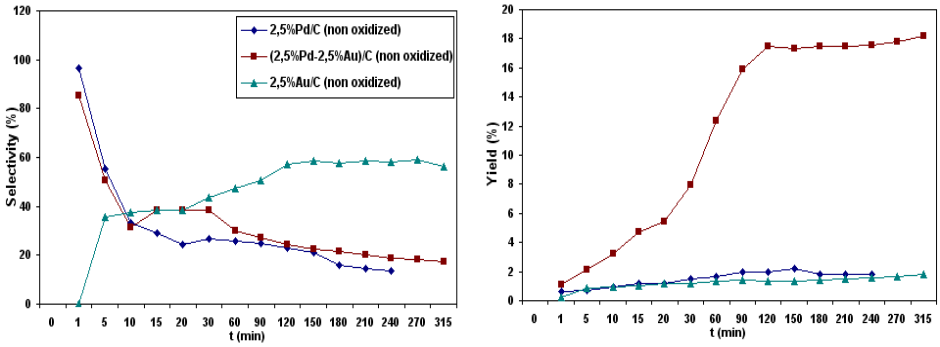

Figure 1. The selectivity and the yield of 2.5 % Au/C, 2.5% Pd/C and 2.5 %Au-2.5 % Pd/C (non-oxidized state of Sibunit was used as the support) for the direct synthesis of H_2O_2

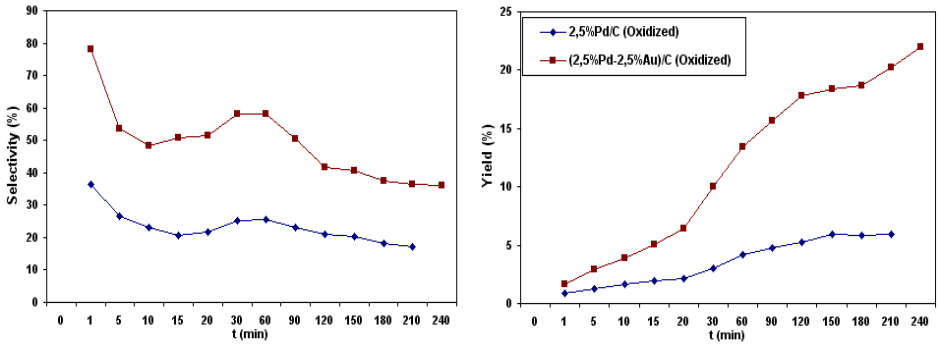

Figure 2.The selectivity and the yield of 2.5 % Pd/C and 2.5 % Au-2.5 % Pd/C (oxidized state of Sibunit was used as the support) for the direct synthesis of H_2O_2

3.2 The effect of support oxidation:

Pre-oxidizing Sibunit enhances the yield for Pd/C catalyst in the direct synthesis of hydrogen peroxide considerably (especially at higher reaction times), slightly diminishing the selectivity at lower reaction times (Fig. 3). This is because pre oxidizing the support increases the catalytic activity of pure Pd/C in the production of both hydrogen peroxide and water by almost the same order of magnitude. Therefore, the yield increases dramatically but the selectivity does not change that much.

Pre-oxidizing of the support for bimetallic Au-Pd/C catalyst made the catalyst more selective decreasing the production of water. It did not have any effect on the activity of the catalyst in the generation of hydrogen peroxide. Therefore, selectivity is increased considerably, especially at the higher reaction times and slightly the yield (Fig. 4)

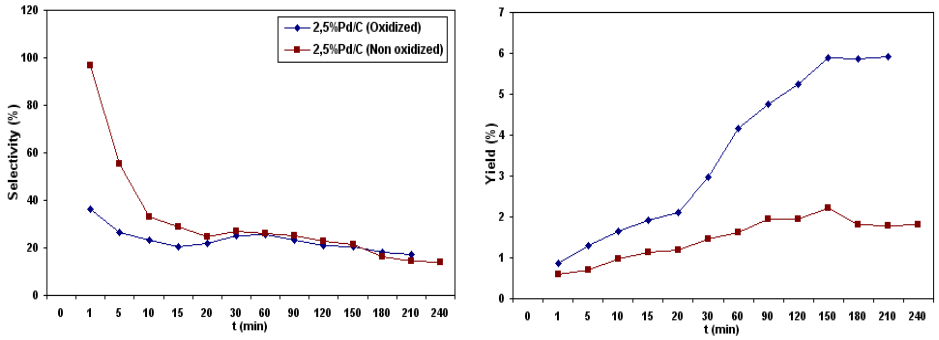

Figure 3.The effect of oxidizing state of the support on the selectivity and the yield of the 2.5%Pd/c for the direct synthesis of H_2O_2

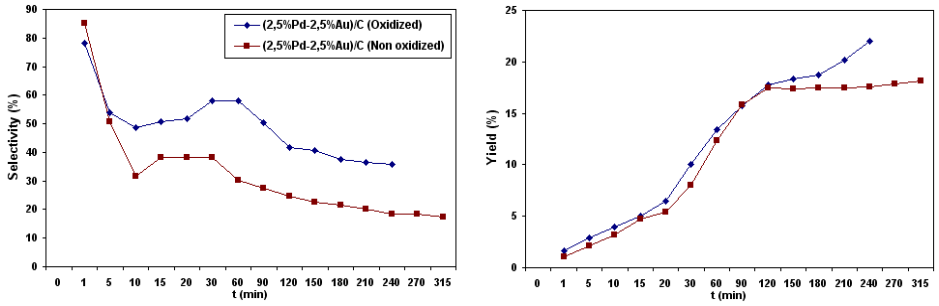

Figure 4. The effect of support oxidation on the selectivity and the yield of 2.5 % Au-2.5 % Pd/C for the direct synthesis of H_2O_2

The better results obtained with the bimetallic catalyst, (Au-Pd)/C, compared to the monometallic Pd/C and Au/C could be related with the properties of the different metals for oxidized supports. Moreover, the higher nominal metal loading (5 wt.% for the bimetallic catalyst vs. 2.5 wt.% for the monometallic ones) certainly has an effect on the catalytic activity. In addition, when oxidizing the support, different functional groups on

the external and porous surface of the Sibunit could be formed. These groups are likely to be surface oxygenated groups that have an acidic character which can influence the activity and selectivity in the hydrogen peroxide direct synthesis. It is expected that the different metals behave differently depending on the type of the support as well. Nonetheless, a more detailed characterization study is needed in order to reveal the structural differences between the oxidized and non-oxidized supports as well as the behaviours of the metals on them.

4. Conclusion

This study shows that bimetallic Au-Pd/C is more active in the direct synthesis of H_2O_2 than monometallic Pd/C and Au/C catalysts especially at higher reaction times. Pre-oxidizing of mesoporous carbon support (Sibunit) also enhances the catalytic performance of both Pd/C and bimetallic Au-Pd/C catalysts in the direct H_2O_2 synthesis considerably. Pre-oxidizing the support in the case of Pd/C increases the production of both hydrogen peroxide and water by almost the same order of magnitude, while for bimetallic Au-Pd/C catalyst on this support the water production is diminished without any considerable effect on the production of hydrogen peroxide.

References

Chanchal S., 2008, Direct synthesis of hydrogen peroxide from hydrogen and oxygen: An overview of recent developments in the process, Appl. Catal. A: General 350,133–149.

Chanchal S. and Choudhary V.R., 2007a, Direct formation of H_2O_2 from H_2 and O_2 and decomposition/hydrogenation of H_2O_2 in aqueous acidic reaction medium over halide-containing Pd/SiO_2 catalytic system, Cat. Commun. 8, 2222-2228.

Chanchal S. and Choudhary V.R., 2007b, Direct synthesis of H_2O_2 from H_2 and O_2 and decomposition/hydrogenation of H_2O_2 in an aqueous acidic medium over halide-modified Pd/Al_2O_3 catalysts, Appl. Catal. A: General 330, 23-32.

Edwards J. K. and Hutchings G. J., 2008, Palladium and gold–palladium catalysts for the direct synthesis of hydrogen peroxide, Angew. Chem. Int. Ed. 47, 9192 – 9198.

N. Ntainjua E., Piccinini M., Pritchard J. C., He Q., Edwards J. K., Carley A. F., Moulijn J. A., Kiely C. J. and Hutchings G. J., 2009, The effect of bromide pretreatment on the performance of supported Au–Pd catalysts for the direct synthesis of hydrogen peroxide, Chem Cat Chem 1, 479 – 484.

Prati L. and Porta F., 2005, Oxidation of alcohols and sugars using Au/C catalysts. Part 1: Alcohols, Appl. Catal. A: General 291, 199-206.

Simakova I. L., Simakova O. A., Romanenko A. V. and Murzin D. M., 2008, Hydrogenation of vegetable oils over Pd on nanocomposite carbon catalysts, Ind. Eng. Chem. Res. 47, 7219–7225.

Simakova O.A., Simonov P.A., Romanenko A.V. and Simakova I.L., 2008, Preparation of Pd/C catalysts via deposition of palladium hydroxide onto Sibunit carbon and their application to partial hydrogenation of rapeseed oil, React. Kinet. Catal. Lett. 95 (1), 3-12.

Villa A., Campione C. and Prati L., 2007, Bimetallic gold/palladium catalysts for the selective liquid phase oxidation of glycerol, Catalysis Letters 115, 133-136.

Publication VI

W. Ratchananusorn, D. Gudarzi, I. Turunen
Catalytic direct synthesis of hydrogen peroxide in a novel microstructured reactor
Chemical Engineering and Processing: Process Intensification (2014)
Available online at http://dx.doi.org/10.1016/j.cep.2014.01.005

G Model
CEP-6379; No. of Pages 7
ARTICLE IN PRESS

Chemical Engineering and Processing xxx (2014) xxx–xxx

Contents lists available at ScienceDirect

Chemical Engineering and Processing: Process Intensification

journal homepage: www.elsevier.com/locate/cep

Catalytic direct synthesis of hydrogen peroxide in a novel microstructured reactor

Warin Ratchananusorn*, Davood Gudarzi, Ilkka Turunen

Department of Chemical Technology, Lappeenranta University of Technology, Lappeenranta FI-53851, Finland

ARTICLE INFO

Article history:
Received 12 August 2013
Received in revised form 23 October 2013
Accepted 16 January 2014
Available online xxx

Keywords:
Microreactor
Hydrogen peroxide
Direct synthesis
Activated carbon cloth
Pd catalyst

ABSTRACT

The direct synthesis of hydrogen peroxide was investigated in a bench-scale continuous process using a novel microstructured reactor. This plate-type reactor was developed to offer favorable hydrodynamic and mass transfer conditions. Supported Pd catalyst on activated carbon cloths was employed. The experiments were conducted with hydrogen and oxygen using methanol as a solvent. Effects of process conditions, e.g. gas composition, gas and liquid flow rates, pressure and amount and composition of catalyst were studied. The promising results and plans for further development of the reactor and process concept are discussed.

1. Introduction

Hydrogen peroxide is a very powerful and green oxidant used in many industries. Currently, hydrogen peroxide is mainly produced by auto-oxidation in anthraquinone process. This process, however, has certain drawbacks. The chemistry is complicated with plenty of side reactions and byproducts. The investment costs are relatively high because of high number of equipment and large capacity is needed to achieve acceptable profitability. Moreover, using of a large amount of organic solvent makes the process less sustainable [1,2].

Direct synthesis of hydrogen peroxide has been studied as an attractive, green alternative over past decades [3]. The main benefits include:

- The chemistry is more straightforward than in the case of anthraquinone process.
- Lower investment and operating costs due to a substantially smaller number of equipment.
- The process is green when compared to anthraquinone process. This is clear if water is used as a solvent. The direct synthesis is greener even with methanol as a solvent because the total volume of organic liquid in the process would be substantially less.
- The process is favorable for on-site production.

However, there are a number of technical challenges in the direct synthesis. Hydrogen and oxygen generate an explosive mixture at wide range of concentrations (5–96 vol% H_2) [4]. Moreover, several side reactions are involved, as shown in Fig. 1. Therefore, selectivity is a challenge.

The safety risk can be decreased by utilizing microreactor technology. Proceeding of explosion could be suppressed by small dimensions of the reaction space. Moreover, the small holdup in microreactor limits the damage to be small even in the case of explosion. Therefore microreactors can be considered as inherently safe tools for hydrogen peroxide synthesis. Microreactors might even be able to be operated at explosive regime of gas mixture [5–8] allowing then also higher gas concentrations in the solvent, leading to higher yield.

The selectivity problem (see Fig. 1) can be solved by catalyst development [9]. Catalyst is very crucial to obtain high yield and selectivity, which tend to be rather low. Supported Pd catalysts, such as Pd/C, Pd/SiO_2, and Pd/Al_2O_3, are traditionally used in the direct synthesis [3]. In recent years, bimetallic Au–Pd catalysts were found to exhibit high activity with high selectivity [10–12].

The direct synthesis has been studied in various types of reactors from conventional ones to microreactors. A number of investigations in batch reactors [9,13–17] and trickle bed reactors has been carried out [12,18,19]. Pd catalysts on various support materials including activated carbon [9,12–15,17], SiO_2, CeS, and ZrO_2 [19] have been used. Many attempts to use single channel and multichannel microreactors have been done [5–8,11,20,21]. Some of the experiments were done in the explosive regime [5–8] and sometimes small explosions were detected by Inoue et al. [7].

* Corresponding author. Tel.: +358 404804963; fax: +358 56212199.
E-mail address: warin.ratchananusorn@lut.fi (W. Ratchananusorn).

0255-2701/$ – see front matter © 2014 Published by Elsevier B.V.
http://dx.doi.org/10.1016/j.cep.2014.01.005

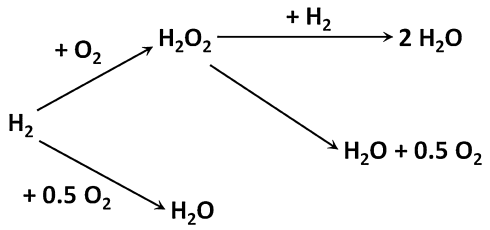

Fig. 1. Reactions in the direct synthesis of H_2O_2.

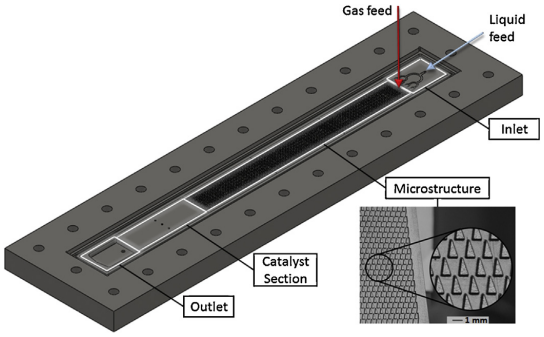

Fig. 2. Microreactor plate in this study.

The goal of this study is to investigate the direct synthesis in a novel microstructured reactor which was developed in previous studies [22]. Pd supported catalysts on activated carbon cloths [9] were used. Effects of gas composition, pressure, catalyst, and hydrodynamic conditions were studied.

2. Experimental setup

2.1. Microreactor

The development of the plate type microstructured reactor used in this study has been reported by Ratchananusorn et al. [22] and Semyonov et al. [23]. This structure was chosen because of several benefits. Firstly, gas–liquid mass transfer might be faster than in the reactor with parallel microchannels. The reason is that the gas slugs in the channels are surrounded by thin liquid films which easily become saturated with gas. In that case, mass transfer can only take place through the ends of the slugs [24], i.e. through reduced interfacial area. Moreover, the reactor can be easily opened for cleaning and catalyst replacement or regeneration. The plugging problem is also expected to be less severe when compared to conventional microreactors with several microchannels. The safety is enhanced by small dimensions and holdup. Moreover, the scale up of this type of microreactor is straightforward. Several parallel plates can be installed (numbering up).

The configuration of the reactor is shown in Fig. 2. It is made of stainless steel and consists of several sections. The reactor plate is installed in vertical position. The inlets for gas and liquid feeds are located at the top section. Bifurcation configuration was used for the liquid feed to improve the distribution and prevent channeling problem. The gas feed takes place through the cover plate which is installed against the microreactor plate. The microstructure section is located below the inlet section. The width of this section is 32 mm, height 300 mm and depth 300 μm. The microstructure consists of number of triangular elements (see Fig. 2). The size of each element is 1 mm × 2 mm × 300 μm (base × height × depth). The elements are arranged in staggered arrays providing void fraction of 75% for reaction space. The holdup for gas/liquid mixture was 3.84 cm^3. The microstructure was designed to improve the mixing of the two phases and to generate high interfacial area. Below the microstructure section is the catalyst bed. Pd catalyst was supported on active carbon cloth. A single layer of the cloth was installed in the catalyst bed between the plates.

2.2. Catalyst

2.2.1. Catalyst support

Carbon supported Pd catalysts have been extensively used in many studies for the direct synthesis with high performance [9,12–15,17]. Acidic pretreatment of the support and oxidized state of the catalyst usually give better performance [9]. Activated carbon has been found in many studies to give better performance than other supports.

In this study, activated carbon cloth (ACC) was used as a catalyst support. Because ACC is a fabric-type support, it can be placed directly between the reaction plate and the cover plate. Thus the replacement and regeneration of the catalyst can be done easily by opening the reactor and taking the ACC out. The packing problems are less difficult than with conventional granulated or powder catalysts.

Activated carbon cloth is flexible and easily applicable, it can be cut to proper size, bent, and rolled to fit into any reactor geometry. A large specific surface area is available (over 2000 m^2/g). The diameter of fibers is small and uniform. Therefore, a good contact between the flowing fluid and the catalyst surface can be obtained and excellent mass transfer characteristics achieved [25].

The catalysts used in this study were developed and tested extensively in an autoclave batch reactor by Gudarzi et al. [9].

ACC is available from many manufacturers with different properties. In this study, ACC was purchased from Kynol GmbH, Germany, and the model number was ACC507-15. The specific surface area (BET) is as high as 1500 m^2/g and the fiber size 9.2 μm. The microstructure of the fiber is uniform with straight pores rather than branched ones in granulated activated carbon.

2.2.2. Catalyst preparation

Series of Pd/ACC catalysts were prepared by precipitation of Pd on ACC. The pretreatment of the support was done with 20% nitric acid for overnight. Acidic solution of $PdCl_2$ was used to prepare the catalysts. The procedure has been described by Gudarzi et al. [9].

SEM images of catalysts with different Pd loading are shown in Fig. 3. The white spots represent metal particles which are well distributed throughout the ACC fibers. According to the images, Pd loading up to 1 wt.% mainly occurred inside the micropores of the ACC, because no particles can be detected on the outer surface of ACC. Increasing the amount of Pd led to development of large Pd particles on the outer surface [9].

2.3. Experimental bench-scale process

A continuous bench scale process for the direct synthesis is shown in Fig. 4. The stainless steel equipment was initially passivated with 20% citric acid at 333.15 K for 12 h to minimize the decomposition of hydrogen peroxide. Methanol was used as a solvent allowing higher solubility of gases. Solvent was saturated with oxygen in a saturation vessel at 20 bar. Excess of oxygen gas was used in order to also strip away dissolved carbon dioxide and hydrogen left in the recycled solvent. The vessel was cooled to maintain solvent temperature at 273.15 K. From the saturation vessel, solvent with dissolved oxygen was fed into the microreactor together

Please cite this article in press as: W. Ratchananusorn, et al., Catalytic direct synthesis of hydrogen peroxide in a novel microstructured reactor, Chem. Eng. Process. (2014), http://dx.doi.org/10.1016/j.cep.2014.01.005

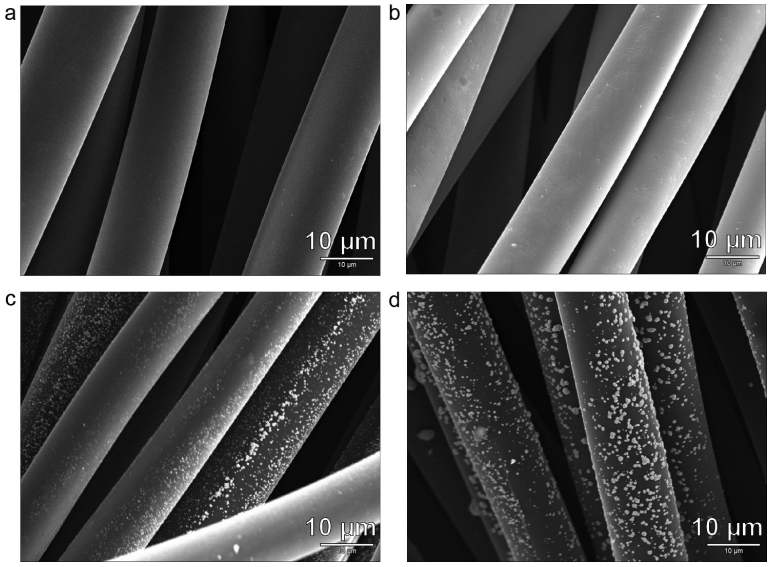

Fig. 3. SEM images for the catalysts used in this study: 0 wt.% (a), 1 wt.% (b) 3 wt.% (c), and 5 wt.% (d).
Reprinted with copyright from Ref. [9].

with mixture of CO_2 and H_2 (95%/5%). The fluids were flowing concurrently downwards in the reactor. At the bottom, gas and liquid phase were separated by gravity. Pressure was controlled by the gas outflow. Part of the outflowing liquid was taken as a product and the rest was recycled back to the saturation vessel. To maintain constant volume of liquid in the system, the equal amount of solvent was added to the saturation vessel as taken away as product stream after the reactor. The instrumentation is shown in Fig. 4.

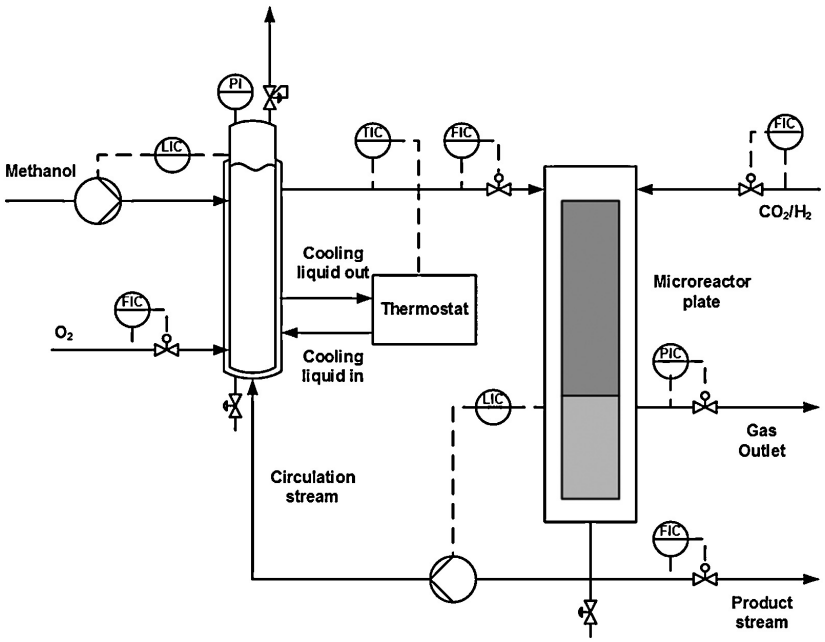

Fig. 4. Experimental setup.

Please cite this article in press as: W. Ratchananusorn, et al., Catalytic direct synthesis of hydrogen peroxide in a novel microstructured reactor, Chem. Eng. Process. (2014), http://dx.doi.org/10.1016/j.cep.2014.01.005

Table 1
Conditions in long-term experiments.

No.	Liquid feed (ml/min)	Gas mixture	Gas feed (ml/min)	Product flow (ml/min)	Pressure (bar)	Catalyst	Amount of catalyst (g)
1	68	CO_2/H_2	102	0.85	20	3 wt.% Pd	0.21
2	68	N_2/H_2	102	0.85	20	3 wt.% Pd	0.21
3	68	CO_2/H_2	102	0.85	10	3 wt.% Pd	0.21

3. Experimental procedure

Typical conditions in the reactor were 273.15 K and 20 bar. In the beginning, the saturation vessel was filled with methanol (0.35 l). Cooling of the liquid was started by feeding ethylene glycol through the jacket of the saturation vessel. Then oxygen flow through the saturation vessel was initiated. Gas sparger was utilized to achieve sufficient gas–liquid interface. After that, circulation of saturated solvent through the process was started. Next, the pressure of the reactor was raised to sufficient level by feeding inert gas. After reaching proper conditions in the whole process, the inert gas feed was changed to the mixture of CO_2 and H_2 and the reaction started.

The variables in the experiments were flow rate of liquid feed into the reactor, flow rate of gas feed into the reactor, pressure, concentration of Pd in the catalysts and amount of catalyst. In addition, two alternative inert gases, CO_2 and N_2, were utilized to dilute hydrogen feed. Temperature was always the same, 273.15 K.

In each experiment, samples were taken from the product stream. Concentration of hydrogen peroxide and water was determined in each sample. The iodometric titration was used for hydrogen peroxide and Karl–Fischer titration for water. The selectivity was calculated according to Eq. (1).

$$\text{Selectivity}(\%) = \frac{\text{Moles of produced } H_2O_2}{\text{Moles of produced } (H_2O_2 + H_2O)} \times 100\% \quad (1)$$

4. Experimental results

4.1. Long-term experiments

In these experiments, two different feed gas mixtures were used, as well as two pressure levels. The experimental conditions are shown in Table 1.

Analyzed concentration of H_2O_2 in the products streams is shown in Fig. 5 as a function of time. It can be seen that the system reached steady state approximately in 20 h. The best results were obtained at higher pressure when carbon dioxide was used as inert gas. The likely explanation for the latter is that carbon dioxide increases the solubility of the gases [26] and stabilizes the produced hydrogen peroxide [27].

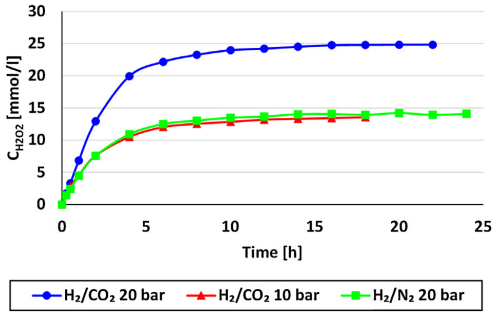

Fig. 5. Concentration of H_2O_2 in long-term experiments.

The cumulative amount of H_2O_2 produced (mmol) as a function of time is shown in Fig. 6. The upper curve represents the real cumulative H_2O_2 production (mmol) and the lower one describes the cumulative H_2O_2 (mmol) in the process circulation.

The total production rate of H_2O_2 in the reactor (mmol/h) is shown in Fig. 7. This is also shown per mass of Pd (mmol/h/g_{Pd}).

Selectivity in the long-term experiments is shown in Fig. 8. It has the highest value at the beginning of the experiments, during the unsteady period. This is understandable because the decomposition of H_2O_2 is directly proportional to the concentration of H_2O_2. The selectivity is the best at high pressure and with CO_2 as inert gas instead of N_2. At higher pressure the rate of decomposition is lower because gas (O_2) is produced during decomposition. As stated above, CO_2 stabilizes H_2O_2 and in that way improves selectivity.

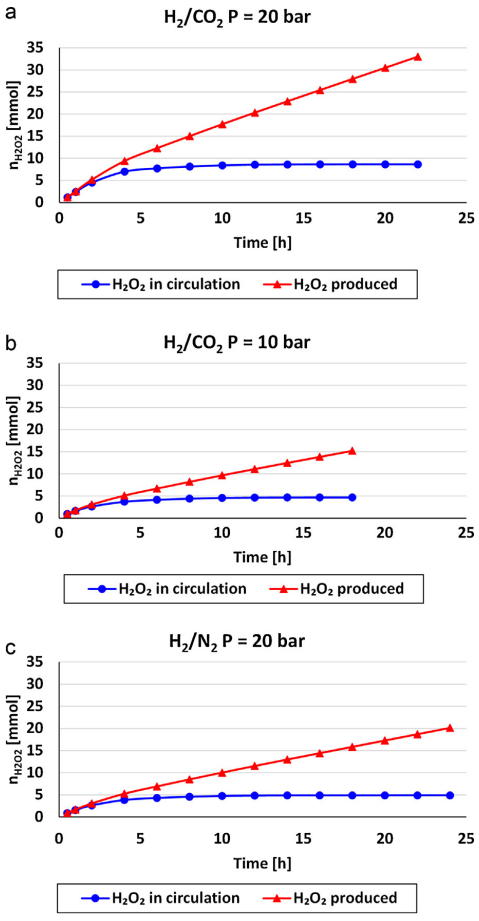

Fig. 6. Cumulative amount of H_2O_2 produced.

Please cite this article in press as: W. Ratchananusorn, et al., Catalytic direct synthesis of hydrogen peroxide in a novel microstructured reactor, Chem. Eng. Process. (2014), http://dx.doi.org/10.1016/j.cep.2014.01.005

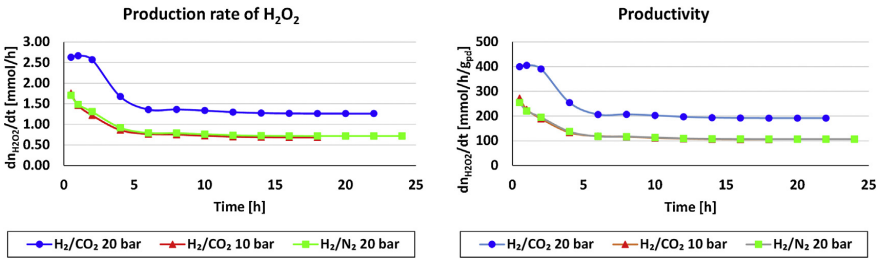

Fig. 7. Production rate of H_2O_2 in the reactor.

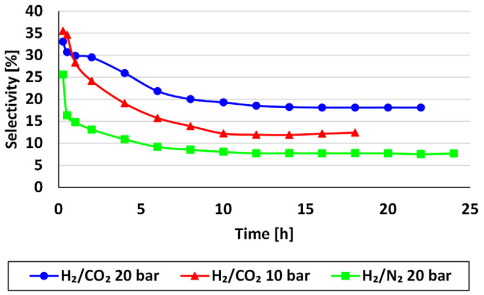

Fig. 8. Selectivity.

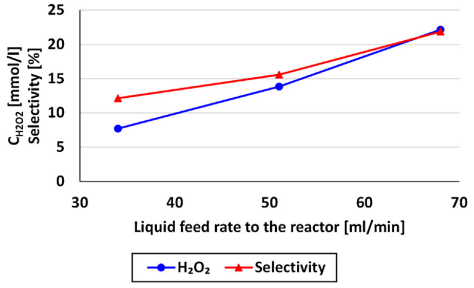

Fig. 9. Effect of liquid feed rate.

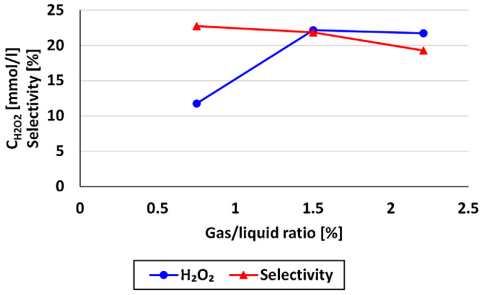

Fig. 10. Effect of gas/liquid feed ratio.

CO_2 also improves the solubility of gases and, therefore, increases the production rate of hydrogen peroxide.

4.2. Effect of the process conditions

Effect of different process conditions were studied with plenty of experiments with residence time of 6 h. Temperature and pressure were the same in all the experiments, namely 273.15 K and 20 bar.

4.2.1. Feed rate

Experiments were done with three different liquid feed rates. Gas/liquid ratio was kept constant in all these experiments. The conditions are shown in Table 2. Pressure was 20 bar, temperature 273.15 K and catalyst loading 0.21 g of 3 wt.% Pd. The product stream taken out after the reactor was 0.85 ml/min.

The results are shown in Fig. 9. Both concentration of H_2O_2 and selectivity seem to increase as a function of liquid feed rate. A reason for this could be improved hydrodynamical conditions in the catalyst bed, causing better surface contact and liquid/solid mass transfer. Another explanation could be faster gas–liquid mass transfer in the microstructure section because of higher velocity of gas/liquid dispersion. However, the interfacial area was extremely high and therefore mass transfer is not limiting the total rate substantially in these experiments.

4.2.2. Gas/liquid feed ratio

In Fig. 10, three different experiments are shown where gas flow rate was changing from 51 ml/min to 150 ml/min. The liquid flow rate was constant (68 ml/min). Therefore, gas/liquid feed ratio had values of 0.75, 1.50 and 2.21. The catalyst loading was 0.21 g of 3 wt.% Pd. The experimental conditions are shown in Table 3.

The results of the experiments are shown in Fig. 10. The increase of H_2O_2 concentration with increasing hydrogen feed is understandable. The decrease of selectivity can be explained by enhanced decomposition of H_2O_2 via hydrogenation (see Fig. 1).

Table 2
Experimental conditions for studies of liquid feed rate.

No.	Liquid feed rate (ml/min)	Gas feed rate (ml/min)
1	34	51
2	51	76.5
3	68	102

Table 3
Experimental conditions for studies of gas/liquid feed ratio.

No.	Liquid feed (ml/min)	Gas feed (ml/min)	Gas/liquid feed ratio (–)
1	68	51	0.75
2	68	102	1.00
3	68	150	2.21

Please cite this article in press as: W. Ratchananusorn, et al., Catalytic direct synthesis of hydrogen peroxide in a novel microstructured reactor, Chem. Eng. Process. (2014), http://dx.doi.org/10.1016/j.cep.2014.01.005

Table 4
Experimental conditions for studies of Pd loading.

No.	Liquid feed (ml/min)	Gas feed (ml/min)	Catalyst (wt.% Pd)	Amount of catalyst (g)
1	68	102	1	0.21
2	68	102	3	0.21
3	68	102	5	0.21

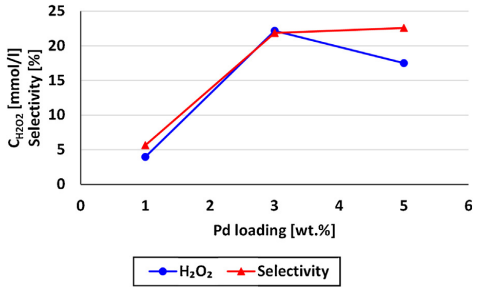

Fig. 11. Effect of Pd loading.

Table 5
Effect of the amount of catalyst.

Amount of catalyst (g)	H_2O_2 concentration (mmol/l)	Selectivity (%)
0.21	22.16	21.85
0.42	14.18	16.00

Reaction conditions: liquid feed rate = 68 ml/min, gas feed rate = 102 ml/min, 3 wt.% Pd catalyst.

4.2.3. Pd loading

The catalysts were prepared with 1 wt.%, 3 wt.%, and 5 wt.% Pd loading. The other conditions are shown in Table 4

The results are shown in Fig. 11. In the case of 1 wt.% Pd catalyst, almost all Pd particles were located inside micropores which are more difficult to access by the reactants. After increasing the amount of Pd to 3 wt.%, particles started to develop on the outer surface of carbon fibers which are easily accessible for the reactants. Further increase of Pd loading to 5 wt.% did not increase the number of active sites. It just led to bigger particles on the outer surface of carbon fibers. Therefore, after 3 wt.% loading of Pd, the concentration of hydrogen peroxide did not increase anymore [9].

4.2.4. Amount of catalyst

Experiments were done with two catalyst amounts, 0.21 and 0.42 g. The results are shown in Table 5.

The reason for the decreased selectivity might be the extra catalyst which caused the produced hydrogen peroxide to be hydrogenated or decomposed to water. This conclusion is supported by the observed decrease in the concentration of hydrogen peroxide.

5. Conclusions

A novel microreactor for direct synthesis of hydrogen peroxide was tested. The construction of the reactor, based on microstructured plates, offer certain advantages over conventional microreactors consisting of parallel channels with small diameter. Pd catalyst supported on carbon cloth was utilized.

The operation of the reactor was tested in a bench-scale process designed for experimental purposes. Effect of several process conditions on productivity and selectivity was studied and promising results achieved.

The microreactor and test process were designed to produce information for R&D purposes. The final goal in our R&D project is a full scale unit which have different design criteria and also partly different operation conditions.

The best strategy for scale-up is to install several parallel microreactor plates to enable sufficient throughput. Longer reactor plates with alternating mixing and catalytic sections would increase the yield. In this kind of reactor configuration several gas feeds through the cover plate, at different height levels, would be needed.

The arrangement of gas feed was designed for the test unit only. Hydrogen and oxygen gases, diluted with carbon dioxide, would be fed directly into the reactor in a production unit. The flow rates and compositions have to be optimized taking into account selectivity, yield and safety. Microreactor technology might offer possibilities to operate safely in the conditions which might be too dangerous with current technology but enhance the yield substantially. This has to be confirmed in a reliable way.

Separation of hydrogen peroxide and water from the circulating methanol stream is an essential part of a full scale process. This can be done with distillation. More promising, but also more challenging would be a membrane-based separation unit.

The research group will continue the development of the process concept according to these guidelines.

References

[1] Hydrogen peroxide, in: B. Elvers, S. Hawkins, M. Ravenscroft, G. Schulz (Eds.), Ullmann's Enclyclopedia of Industrial Chemistry, vol. A13, VCH, Weinheim, 1989.
[2] Ch. 8: Direct synthesis of hydrogen peroxide: recent advances, in: G. Centi, S. Perathoner, S. Abate, N. Mizuno (Eds.), Modern Heterogeneous Oxidation Catalysis: Design, Reactions and Characterization, Wiley-VCH, Weinheim, 2009.
[3] C. Samanta, Direct synthesis of hydrogen peroxide from hydrogen and oxygen: an overview of recent developments in the process, Appl. Catal. A 350 (2008) 133–149.
[4] C.E. Baukal Jr., Oxygen-Enhanced Combustion, CRC, New York, 1998.
[5] Y. Voloshin, R. Halder, A. Lawal, Kinetics of hydrogen peroxide synthesis by direct combination of H_2 and O_2 in a microreactor, Catal. Today 125 (2007) 40–47.
[6] X. Wang, Y. Nie, J.L. Lee, S. Jaenicke, Evaluation of multiphase microreactors for the direct formation of hydrogen peroxide, Appl. Catal. A 317 (2007) 258–265.
[7] T. Inoue, Y. Kikutani, S. Hamakawa, K. Mawatari, F. Mizukami, T. Kitamori, Reactor design optimization for synthesis of hydrogen peroxide, Chem. Eng. J. 160 (2010) 909–914.
[8] T. Inoue, K. Ohtaki, S. Murakami, S. Matsumoto, Direct synthesis of hydrogen peroxide based on microreactor technology, Fuel Process. Technol. 108 (2013) 8–11.
[9] D. Gudarzi, W. Ratchananusorn, I. Turunen, T. Salmi, M. Heinonen, Preparation and study of Pd catalysts supported on activated carbon cloth (ACC) for direct synthesis of H_2O_2 from H_2 and O_2, Top. Catal. 56 (2013) 527–539.
[10] J.K. Edwards, B.E. Solsona, P. Landon, A.F. Carley, A. Herzing, C.J. Kiely, G.J. Hutchings, Direct synthesis of hydrogen peroxide from H_2 and O_2 using TiO_2-supported Au–Pd catalysts, J. Catal. 236 (2005) 69–79.
[11] S.J. Freakley, M. Piccinini, J.K. Edwards, E.N. Ntainjua, J.A. Moulijn, G.J. Hutchings, Effect of reaction conditions on the direct synthesis of hydrogen peroxide with a AuPd/TiO_2 catalyst in a flow reactor, ACS Catal. 3 (2013) 487–501.
[12] P. Biasi, F. Menegazzo, F. Pinna, K. Eränen, T.O. Salmi, Continuous H_2O_2 direct synthesis over PdAu catalysts, Chem. Eng. J. 176-177 (2011) 172–177.
[13] P. Biasi, N. Gemo, J.R.H. Carucci, K. Eränen, P. Canu, Kinetics and mechanism of H_2O_2 direct synthesis over Pd/C catalyst in a batch reactor, Ind. Eng. Chem. Res. 51 (2012) 8903–8912.
[14] N. Gemo, P. Biasi, P. Canu, T.O. Salmi, Mass transfer and kinetics of H_2O_2 direct synthesis in a batch slurry reactor, Chem. Eng. J. 207–208 (2012) 539–551.
[15] T. Moreno, J. García-Serna, M.J. Cocero, Direct synthesis of hydrogen peroxide in methanol and water using $scCO_2$ and N_2 as diluents, Green Chem. 12 (2010) 282–289.
[16] R. Burch, P.R. Ellis, An investigation of alternative catalytic approaches for the direct synthesis of hydrogen peroxide from hydrogen and oxygen, Appl. Catal. B 42 (2003) 203–211.
[17] D. Gudarzi, O.A. Simokova, J.R.H. Carucci, P. Biasi, K. Eränen, E. Kolehmainen, I. Turunen, D.Y. Murzin, T. Salmi, Direct synthesis of H_2O_2 from H_2 and O_2 over carbon supported Au, Pd and Au–Pd/C bimetallic catalysts, Chem. Eng. Trans. 21 (2010) 925–930.
[18] P. Biasi, F. Menegazzo, F. Pinna, K. Eränen, P. Canu, T.O. Salmi, Hydrogen peroxide direct synthesis: selectivity enhancement in a trickle bed reactor, Ind. Eng. Chem. Res. 49 (2010) 10627–10632.

Please cite this article in press as: W. Ratchananusorn, et al., Catalytic direct synthesis of hydrogen peroxide in a novel microstructured reactor, Chem. Eng. Process. (2014), http://dx.doi.org/10.1016/j.cep.2014.01.005

[19] P. Biasi, P. Canu, F. Menegazzo, F. Pinna, T.O. Salmi, Direct synthesis of hydrogen peroxide in a trickle bed reactor: comparison of Pd-based catalysts, Ind. Eng. Chem. Res. 51 (2012) 8883–8890.
[20] J.F. Ng, Y. Nie, G.K. Chuah, S. Jaenicke, A wall-coated catalytic capillary microreactor for the direct formation of hydrogen peroxide, J. Catal. 268 (2010) 302–308.
[21] S. Maehara, M. Taneda, K. Kusakabe, Catalytic synthesis of hydrogen peroxide in microreactors, Chem. Eng. Res. Des. 86 (2008) 410–415.
[22] W. Ratchananusorn, D. Semyonov, D. Gudarzi, E. Kolehmainen, I. Turunen, Hydrodynamics and mass transfer studies on a plate microreactor, Chem. Eng. Process. Process Intensif. 50 (2011) 1186–1192.
[23] D. Semyonov, W. Ratchananusorn, I. Turunen, Hydrodynamic model of a microstructured plate reactor, Comput. Chem. Eng. 52 (2013) 145–154.
[24] R. Pohorecki, Effectiveness of interfacial area for mass transfer in two-phase flow in microreactors, Chem. Eng. Sci. 62 (2007) 66495–66498.
[25] R.T. Yang, Adsorbents: Fundamentals and Applications, John Wiley & Sons, Inc., New Jersey, 2003.
[26] N. Gemo, P. Biasi, T.O. Salmi, P. Canu, H_2 solubility in methanol in the presence of CO_2 and O_2, J. Chem. Thermodyn. 54 (2012) 1–9.
[27] J.K. Edwards, G.J. Hutchings, Palladium and gold–palladium catalysts for the direct synthesis of hydrogen peroxide, Angew. Chem. Int. Ed. 47 (2008) 9192–9198.

Please cite this article in press as: W. Ratchananusorn, et al., Catalytic direct synthesis of hydrogen peroxide in a novel microstructured reactor, Chem. Eng. Process. (2014), http://dx.doi.org/10.1016/j.cep.2014.01.005

PublicationVII

W. Ratchananusorn, D. Semyonov, D. Gudarzi, E. Kolehmainen, I. Turunen
Hydrodynamics and mass transfer studies on a plate microreactor
Chemical Engineering and Processing: Process Intensification 50 (2011) 1186-1192

Chemical Engineering and Processing 50 (2011) 1186–1192

Contents lists available at SciVerse ScienceDirect

Chemical Engineering and Processing: Process Intensification

journal homepage: www.elsevier.com/locate/cep

Hydrodynamics and mass transfer studies on a plate microreactor

Warin Ratchananusorn*, Denis Semyonov, Davood Gudarzi, Eero Kolehmainen, Ilkka Turunen

Department of Chemical Technology, Lappeenranta University of Technology, P.O. Box 20, FI-53851 Lappeenranta, Finland

ARTICLE INFO

Article history:
Received 21 April 2011
Received in revised form 13 July 2011
Accepted 19 August 2011
Available online 26 August 2011

Keywords:
Microreactor
Multiphase flow
Gas holdup
Interfacial area
Mass transfer

ABSTRACT

Prototype of structured microreactor plates with 300 μm deep flow channels was developed. Two plates with different structural elements, square and triangular, were used in the study. Flow behavior was investigated and the results showed excellent mixing behavior of gas and liquid phases. Hydrodynamic parameters and volumetric gas–liquid mass transfer coefficients were determined at various flow conditions. Gas holdup and the gas–liquid interfacial area were determined by an optical method using image processing software. Volumetric mass transfer coefficients were measured using nitrogen to strip oxygen from deionized water. The experimental results indicate a high mass transfer rate. Gas holdup and the total gas–liquid interfacial area were in the range of 20–45% and 2600–5600 $m^2\,m^{-3}$, respectively. Volumetric mass transfer coefficients were as high as 1.1 s^{-1}. An empirical correlation for the mass transfer coefficient was derived.

1. Introduction

Microreactors have recently been of great interest for multiphase reaction applications, mainly because of their high heat and mass transfer capacities and perceived safety advantages [1,2]. Due to the small size of the flow channels, extremely high surface to volume ratios can be obtained, allowing excellent heat transfer properties. As a consequence, hotspots in exothermic reactions can be avoided because of the maintenance of uniform temperatures throughout the reactor [3]. In multiphase catalytic reactions, gas–liquid mass transfer sometimes represents significant resistance [4,5]. Microreactors can provide a high gas–liquid interfacial area and therefore enhance mass transfer by up to 100 times compared to conventional scale reactors [6,7]. Multiphase microreactors include both non-catalytic gas–liquid reactors and gas–liquid-solid reactors, where a catalyst may be fixed on the channel walls.

Typically, such reactors consist of a large number of parallel channels. The diameter of the channels can sometimes be even less than 100 μm, thus the flow in microchannels is usually laminar and mainly dominated by viscosity, surface tension, and wall friction forces. Hydrodynamics of gas liquid flow in direct microchannels has been extensively studied [8–11]. The favorable flow pattern is slug (Taylor) flow, where elongated gas bubbles, occupying the whole cross section of the channel, alternate with liquid slugs. Only a thin liquid film then separates the gas slugs from the channel walls. As presented by Pohorecki [12], in some conditions, this thin liquid film might be saturated by dissolved gas. In these cases, only the ends of the gas slugs provide an active interfacial area for mass transfer, which might decrease the mass transfer performance remarkably. However, if the walls are covered with catalyst, the gas may be consumed and no saturation would occur.

A number of studies have been conducted to investigate mass transfer characteristics associated with different flow patterns in different types of microscale gas–liquid contactors. Yue et al. [3,13] investigated the mass transfer characteristics of gas–liquid flow in rectangular microchannels with hydraulic diameter of 200, 400, and 667 μm. The results exhibited that the specific gas–liquid interfacial area and mass transfer coefficient in microscale gas–liquid contactors were found to be at least one or two orders of magnitude higher than those in conventional scale gas–liquid contactors. Shao et al. [14] demonstrated the work on CFD modeling to investigate the mass transfer characteristics with slug flow pattern in micro-capillaries with diameter less than 1 mm. The results were compared and reported to be in the same range with the values from Yue et al. [3]. Losey et al. [6,7] designed and fabricated a novel type of multichannel packed-bed microreactors for hydrogenation reaction. The reactor consists of ten parallel channels with microstructure situated inside the channels. Extremely high mass transfer coefficient and gas–liquid interfacial area, by two orders of magnitude larger than in conventional scale gas–liquid contactors, were achieved in their study.

The current study was performed with novel microreactor plates designed for multiphase reactions. Gas holdup, the gas–liquid interfacial area, and the mass transfer coefficient were determined at various flow conditions.

* Corresponding author.
E-mail address: warin.ratchananusorn@lut.fi (W. Ratchananusorn).

0255-2701/$ – see front matter © 2011 Elsevier B.V. All rights reserved.
doi:10.1016/j.cep.2011.08.010

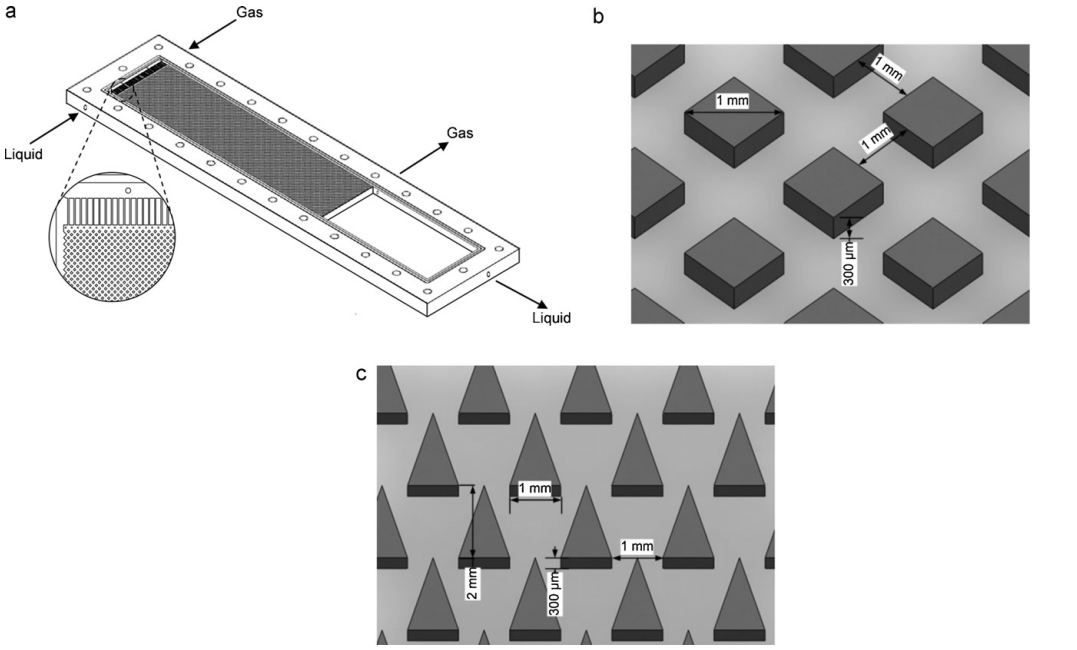

Fig. 1. Microreactor plate: (a) Microreactor plate showing inlet and outlet of gas and liquid. (b) Square structure layout and dimensions. (c) Triangular structure layout and dimensions.

2. Microreactor plate

A novel microreactor was constructed from parallel plates and the reaction space was located between them. This structure was selected in order to gain several advantages over more conventional multichannel structures. Firstly, plugging problems were expected to be less severe and more uniform fluid distribution was anticipated. Secondly, changing and regeneration of the catalyst were assumed to be less complex, because the plates can be easily separated from each other. An overview of the microreactor plate is shown in Fig. 1(a) and its detailed structure in Fig. 1(b) and (c).

The microreactor plate is made of stainless steel and consists of three sections: the inlet, reaction, and outlet section. Liquid and gas enter into the reactor at the inlet section from opposite sides and are divided into a number of substreams. The mixing and dispersion occurs in the reaction section, which consists of the structural elements. The size of the reaction section is 10 cm × 40 cm. Two types of structural elements, square and triangle, are used. The layout and dimensions of these structures is shown in Fig. 1(b) and (c). The structural elements are arranged in staggered arrays forming a number of parallel microchannels and providing a fraction of free space of 0.83 in the square structure configuration and 0.75 in the triangular structure configuration. The distance between the plates is 300 μm. The reactor is vertically operated, allowing the fluids to flow downwards through the reaction section to the outlet section where the gas and liquid are separated by gravity. The liquid is then removed from the bottom and the gas is removed from the top of the outlet section.

3. Hydrodynamic measurement

The experimental setup is shown in Fig. 2. A water–air system was used. The reactor plate was covered by transparent acrylic plate to enhance visual observation. A high speed camera was used to capture still images at different flow conditions in order to be able to determine hydrodynamic parameters.

Because the top and bottom plates are made of different materials, they have different wetting properties. The contact angle measurement was done with KSV CAM100 contact angle meter. The contact angle of water on steel was 72 and on the acrylic was 77. The difference in wetting properties might have small effect on the hydrodynamic behavior in the reactor.

The experiments were performed by feeding water at a certain flow rate ranging from 20 to 100 ml/min into the reactor so that all the flow channels were fully occupied. Air was then fed into the reactor with a flow rate ranging between 36 and 180 ml_n/min. The

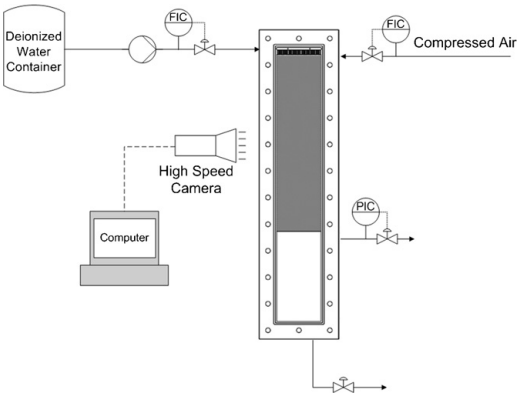

Fig. 2. Experimental setup for hydrodynamics measurement.

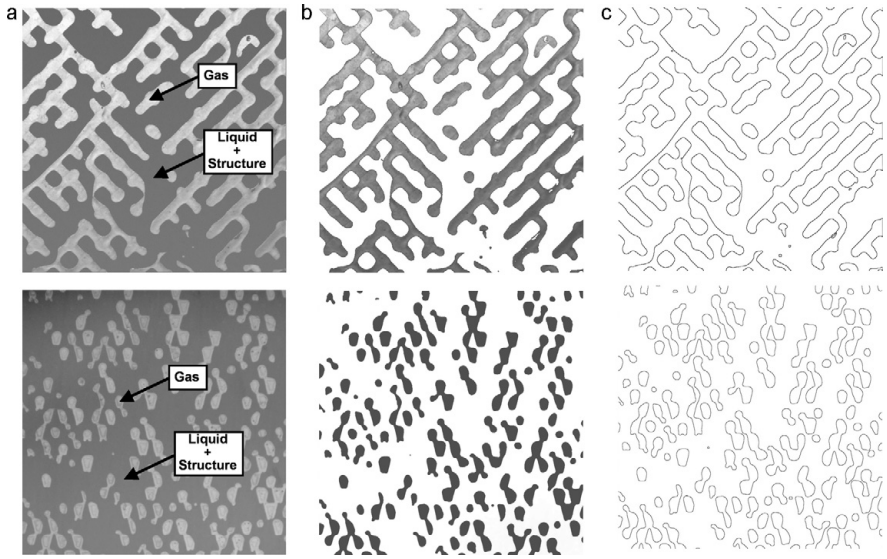

Fig. 3. Image processing steps for gas holdup and gas–liquid interfacial area measurements: (a) original image, (b) processed image showing the area of the gas slugs, (c) processed image showing the perimeters of the gas slugs.

feed flow rates correspond to a superficial velocity of 11–55 mm s^{-1} and 20–100 mm s^{-1} for water and air, respectively. Ambient temperature and pressure prevailed.

A favorable flow pattern was achieved. The flow in the microreactor demonstrated excellent mixing behavior by breaking and recombining the gas and liquid slugs throughout the reactor. Thus, an extremely high gas–liquid interfacial area was achieved.

From the investigation of flow behavior, the flow in microreactor plates was considerably unstable. The flow trajectories changed continuously due to the breaking–recombining behavior caused by the structural elements inside the reactors. The determination of hydrodynamic parameters by image analysis was done carefully in order to limit the uncertainty from the unstable flow and to prove the reproducibility of the results. Several sample images from each flow combination were taken at different time spans. The images were captured from the reaction section where the two phase flow was fully developed and the hydrodynamic parameters were determined as average values. The image processing software, ImageJ, was used to determine the hydrodynamic parameters. The images from square and triangular structure microreactor were cropped to 800×800 pixel and 1440×1440 pixel, respectively. The scales of the images were 43 pixel/mm for the square structure reactor and 30 pixel/mm for the triangular structure reactor. The software calculated the area occupied by the gas by subtracting the area occupied by the liquid and the structural elements from the total plate area. The steps in image analysis for gas holdup and gas–liquid interfacial area measurements in the square structure microreactor (upper) and triangular structure microreactor (lower) are presented in Fig. 3. Brighter parts in Fig. 3(a) represent the gas phase, while darker parts represent the liquid phase and structural elements. Fig. 3(a) was processed by inverting the colors so that the gas phase has dark color in Fig. 3(b). The perimeter of the gas phase in Fig. 3(b) was generated and is shown in Fig. 3(c). The area of the gas slugs determine gas holdup which is presented in Fig. 4. Fig. 5 presents the gas–liquid interfacial area determined from (a) only the perimeter of gas slugs, denoted by the subscript *per*, and (b) both from the perimeter of gas slugs and the area against the bottom and cover plate, denoted by the subscript *tot*. The latter represents the real interfacial area. However, in some applications only the area a_{per} might be active in mass transfer. The gas–liquid interfacial area was determined both as the area per volume of fluid, denoted by the subscript *f*, and per volume of the reactor, denoted by the subscript *r*.

Gas holdup determined from the experiments was in the range of 20–45%. The values of the total gas–liquid interfacial area were high up to 4800 and 5600 $m^2\ m^{-3}$ for the square and triangular

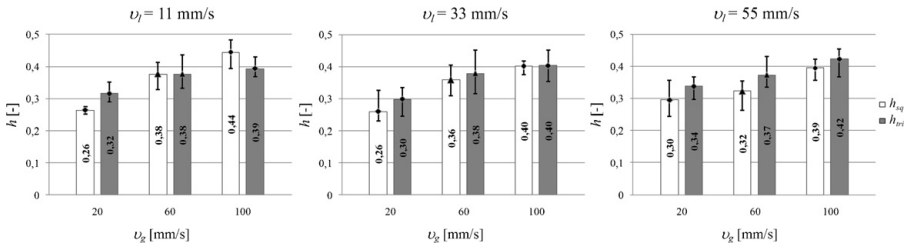

Fig. 4. Experimental results: gas holdup at various flow conditions.

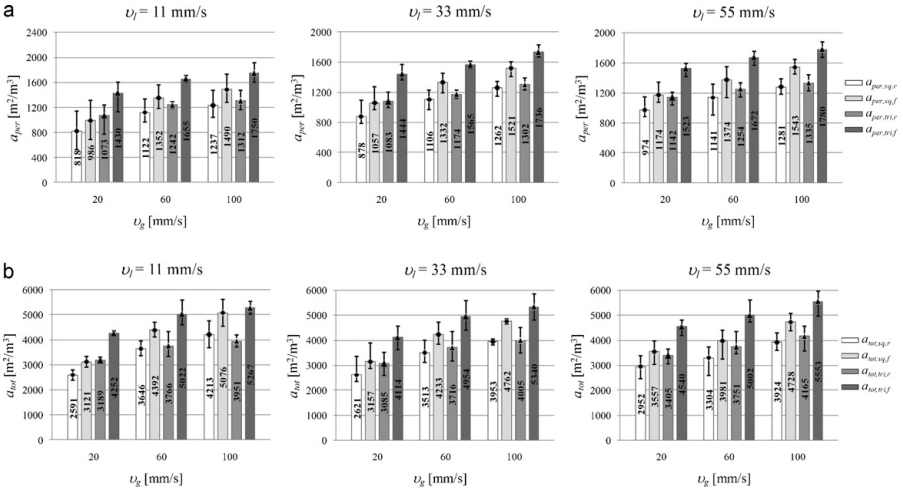

Fig. 5. Experimental results: gas–liquid interfacial area at various flow conditions: (a) determined from only the perimeter of gas slugs, (b) determined from the perimeter of gas slugs and area against the bottom and cover plate.

structure microreactor, respectively, which is much higher than in typical commercial gas–liquid reactors, where 1000 $m^2\ m^{-3}$ is seldom exceeded. The uncertainty of the results obtained from the images at each flow combination was found to be in the range of ±20% where the maximum value at ±30% was found at the lowest gas and liquid flow rate in the square plate. The uncertainty tended to be decreased at higher gas and liquid flow rate. This can be explained by the poor hydrodynamic behavior which was exhibited as fingered flow (channeling flow). This type of flow was observed at low gas and liquid flow rate where the gas and liquid phases flowed through the certain part of the reactor plate and breaking–recombining behavior sometimes occurred during the investigation.

The gas and liquid slugs in the triangular plate were splitted into smaller gas bubbles and liquid slugs than the ones in the square plate; a result caused from the difference in the void fraction and in the shape of the structural elements. As a result, the gas–liquid interfacial area was slightly higher in the plate with triangular elements. The gas superficial velocity strongly influenced both gas holdup and the gas–liquid interfacial area, while the effect of the liquid superficial velocity was insignificant.

4. Mass transfer measurements

The experimental setup is shown in Fig. 6. A water–nitrogen–oxygen system was used. Deionized water was saturated with oxygen, and nitrogen was used to strip oxygen out from the liquid phase. An in-line oxygen concentration analyzer was employed to measure the concentration of oxygen at the inlet and outlet of the reactor. The ranges of the gas and liquid flow rates were the same as in hydrodynamic measurements.

Oxygen was transferred from the liquid phase to the gas phase and nitrogen vice versa. Changes in the oxygen and nitrogen molar flow in the gas phase along the microreactor can be described as:

$$\frac{d\dot{n}_{O_2}}{dL} = -k_l a(C^*_{O_2} - C_{O_2})(1-\varepsilon_s)A_{cr} \quad (1)$$

$$\frac{d\dot{n}_{N_2}}{dL} = -\frac{D_{N_2}}{D_{O_2}} k_l a(C'^*_{N_2} - C_{N_2})(1-\varepsilon_s)A_{cr} \quad (2)$$

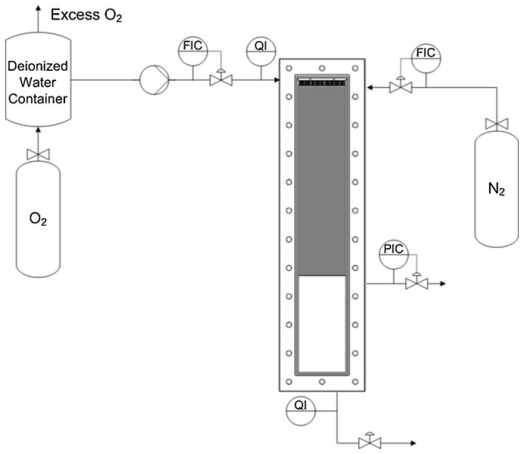

Fig. 6. Experimental setup for mass transfer study.

Concentrations of oxygen and nitrogen in the liquid phase change according to the following equations

$$\frac{dC_{O_2}}{dL} = k_l a(C^*_{O_2} - C_{O_2})\frac{A_{cr}(1-\varepsilon_s)(1-\varepsilon_g)}{\dot{V}_l} \quad (3)$$

$$\frac{dC_{N_2}}{dL} = \frac{D_{N_2}}{D_{O_2}} k_l a(C^*_{N_2} - C_{N_2})\frac{A_{cr}(1-\varepsilon_s)(1-\varepsilon_g)}{\dot{V}_l} \quad (4)$$

The saturation concentrations of the nitrogen and oxygen can be calculated by Henry's law as:

$$C^*_{N_2} = \frac{p_{N_2}}{H_{N_2}} \quad (5)$$

$$C^*_{O_2} = \frac{p_{O_2}}{H_{O_2}} \quad (6)$$

$$p_{N_2} = \frac{\dot{n}_{N_2}}{\dot{n}_{O_2} + \dot{n}_{N_2}} \cdot P \quad (7)$$

Table 1
Parameter values and correlation for mass transfer coefficient.

Element type	α_1	α_2	α_3	Correlation
Square (♦)	0.177	0.874	0.179	$k_l a = 0.177\left(\frac{\upsilon_g}{0.02}\right)^{0.874}\left(\frac{\upsilon_l}{0.02}\right)^{0.179}$
Triangular (▲)	0.175	0.899	0.432	$k_l a = 0.175\left(\frac{\upsilon_g}{0.02}\right)^{0.899}\left(\frac{\upsilon_l}{0.02}\right)^{0.432}$

$$p_{O_2} = \frac{\dot{n}_{O_2}}{\dot{n}_{O_2} + \dot{n}_{N_2}} \cdot P \quad (8)$$

where $H_{N_2} = 1468.90\,dm^3\,bar\,mol^{-1}$ and $H_{O_2} = 732.62\,dm^3\,bar\,mol^{-1}$ [15].

A closed system of four ordinary differential equations (ODE) describes the two-phase mass transfer in the microreactor.

The following correlation was used to describe the dependency of the mass transfer coefficient from the superficial velocities:

$$k_l a = \beta_1 \upsilon_g^{\beta_2} \upsilon_l^{\beta_3} \quad (9)$$

For better numerical performance the following normalized form of the equation was used:

$$k_l a = \alpha_1 \left(\frac{\upsilon_g}{\upsilon_{g,norm}}\right)^{\alpha_2} \left(\frac{\upsilon_l}{\upsilon_{l,norm}}\right)^{\alpha_3} \quad (10)$$

where $\upsilon_{g,norm}$ and $\upsilon_{l,norm}$ are equal to $0.02\,m\,s^{-1}$.

A set of experiments was performed on both the square and triangular structure microreactors. In each experiment O_2 concentration in the liquid was measured at the inlet ($L = 0$ mm) and outlet of the microreactor ($L = 400$ mm) for each gas and liquid flow rate. Inlet measurements defined initial conditions for the ODE system and outlet measurements were used to fit the model parameters. An Euler method was then used to solve the ODE system. It was found that this method is very fast and robust enough in this case. Conducted error analysis revealed that it gives an accuracy of the estimated parameters of 0.2–0.5% when the number of subintervals is only 200.

$k_l a$ values were estimated by minimizing the sum of the squared differences between the estimated and the measured values at the outlet of the reactor. Corresponding estimated optimal parameter values are shown in Table 1.

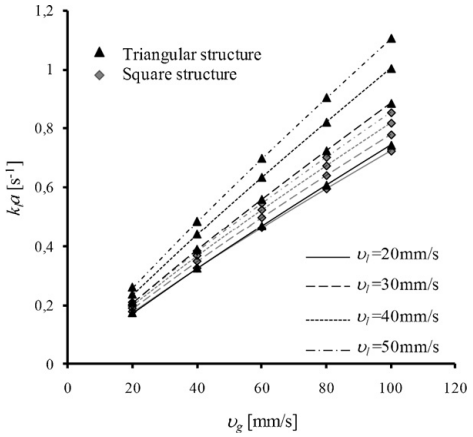

Fig. 7. Estimated $k_l a$ dependency on υ_g and υ_l.

Fig. 7 shows that mass transfer in the triangular structure microreactor was better than in the square structure one. The maximum $k_l a$ values in the triangular structure microreactor were as high as $1.10\,s^{-1}$, which was approximately 25% higher than in the square structure reactor, where the highest value was $0.85\,s^{-1}$. The comparison of mass transfer coefficient obtained from this study and from literature [3,6,7,13,14,16–19] in microscale and conventional scale gas–liquid contactors is presented in Table 2. The mass transfer coefficients from this study are in the range from 0.17 to $1.10\,s^{-1}$, which are one or two orders of magnitude higher than

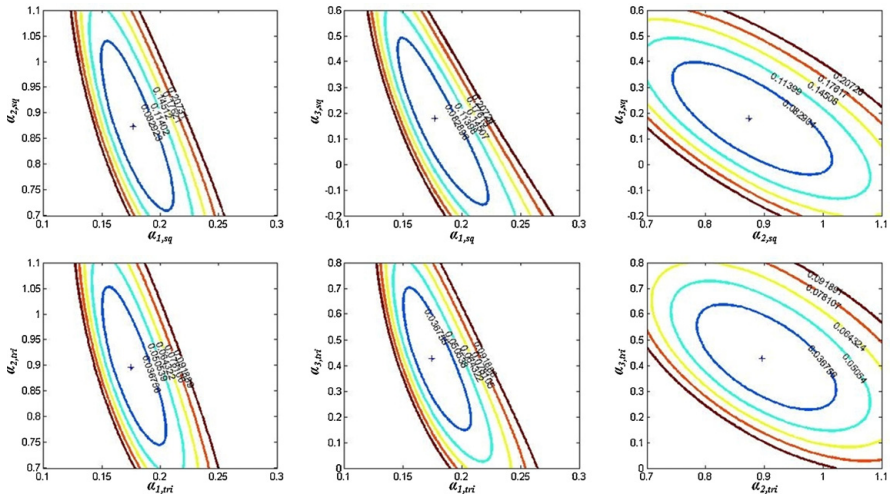

Fig. 8. Sensitivity plots of estimated parameters for volumetric mass transfer coefficient.

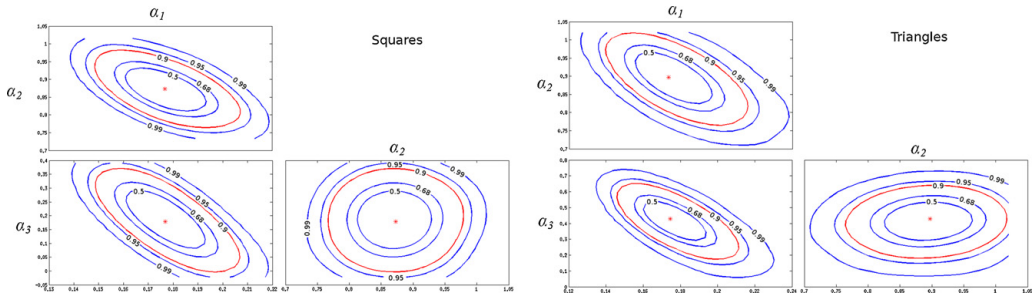

Fig. 9. Confidence level of marginal distribution of parameters.

Table 2
Comparison of gas–liquid interfacial area and mass transfer coefficients in different gas–liquid contactors.

Type of contactor	a [$m^2\ m^{-3}$]	$k_l a$ [s^{-1}]
Bubble column [16]	180–670	0.07–0.25
Trickle bed reactor [17]	150–1500	0.01–0.08
Three-phase fluidized bed [18]	30–160	0.08–0.64
Static mixer [19]	100–1000	0.1–2.4
Microchannel [3,13]	3400–9000	0.3–21
Micro-capillaries [14]	1000–7500	0.3–1.5
Micro packed-bed reactor [6,7]	1500–16,000	5–15
Microreactor in this study	2600–5600	0.17–1.1

conventional scale gas–liquid contactors and in the same range as in other microscale gas–liquid contactors.

Sensitivity analysis of the estimated parameters (α_1, α_2, and α_3) was carried out to determine their identifiability and the goodness of the fit. The aim of the analysis was to determine the shape of the objective function representing the sum of squares SS(α_1,α_2,α_3) used to find the parameters. Its minimum indicates the optimal point and the best parameter values. The shape of the function tells how well every parameter is identified and if there is a correlation between them. In this case the objective function is a surface in a four-dimensional space, so it cannot be explicitly plotted. Instead, two-dimensional cross-sections of this function at the optimal point can be studied to get an insight of it. The cross-section is done along coordinate planes (α_1,α_2), (α_1,α_3) and (α_2,α_3). Corresponding contour-plots are presented in Fig. 8. Top row is for the square structure, bottom row – for triangle. These plots indicate that the parameters are well-identified, although a slight correlation exists between them, especially between the α_1–α_2 and α_1–α_3 in both cases.

Confidence levels of marginal distributions of the estimated parameters are presented in Fig. 9. Three plots on the left are for the squared structure reactor and three on the right are for the triangle. These distributions were estimated using Monte-Carlo Markov Chain (MCMC) simulation. They are in a good accordance with the objective function contour-plots and also indicate the same correlation between the α_1–α_2 and α_1–α_3 for both cases.

5. Conclusion

Hydrodynamic and mass transfer behavior of a novel plate type microreactor was studied. The reactor has certain advantages when compare to conventional microreactor consisted of parallel direct microchannels. Firstly, less plugging problem can be expected. Secondly, changing and regenerating catalyst is easier because the reactor can be easily opened.

Relatively uniform gas–liquid distribution without serious channeling was obtained. Hydrodynamics and mass transfer performance of the microreactor were considerably better than in conventional multiphase chemical reactors. The total interfacial area was in the range of 2600–5600 $m^2\ m^{-3}$ and the volumetric mass transfer coefficient was in the range of 0.17–1.10 s^{-1}. The volumetric mass transfer coefficient correlated well with the superficial velocities of the gas and liquid. The parameters of the correlation were well determined.

It was found that the triangular structural elements gave slightly better hydrodynamic behavior than the square ones. As a consequence, also the mass transfer was faster with the triangular elements.

Appendix A. Nomenclature

a	specific surface area ($m^2\ m^{-3}$)
A	area (m^2)
C	concentration ($mol\ m^{-3}$)
C^*	saturation concentration ($mol\ m^{-3}$)
D	diffusivity ($m^2\ s^{-1}$)
h	holdup (–)
H	Henry's constant ($dm^3\ bar\ mol^{-1}$)
k	volumetric mass transfer coefficient ($m\ s^{-1}$)
L	length of the microreactor plate (m)
p	partial pressure (bar)
P	total pressure (bar)
$\dot{V}$	volumetric flow rate ($m^3\ s^{-1}$)

Greek symbols

ε	volume fraction (–)
υ	superficial velocity ($mm\ s^{-1}$)

Subscripts

cr	cross sectional
f	fluid
g	gas
l	liquid
norm	normalized
per	perimeter
r	reactor
s	structured plate reactor
sq	square structure plate
tot	total
tri	triangular structure plate

References

[1] W. Ehrfeld, V. Hessel, H. Löwe, Microreactors: New Technology for Modern Chemistry, Wiley-VCH, Weinheim, 2002.
[2] K. Jähnisch, V. Hessel, H. Löwe, M. Baerns, Chemistry in microstructured reactors, Angew. Chem. Int. Ed. 43 (2004) 406–446.

[3] J. Yue, G. Chen, Q. Yuan, L. Luo, Y. Gontier, Hydrodynamics and mass transfer characteristics in gas–liquid flow through a rectangular microchannel, Chem. Eng. Sci. 62 (2007) 2096–2108.
[4] L. Kiwi-Minsker, A. Renken, Microstructured reactors for catalytic reactions, Catal. Today 110 (2005) 2–14.
[5] St. Walter, St. Malmberg, B. Schmidt, M.A. Liauw, Mass transfer limitations in microchannel reactors, Catal. Today 110 (2005) 15–25.
[6] M.W. Losey, M.A. Schmidt, K.F. Jensen, Microfabricated multiphase packed-bed reactor: characterization of mass transfer and reactions, Ind. Eng. Chem. Res. 40 (2001) 2555–2562.
[7] M.W. Losey, J. Rebecca, S.L. Firebaugh, M.A. Schmidt, K.F. Jensen, Design and fabrication of microfluidic devices for multiphase mixing and reaction, J. Microelectromech. Syst. 11 (2002) 709–717.
[8] J.W. Coleman, S. Garimella, Characterization of two-phase flow patterns in small diameter round and rectangular tubes, Int. J. Heat Mass Transf. 42 (1999) 2869–2881.
[9] A. Kawahara, P.M.Y. Chung, M. Kawaji, Investigation of two-phase flow pattern, void fraction and pressure drop in a microchannel, Int. J. Multiphase Flow 28 (2002) 1411–1435.
[10] S. Waelchli, P.R. von Rohr, Two-phase flow characteristics in gas–liquid microreactors, Int. J. Multiphase Flow 32 (2006) 791–806.
[11] R. Pohorecki, P. Sobieszuk, K. Kula, W. Moniuk, M. Zieliński, P. Cygański, P. Gawiński, Hydrodynamic regimes of gas–liquid flow in a microreactor channel, Chem. Eng. J. 135S (2008) 185–190.
[12] R. Pohorecki, Effectiveness of interfacial area for mass transfer in two-phase flow in microreactors, Chem. Eng. Sci. 62 (2007) 6495–6498.
[13] J. Yue, L. Luo, Y. Gonthier, G. Chen, Q. Yuan, An experimental study of air–water Taylor flow and mass transfer inside square microchannels, Chem. Eng. Sci. 64 (2009) 3697–3708.
[14] N. Shao, A. Gavriilidis, P. Angeli, Mass transfer during Taylor flow in microchannels with and without chemical reaction, Chem. Eng. J. 160 (2010) 873–881.
[15] R.H. Perry, Perry's Chemical Engineers' Handbook, 7th edition, McGraw-Hill Inc., USA, 1999.
[16] K.M. Singh, S.K. Majumder, Co- and counter-current mass transfer in bubble column, Int. J. Heat Mass Transf. 54 (2011) 2283–2293.
[17] M.H. AlDahhan, F. Larachi, M.P. Dudukovic, A. Laurent, High-pressure trickle-bed reactors: a review, Ind. Eng. Chem. Res. 36 (8) (1997) 3292–3314.
[18] W. Yang, J. Wang, T. Wang, Y. Jin, Experimental study on gas–liquid interfacial area and mass transfer coefficient in three-phase circulating fluidized beds, Chem. Eng. J. 84 (2001) 485–490.
[19] A. Heyouni, M. Roustan, Z. Do-Quang, Hydrodynamics and mass transfer in gas–liquid flow through static mixers, Chem. Eng. Sci. 57 (2002) 3325–3333.

ACTA UNIVERSITATIS LAPPEENRANTAENSIS

559. GRÖNMAN, KAISA. Importance of considering food waste in the development of sustainable food packaging systems. 2013. Diss.

560. HOLOPAINEN, SANNA. Ion mobility spectrometry in liquid analysis. 2013. Diss.

561. NISULA, ANNA-MAIJA. Building organizational creativity – a multitheory and multilevel approach for understanding and stimulating organizational creativity. 2013. Diss.

562. HAMAGUCHI, MARCELO. Additional revenue opportunities in pulp mills and their impacts on the kraft process. 2013. Diss.

563. MARTIKKA, OSSI. Impact of mineral fillers on the properties of extruded wood-polypropylene composites. 2013. Diss.

564. AUVINEN, SAMI. Computational modeling of the properties of TiO2 nanoparticles. 2013. Diss.

565. RAHIALA, SIRPA. Particle model for simulating limestone reactions in novel fluidised bed energy applications. 2013. Diss.

566. VIHOLAINEN, JUHA. Energy-efficient control strategies for variable speed controlled parallel pumping systems based on pump operation point monitoring with frequency converters. 2014. Diss.

567. VÄISÄNEN, SANNI. Greenhouse gas emissions from peat and biomass-derived fuels, electricity and heat – Estimation of various production chains by using LCA methodology. 2014. Diss.

568. SEMYONOV, DENIS. Computational studies for the design of process equipment with complex geometries. 2014. Diss.

569. KARPPINEN, HENRI. Reframing the relationship between service design and operations: a service engineering approach. 2014. Diss.

570. KALLIO, SAMULI. Modeling and parameter estimation of double-star permanent magnet synchronous machines. 2014. Diss.

571. SALMELA, ERNO. Kysyntä-toimitusketjun synkronointi epävarman kysynnän ja tarjonnan toimintaympäristössä. 2014. Diss.

572. RIUNGU-KALLIOSAARI, LEAH. Empirical study on the adoption, use and effects of cloud-based testing. 2014. Diss.

573. KINNARINEN, TEEMU. Pressure filtration characteristics of enzymatically hydralyzed biomass suspensions. 2014. Diss.

574. LAMMASSAARI, TIMO. Muutos kuntaorganisaatiossa – tapaustutkimus erään kunnan teknisestä toimialasta. 2014. Diss.

575. KALWAR, SANTOSH KUMAR. Conceptualizing and measuring human anxiety on the Internet. 2014. Diss.

576. LANKINEN, JUKKA. Local features in image and video processing – object class matching and video shot detection. 2014. Diss.

577. AL-SAEDI, MAZIN. Flexible multibody dynamics and intelligent control of a hydraulically driven hybrid redundant robot machine. 2014. Diss.

578. TYSTER, JUHO. Power semiconductor nonlinearities in active d*u*/d*t* output filtering. 2014. Diss.

579. KERÄNEN, JOONA. Customer value assessment in business markets. 2014. Diss.

580. ALEXANDROVA, YULIA. Wind turbine direct-drive permanent-magnet generator with direct liquid cooling for mass reduction. 2014. Diss.

581. HUHTALA, MERJA. PDM system functions and utilizations analysis to improve the efficiency of sheet metal product design and manufacturing. 2014. Diss.

582. SAUNILA, MINNA. Performance management through innovation capability in SMEs. 2014. Diss.

583. LANA, ANDREY. LVDC power distribution system: computational modelling. 2014. Diss.

584. PEKKARINEN, JOONAS. Laser cladding with scanning optics. 2014. Diss.

585. PELTOMAA, JYRKI. The early activities of front end of innovation in OEM companies using a new FEI platform as a framework for renewal. 2014. Diss.

586. ROZHANSKY, IGOR. Resonant tunneling effects in semiconductor heterostructures. 2014. Diss.

587. PHAM, THUY DUONG. Ultrasonic and electrokinetic remediation of low permeability soil contaminated with persistent organic pollutants. 2014. Diss.

588. HOKKANEN, SANNA. Modified nano- and microcellulose based adsorption materials in water treatment. 2014. Diss.

589. HINKKANEN, JUHA. Cooperative strategy in emerging markets – analysis of interfirm R&D cooperation and performance in Russian manufacturing companies. 2014. Diss.

590. RUSKOVAARA, ELENA. Entrepreneurship education in basic and upper secondary education – measurement and empirical evidence. 2014. Diss.

591. IKÄHEIMONEN, TUULI. The board of directors as a part of family business governance – multilevel participation and board development. 2014. Diss.

592. HAJIALI, ZUNED. Computational modeling of stented coronary arteries. 2014. Diss.

593. UUSITALO, VILLE. Potential for greenhouse gas emission reductions by using biomethane as road transportation fuel. 2014. Diss.

594. HAVUKAINEN, JOUNI. Biogas production in regional biodegradable waste treatment – possibilities for improving energy performance and reducing GHG emissions. 2014. Diss.

595. HEIKKINEN, JANNE. Vibrations in rotating machinery arising from minor imperfections in component geometries. 2014. Diss.

596. GHALAMCHI, BEHNAM. Dynamic analysis model of spherical roller bearings with defects. 2014. Diss.

597. POLIKARPOVA, MARIIA.Liquid cooling solutions for rotating permanent magnet synchronous machines. 2014. Diss.

598. CHAUDHARI, ASHVINKUMAR. Large-eddy simulation of wind flows over complex terrains for wind energy applications. 2014. Diss.

599. PURHONEN, MIKKO. Minimizing circulating current in parallel-connected photovoltaic inverters. 2014. Diss.

600. SAUKKONEN, ESA. Effects of the partial removal of wood hemicelluloses on the properties of kraft pulp. 2014. Diss.